BIFURCATION SUBSYSTEM METHOD AND ITS APPLICATIONS IN ANALYSIS AND CONTROL DESIGN FOR POWER SYSTEMS

By

Meng Yue

A DISSERTATION

Submitted to
Michigan State University
in partial fulfillment of the requirements
for the degree of

DOCTOR OF PHILOSOPHY

Department of Electrical and Computer Engineering

2002

ABSTRACT

BIFURCATION SUBSYSTEM METHOD AND ITS APPLICATIONS IN ANALYSIS AND CONTROL DESIGN FOR POWER SYSTEMS

By

Meng Yue

Two generic bifurcations, saddle-node and Hopf bifurcation, have been proven to cause various instability problems in the power systems. The size, complexity, and nonlinearity is the main obstacle to analyzing, diagnosing, and stabilizing power system bifurcations. A bifurcation subsystem method, a novel model reduction method, is able to identify a small order subsystem that (1) experiences, produces, causes, and provides the cures for power system instability problems; (2) captures the critical dynamics (the center manifold) and preserves the dynamic behaviors of the full system; (3) does not utilize a nonlinear or linear transformation that requires significant computation; (4) retains the physically meaningful state variables and parameter structure of the full system due to the fact that no linear or nonlinear transformation is needed; (5) makes the classification of the power system bifurcations possible by noting that states of the generator or load devices in the bifurcation subsystem model; and (6) can be used to design stabilizing control to be applied to the full system bifurcation. The complete theoretical framework for the bifurcation subsystem method is established in the first part of this thesis and applied to an example power system.

The second part of this thesis is dedicated to the design of robust control based on

the bifurcation subsystem method using a methodology that can provide and clearly demonstrate advantages over classical control design methods. The first component of this methodology is the use of the *RGA* analysis to show that the robust control design produced by this methodology (1) breaks the external system into subsystems that are decoupled from one another and from the bifurcation subsystem and (2) shows the effectiveness of the control in each subsystem. The second component is to use a structured uncertainty that captures the nonlinear change in linear model due to the bifurcation parameter change from the nominal value to the bifurcation value. The third component is the use of the bifurcation subsystem model for design of the controller rather than the full system model. The fourth component is the selection of the performance index, weighting matrix, measurements and control that are based on the bifurcation and the bifurcation subsystem being stabilized.

H_∞ control attempts to find the control that minimize the performance index for the possible uncertainty that occurs at the frequency where the system is most vulnerable. The design methodology preselects and coordinates the frequency uncertainty and subsystem at which the robust controller should have effect. The frequency where the system is most vulnerable is the bifurcation frequency ($\omega = 0$ for saddle-node and $\omega = \omega_0$ for Hopf bifurcation), the uncertainty produces the bifurcation at this frequency and the subsystem is the bifurcation subsystem for this bifurcation. This coordination within this design methodology enables the very significant control performance improvements enabled.

The complete robust control design methodology for power system stabilizer, SVC, and mixed power system stabilizer/SVC, is described by studying a single bifurcation (saddle-node or Hopf bifurcation) and multiple bifurcations (interarea oscillation and local oscillation). The nonlinear effects of the robust control design is also studied.

To my parents

ACKNOWLEDGEMENTS

I am grateful for the invaluable understanding, concern, and support my parents give me throughout my life.

I am greatly indebted to my advisor, Dr. Schlueter, for giving me the opportunity to pursue my study here. His encouragement, guidance, assistance, and consideration make this thesis possible.

I would also like to express my gratitude to the other committee members, Professors Jerry Schuur, Hassan Khalil, Steve Shaw, and Michael Frazier for their valuable comments, time, and advice.

Special thanks to my brothers, Gang, Yong, and my sister, Lin for their support. Last but not the least, sincere gratitude is extended to my friends, Lin Zhou, Yongsheng He, Shen Lu, and Yun Tang for their constant encouragement and support.

Contents

List of Figures

List of Tables

Chapter 1

Introduction

1.1 Objectives

The thesis is to be formulated in an effort to achieve the following objectives:

1. provide theoretical framework for the bifurcation subsystem method:

   (a) by showing that the properties of trajectories, the size and the nature of the orbits, the equilibrium, the bifurcation point, the bifurcating eigenvalue, and the center manifold dynamics of the reduced system persist for the full system with both fast and slow singularly perturbed external dynamics provided that singular perturbation is small. Simultaneous application of both fast and slow singular perturbations for the external system of a regular internal dynamic system has never been previously attempted, but is required to define the concept of the bifurcation subsystem for both saddle-node and Hopf bifurcation based on the bifurcation theory. The definition of a bifurcation subsystem is based on the closeness of equilibrium and bifurcation points of the full system and those for the fast singularly perturbed and slow singularly perturbed external system

model;

(b) by developing a set of sufficient conditions for a bifurcation subsystem to exist. These conditions are referred to as bifurcation subsystem condition, and geometric decoupling condition that establish the conditions for the bifurcation subsystem to exist. Knowing the test conditions for a bifurcation subsystem to exist does not imply that one could ever satisfy these conditions. Moreover, one could not be assured that one should be able to find the bifurcation subsystem in most if not all cases when a bifurcation occurs. It is proven that finding a bifurcation subsystem of some order is a very high probability event. If the external system is extremely fast compared to the bifurcation subsystem dynamics, then the bifurcation subsystem exists. This requirement is generally true 1) if the bifurcation subsystem is experiencing saddle-node bifurcation, 2) if the coupling of the bifurcation subsystem to the external system is null in the direction of the right eigenvector at bifurcation point, 3) if the coupling of the external system to the bifurcation bifurcation subsystem is null in the direction of the right eigenvector approximation to the center manifold at bifurcation. These results allow the proof that the identification of a bifurcation subsystem for any bifurcation is a highly probable event and that the order of the bifurcation subsystem model is very likely to be small;

(c) these results also allow the comparison of the bifurcation subsystem method with the slaving principle [27] and a method of clustering dynamics by α-decomposition [22]. The objectives of the slaving principle and α-decomposition are respectively to obtain the reduced order model that describes the bifurcation (slaving principle) or to obtain a reduced order model that allows accurate approximation of the response of the full

system model when disturbances are restricted to the internal subsystem (α-decomposition). The objective of the bifurcation subsystem method does not necessarily desire to perform and justify model reduction or to obtain a reduced order model that describes the bifurcation. The objective of bifurcation subsystem method is to describe the subsystem that experiences, produces, and causes the bifurcation in the full system so that better control can be achieved to correct the instability, and stabilize the center manifold dynamics of the full system. The ability to determine a bifurcation subsystem would greatly aid in the design of the control system;

(d) by proving that the bifurcation subsystem dynamics produce nearly the same center manifold, orbits and their frequencies, trajectories near the center manifold, bifurcation points, equilibrium points as the full system model. It is also to be proven that 1) a very small order bifurcation subsystem is a good approximation of the center manifold dynamics, and 2) that a bifurcation subsystem model contains the center manifold of the full system model without requiring the nonlinear transformation used to determine the center manifold dynamic model for a particular saddle-node or Hopf bifurcation.

2. provide the theoretical justification of the algorithm for identification of the bifurcation subsystem and the computational justification of the bifurcation subsystem method:

(a) by developing an algorithm for identification of the bifurcation subsystem out of the full system model which has relatively small dimension and includes the center manifold dynamics of the full system based on the above theoretical results. The bifurcation subsystem identification

algorithm must be theoretically justified for both saddle-node and Hopf bifurcation systems;

(b) by obtaining different bifurcation subsystems (both saddle-node and Hopf bifurcation) by applying the bifurcation subsystem identification algorithm on a two-area example system with different bifurcation parameters.

3. design μ-synthesis based robust controls for the two-area example power system to stabilize bifurcation and improve the control performance and robustness based on the bifurcation subsystem information:

(a) by modeling the uncertainty of power system with the structural information of the system. The structural uncertainty is caused by the variation of a specific bifurcation parameter. This uncertainty modeling should not lead much conservativeness for control design;

(b) by designing H_∞ robust controller [35] for the two area power system based on the bifurcation subsystem information and the uncertainty model caused by bifurcation parameter. Robust control of power system stabilizer and SVC devices will be designed and the control performance will be compared. The dynamic performance of robust controls will be also compared for conventional power system stabilizer control design and conventional SVC control with and without inverse generator dynamics;

(c) by studying the RGA matrix of the system with and without robust control. The RGA matrix [35] (relative gain array) indicates the measure for observing the structure of decentralized control and for indicating the sensitivity to the uncertainty at different frequencies. The RGA matrix based on the robust decentralized control will be compared with RGA

matrix computed for an existing conventional controller. This will explains how and why the robust control improves the control performance compared to the conventional power system control design.

When the bifurcation parameters change the full system could experience a sequence of different bifurcations, even chaos. Currently, our program does not have the ability to trace out this bifurcation sequence. It is not one of the tasks in this thesis but is left as a topic for future research.

1.2 Why a Bifurcation Subsystem Method

The recurrent problem in diagnosing and analyzing a specific power system stability problem is that of the size, complexity, and nonlinearity of the model. Although it seems that a large number of variables are involved in the power system stability problem, only a small subset of these variables are hypothesized to be critical to the problem.

Model reduction approach, including modal analysis method [12], singular perturbation method [10], coherent reduction [14], Kalman minimal realization method [13], decomposition methods [22], and quasi-steady-state approximation [9], has been applied to determine a reduced order model that retains the dynamics of an internal system and approximates the dynamics of the external system.

1.2.1 Comparison with Modal Methods

With modal analysis method [12] the location and the states of the system involved in the response and control of a particular bifurcation eigenvalue are obtained from the information of right eigenvector, left eigenvector, and participation factor matrix of the bifurcating eigenvalue when system instability is being approached. The mag-

nitude of the eigenvalue of the normalized modal transformed system represents the relative measure to proximity to the bifurcation, the elements of the left eigenvector can be interpreted as indicating a direction normal to the operational boundary of the system, and right eigenvector indicates the degree to which given variables respond for a given mode. The highest correlation of the right eigenvector with rows of the output matrix can be used to select measurements to observe the response of the model. The highest correlation of the left eigenvector of a mode with the columns of the input matrix can be used to select the control inputs that best control the response. The participation factor matrix indicates the relative involvement of system components in the unstable mode or the collapse region. The participation factor matrix determines states where the mode is most evident in terms of both control and measurement, but does not necessarily determine the subsystem that experiences and the subsystem that produces the bifurcation. A study on the BC Hydro system conducted in [8] shows that the results obtained by modal analysis can be misleading or insufficient for determining the portion of the system that is causing the instability in the full system.

1.2.2 Comparison with Singular Perturbation Method

The singular perturbation technique [10] [9] cannot always be applied for problem diagnosis that occurs after a power system disturbance since the states most involved in an unstable behavior in a power system cannot always be classified into either the slow or the fast dynamics groups so that the reduced model will always describe the instability. Transient stability often involves both fast and slow dynamics. However, voltage instability and interarea oscillation are often associated with the slow dynamics of coherent bus groups and thus appears to be appropriate for an analysis via reduced models. When the singularly perturbed models are useful to focus on

the dynamics experiencing, producing, and causing the bifurcation that are observed as voltage stability and interarea oscillation, it is anticipated that bifurcation subsystem method can be applied. In fact, bifurcation subsystems are only possible when bifurcation subsystem can be modeled simultaneously by the reduced model of a fast singularly perturbed model of the external system and by the reduced model of a slow singularly perturbed model of the external system to the bifurcation subsystem. Since both inter-area oscillation and generator oscillation modes each lie in a separate narrow band of frequencies, this singular perturbation approach seems to be inadequate to establish the bifurcation subsystem for a single mode in one of the narrow band of oscillations.

1.2.3 A Brief Comparison with the Center Manifold

Center manifold dynamics [18] is a subsystem of the full system dynamics which experiences, produces, and causes the bifurcation in the full model. However, center manifold dynamics is not considered a bifurcation subsystem since

1. the center manifold dynamics are obtained by a nonlinear transformation of the full dynamics, and thus are not expressed in terms of physically meaningful variables;

2. it is generally impossible to use a nonlinear transformation to analyze how operating condition changes or model parameter changes cause bifurcation for a very large system model. On the other hand, these problems are not difficulties when a bifurcation subsystem is used.

1.2

1.2.4 Comparison with Decomposition Methods

The α-decomposition method [22] clusters the subsystems which have frequencies of oscillation in each subsystem that are close to each other. Effectively, the full system dynamics can be simplified to a set of subsystems with almost same internal frequencies of oscillation and weak coupling between subsystems. The α-decomposition method does not intend to look for the subsystem which experiences, produces, and causes the bifurcation of the full dynamics, nor preserves the center manifold dynamics of the full system for any bifurcation.

The property of the clustered system is rigorously established, and it has been verified that the power system model is a singular perturbation model consisting of slow intercluster dynamics and fast intracluster dynamics in [22]. The goal of the α-decompostion method is to determine the fast intracluster dynamics so they can be eliminated to produce a model reduction that hopefully approximates the slow intercluster dynamics.

The results of α-decomposition method applied in the dynamic equations reveals that the eigenvalues of the decomposed state matrix should be close to those of the full model and the closeness is determined by the choice of α.

Power system differential-algebraic models have both slow and fast dynamics and thus evolve over different time scales. In this case, time-scale decomposition [9] could be used based on singular perturbation. Denoting the slow and fast variables of the dynamic state variables, quasi-steady-state approximation [9] of the slow subsystem becomes the differential-algebraic form. The slow manifold can be approximated using a series expansion in perturbation ϵ to the desired accuracy. The slow and fast dynamics can be represented by the slow manifold. The fast dynamics may undergo bifurcation when the slow dynamics envolve. In this case the slow time-scale-decomposition fails since this slow assumptions which assure the validity of

time-scale-decomposition are violated. Then a fast-time scale decomposition is used to produce a differential model.

1.2.5 Comparison with Dynamic Equivalent Methods

Modal analysis [12], coherency based method [14], and singular perturbation method [10] are motivated to obtain the simplified system model such that the approximated response of the original system can be achieved. These methods identify the fast or weakly coupled subsystem that are then aggregated to produce the approximate slow model of the external system. Modal analysis has also been used to obtain a dynamic equivalent of the system external to a particular utility. This model reduction method does not attempt to preserve the dynamics experiencing, producing, and causing a bifurcation or the center manifold dynamics for a specific bifurcation. Although this modal analysis approach [12] has completely different objectives than the bifurcation subsystem method as just noted, it does attempt to aggregate dynamics and those weakly coupled to the internal system. Thus, this use of modal analysis exploits the same structural properties of systems that is so much more effectively exploited in the bifurcation subsystem method. The model approximation methods [12] [10] [14] are not intended to identify and preserve or even approximate the center manifold dynamics of the internal system for one bifurcation or all bifurcations that affect the utility under study which is referred to as the internal system.

For determining the center manifold of the original full system the large computational requirement to determine the nonlinear transformation limits its application to small system only. On the other hand, bifurcation subsystem method can be applied to both large and small system.

The bifurcation subsystem method exploits the same singular perturbation properties as the α-decomposition method [22] to obtain a reduced model of the fast

singular perturbed external dynamics separated from the bifurcation subsystem by weak coupling but with the objectives of a) focusing on the internal subsystem that preserves the center manifold dynamics and experiences, produces, and causes the bifurcation, and b) more effectively exploiting the same structural properties to obtain stronger results.

From the above discussion, capturing the nature of the original system dynamics cannot be guaranteed except for center manifold method, which does not have clear physical meaning and is not applicable for relatively complex systems.

1.2.6 Comparison with Slaving

Slaving principle [27], a second approach that is different from model reduction, is looking for the dominant dynamic response for a system experiencing bifurcation that may include the dynamics which produces and causes the instability in the full system. Slaving is not intended as a model reduction or approximation method. The slaving principle attempts to identify the subsystem dynamics that dominates the behaviors of a full system model that is experiencing the bifurcation. The approach through the adiabatic approximation allow us to express the fast external variables as a nonlinear function of the slow-changing internal variables provided that: the internal system is very slow and bounded in a small neighborhood around the equilibrium point; the external system is very fast; and the coupling between internal and external systems is weak. Therefore, in dealing with system with very many variables, which are slaved by very few slow variables, we are able to simplify our understanding of the complex system considerably. In this situation the slow internal variables are called order parameters.

The slaving principle has been broadly applied to economic, biological, chemical, and physics based systems, and has been applied to study saddle-node and Hopf bifurca-

tions and to sequences of bifurcations that lead to chaos [27]. It will be shown that identifying when slaving exists in a system is the first step in identifying a bifurcation subsystem which experiences, produces, and causes the full system to bifurcate. This bifurcation subsystem will be argued to exist and be identifiable for most bifurcations for much weaker conditions than required by slaving. Slaving thus may be a much generic property of systems because a) it is true for any bifurcation subsystem; b) the bifurcation subsystem is identifiable based on much weaker conditions than required for slaving to occur [27]; and c) these weaker conditions are proven to have solutions with a high probability.

1. singular perturbation has been argued as being useful in eliminating either the fast or slow model in [9] to study bifurcation, but slaving only would allow the elimination of the fast dynamics when the separation between fast and slow dynamics is sufficiently large;

2. reduced singularly perturbed models have been used to study the bifurcation. The quasi-steady-state approximation [9] is an example where a singularly perturbed model is used to reduce the fast dynamics;

3. the hybrid slow dynamics and network have been reduced from a singularly perturbed model to produce a fast dynamic model [9];

4. tests for bifurcation have been developed for the reduced models and shown to apply to the full system model [9] [8];

5. no theoretical justification is given that the reduction of a singularly perturbed model will preserve the equilibrium point, the orbits, the trajectories, the frequencies, and the center manifold of the full system;

6. this singularly perturbed approach in [10] could be theoretically justified using the same process that will be used to theoretically justify the bifurcation

subsystem method. This theoretical justification of the bifurcation subsystem method also be used to theoretically justify using reduced models of singular perturbed models in item 2 and 3 above.

The goal of bifurcation subsystem method is not model reduction but identification of the subsystem model that experiences, produces, and causes the full system model bifurcation.

Bifurcation subsystem method has a much stronger set of objectives than that for slaving because the bifurcation subsystem should not only act to slave the system external to it, but is also required to have no coupling to the external system. The requirement that the bifurcation subsystem slave the external system and be simultaneously decoupled from it requires the bifurcation occur and be produced in the bifurcation subsystem [8]. Thus the bifurcation subsystem is said to experience that bifurcation of the full system model, and finally that the parameters that cause and cure of the bifurcation are either in the bifurcation subsystem or its boundary [8]. Although the slaving method is not stated in a rigorous manner [27]:

1. there is an assumption that the external system is fast compared to the internal (bifurcation) subsystem (A_{11}) (the norm on A_{22} and the condition on it are not stated);

2. there is an assumption that the coupling between the internal and external system be weak (the norm on A_{12} and A_{21} is not stated nor is some inequality condition on these norms stated);

3. the requirement that the internal (bifurcation) subsystem A_{11} dominate the external system amounts to requiring that the reduced subsystem of a fast singularly perturbed model of the external system have an equilibrium point and bifurcation point that are close to that of the full system model even

though there is no formal theory to support and prove this.

The theory developed for bifurcation subsystem will necessarily make the above conditions for slaving rigorous. It will be shown that one does not need to require A_{12} or A_{21} to be small or null, but only column dependent in the center manifold direction that is approximated by the right eigenvector of the bifurcating eigenvalue. The theory in this thesis proves that the existence of a bifurcation subsystem using the bifurcation subsystem method requires the reduced models of both a fast singularly perturbed model of the external system and a slow singularly perturbed model of the external system have equilibria and bifurcation points close to those of the full system. Furthermore, conditions on 1) a norm on A_{22}, and 2) vector based norms on A_{21} and A_{12} are given and only one of these three conditions needs to be satisfied for the bifurcation subsystem to exist. Slaving requires much more stronger requirements on all three matrices as noted above. Each of the bifurcation subsystems produced by satisfaction of norms on A_{22}, A_{12}, and A_{21} would be of different order with very different structure.

Finally the slaving method [27] did not attempt to discuss whether the bifurcation, center manifold, trajectories near the center manifold, orbits, and other dynamic subsystem properties for the reduced model are preserved by slaving and are close to those of the full system. The theory presented in this thesis proves such results not only for the fast singularly perturbed model, but also for the slow singularly perturbed model of the external system so that these dynamic system properties (center manifold, trajectories near the center manifold, orbits etc) are preserved or persist when a bifurcation subsystem model is used to analyze the full system model near bifurcation. The bifurcation subsystem method result is thus a significant extension of slaving in terms of

1. what can be stated about the subsystem (experience, produce, and cause bi-

furcation rather than just dominate the external dynamics);

2. much weaker and more precise statements of the conditions on what is required for a bifurcation subsystem to exist compared to those required by slaving method;

3. proof that the probability of existence of bifurcation subsystem is high where no statement is possible for slaving;

4. a method for identification of bifurcation subsystems that can be applied to large systems where no such method exists for the slaving principle;

5. a proof that the bifurcation persists in the bifurcation subsystem model and that the bifurcation subsystem captures the center manifold, trajectories near the center manifold, and orbits of the full system near bifurcation.

This last result is so important because it allows one to focus on a reduced model for diagnosis of causes and cures of the bifurcation and control design because this reduced model captures the most important dynamic system properties of the full system model.

1.2.7 Comparison with Bifurcation Theory

Bifurcation theory has been well-developed [18] and it

1. can identify the center manifold dynamics that precisely describe the nature of the bifurcation. The bifurcation point, the trajectories at or near the center manifold, the size and the nature of orbits, the frequency of the oscillations, and the equilibrium point all can be described precisely;

2. can describe the sequence of the bifurcations and how and why one bifurcation develops from another;

3. has allowed nearly complete description of bifurcations and bifurcation sequences for multiple bifurcation parameters. Such complete studies have been limited to small systems (usually less than fifth order systems) due to the computational requirements and complexity as the order increases;

4. has had limited application to large systems of order of 500 or larger;

Bifurcation subsystem method is not as complete a description of a bifurcation as bifurcation theory could provide. Bifurcation subsystem method is hypothesized to have the following desired properties that will be proven in Chapter 2 and 3

1. experiences, produces, and causes the bifurcation of the full system model for both saddle-node and Hopf bifurcations;

2. identifies a small subsystem model within which the center manifold resides or can contain the center manifold, describes trajectories that are close to those of the full system at or near the center manifold, describes the size and the nature of the orbits and their frequency that is again close to that of the full system model, has equilibrium point and bifurcation parameters close to that of the full system model. We note that the center manifold dynamics play a very important part in the representation of the system dynamics, thus the bifurcation subsystem should contain the center manifold of the full system. The center manifold is a minimum order representation of the full system dynamics that experiences, produces, and causes that bifurcation. It retains the bifurcation orbits, frequencies, bifurcation point, and progression of bifurcation sequences that is essential to fully describing the bifurcation process;

3. does not require a nonlinear or a linear transformation of variables and therefore can be expressed in physically meaningful state variables, This lack of any requirement to perform a nonlinear or linear transformation perfectly pre-

serves the system state variables and parametric structure of the full system model. This may assist in finding the function of multiple parameters in the bifurcation subsystem model that is the bifurcation parameter in the center manifold dynamics. It may be possible to find more than one such function that produces a bifurcation parameter of the center manifold dynamics;

4. does not require significant computation to identify a bifurcation subsystem and thus can be applied to very large systems where computational requirements of obtaining a center manifold would make its application impractical;

5. can provide insight into the dynamics of the subsystem that experiences, produces, and causes the bifurcation that may not be captured by the right or left eigenvector evaluated at an equilibrium. The right eigenvector is a linear approximation of the center manifold at equilibrium, but can indicate that states outside the bifurcation subsystem are so excited by the bifurcation that their response can dominate that of the bifurcation subsystem that experiences, produces, and causes the bifurcation. The left eigenvector is orthogonal to the right eigenvector and is interpreted as indicating the controls that are most effective in controlling the response observed in the right eigenvector. If dominant response to a bifurcation is outside the bifurcation subsystem based on right eigenvector information and the identified bifurcation subsystem, then the selection of a subset of control actuators based on the left eigenvector information may better control the response to the bifurcation rather than control the bifurcation subsystem itself. This may make stabilization of the bifurcation subsystem difficult if not impossible. The right eigenvector is often used to select sensors to observe the response of the bifurcation and may not then effectively measure and thus observe the bifurcation subsystem response. Thus knowledge of bifurcation subsystem may provide improved method for selecting

the output signals to be measured and control input signals to be governed by control laws than those to be chosen by eigenvector methods on the full system model. When right eigenvector correctly predicts the bifurcation subsystem, then eigenvector and bifurcation subsystem method might select a similar or identical set of sensors and actuators for controlling a particular mode; Results in [8] show that the right eigenvector did not correctly predict the bifurcation subsystems on a single machine infinite bus (SMIB) model;

6. identifies the essence of center manifold structure and dynamic properties if that bifurcation subsystem model is sufficiently small. This is particularly true if the bifurcation model is approximately of the same order as the center manifold dynamics. Even if the bifurcation subsystem model order is somewhat larger than the center manifold dynamics, the determination of the bifurcation subsystem can still provide information for control design that is not easily obtained or may be impossible to obtain when the full system model is very large;

7. provides a taxonomic methodology for finding the classes and agents for each type of bifurcation in a power system model. This will be further discussed in next section;

8. bifurcation subsystem method could provide a simple lower order model and very important information for the design of hierarchical control systems to cure or stabilize the specific type and class of bifurcation for large complex nonlinear systems.

The bifurcation subsystem method will be argued to be a stronger yet more generic property than slaving. It requires conditions on decoupling that are much weaker than either slaving or α-decomposition based model reduction methods. The values of bifurcation subsystem method goes considerably beyond that of determining the

submodel that dominates or approximates the full system dynamics because it experiences, produces, and causes these dominant bifurcation dynamics and contains all the dynamic system properties of that bifurcation in the full system model. It is therefore much more useful in model stabilization, developing operating schedules, and deciding when control actions are taken to avoid instability than model reduction, slaving, or the full system model with all its complexity.

1.3 Classification of Types, Classes, and Agents for Bifurcation

It has been hypothesized in [26] that there can be a countable but very large number of bifurcation in a large power system model. There is no automated procedure for deciding what measurements and controls as well as what control laws are necessary for stabilizing an instability caused by one of these bifurcation. There is no automated procedure for adjusting model parameters via FACTS devices or operating conditions to cure a particular bifurcation. If an intelligent control is to be developed for a system with so many different bifurcation, one needs a classification procedure similar to the one developed over the centuries by the medical profession. One needs to know:

1. types of local bifurcation: saddle-node, Hopf, load flow bifurcation, and singularity induced bifurcation etc.

2. classes of each type of bifurcation: a subset of the variables of generator and load dynamics, controls, and network equations that experience and produce a specific type of bifurcation;

3. agents of a particular type and class of bifurcation: differ in terms of the specific

generator and load devices that lie in the bifurcation subsystem, but not the subset of variables in the models of these devices that belong to its bifurcation subsystem.

All classes of a particular type of bifurcation are anticipated to have many agents but not all agents within each class have a high risk of ever experiencing bifurcation. The subset of the variables of these different devices constitute the class of which an agent is a member when the generator and load devices that are associated with these variables in a bifurcation of that class specify the agent of that class. As an example, classes of saddle-node bifurcation are those that occur in solely induction motors dynamics, those that occur in generator dynamics, and possibly those that belong to both induction and generator dynamics. Agents of the induction motor class of saddle-node bifurcation occur on different induction motors or groups of induction motors in a particular plant or subregion. Bifurcation subsystem method should hopefully be the diagnostic tool required to identify specific classes of bifurcation and all agents in each class. All classes of a particular type of bifurcation are anticipated to have many agents but not all agents within each class have a high risk of ever experiencing bifurcation.

If the bifurcation occurs to the power system, usually two types of bifurcations, saddle-node and Hopf bifurcations, can be found. In the case of saddle-node bifurcation the system may experience slow monotonic instability, i.e., collapse type of instability. Saddle-node bifurcation has been observed in generator flux decay dynamics, in generator inertial dynamics, and induction motor inertial dynamics [9] [8]. The Hopf bifurcation, which usually represents the interarea oscillations of the power system, has been observed in the generator inertial dynamics, and in the generator flux decay excitation system dynamics [6]. Two different Hopf bifurcations exist: a supercritical Hopf bifurcation occurs when a stable limit cycle exists around an

unstable equilibrium point and where the orbits of the limit cycle grows as the bifurcation parameter(s) moves away from the bifurcation value; a subcritical Hopf bifurcation occurs when an unstable limit cycle exists around the stable equilibrium, where the orbit (a) is a region of stability boundary for excursions in the direction of that orbit, and (b) shrinks to zero as a bifurcation parameter approaches the bifurcating value. Classification of types, classes, and agents will be discussed in following chapters. It will be shown that classification of bifurcations is more than a taxonomy and it will provide the causes of each specific type and class of stability problems and thus prescribes the cure for the dynamic bifurcation as in [30] for the network model.

1.4 Robust Control Design

Basically robust control is a linear control technique, but may take on nonlinear properties if the nonlinear change in bifurcation parameter to the point of bifurcation is modeled as uncertainty in the linear form. The control objective is that robust stability and/or robust performance of the perturbed system can be achieved over the range of the parameter uncertainty. Robust control has been applied broadly and would seem to be very promising for power system control design.

Recently robust control techniques including H_∞-optimization and μ-synthesis have been applied to power system controller design. Most of robust control applications are dedicated to dampen local or interarea oscillation in a power system. A H_∞-based power system stabilizer [36] was designed for a single machine infinite bus system. The input uncertainty was modeled simply by a transfer function, which was claimed to be obtained by lumping various physical variations. The control objectives were nominal performance and robust stability measures. The simulation showed that nominal performance and robust stability were obtained for loading changes and

ground faults and the results were compared with the conventional power system stabilizer.

Based on H_∞ mixed-sensitivity technique a robust controller design for a SVC was presented [37]. The control design was formulated to increase the power system damping since the PI SVC control did not provide this contribution no matter how it was tuned. In this design PI controller was included in the nominal plant. A multiplicative form of uncertainty was modeled and corresponding weighting functions were selected. The design achieved robust stability and provided an increase in damping.

A robust thyristor controlled series compensator (TCSC) [38] was used to increased the damping of an interarea mode for the New York State power system. This large system was significantly simplified with coherency reduction. The model uncertainty was modeled in both an additive and a multiplicative form. Again, H_∞ mixed-sensitivity design was used.

A structural singular value (SSV) based method was proposed in [41] to perform the robust stability analysis rather than robust control design. This paper focused on the uncertainty representation. A novel method for modeling the network uncertainties was developed based on the fact that only some of the state matrix elements would change over the range of operating conditions. This conclusion facilitates the uncertainty modeling undertaken in this paper. By casting the problem into $M\Delta$ form, μ-synthesis was applied to evaluate the system performance.

In [46] several control design techniques for a power system stabilizer, including classical design, μ-synthesis, linear matrix inequality (LMI) approaches, were compared. The representation of the uncertainty, which was caused by the tie line reactance, was similar to that in [41]. The μ controller was obtained for a power system model which was simplified by Hankel norm approximation. The order of this controller was

further reduced using coprime factorization. It showed that the μ-synthesis based controller achieves the same damping enhancement with much smaller gain than the other two designs. However, the time simulation showed that the μ-synthesis controller does not obviously improve the control performance compared to the conventional power system stabilizer design.

H_∞-approach was systematically described in [25]. The dynamic positive feedback controller for SVC was synthesized with tie line current as an input signal. Robust H_∞ loop shaping technique was used to design the control to damp the interarea oscillation and be robust to coprime factor perturbations. This ensured the robustness to changes in the coprime factors of a shaped plant and increases the damping. The controller's overall performance was evaluated. The addition of damping control reduced the system load disturbance rejection performance.

One of the difficulties in power system control design is that of using high order model and computing a high order controller. SMIB model has been adopted in many control designs as noted in [36]. For a large power system, the SMIB model is not capable of representing the system dynamics appropriately. Although in [46] a lower order controller was proposed using coprime factors and LMI, it is still difficult to design, compute and implement the full order controller when power system model is very large.

The system uncertainty plays a very important role in achieving the desired design performance despite the fact that the modeling of the system uncertainties is difficult. Structural uncertainty has not been studied in above research [36] [37] [38] [41] [46] [25] even though some degree robustness of the controller has been obtained without using structured uncertainty models. Bifurcation subsystem will provide lower order models and the bifurcation parameter that produces the bifurcation within the bifurcation subsystem will be used to obtain a structured uncertainty model. The

structured uncertainty captures the nonlinear change in the linearized model that occurs as the bifurcation parameter changes and reaches the bifurcation value.

The design and implementation of the robust controller in our research will attempt to stabilize a single bifurcation and furthermore increase the feasibility region in the direction of a specific bifurcation parameter. Multiple bifurcations produced by more than one bifurcation parameters in the full system model will also be studied in an effort to increase the range of the bifurcation parameter (feasibility region) where the system remains stable. The robust control design will be based on the bifurcation subsystem as well as the full system model since the center manifold dynamics of the full system lie in or are totally contained in the bifurcation subsystem. The bifurcation subsystem indicates the states and the model experiences, produdes, and causes the bifurcation in full system model. These states are required to be controlled in order to stabilize the system and cure the bifurcation. It is also hypothesized and proven that when bifurcation occurs the *RGA* matrix of the closed-loop system with robust control becomes block diagonal. The off-diagonal blocks approach zero, and the upper diagonal block approaches the *RGA* matrix of the internal system or bifurcation subsystem with the external system truncated. The lower diagonal block approaches the *RGA* matrix of the external system with the internal system truncated. The proof is given in Appendix B. The control of the bifurcation subsystem is completely independent of the external system based on this *RGA* structure.

A power system is typically a MIMO system and power system control is a multivariable control problem. The *RGA* matrix is a simple but a powerful tool for multivariable system control design. The *RGA* matrix has not been studied or exploited in any of the references [36] [37] [38] [41] [46] [25]. It is impossible to achieve the desired control performance without thoroughly considering the control structure design, the effectiveness and disturbance rejection properties of MIMO system control as well as the uncertainty representation for MIMO system as observed by

its impact on the RGA matrix.

In this thesis, μ-synthesis will be used to design the power system stabilizer. We are trying to achieve better control performance with the help of bifurcation subsystem method from the very beginning of controller synthesis to achieve significant control structure improvement, lower order controller simplification, and improved control performance test. The following topics of power system stabilizer design for a single bifurcation or multiple bifurcations are studied: (1) determination of which generator the power system stabilizer is the most effective; (2) how to define the performance index for the best performance to be achieved; (3) how to simplify the high order controller and yet achieve excellent performance; (4) whether the controller designed for one bifurcation is effective for different bifurcations produced by different parameter variations as well as for what types and classes of bifurcation will a specific controller be applicable; (5) how to evaluate the control performance and whether the control performance is improved (degenerated) based on these measures; and (6) whether the overall performance of robust power system stabilizer is acceptable.

FACTS control has achieved significant applications in enhancing power system performance via high speed and continuous response. Static var compensator (SVC), as one of the FACTS control devices, can be used to provide the voltage support on long transmission lines by injecting or absorbing reactive power. In fact, SVC can also increase the power system damping with supplemental signal. Robust SVC controller will be designed in order to damp the interarea oscillations of power systems over a given operating range as well as providing the effective voltage control over the network. The nonlinear effects of the robust control over the power system will also be studied in this thesis.

1.5 Contributions of This Thesis

A bifurcation subsystem experiences, produces, and causes the full system bifurcation when satisfying the same conditions for bifurcation as satisfied by the full system dynamics. In comparison with center manifold dynamics, a bifurcation subsystem is a subsystem of the state space model with physically meaningful variables, and is not a reduced model that can be necessarily be simulated or analyzed apart from the singularly perturbed full system model.

The bifurcation subsystem method proposed in [8] had not been proven but came out of the hypothesis that bifurcation subsystems are a generic phenomena that can be applied to almost every bifurcation in a large power system model. This hypothesis will be proven in the thesis.

The original work on the bifurcation subsystem in [3] was heuristic in a manner similar to slaving but did extend the concept by establishing a precise definition and the two existence conditions (bifurcation subsystem condition and geometric decoupling condition) where the slaving principle only required one condition that the external system be represented by the reduced algebraic model that could be viewed as coming from a fast singularly perturbed model of the external system.

In this proposal, the bifurcation subsystem method and its applications, and the identification of bifurcation subsystems are described systematically.

1. we define the bifurcation subsystem based on preserving the equilibria, bifurcation points and bifurcating eigenvalues when the reduced system of a fast singularly perturbed external system model and a slow singularly perturbed external system model are both arbitrarily close to those of the full system for both saddle-node and Hopf bifurcations [3];

2. we derive sufficient conditions for a bifurcation subsystem to exist for both

saddle-node and Hopf bifurcations. These conditions are referred to as the bifurcation subsystem condition and the geometric decoupling condition [3];

3. we show that the properties of trajectories, the size and the nature of the orbits, the equilibria, the bifurcation point, the bifurcating eigenvalue, and the center manifold dynamics of the reduced system persist for the full system with both fast and slow singularly perturbed external dynamics provided that singular perturbation is small enough. We will also show that the center manifold of the bifurcation is in the bifurcation subsystem and is contained within the bifurcation subsystem if additional conditions are satisfied. To identify the bifurcation subsystem it is necessary to study the persistence of full system bifurcation when bifurcation occurs in the subsystem. The effects of slow or fast external dynamics on the full system should be considered.

   The work by Chiang in [2] summarized the theoretical results about the persistence saddle-node bifurcation with singularly perturbed slow or/and fast unmodeled external dynamics. As long as the perturbation is small enough in the presence of either the fast or the slow external system dynamics, the persistence of the saddle-node bifurcation of subsystem can be guaranteed, and the center manifold dynamics of the full system will be preserved in the internal subsystem. Based on the theoretical results for the persistence of saddle-node bifurcation under singularly perturbed slow or fast external unmodeled dynamics in [2], the persistence of the bifurcation in the bifurcation subsystem and the preservation of center manifold dynamics within the bifurcation subsystem are proven in Chapter 2.

   In [4], the persistence of Hopf bifurcation is discussed in detail in the presence of fast external dynamics. The equilibrium point, the orbits, the period of the periodic solutions of the full system and the reduced system are discussed.

Although the center manifold dynamics of the full system and the subsystem is not mentioned in [4], the method in [5] is applied to discuss this in this proposal;

4. we prove that solutions can be found to these sufficient conditions for the existence of a bifurcation subsystem exist and these solutions have a high probability of occurrence. This is important because there otherwise is no assurance that one could ever find a solution to the sufficient conditions and what the probability of finding the solutions might be;

   The fact that α-decomposition is applicable for power system dynamics model of the generator inertial dynamics indicates that power system model can be clustered as slow and fast subsystem which are weakly coupled, not just in the direction of the center manifold. This shows that the power system internal dynamics have a natural structure that lends itself to bifurcation subsystem method. The fact that all that is needed for a bifurcation subsystem to exist is that the bifurcation subsystem and internal system model be decoupled in the center manifold direction is a much weaker condition than α-decomposition and will be proven to make the finding of bifurcation subsystem a high probability event even when the dynamics do not satisfy α-decomposition conditions for decoupling.

   The effectiveness of α-decompostion is that these methods reveal that power system state Jacobian for the classical power system dynamic models [22] can be represented by a block diagonal matrix, i.e., the coupling between the internal system and the external system can be considered null. Although this conclusion is only an approximation of the real system model, we require a similar but much weaker condition between the internal and external subsystems to be able to identify a bifurcation subsystem model. The weaker condition

requires only that the internal and external system be coupled weakly enough in the center manifold direction rather than completely decoupled as required for α-decomposition method. When the bifurcation occurs, for system that satisfies the α-decompostion condition, geometric decoupling is automatically satisfied. Thus the bifurcation subsystem and geometric decoupling conditions are both satisfied automatically for both an algebraic model of the power system and/or a classical dynamics model external to the bifurcation system and bifurcation subsystem itself [7].

Since the power system dynamics can be clustered as slow dynamics and fast dynamics with weak coupling between them [22], the bifurcation subsystem identification method can be studied with the singular perturbation technique. The power system dynamics takes the form of regular dynamics with unmodeled slow or fast external dynamics. These facts support that finding of the bifurcation subsystem with small order is highly probable;

5. it has been clear from 3 and 4 that a very small order bifurcation subsystem could be obtained and would be a good approximation of the center manifold dynamics of the full system model. This bifurcation subsystem would be determined without requiring the nonlinear transformation needed to obtain a center manifold for a particular saddle-node or Hopf bifurcation;

6. a bifurcation subsystem of small or moderate order contains the center manifold dynamics and preserves all the dynamic properties even if it does not have smaller order and the exact form of the center manifold dynamics that experiences, produces, and causes the bifurcation in the full system model. This model would facilitate and possibly improve the design of prescriptive corrective operating schedules and stabilizing control for the bifurcation;

7. a bifurcation subsystem identification algorithm, which is capable of finding the

very small order bifurcation subsystem, is developed and theoretically justified for both saddle-node and Hopf bifurcation subsystems;

8. the bifurcation subsystem method is extended to a relatively large two-area multiple generator system modeled by the differential algebraic equation rather than SMIB system [3]. A set of numerical examples are presented and discussed. The different bifurcation subsystems are obtained (both saddle-node and Hopf bifurcation) by applying the bifurcation subsystem identification algorithm on a two-area example system with different bifurcation parameters;

9. a diagnosis procedure based on bifurcation subsystem method [7] has been developed to find cures for a blackout that may not be found after an average of after 15 hours of computing and engineering effort to perform the diagnosis.

10. The various types and classes of bifurcation are investigated as a function of the network, load or transfer level, and the load models. By applying bifurcation subsystem method, the following problems are addressed: (a) what is the relation between network and dynamic bifurcation? (b) how and why interarea and local modes are produced? (c) what are the classes and types of bifurcation for different load models? and (d) how to find the bifurcation subsystem and the system behaviors when singularity induced bifurcation occurs? It is shown that the bifurcation subsystem method can identify the different classes of bifurcation (those with different variables in the bifurcation subsystem) as well as the agents for each bifurcation class (those with the same bifurcation subsystem but involving the same subset of variables in different generator, load, devices, and different network buses). The classification of bifurcation is more than a taxonomy and it will provide the causes of each specific type and class of stability problem and thus prescribe the cure for the bifurcation as in [30] for the network model.

The bifurcation subsystem was stated and justified based on conditions on both a fast and slow singularly perturbed model of the external system in [3]. The bifurcation subsystem concept was applied to an algebraic power system in [6] and has provided a theoretical underpinning to a procedure for (a) identification of all the bifurcation subsystem (agents) in that model; (b) identification of what causes and cures instability in each agent; (c) contingency selection and ranking on each agent; (d) identification of vulnerable agents; (e) the condition which must occur for cascading instability of agents to develop and produce the voltage collapse that produces the blackout.

The success in algebraic model [3] will hopefully be extended to the differential algebraic model at some future date. The bifurcation subsystem algebraic (loadflow) model permits making stronger linkages to previously discussed model reduction methods in the differential model and in an algebraic model of a power system.

It should be noted that the results stated may be incorrectly taken as a justification of model reduction of huge power system models since the development of bifurcation are dependent on the affects of the global response of the model and many discrete control actions and their sequence throughout the portion of the model being reduced would almost certainly change the equilibrium and destroy the validity of the model at the equilibrium. The full system model needs to be retained so that the foundation for focusing on a bifurcation subsystem have validity at bifurcation of the full system model.

It is common to view the finding of the center manifold dynamics as an effort to identify the representation of the full system dynamics. Bifurcation subsystem method can be considered as a trade-off between the investigations of the center manifold dynamics and full system dynamics since it is less precise in analyzing, observing the bifurcation and the trajectories near the bifurcation point than the center manifold

dynamics. A bifurcation subsystem does not have same order as center manifold, it just contains the center manifold dynamics with physically meaningful system states. It experiences the bifurcation as does the center manifold dynamics. Despite that we do not see the center manifold dynamics directly in the bifurcation subsystem, we do have everything necessary to investigate how to produce, cause and cure the bifurcation of the full system that lies in the bifurcation subsystem. The dimension of the bifurcation subsystem depends on the complexity of the full system dynamics.

The identification of the bifurcation parameters is usually difficult to find but is required to study the particular bifurcation. The bifurcation parameters are included in the bifurcation subsystem and it will be relatively easy the find them. The determination of the bifurcation parameters and the bifurcation subsystem will provide necessary information for the analysis and control design, which is not easily obtained or even impossible to determine with other methods when the full system is very large.

The second part of this thesis presents the μ-synthesis robust control for the power system based on the bifurcation subsystem information

1. by modeling the uncertainty of the power system with the second order matrix polynomial for a specific bifurcation parameter or multiple bifurcation parameters acting as the uncertainty parameter. Since the structural information of the system is utilized in the modeling, this uncertainty model will lead to almost no conservativeness of the control design;

2. by providing a systematic robust design methodology for power systems. This includes the use of RGA matrix to observe the subsystems, decoupling of subsystem, effectiveness of control disturbance rejection, and the lack of competition for control of each subsystem; the use of structured uncertainty to increase the feasibility region in the bifurcation subsystem direction; the use

of the structured and dynamical system uncertainty to provide a subsystem structure in the external system as well as an effective disturbance rejection, and noncompetitive control within each subsystem including the bifurcation subsystem;

3. by posing the standard μ-synthesis robust power system stabilizer and/or SVC control design problem for the two area example power system. The performance index and the weighting transfer function that are expected to improve the control performance of the system are defined based on the bifurcation subsystem information;

4. by designing a μ-synthesis robust power system stabilizer (MPSS). The order of the resulting MPSS is reduced based on the bifurcation subsystem information and is applied to the full system. The control performance of the MPSS and MPSS with inverse dynamics is compared to the performance of the open loop system with conventional power system stabilizer (CPSS);

5. by designing several μ-synthesis robust SVC controls (MSVC). The control performance of MSVC is compared to that of both open loop system with conventional SVC (CSVC) and the closed-loop system with MPSS. This tells us whether MSVC or MPSS is more effective in terms of control performance. The following topics of MSVC control design are also studied (1) MSVC control effects for voltage coherent buses within groups in the system external to the bifurcation subsystem; (2) BMSVC design using only the bifurcation subsystem model rather than the full system model; (3) MSVC design for input uncertainty and measurement noise; (4) MSVC design for saddle-node bifurcation; and (5) MSVC for input uncertainty and measurement noise;

6. by designing different kinds of μ-synthesis robust control, including multiple-output multiple-input robust power system stabilizer and SVC control, for

multiple bifurcations. This is a very important step for robust control application since there usually exist more than one bifurcation to be stabilized in large power systems;

7. by analyzing the RGA matrix information of the closed-loop system. The RGA matrix of the above μ-synthesis robust designs will be compared with RGA matrix computed for an existing conventional controller. This will reveal whether and why the robust control designs improves the control performance;

8. by studying the second order interaction with and without robust control for a two-area power system. This study shows that the robust control has tremendous effect over the power system up to second order.

1.6 Organization

After the bifurcation theory and bifurcation subsystem method is briefly introduced in Chapter 1, the saddle-node and Hopf bifurcation subsystem for both fast and slow unmodeled external dynamics are discussed in Chapter 2 and 3, respectively. The saddle-node and Hopf bifurcation subsystem are defined using singular perturbation technique. With the help of Fenichel's theory, which is summarized in Appendix A. The persistence of the equilibrium, the bifurcation point, the orbits at or near the equilibrium point, the trajectories, and bifurcation parameters are proven in Chapter 3. The bifurcation subsystem condition and the geometric decoupling condition, which are the sufficient conditions for existence of both both saddle-node and Hopf bifurcation subsystems are derived from the conditions for an existence of bifurcation in the reduced models of the singularly perturbed fast external model and the singularly perturbed slow external model.

The detailed demonstration of the bifurcation subsystem method is shown in Chapter

4. The bifurcation subsystem identification algorithm is presented and proven to obtain the relatively small dimensional bifurcation subsystem. A series of theorems are presented and proven, which extend and prove the near generality for satisfaction of both bifurcation subsystem condition and geometric decoupling condition. These results justify the bifurcation subsystem method as being applicable for most if not all saddle-node and Hopf bifurcations in a differential model.

A set of examples for a two-area power system in Chapter 5 verify numerically the bifurcation subsystem method. Different bifurcation subsystem with small order are obtained and discussed for different bifurcation parameters. The classification of bifurcations are also discussed in detail in this chapter. In Chapter 6 the future research in robust control design based on the bifurcation subsystem is presented.

In Chapter 6, μ-synthesis based robust control is systematically studied. After a brief description of robust control theory, a μ-synthesis based power system stabilizer (MPSS) is designed using bifurcation subsystem information. The control performance is compared with the conventional power system stabilizer (CPSS) by studying both RGA matrix and the time simulation. The MPSS is shown to be much more effective than the conventional power system stabilizer.

FACTS controls have been broadly used and proven to be very effective in enhancing the power system stability. μ-synthesis robust SVC control is studied in Chapter 6. By again using the bifurcation subsystem information, a robust SVC control (MSVC) is obtained. The time simulation and RGA matrix information both show that MSVC provides better control performance that both MPSS and CPSS. Also in this section, MSVC with input uncertainty and measurement noise and MSVC that is designed based on bifurcation subsystem (BMSVC) are studied.

Multiple bifurcation phenomena is observed in this two area power system. To stabilize the system when multiple bifurcations develop, several different kind of μ-

synthesis robust control, including both power system stabilizer and SVC control, are designed and compared. The conclusion is drawn for multiple bifurcation stabilization. This will provide important robust control design information for large power systems since multiple bifurcation are frequently encountered in large systems.

The nonlinear effects of conventional and robust power system control are studied in Section 6.7. The computation of the second order interactions shows that robust control not only greatly improves the control performance and robustness, but also dominates the nonlinear response of the system.

Chapter 2

Bifurcation Subsystem for Saddle-node Bifurcation

2.1 Objective

The singular perturbation theory underlying the definition of a bifurcation subsystem and the sufficient conditions for the existence of a bifurcation subsystem has been developed in [2] and [3] and are reviewed in this chapter. The theory in [2] underlying definition of the bifurcation subsystem, is more precisely discussed in this chapter than in [3] and needed to justify the modified definition of a bifurcation subsystem. This chapter is arranged to demonstrate the theoretical results related to saddle-node bifurcation. Some preliminaries are introduced in section 2.2. In section 2.3 the conclusions on the persistence of saddle-node bifurcation under singularly perturbed slow and fast unmodeled dynamics are reviewed. The saddle-node bifurcation subsystem is defined and discussed in section 2.4.

2.2 Preliminaries

Generally a set of ordinary differential equations can be used to represent the engineering system which involving dynamics:

$$\dot{x} = f(x) \tag{2.2.1}$$

where $x \in R^n$, and $f_i, i = 1, 2, ..., n$ is a nonlinear function of all the states $x_i, i = 1, 2, ..., n$.

The equilibrium points represent the true characteristic of the behavior of the dynamic system and are defined as the points on the trajectory with zero velocity. The equilibrium points are those points where the derivatives $\dot{x}$ are simultaneously zero, i.e.,

$$0 = f(x)$$

Unlike the linear system, the nonlinear system may have more than one equilibrium point. The region of a stable equilibrium may be limited, therefore the existence of a stable equilibrium does not assure the stability in a neighborhood of the equilibrium point.

Usually, the stability of a nonlinear system equilibrium is studied via linearized system in a neighborhood of an equilibrium point x^0. Define:

$$\Delta x = x - x^0$$

Ignoring the high-order terms of the Taylor series expansion around x^0 gives:

$$\Delta \dot{x} = D_x f|_{x^0} \Delta x$$

$D_x f|_{x^0}$ is the Jacobian of vector field f. The local stability of the nonlinear system

can be judged by the eigenvalues of the state Jacobian. The different eigenvalue combinations generate the corresponding trajectory behaviors, such as focus, node, center, and saddle, around the equilibrium points. When there exists a zero eigenvalue or eigenvalues with zero real parts, the linearization fails and we cannot say anything about the stability. In this case, the center manifold can be computed to study the behaviors of the trajectories at or near bifurcation.

The bifurcation phenomena in the nonlinear system refers to characterizing the qualitative change of the fixed points of the system for a smooth continuous change in a parameter, say μ, over a specified range. For one-dimensional vector fields

$$\dot{x} = f(x, \mu) \tag{2.2.2}$$

a fixed point (x, μ) is said to undergo a bifurcation at $\mu = 0$ if the flow for μ near zero and x near zero is not qualitatively the same as the flow near $x = 0$ at $\mu = 0$.

As μ varies, the Implicit Function Theorem implies that fixed points are described by the smooth functions of μ away from those points at which the Jacobian $D_x f(\mu)$ with respect to x, has a simple zero eigenvalue. This is called saddle-node bifurcation. If the Jacobian $D_x f(\mu)$ has a pair of complex conjugate eigenvalues on the imaginary axis, it's called Hopf bifurcation. The precise conditions for defining when saddle-node and Hopf bifurcation occurs is given in [18]. A value μ_0 of equation (2.2.3) for which the flow of (2.2.3) is not structurally stable is a bifurcation value of μ [21].

In most of the cases, the system dynamics are modeled by ignoring the small time constants, such as small time constant, capacitance, or parasitic parameters, or considering the system with a large time constant as a time invariant system. The analysis based on the "oversimplified" models could be too far from reality. These unmodeled dynamics with small and large time constants, which are called fast dynamics and slow dynamics, respectively, may have significant influence on the

dynamic behaviors of the full system [11].

The dynamic system with slow or fast dynamics can be represented in the form of (2.2.3) and (2.2.4), respectively.

$$\begin{aligned} \dot{x} &= f(x, y, \mu, \epsilon) \\ \dot{y} &= \epsilon g(x, y, \mu, \epsilon) \end{aligned} \tag{2.2.3}$$

$$\begin{aligned} \dot{x} &= f(x, y, \mu, \epsilon) \\ \epsilon\dot{y} &= g(x, y, \mu, \epsilon) \end{aligned} \tag{2.2.4}$$

where ϵ is small real positive number that is called perturbation, and $\mu \in R$ is a parameter subject to variation.

Singular perturbation technique can be applied to this set of problems by separating time scales, and studying the reduced system ($\epsilon = 0$) and the boundary-layer problem (ϵ is sufficiently small), respectively.

In the case of a system with fast external dynamics the fast reduced system is obtained by setting $\epsilon = 0$:

$$\begin{aligned} \dot{x} &= f(x, y, \mu, 0) \\ 0 &= g(x, y, \mu, 0) \end{aligned} \tag{2.2.5}$$

This reduced system represents the fast time phenomena, which is dominant in a lot of applications. By rescaling $\tau = t/\epsilon$ the boundary-layer problem is defined from

(2.2.4) as:

$$\begin{aligned} x' &= \epsilon f(x, y, \mu, \epsilon) \\ y' &= g(x, y, \mu, \epsilon) \end{aligned} \tag{2.2.6}$$

For the system with slow external dynamics setting $\epsilon = 0$ gives the reduced system:

$$\begin{aligned} \dot{x} &= f(x, y, \mu, 0) \\ \dot{y} &= 0 \end{aligned} \tag{2.2.7}$$

Usually we are interested in the behaviors in some neighborhood of the equilibrium point for sufficiently small perturbation.

2.3 Persistence of Saddle-node Bifurcation with Singularly Perturbed Slow and Fast External Dynamics

In this section, the persistence of saddle-node bifurcation under singular perturbation with presence of slow and fast external dynamics is studied. The relation of the reduced and the full system dynamics when a saddle-node bifurcation occurs is discussed in detail. The theory summarized in section 2.3.1 and 2.3.2 for slow and fast singularly perturbed models, respectively, is taken from [2]. We use the notations $\hat{x}$, $\tilde{x}$, and $\bar{x}$ to represent the dynamic properties of the full system, the reduced system with fast external dynamics, and the reduced system with slow external dynamics, respectively, where x can be equilibrium points, bifurcation points, trajectories or orbits etc.

2.3.1 Singular Perturbation with Slow External Dynamics

Consider the nonlinear system with slow external dynamics in the form of of equation (2.2.3), and the corresponding reduced system given in (2.2.7).

(H1) All the eigenvalues of $D_y g$ at equilibrium point $\bar{m}^* = (\bar{x}^*, y_0)$ for $\mu = \bar{\mu}^*$ are in the left-half plane

(H2) The slow reduced system (2.2.7) undergoes saddle-node bifurcation at $\bar{m}^* = (\bar{x}^*, y_0)$ for $\mu = \bar{\mu}^*$

Let $\bar{m}^* = (\bar{x}^*, y_0)$ be equilibrium point of the reduced system for $\mu = \bar{\mu}^*$, then under assumption (H1) and (H2) there exist an $\epsilon_0 > 0$ such that the following results hold for the full system (2.2.3) with $0 < \epsilon < \epsilon_0$[2]:

1. The full system undergoes the saddle-node bifurcation at equilibrium point $\hat{m}^* = (\hat{x}^*, \hat{y}^*)$ of the full system with $\| \hat{m}^* - \bar{m}^* \| = O(\epsilon)$ and $\| \hat{\mu}^* - \bar{\mu}^* \| = O(\epsilon)$.

Denote a neighborhood of $\bar{m}^*$ by $N = N_{(x,y)} \times N_\mu$. Let $\bar{\gamma} = (\bar{x}(t, \mu_0), y_0)$ be the solution of the reduced system near $W^c_+(\bar{x}^*, y_0)$ with $\mu = \bar{\mu}^*$ and initial condition x_0, y_0 in $N_{x,y}$, and $\hat{\gamma} = (\hat{x}(t, \epsilon), \hat{y}(t, \epsilon))$ be the solution of the full system near $W^{c,\epsilon}(\hat{x}^*, \hat{y}^*)$ with $\mu = \hat{\mu}^*$ and initial condition $(x_0 + O(\epsilon), y_0 + O(\epsilon))$ in $N_{x,y}$, then

2 There is $T > 0$ and $\epsilon_0 > 0$ such that $\| \hat{\gamma} - \bar{\gamma} \| = O(\epsilon)$ for at least $t \in (0, T]$ and $0 \leq \epsilon \leq \epsilon_0$.

3 $\| W^{c,\epsilon}_+(\hat{x}^*, \hat{y}^*) \cap N - W^c_+(\bar{x}^*, y_0) \| = O(\epsilon)$ for $0 \leq \epsilon \leq \epsilon_0$.

This states the persistence of the saddle-node bifurcation in the reduced system when a saddle-node bifurcation occurs to the full system. Also, the dynamic properties, including the equilibrium point and center manifold dynamics of the full system after the bifurcation are preserved in the reduced system to the order of $O(\epsilon)$.

2.3.2 Singular Perturbation with Fast External Dynamics

(H3) All the eigenvalues of $D_y g$ at equilibrium point $(\tilde{x}^*, \tilde{y}^*)$ for $\mu = \tilde{\mu}^*$ are in the left-half plane

(H4) The fast reduced system (2.2.5) undergoes saddle-node bifurcation at equilibrium point $(\tilde{x}^*, \tilde{y}^*)$ for $\mu = \tilde{\mu}^*$

The full system with fast external dynamics is in the form of equation (2.2.4), and the fast reduced system is given as (2.2.5), where $f, g \in C^r, r \geq 2$. The suspended system is given by:

$$\begin{aligned} \dot{x} &= \epsilon f(x, y, \mu, \epsilon) \\ 0 &= g(x, y, \mu, \epsilon) \\ \dot{\mu} &= 0 \\ \dot{\epsilon} &= 0 \end{aligned}$$

Under assumption (H3) and (H4) there exists a center manifold $C \subset R^{n+2}$. For the suspended system, the Implicit Function Theorem suggests that there is an unique solution $y = u(x, \mu, 0)$ satisfying $0 = g(x, y, \mu, 0)$ at equilibrium point $\tilde{m}^* = (\tilde{x}^*, \tilde{y}^*)$ for $\mu = \tilde{\mu}^*$. Thus, there is a local representation of the reduced system:

$$\dot{x} = f(x, u(x, \mu, 0), \mu, 0) \tag{2.3.8}$$

It is reasonable to define that the reduced system is undergoing saddle-node bifurcation if the local representation of the reduced system has the same behavior.

Let $\tilde{m}^* = (\tilde{x}^*, \tilde{y}^*)$ be an equilibrium point of the reduced system for $\mu = \tilde{\mu}^*$, then under assumption (H3) and (H4) there exist an $\epsilon_0 > 0$ such that:

1. The full system undergoes the saddle-node bifurcation at equilibrium point

$$\hat{m}^* = (\hat{x}^*, \hat{y}^*) \text{ for } \mu = \hat{\mu}^* \text{ with } \| \hat{m}^* - \tilde{m}^* \| = O(\epsilon) \text{ and } \| \hat{\mu}^* - \tilde{\mu}^* \| = O(\epsilon)$$

Let $N = N_{(x,y)} \times N_\mu$ be a neighborhood of $\tilde{m}^*$. Let $\tilde{\gamma} = (\tilde{x}(t, \mu_0), \tilde{y}(t, \mu_0))$ be the solution of the reduced system near $W^c_+(\tilde{x}^*, \tilde{y}^*)$ with $\mu = \tilde{\mu}^*$ and initial condition $x_0, y_0 = u(x_0, \tilde{\mu}^*)$ in N and $\hat{\gamma} = (\hat{x}(t, \epsilon), \hat{y}(t, \epsilon))$ be the solution of the full system near $W^{c,\epsilon}(\hat{x}^*, \hat{y}^*)$ with $\mu = \hat{\mu}^*$ with initial condition $(x_0 + O(\epsilon), y_0 + O(\epsilon))$ in N. If y_0 lies in the stability region of $u(x, \tilde{\mu}^*)$ of the fast system,

2 There is $T > 0$ and $\epsilon_0 > 0$ such that

$$\| \hat{x}(t, \epsilon) - \tilde{x}(t) \| < C\epsilon$$
$$\| \hat{y}(t, \epsilon) - u(\tilde{x}(t), \mu, 0) \| < C\epsilon$$

for $t \in [0, T]$, and $\epsilon \in (0, \epsilon_0)$;

3 $\| W^{c,\epsilon}_+(\hat{x}^*, \hat{y}^*) \cap N - W^c_+(\tilde{x}^*, \tilde{y}^*) \| = O(\epsilon)$ for $\epsilon \in (0, \epsilon_0)$.

The conclusions in section 2.3 reveal that the bifurcation point and the equilibrium point of the reduced system are close to that of the full system of order ϵ. The more important fact is that the dynamic behaviors of the reduced system will persist around the equilibrium point at the bifurcation point. When saddle-node bifurcation occurs the trajectories and the center manifold dynamics of the reduced system will be close to that of the full system provided that the perturbation is small.

2.4 Saddle-node Bifurcation Subsystem

Consider a parameter-dependent $(n + m)$-dimensional nonlinear system:

$$\dot{x} = f(x, y, \mu) \tag{2.4.9}$$
$$\dot{y} = g(x, y, \mu) \tag{2.4.10}$$

The linearized model at an equilibrium point $m_0(\mu) = (x_0(\mu), y_0(\mu))$ is:

$$\begin{bmatrix} \Delta\dot{x} \\ \Delta\dot{y} \end{bmatrix} = \begin{bmatrix} D_x f & D_y f \\ D_x g & D_y g \end{bmatrix} \begin{bmatrix} \Delta x \\ \Delta y \end{bmatrix} \tag{2.4.11}$$

Define:

$$A = \begin{bmatrix} A_{11} & A_{12} \\ A_{21} & A_{22} \end{bmatrix} = \begin{bmatrix} D_x f & D_y f \\ D_x g & D_y g \end{bmatrix}$$

The saddle-node or Hopf bifurcation can occur if an equilibrium point becomes non-hyperbolic, that is there is a zero eigenvalue or a pair of eigenvalues which have zero real part, and the appropriate nondegeneracy and trasversality conditions hold [21]. If system (2.4.9) and (2.4.10) contain subsystems that are decoupled from one another, that is the state Jacobian $A = diag(A_{11}, A_{22})$, then the bifurcation in any subsystem results in bifurcation being experienced in the full system.

In most of cases the state Jacobian is coupled. Testing for the occurrence of saddle-node bifurcation requires testing for singularity of state Jacobian. From Schur's theorem, testing singularity of A is equivalent to testing the reduced order matrix A_{SN}:

$$A_{SN} = A_{11}(\mu) - A_{12}(\mu)A_{22}^{-1}(\mu)A_{21}(\mu) \tag{2.4.12}$$

and the nonsingular $A_{22}(\mu)$. This condition on nonsingularity of A_{22} is required for persistence of bifurcation in fast and slow singularly perturbed models. The test condition (2.4.12) is used in the slaving method when appropriate additional assumptions on decoupling and external system speed of response on matrices A_{12}, A_{22}, and A_{21} are made as noted in Chapter 1. This implies that as long as these conditions are satisfied an arbitrary subset of states x, an arbitrary subset A_{11} of the

system matrix in (2.4.11) and the reduced-order linearized subsystem

$$\Delta\dot{x} = [A_{11} - A_{12}A_{22}^{-1}A_{21}](\mu)\Delta x$$

will capture the existence of a bifurcating eigenvalue in the full system model. There could be a very large number of such subsystems with different subsets of variables in x and y, and each of them indicates the occurrence of the saddle-node bifurcation but likely providing misleading information on causes and cures in the full system. The selection of the bifurcation subsystem, which experiences and produces the bifurcation in the full system and clearly indicates the causes and cures for the bifurcation, requires selecting the correct number of variables, the correct subset of variables of that dimension, and the correct subset of the equations of that dimension that satisfy the definition and conditions defined as below.

The linearized model of the first equation in (2.2.7) of the reduced system with slow external dynamics is given by

$$\Delta\dot{x} = A_{11}\Delta x \tag{2.4.13}$$

with $y = y_0$. Since y is constant at the bifurcation point $(\bar{x}^*(\bar{\mu}^*), y_0)$ the dynamics is restricted to the invariant manifold associated with the bifurcation subsystem dynamics of the bifurcating eigenvalue. The slow unmodeled dynamics external to the bifurcation subsystem is used to represent the fact that the bifurcation subsystem (the first equation in (2.2.4)) must experience and produce the bifurcation of the full system for a bifurcation subsystem to exist.

The linearized model of reduced system with fast external dynamics is:

$$\Delta\dot{x} = A_{11}\Delta x + A_{12}\Delta y \tag{2.4.14}$$

$$0 = A_{12}\Delta x + A_{22}\Delta y \tag{2.4.15}$$

This linearized model represents that when the full system is approaching the bifurcation at bifurcation point $(\hat{x}(\hat{\mu}^*), \hat{y}(\hat{\mu}^*))$ the external subsystem appears arbitrarily fast compared to the center manifold response that occurs at the bifurcation point. This model provides the bifurcation conditions for the full system to define and determine a bifurcation subsystem. Note that if A_{22} is nonsingular this linearized model of the reduced model with fast external dynamics can be tested by finding a zero eigenvalue or complex eigenvalues with zero real part of (2.4.12). This is the slaving condition discussed earlier.

The apparent contradiction that the external system can be represented by unmodeled slow and fast dynamics is required to define a bifurcation subsystem and derive the two conditions for existence of a bifurcation subsystem, i.e., a condition for bifurcation in the subsystem as well the condition for bifurcation in the full system when the response is restricted to the invariant manifold of the bifurcation subsystem's bifurcating eigenvalue.

The theoretical results of the singular perturbed saddle-node bifurcation with slow and fast external dynamics state that the bifurcation point $(\hat{x}(\hat{\mu}^*), \hat{y}(\hat{\mu}^*))$, the trajectory $\hat{\gamma}$, the center manifold $W^c_+(\hat{x}^*(\hat{\mu}^*), \hat{y}^*(\hat{\mu}^*))$ of the full system are ϵ_1-close to bifurcation point $(\tilde{x}^*(\tilde{\mu}^*), \tilde{y}^*(\tilde{\mu}^*))$, the trajectory $\tilde{\gamma}$, the center manifold $W^{c,\epsilon_1}_+(\tilde{x}^*(\tilde{\mu}^*), \tilde{y}^*(\tilde{\mu}^*))$ of reduced system (2.2.5), and ϵ_2-close to bifurcation point $(\bar{x}^*(\bar{\mu}^*), \bar{y}^*(\bar{\mu}^*))$, the trajectory $\bar{\gamma}$, the center manifold $W^{c,\epsilon_2}_+(\bar{x}^*(\bar{\mu}^*), \bar{y}^*(\bar{\mu}^*))$ of reduced system (2.2.7).

The bifurcation subsystem for a saddle-node bifurcation is ready to be defined [3]:

Definition 2.4.1: The reduced-order subsystem (2.2.7) with linear model (2.4.13), where y is constant and Δy is assumed to be zero, is called a bifurcation subsystem for saddle-node bifurcation if following conditions are satisfied:

1. A_{22} is nonsingular, so that the fast subsystem linearized model $\Delta\dot{x} = [A_{11} - A_{12}A_{22}^{-1}A_{21}](\mu)\Delta x$ is well-defined.

2. The fast subsystem linearized model $[A_{11} - A_{12}A_{22}^{-1}A_{21}](\mu)$ has an eigenvalue $\tilde{\lambda}(\mu)$ with an R^{n_1} eigenvector $\tilde{u}(\mu)$ such that $\tilde{\lambda}(\mu) \to 0$ as $\mu \to \tilde{\mu}^*$.

3. The bifurcation subsystem linearized model $A_{11}(\mu)$ has an eigenvalue $\bar{\lambda}(\mu)$ with an R^{n_1} eigenvector $\bar{u}(\mu)$ such that $\bar{\lambda}(\mu) \to 0$ as $\mu \to \bar{\mu}^*$.

4. $\begin{bmatrix} A_{11} & A_{12} \\ A_{21} & A_{22} \end{bmatrix}(\hat{\mu}^*) \begin{bmatrix} \hat{w}_1(\hat{\mu}^*) \\ \hat{w}_2(\hat{\mu}^*) \end{bmatrix} = \begin{bmatrix} 0 \\ 0 \end{bmatrix}$, where $\hat{w}(\hat{\mu}^*) = \begin{bmatrix} \hat{w}_1(\hat{\mu}^*) \\ \hat{w}_2(\hat{\mu}^*) \end{bmatrix}$ is the right eigenvector of $A(\hat{\mu}^*)$.

5. $\tilde{m}^* = (\tilde{x}^*, \tilde{y}^*, \tilde{\mu}^*)$ and $\bar{m}^* = (\bar{x}^*, \bar{y}^*, \bar{\mu}^*)$ are $O(\epsilon_1)$ and $O(\epsilon_2)$ from $\hat{m}^* = (\hat{x}^*, \hat{y}^*, \hat{\mu}^*)$ and

6. $\tilde{u}(\tilde{\mu}^*)$ and $\bar{u}(\bar{\mu}^*)$ are respectively $O(\epsilon_1)$ and $O(\epsilon_2)$ close to $\hat{u}(\hat{\mu}^*) = \hat{w}_1(\hat{\mu}^*)$, and $\tilde{\lambda}(\tilde{\mu}^*)$ and $\bar{\lambda}(\bar{\mu}^*)$ are respectively $O(\epsilon_1)$ and $O(\epsilon_2)$ close to $\hat{\lambda}(\hat{\mu}^*)$.

Condition 5 should hold from condition 1 for slow and fast singularly perturbed conditions. Condition 6 should hold from conditions 2 and 3 for fast singularly perturbed systems.

The definition of a bifurcation subsystem requires that (2.2.4) experience bifurcation at $\hat{\mu}^*$ with bifurcation point $(\hat{x}^*(\hat{\mu}^*), \hat{y}^*(\hat{\mu}^*))$; (2.2.7) experience bifurcation at $\bar{\mu}^*$ with bifurcation point $(\bar{x}^*(\bar{\mu}^*), y_0)$, (2.2.5) experience bifurcation at $\tilde{\mu}^*$ with bifurcation point $(\tilde{x}^*(\tilde{\mu}^*), \tilde{y}^*(\tilde{\mu}^*))$ and condition 5 and 6 above hold.

Lemma 2.4.1: If

$$\begin{aligned} \| A_{11}\hat{u}(\mu) \| &\to \epsilon_2 + H.O.T(\epsilon_2) \\ \| [A_{11} - A_{12}A_{22}^{-1}A_{21}]\hat{u}(\mu) \| &\in (0, \epsilon_{10}] \end{aligned}$$

then $\| A_{12}A_{22}^{-1}A_{21}\hat{u}(\mu) \| \in (0, \epsilon_{30}]$, where $\epsilon_{10} = \epsilon_1 + H.O.T(\epsilon_1)$, and $\epsilon_{30} = \epsilon_1 + \epsilon_2 + H.O.T(\epsilon_1) + H.O.T(\epsilon_2)$.

Proof:

Suppose $\| [A_{11} - A_{12}A_{22}^{-1}A_{21}]\hat{u}(\mu) \| \rightarrow \epsilon_1 + H.O.T(\epsilon_1) \in (0, \epsilon_{10}]$, since

$$\| A_{12}A_{22}^{-1}A_{21}\hat{u}(\mu) \| - \| A_{11}\hat{u}(\mu) \| \leq \| [A_{11} - A_{12}A_{22}^{-1}A_{21}]\hat{u}(\mu) \|$$

Therefore:

$$\begin{aligned} \| A_{12}A_{22}^{-1}A_{21}\hat{u}(\mu) \| &\leq \epsilon_2 + \epsilon_1 + H.O.T(\epsilon_2) + H.O.T(\epsilon_1) \\ &\in (0, \epsilon_{30}] \end{aligned}$$

This lemma establishes the geometric decoupling condition as a result of satisfying conditions for a bifurcation subsystem existence based on the persistence of saddle-node bifurcation in the slow/fast reduced system models. The theorem that follows establishes that bifurcation in the slow singularly perturbed system and geometric decoupling results in satisfying the condition for saddle-node bifurcation in the fast singularly perturbed system and in the full system by Schur's Theorem.

Theorem 2.4.1 [3]: The sufficient conditions for saddle-node bifurcation subsystem to exist is that near $\hat{\mu}^*$ the following conditions hold at some nonzero R^{n_1} eigenvector $\hat{u}(\mu) = \hat{w}_1(\mu)$ component of $\hat{w}(\mu)$:

$$\| A_{11}\hat{u}(\mu) \| \rightarrow \epsilon_2 + H.O.T(\epsilon_2) \tag{2.4.16}$$

$$\| [A_{12}A_{22}^{-1}A_{21}]\hat{u}(\mu) \| \in (0, \epsilon_{30}] \tag{2.4.17}$$

as $\mu \rightarrow \hat{\mu}^*$, then $\| [A_{11} - A_{12}A_{22}^{-1}A_{21}]\hat{u}(\mu) \| \in (0, \epsilon_1 + 2\epsilon_2 + H.O.T(\epsilon_1) + H.O.T(\epsilon_2)]$ as $\mu \rightarrow \hat{\mu}^*$.

Proof:

The proof is straightforward by using Lemma 2.4.1 and is omitted here.

Equation (2.4.16) is called bifurcation subsystem condition, and (2.4.17) is called geometric decoupling condition. (2.4.16) tests whether the subsystem $\dot{x} = f(x, y_0)$ with linear approximation (2.4.14) experience bifurcation. Conditions (2.4.16) and (2.4.17) indicate the bifurcation of the subsystem model produces the bifurcation in the full system since bifurcation occurs in bifurcation subsystem and the bifurcation subsystem is completely decoupled along the right eigenvector. Since the slow subsystem (2.2.5) and bifurcation subsystem (2.2.7) experience bifurcation when the conditions of Theorem 2.4.1 are satisfied, the full system experiences the bifurcation that is experienced and produced in the bifurcation subsystem. There are three different ways one can produce bifurcation in the bifurcation in the full system depending on which of the conditions experience change as $\mu \to \hat{\mu}^*$, which will be elaborated in Chapter 4.

The difficulty with these test conditions is whether there is a solution, i.e., a bifurcation subsystem exists. The second difficulty is finding these solutions since there are so many combinations of variables that potentially could be inside and outside any order bifurcation subsystem and need to be tested to determine whether that combination produces a bifurcation subsystem for a specific proposed order n_1. This process must be repeated for each order n_1 to find all orders n_1 that have a bifurcation subsystem. The desire is to find n_1^* that is the largest bifurcation subsystem since it will give the greatest flexibility for design of a control system that stabilizes the bifurcation. This apparent difficulty in finding the bifurcation subsystem is greatly exaggerated because one can directly find the variables in the bifurcation subsystem of any order based on the ranking of elements in right eigenvector based on the results in Chapter 4.

Conditions (2.4.16) and (2.4.17) are tests for the existence of the bifurcation subsystem , but are not a complete algorithm for finding bifurcation subsystem. A description of systematic bifurcation subsystem identification algorithm based on

the magnitude of the right eigenvector is given in Chapter 4.

It has been stated that the center manifold dynamics persists in reduced system for both fast and slow external dynamics. The fact that A_{11} and $A_{11} - A_{12}A_{22}^{-1}A_{21}$ are singular when A_{22} is nonsingular suggests the bifurcation is in the bifurcation subsystem. Since the right eigenvector w_1 of A_{11} and $A_{11} - A_{12}A_{22}^{-1}A_{21}$ approximates the center manifold of the full system that persists in these two reduced subsystems, the center manifold lies in the bifurcation subsystem. It can be shown that if $A_{21}w_1 = 0$, then the center manifold is contained in the bifurcation subsystem when the center manifold trajectories are sufficiently close to the equilibrium since the external system is not at all excited linearly by the bifurcating eigenvalue. If $A_{21}w_1 \neq 0$ near the equilibrium point, then the external system can respond but its response is small if $A_{22}^{-1}A_{21}w_1$ is small. It should be noted without proving the persistence of the center manifold in the fast and slow singularly perturbed external models, the ability to prove that the center manifold lies in or within the bifurcation subsystem is not possible.

Remarks:

1. The bifurcation subsystem and geometric decoupling conditions are not only sufficient conditions for a bifurcation subsystem to exist, but will also act as a test condition to help find a relatively lower-ordered bifurcation subsystem. Bifurcation subsystem method is developed to cure the bifurcation, and one of the significant issues is to determine the bifurcation parameters. The reduced order bifurcation subsystem will contain fewer parameters. Thus, it is relatively easy to obtain the bifurcation parameter from the bifurcation subsystem.

2. Given that the center manifold and trajectories of the full system persist in either the fast or slow singularly perturbed external system, respectively, for $\epsilon_1 < \epsilon_{10}$ and $\epsilon_2 > \epsilon_{20}$, including $\epsilon_1 = \epsilon_2 = 0$, and assuming that the center

manifold and the trajectories of the full system should persist when both the external system is modeled as simultaneously a fast and a slow singularly perturbed model (when the fast singular perturbation tends to zero first), then the center manifold and the trajectories near the center manifold should be within the bifurcation subsystem or its boundary defined as occurring when the external model is simultaneously both fast and slow.

Chapter 3

Bifurcation Subsystem for Hopf Bifurcation

3.1 Objective

Singular perturbation theory underlying the definition of Hopf bifurcation subsystem and the sufficient conditions for existence of a Hopf bifurcation subsystem are developed in this chapter since it was never thoroughly developed in [3] and [4] for both fast and slow singularly perturbed models. In section 3.2, the Hopf bifurcation is introduced. The persistence of Hopf bifurcation with fast external dynamics is presented in section 3.3 and 3.4 based on [4]. Motivated by the results in section 3.3 and 3.4, the persistence of singularly perturbed Hopf bifurcation with slow external dynamics is proven in section 3.5. The closeness of the bifurcation value, the eigenvalues, and the equilibrium points are concluded in this section. The application of geometric singular perturbation theory in [5] gives the preservation of the nature and size of the periodic orbits. By applying overflowing invariant manifolds theory and conclusions of α-decomposition, the persistence of the center manifold dynamics

with slow and fast external dynamics is proven section 3.6. In section 3.7 the Hopf bifurcation subsystem is defined and the sufficient conditions for the existence of a Hopf bifurcation subsystem are given.

3.2 Hopf Bifurcation

Considering the nonlinear system:

$$\dot{x} = f(x, \mu) \tag{3.2.1}$$

where $x = x(t) \in R^n$, $f : R^n \times R \to R^n$ is a C^r smooth function. Suppose $f(0, \mu) = 0$. For a Hopf bifurcation to occur two hypotheses are required:

(H1) The Jacobian $D_x f(0, \mu)$ possesses a pair of complex-conjugate simple eigenvalues $\lambda(\mu) = \alpha(\mu) + i\omega(\mu)$, such that $\alpha(0) = 0$, $\alpha'(0) \neq 0$ and $\omega_c := \omega(0) > 0$.

(H2) $\pm i\omega_c$ are the only pure imaginary eigenvalues of the critical Jacobian $D_x f(0, 0)$.

Hypotheses (H1) means that the linearization of (3.2.1) has a pair of complex eigenvalues which cross the imaginary axis transversally as μ is varied through the critical value $\mu = 0$. Therefore, the Hopf theorem asserts the existence of a one-parameter family $\{\gamma_\nu, 0 \leq \nu \leq \nu_0\}$ of nonconstant periodic solutions of (3.2.1) emerging from the equilibrium $x = 0$ at $\mu = 0$. Here ν is the amplitude of the periodic solutions and ν_0 is sufficiently small.

3.3 Persistence of Hopf Bifurcation under Singularly Perturbed Fast External Dynamics [4]

Consider the perturbation problems with fast unmodeled dynamics of the form:

$$\begin{aligned} \dot{x} &= f(x, y, \mu, \epsilon) \\ \epsilon \dot{y} &= g(x, y, \mu, \epsilon) \end{aligned} \tag{3.3.2}$$

where $x \in R^n$, $y \in R^m$, μ, $\epsilon \in R$ and ϵ is a small, but nonzero number. μ is the bifurcation parameter and ϵ is the singular perturbation parameter. System (3.3.2) is called full system. When $\epsilon = 0$ the full system degenerates to the reduced system:

$$\begin{aligned} \dot{x} &= f(x, y, \mu, 0) \\ 0 &= g(x, y, \mu, 0) \end{aligned} \tag{3.3.3}$$

Let $\tilde{m}^* = (\tilde{x}^*, \tilde{y}^*)$ denote the equilibrium point of the reduced system (3.3.3) and suppose that $D_y g(\tilde{x}^*, \tilde{y}^*, 0, 0)$ is nonsingular. According to Implicit Function theorem there exists an unique solution $y = h(x, \mu)$ in the neighborhood of $(\tilde{x}^*, \tilde{y}^*, \tilde{\mu}^* = 0)$ which satisfies $0 = g(x, h(x, \mu), \mu, 0)$.

Definition 3.3.1: The reduced system undergoes a Hopf bifurcation at the equilibrium point $\tilde{m}^*$ when $\mu = \tilde{\mu}^* = 0$ if this behavior occurs for the local representation $\dot{x} = f(x, h(x, \mu), \mu, 0)$.

The following four Hypotheses are required:

(H1) f and g are smooth enough in x, y, μ, ϵ in a neighborhood of $(\tilde{m}^*, 0, 0)$.

(H2) $\det D_y g(\tilde{x}^*, \tilde{y}^*, 0, 0) \neq 0$

(H3) The reduced system undergoes a Hopf bifurcation at $\tilde{m}^*$ for $\mu = \tilde{\mu}^* = 0$.

(H4) $D_y g(\tilde{x}^*, \tilde{y}^*, 0, 0)$ has no eigenvalue with zero real part.

Let:

$$J(\mu, \epsilon) = \begin{bmatrix} D_x f & D_y f \\ \epsilon^{-1} D_x g & \epsilon^{-1} D_y g \end{bmatrix}$$
$$A(\mu) = (D_x f + D_y f D_x h)|_{\tilde{x}^*(\mu)}$$

where $J(\cdot, \cdot)$ and $A(\cdot)$ denote the Jacobian of the full system (3.3.2) and the reduced system (3.3.3), respectively. Under hypotheses H1-H4 we have following conclusions [4]:

1. *Closeness of eigenvalues*

   $$\sigma(J(\mu, \epsilon)) = [\sigma(A(\mu)) + O(|(\mu, \epsilon)|)] \cup [\epsilon^{-1} \sigma(D_y g(\tilde{x}^{*,\mu,\epsilon}, \tilde{y}^{*,\mu,\epsilon}, \mu, \epsilon)) + O(1)]$$

   for small ϵ, μ, where σ denotes the eigenvalues.

2. *Persistence of Hopf bifurcation/Closeness of Equilibrium*

   There is an $\epsilon_0 > 0$ and for each $\epsilon \in (0, \epsilon_0]$ the full system undergoes a Hopf bifurcation at equilibrium $\hat{m}^{*,\mu,\epsilon}$ of the full system near $\tilde{m}^*$ for $\mu, \epsilon \in (0, \epsilon_0)$.

3. *Transversality persistence*

   $$\lim_{\epsilon \to 0} \frac{\partial}{\partial \mu} Re\lambda_1(\mu, \epsilon) = \alpha'(0)$$

   where $\lambda_1(\mu, \epsilon)$ is the bifurcating eigenvalue of $A(\mu)$ for $\mu = 0$.

3.4 Regular Degeneration of Periodic Orbits with Singularly Perturbed Fast External Dynamics [4]

To study the convergence of the bifurcated periodic orbits consider the suspended system:

$$\begin{aligned} \dot{x} &= f(x, y, \mu, \epsilon) \\ \epsilon\dot{y} &= g(x, y, \mu, \epsilon) \\ \dot{\mu} &= 0 \\ \dot{\epsilon} &= 0 \end{aligned} \tag{3.4.4}$$

Setting $\epsilon = 0$ gives the associated reduced system:

$$\begin{aligned} \dot{x} &= f(x, y, \mu, 0) \\ 0 &= g(x, y, \mu, 0) \\ \dot{\mu} &= 0 \\ \dot{\epsilon} &= 0 \end{aligned} \tag{3.4.5}$$

Let $\phi_t(x, y, \mu, \epsilon)$ be the flow of the suspended system (3.4.4) at time t. Let $I(U)$ represent the set $I(U) = \{(x, y, \mu, \epsilon) \in U | \phi_t(x, y, \mu, \epsilon) \in U \text{ for } t \in (-\infty, \infty)\}$ for any open set $U \subset R^n \times R^m \times R \times R$. Then, $I(U)$ is the U-invariant subset of U.

By the associated reduced system (3.4.5) we have that $0 = g(x, y, \mu, 0)$ holds, then there exists a manifold χ near $\tilde{m}^*$ and a neighborhood U of $\tilde{m}^*$ such that $I(U) \in \chi$ for the suspended system [5]. Actually χ is a center manifold near $\tilde{m}^*$ of the fast time system corresponding to the suspended system. Hence, χ contains all locally

recurrent trajectories of the suspended system, including the family of bifurcated periodic solutions for the full system.

Concerning the bifurcated periodic orbits we have the following theorem [4], where ν is the amplitude of the periodic orbits:

Theorem 3.4.1 Let hypotheses (H1) - (H4) hold. Then there exist positive numbers ν_0, ϵ_0 and a C^{r-2} function $\mu(\nu, \epsilon)$ such that the full system has a periodic solution $\hat{\gamma}_{\nu,\epsilon}$ near $\tilde{m}^*$ and of period near $2\pi\omega_c^{-1}$ for the parameter value $\mu = \mu(\nu, \epsilon)$, for any (ν,ϵ) $\in (0, \nu_0] \times (0, \epsilon_0]$. For a given $\epsilon \in (0, \epsilon_0]$, the one-parameter family $\hat{\gamma}_{\nu,\epsilon}, \nu \in (0, \nu_0]$ is identical to the bifurcated family of periodic solutions. At $\epsilon = 0$ the bifurcated family of periodic solutions $\tilde{\gamma}_\nu$ of the reduced system occur for the parameter values $\mu_0(\nu) = \mu(\nu, 0), \nu \in (0, \nu_0]$. Let $\nu \in (0, \nu_0]$. Then for any $\rho > 0$ there is an $\epsilon_1 \in (0, \epsilon_0]$ such that the periodic solution $\hat{\gamma}_{\nu,\epsilon}$ lies in a ρ-neighborhood of $\tilde{\gamma}_\nu$ and such that the period of $\hat{\gamma}_{\nu,\epsilon}$ differs from that of γ_ν by no more than ρ whenever $0 < \epsilon \leq \epsilon_1$.

This theorem can be summarized in the following statements:

(a) *Local attractive property*:

The center manifold χ contains all locally recurrent trajectories of the suspended system (3.4.4). Let χ_ϵ denote the ϵ =constant slices of χ. Then the ϵ-sliced manifolds χ_ϵ can be parameterized as the graph of function $y = u(x, \mu, \epsilon)$ near $\tilde{m}^*$ from (H4). Therefore, for small enough μ the slow dynamics x obeys

$$\dot{x} = f(x, u(x, \mu, \epsilon), \mu, \epsilon) \tag{3.4.6}$$

on χ_ϵ.

(b) *Invariance of critical bifurcation parameter*

For any small $\epsilon > 0$, the critical bifurcation parameter value for full system (3.4.4) and the local representation of the reduced system (3.4.6) at bifurcation

points $(\hat{x}^{*,\mu,\epsilon}, \hat{y}^{*,\mu,\epsilon})$, and $\tilde{x}^{*,\mu,\epsilon}$, respectively, are both zero.

(c) *Invariance of the frequency of periodic solution*

For any small $\epsilon > 0$, the bifurcation eigenvalues for the full system and (3.4.6) cross the imaginary axis at same point.

(d) *Persistence of the periodic orbits*

For each small ϵ, the periodic solution (the orbits) for the full system are identical to the periodic solutions of the reduced system (3.4.5) and yet $\gamma_{\nu,\epsilon}$ lies in a ρ-neighborhood of γ_ν and the period of $\tilde{\gamma}_{\nu,\epsilon}$ differs from that of $\hat{\gamma}_\nu$ by no more than ρ whenever $0 < \epsilon \leq \epsilon_1$.

3.5 Persistence of Hopf Bifurcation under Singularly Perturbed Slow External Dynamics

Consider the ordinary differential equations with singularly perturbed external dynamics:

$$\begin{aligned} \dot{x} &= f(x, y, \mu, \epsilon) \\ \dot{y} &= \epsilon g(x, y, \mu, \epsilon) \end{aligned} \tag{3.5.7}$$

The reduced system is given by setting $\epsilon = 0$ in (3.5.7) and the corresponding equilibrium of the reduced system is $\bar{m}^* = (\bar{x}^*, y_0)$. Generally the equilibrium points are isolated. For the fast time systems of singular perturbation problem this is not true.

Let's make another assumption:

(H5) $\det D_x f(\bar{x}^*, y_0, 0, 0) \neq 0$

By rescaling the full system, it is transformed to be:

$$\begin{aligned} \epsilon x' &= f(x, y, \mu, \epsilon) \\ y' &= g(x, y, \mu, \epsilon) \end{aligned} \tag{3.5.8}$$

where $'$ represents the derivative with respect to fast time $\tau = t/\epsilon$, and the corresponding reduced system when $\epsilon = 0$ is given by:

$$\begin{aligned} 0 &= f(x, y, \mu, 0) \\ y' &= g(x, y, \mu, 0) \end{aligned} \tag{3.5.9}$$

Note that the equilibrium point of the reduced system (3.5.9) is still $\bar{m}^* = (\bar{x}^*, y_0)$ since rescaling does not change the equilibrium point. Under assumption (H5), there exists a unique solution $x = h(y, \mu)$ in a neighborhood of $\bar{m}^*$, which satisfies $0 = f(x, y, \mu, \epsilon)$ by the Implicit Function Theorem.

$$y' = g(h(y, \mu), y, \mu, 0) \tag{3.5.10}$$

Denote the Jacobian of (3.5.10) by $A(\mu)$ and (H5) implies that:

$$\begin{aligned} A(\mu) &= (D_x g D_y h + D_y g)|_{y_0(\mu)} \\ &= (-D_x g (D_x f)^{-1} D_y f + D_y g)|_{y_0(\mu)} \\ &\neq 0 \end{aligned}$$

The determinant of Jacobian of the reduced system (3.5.9) is given by (H5) and

Schur's theorem:

$$\begin{aligned}
\det(J) &= \begin{bmatrix} D_x f & D_y f \\ D_x g & D_y g \end{bmatrix} \\
&= \det(D_x f)\det(D_y g - D_x g(D_x f)^{-1} D_y f) \\
&= \det(D_x f)\det(A(\mu)) \\
&\neq 0
\end{aligned}$$

By the Implicit Function Theorem, there exists the isolated equilibrium point $\hat{m}^{*,\mu,\epsilon} = (\hat{x}^{*,\mu,\epsilon}, y_0^{\mu,\epsilon})$ of the full system (3.5.7) lies in a small neighborhood of $\bar{m}^* = (\bar{x}^*, y_0)$ for small μ, and small ϵ. Since the equilibrium point of the rescaled system (3.5.8) does not change we are able to say that the persistence of the equilibrium under small singular perturbation.

To study the persistence of the Hopf bifurcation, let's return to full system (3.5.7) again. When $\epsilon = 0$ the suspended system of full system (3.5.7) is given as:

$$\begin{aligned}
\dot{x} &= f(x, y, \mu, 0) \\
\dot{y} &= 0 \\
\dot{\mu} &= 0 \\
\dot{\epsilon} &= 0
\end{aligned} \tag{3.5.11}$$

Denote by $\bar{m}^* = (\bar{x}^*, y_0)$ the equilibrium point of the reduced system. Then, in the neighborhood of $(\bar{m}^*, \mu = 0)$ we have

$$y = u(y_0, \mu, 0) \tag{3.5.12}$$

which satisfies $\dot{y} = 0$, and the dynamics of x in (3.5.7) is equivalent to:

$$\dot{x} = f(x, u(y_0, \mu, 0), \mu, 0) \tag{3.5.13}$$

The full system (3.5.7) can be evaluated in the neighborhood of $(\bar{m}^*, \mu = 0)$

$$\dot{y} = D_y u(y_0, \mu, 0) = 0$$

Therefore:

$$\epsilon g(x, u(y_0, \mu, 0), \mu, \epsilon) = D_y u(y_0, \mu, 0) = 0 \tag{3.5.14}$$

Again, since the bifurcated periodic solutions of the reduced system emerges from the equilibrium point $\bar{m}^*$, let's define that the full system undergoes a Hopf bifurcation if the reduced system (3.5.13) does by noting that system (3.5.13) is equivalent to (3.5.11) in the neighborhood of $(\bar{m}^*, \mu = 0)$.

The Jacobian of the full system (3.5.7) and the reduced system around the equilibrium point $\bar{m}^* = (\bar{x}^*, y_0)$ is given by:

$$J(\mu, \epsilon) = \begin{bmatrix} D_x f & D_y f \\ \epsilon D_x g & \epsilon D_y g \end{bmatrix}_{\bar{m}^*}$$

and

$$A(\mu) = D_x f(x, u(y_0, \mu, 0))|_{\bar{x}^*(\mu)}$$

By equation (3.5.12) the local representation of the full system Jacobian $J(\mu, \epsilon)$ around (3.5.12) is given by:

$$J(\mu, \epsilon) = \begin{bmatrix} D_x f(x, u(y_0, \mu, 0), \mu, 0) & \dagger \\ 0 & 0 \end{bmatrix}_{\bar{m}^*} \tag{3.5.15}$$

where † is the term we do not care. When the Hopf bifurcation occurs (3.5.15) implies that n eigenvalues of $J(\mu, \epsilon)$ are exactly the n eigenvalues of $A(\mu)$. Thus, both full system and reduced system are bifurcating at the same bifurcating parameter $\hat{\mu}^* = \bar{\mu}^*$ when ϵ is small.

Also, we can see that one of the eigenvalues of $J(\mu, \epsilon)$ crosses the imaginary axis transversally if and only if the corresponding eigenvalue of $A(\mu, \epsilon)$ does. Therefore, we are able to state the persistence of the bifurcation as well as the critical value of the bifurcation parameter are same. We have thus proven 1-3, given for fast external dynamics in section 3.3, for the slow external dynamics.

The periodic orbits structure of the reduced system with fast or slow external subsystem for small perturbation is described by Theorem 13.1 in [5]. It has been proven that the periodic orbit of the full system $\hat{\gamma}$ is hyperbolic in case the orbit of reduced system $\tilde{\gamma}$ or $\bar{\gamma}$ is hyperbolic. Moreover, $\hat{\gamma}$ and the period of $\hat{\gamma}$ depends smoothly on the perturbation ϵ. This implies the persistence of the periodic orbits for the reduced system.

3.6 Persistence of the Center Manifold [19]

The only question to be answered is if the center manifold dynamics persists in the reduced system when the saddle-node bifurcation occurs in the full system. There is no general conclusion for nonlinear dynamic systems. Here we consider the linearized model of the nonlinear systems. The generalized singularly perturbed nonlinear system can be represented by:

$$\begin{aligned} \dot{x} &= f(x, y, \epsilon) \\ \dot{y} &= g(x, y, \epsilon) \end{aligned}$$

where $x \in R^n$, $y \in R^m$.

The linearization around the equilibrium point $(x, y, 0)$ is:

$$\begin{bmatrix} \delta\dot{x} \\ \delta\dot{y} \\ \delta\dot{\epsilon} \end{bmatrix} = \begin{bmatrix} D_x f & D_y f & D_\epsilon f \\ D_x g & D_y g & D_\epsilon g \\ 0 & 0 & 0 \end{bmatrix} \begin{bmatrix} \delta x \\ \delta y \\ \delta\epsilon \end{bmatrix}$$

If

$$Re\lambda_i(D_x f) < 0, Re\lambda_j(D_y g) = 0$$

for $1 \leq i \leq n$, $1 \leq j \leq m$, there will be $m + 1$-dimensional center manifold. The persistence of (m+1)-dimensional center manifold dynamics in the unperturbed system ($\epsilon = 0$) is guaranteed in [19] by applying overflowing invariant manifold theory when $Re\{\lambda(D_y g)\} = 0$ if $D_y f$, $D_\epsilon f$, and $D_x g$ vanish at the equilibrium point. For a power system this can be the case if we recall the α-decomposition theory [22], where due to the sparse nature of power systems the dynamics can be represented in the block diagonal form.

By adding a small C^∞ "bump" function an overflowing invariant manifold (the center manifold) is well-defined. The persistence theorem for overflowing invariant manifolds is thus applied (see details in [19]). Therefore, we can state that the center manifold dynamics of the reduced system will approximate that of the full system for the small perturbation.

The persistence of center manifold for the full system in the reduced system helps assure the center manifold of the full system is captured in the bifurcation subsystem by assuring it persists for both fast and slow reduced models. This theory is not in [2] and [3] but is essential to the results that the center manifold dynamics of the full system lies in or within the bifurcation subsystem.

It has been proven that the center manifold dynamics of the full system persists in

the reduced system. The statements in section 3.5 not only show that the bifurcation point and the equilibrium point of the reduced system are close to that of the full system of order ϵ, but also assure that the *dynamic behaviors* of the reduced system will persist around the equilibrium point at the bifurcation point. When Hopf bifurcation occurs the periodic orbits, the frequencies of the periodic orbits, and the center manifold dynamics of the reduced system will be close to that of the full system. Thus, it can be concluded that the critical bifurcation parameter value, the frequency of the periodic solution are invariant, and the periodic orbits of the full system persist in the reduced system for the full system with slow external dynamics. Thus, it can be concluded that the invariance properties (b)-(d) for singularly perturbed fast external dynamics do hold but not exactly the same for singularly perturbed slow external dynamics.

Remarks:

1. The persistence of Hopf bifurcation with slow external dynamics under singular perturbation cannot be guaranteed by merely rescaling the system with different time frame and applying method in [4]. Since the rescaled system is given by equation (3.5.9), if we used the method in [4] we would have the conclusion that the persistence of Hopf bifurcation of the full system when Hopf bifurcation occurs in subsystem g, rather than f. Remember that we are still studying persistence when the Hopf bifurcation occurs in $\dot{x} = f(x, y, \mu, \epsilon)$. Thus, there is a need for the results of the generalized form given in [5].

2. In [5] the perturbation also acts as a bifurcation parameter. The only difference is the dimension of center manifolds of the reduced system and the full system models (see equation (3.4.4)).

The persistence of Hopf bifurcation for full system with singular perturbed slow and fast dynamics can be summarized here.

Proposition 3.6.1

When the reduced system undergoes Hopf bifurcation at equilibrium point $\tilde{m}^*$ (with fast external dynamics) or $\bar{m}^*$ (with slow external dynamics), for any $\rho > 0$ there exists ϵ_0 such that the differences between equilibrium point $\hat{m}^{*,\mu,\epsilon_i}$, the period and the size of the periodic orbits $\hat{\gamma}^{*,\mu,\epsilon_i}$, the bifurcation parameter $\hat{\mu}^{*,\mu,\epsilon_i}$ of the full system and those of the reduced systems are no more than ρ for $0 < \epsilon_i < \epsilon_0$, where $i = 1$ for fast external dynamics and $i = 2$ for slow external dynamics. There exist constant T such that the center manifold $\| W_+^{\epsilon_i}(\hat{m}^{*,\mu,\epsilon_i}) - W_+^{\epsilon_i}(\tilde{m}^{*,\mu,\epsilon_i}) \| \leq \epsilon'$, and $\| W_+^{\epsilon_i}(\hat{m}^{*,\mu,\epsilon_i}) - W_+^{\epsilon_i}(\bar{m}^{*,\mu,\epsilon_i}) \| \leq \epsilon''$, for $t = T$, where $\epsilon', \epsilon'' \in (0, \epsilon_0)$.

From Proposition 3.6.1, the reduced system not only preserves the parameters of the full system, but also preserves the dynamic behaviors of the full system at the bifurcation point.

3.7 Hopf Bifurcation Subsystem

In the definition of saddle-node bifurcation subsystem only the right eigenvector of the bifurcating eigenvalue is used. When the Hopf bifurcation occurs, there will be two right eigenvectors involved. Before we proceed to define the Hopf bifurcation subsystem we will show that only one of the right eigenvectors is required to describe the system response and thus define the bifurcation subsystem for Hopf bifurcation.

Proposition 3.7.1 Consider the linear system:

$$\dot{x} = Ax \tag{3.7.16}$$

where $A \in R^{n \times n}$. Only one eigenvector of the conjugate complex eigenvalues is needed to represent the solution of (3.7.16).

Proof:

The states of (3.7.16) can be expanded in terms of right eigenvector as:

$$x = \Sigma_{i=1}^{n} z_i w_i$$

where w_i is the i^{th} right eigenvector of A.

The scalar coefficient z_i can be obtained by pre-multiplying the i^{th} left eigenvector v_i. Due to the orthogonality of right and left eigenvectors we can see that:

$$z_i = v_i x$$

Substituting z_i into (3.7.16) gives:

$$\dot{z}_i = \lambda_i z_i$$

Thus,

$$z_i = e^{\lambda_i t} z_i(0)$$

Let $\lambda_k = \alpha_k + j\beta_k$ and $\lambda_{k+1} = \lambda_k^H$ be the eigenvalues of A, where ^{H} represents the complex conjugate.

$$\begin{aligned} x &= \Sigma_{i=1}^{n} e^{\lambda_i t} w_i z_i(0) \\ &= \Sigma_{i=1}^{k-1} e^{\lambda_i t} w_i z_i(0) + e^{(\alpha_k + j\beta_k)t} w_k z_k(0) + e^{(\alpha_k - j\beta_k)t} w_{k+1} z_{k+1}(0) + \Sigma_{i=k+2}^{n} e^{\lambda_i t} w_i z_i(0) \\ &= \Sigma_{i=1}^{k-1} e^{\lambda_i t} w_i z_i(0) + \Sigma_{i=k+2}^{n} e^{\lambda_i t} w_i z_i(0) + e^{\alpha_k t} \Delta z_k(0) + e^{\alpha_k t} \Delta^H z_{k+1}(0) \end{aligned}$$

where $\Delta = e^{j\beta_k t} w_k$ and note that $w_k = w_{k+1}^H$.

Let's calculate each element of Δ_i. Denote l^{th} element of Δ_i by Δ_{i_l}.

$$\begin{aligned}\Delta_{i_l} &= (\cos\beta_k t + j\sin\beta_k t)(Re\{w_{k_l}\} + jIm\{w_{k_l}\})z_k(0) \\ &= |w_{k_l}|\{[\frac{R_{k_l}}{|w_{k_l}|}\cos\beta_k t - \frac{I_{k_l}}{|w_{k_l}|}\sin\beta_k t] + j[\frac{R_{k_l}}{|w_{k_l}|}\sin\beta_k t + \frac{I_{k_l}}{|w_{k_l}|}\cos\beta_k t]\}z_k(0)\end{aligned}$$

where $R_{k_l} = Re(w_{k_l})$ and $I_{k_l} = Im(w_{k_l})$.

Let $\tan\phi_{k_l} = I_{k_l}/R_{k_l}$. Then, $\cos\phi_{k_l} = \frac{R_{k_l}}{|w_{k_l}|}$ and $\sin\phi_{k_l} = \frac{I_{k_l}}{|w_{k_l}|}$. Δ_{i_l} can be rewritten as:

$$\begin{aligned}\Delta_{i_l} &= |w_{k_l}|\{[\cos\phi_{k_l}\cos\beta_k t - \sin\phi_{k_l}\sin\beta_k t] + j[\cos\phi_{k_l}\sin\beta_k t + \sin\phi_{k_l}\cos\beta_k t]\}z_k(0) \\ &= |w_{k_l}|\{[\cos(\beta_k t + \phi_{k_l}) + j\sin(\beta_k t + \phi_{k_l})]\}z_k(0) \\ &= |w_{k_l}|e^{j(\beta_k t + \phi_{k_l})}z_k(0)\end{aligned}$$

For the real matrix A, the eigenvalues of A are either real or complex conjugate. Also, z_k and z_{k+1} are complex conjugate. Therefore, the imaginary parts disappear and the solution of (3.7.16) can be written in the form of:

$$x_l = \Sigma_{i=1}^{n} e^{\alpha_i t}|w_{i_l}|[\cos(\beta_i t + \phi_{i_l})Re\{z_i(0)\} - \sin(\beta_i t + \phi_{i_l})Im\{z_i(0)\}]$$

where $i = 1, 3, ..., n-1$, and x_l is l^{th} state of the system. This reveals the time response can be represented by only one of the conjugate eigenvectors, and the magnitude of the time response is determined only by the magnitude of the eigenvector.

Analogous to saddle-node bifurcation subsystem Hopf bifurcation subsystem is defined with only one of the conjugate eigenvectors of the bifurcating eigenvalue according to Proposition 3.7.1:

Definition 3.7.1: The reduced-order subsystem (2.2.7) with linear model (2.4.13), where y is constant and Δy is assumed to be zero is called a bifurcation subsystem

for Hopf bifurcation if following conditions are satisfied:

1. $A_{22} - j\omega_0 I$ is nonsingular, so that the fast subsystem linearized model $\Delta\dot{x} = [(A_{11} - j\omega_0 I) - A_{12}(A_{22} - j\omega_0 I)^{-1}A_{21}](\mu)\Delta x$ is well-defined.

2. The fast subsystem linearized model $[A_{11} - A_{12}A_{22}^{-1}A_{21}](\mu)$ has an eigenvalue $\tilde{\lambda}(\mu)$ with an R^{n_1} eigenvector $\tilde{u}(\mu)$ such that $\tilde{\lambda}(\mu) \to j\omega_0$ as $\mu \to \tilde{\mu}^*$.

3. The bifurcation subsystem linearized model $A_{11}(\mu)$ has an eigenvalue $\bar{\lambda}(\mu)$ with an R^{n_1} eigenvector $\bar{u}(\mu)$ such that $\bar{\lambda}(\mu) \to j\omega_0$ as $\mu \to \bar{\mu}^*$.

4. $\begin{bmatrix} A_{11} - j\omega_0 I & A_{12} \\ A_{21} & A_{22} - j\omega_0 I \end{bmatrix}(\hat{\mu}^*) \begin{bmatrix} \hat{w}_1(\hat{\mu}^*) \\ \hat{w}_2(\hat{\mu}^*) \end{bmatrix} = \begin{bmatrix} 0 \\ 0 \end{bmatrix}$, $\hat{w}(\hat{\mu}^*) = \begin{bmatrix} \hat{w}_1(\hat{\mu}^*) \\ \hat{w}_2(\hat{\mu}^*) \end{bmatrix}$ is the right eigenvector of $A(\hat{\mu}^*)$.

5. $\tilde{m}^* = (\tilde{x}^*, \tilde{y}^*, \tilde{\mu}^*)$ and $\bar{m}^* = (\bar{x}^*, \bar{y}^*, \bar{\mu}^*)$ are $O(\epsilon_1)$ and $O(\epsilon_2)$ close to $\hat{m}^* = (\hat{x}^*, \hat{y}^*, \hat{\mu}^*)$.

6. $\tilde{u}(\tilde{\mu}^*)$ and $\bar{u}(\bar{\mu}^*)$ are respectively $O(\epsilon_1)$ and $O(\epsilon_2)$ close to $\hat{u}(\hat{\mu}^*) = \hat{w}_1(\hat{\mu}^*)$, and $\tilde{\lambda}(\tilde{\mu}^*)$ and $\bar{\lambda}(\bar{\mu}^*)$ are respectively $O(\epsilon_1)$ and $O(\epsilon_2)$ close to $\hat{\lambda}(\hat{\mu}^*)$.

Theorem 3.7.1: The sufficient conditions for Hopf bifurcation subsystem to exist is that near $\hat{\mu}^*$ the following conditions hold for some nonzero R^{n_1} eigenvector $\hat{u}(\mu)$ component of $\hat{w}(\mu)$:

$$\| (A_{11} - j\omega_0 I)\hat{u}(\mu) \| \to \epsilon_2 + H.O.T(\epsilon_2) \tag{3.7.17}$$

$$\| [A_{12}(A_{22} - j\omega_0 I)^{-1}A_{21}]\hat{u}(\mu) \| \in (0, \epsilon_{30}] \tag{3.7.18}$$

as $\mu \to \hat{\mu}^*$, then $\| [(A_{11} - j\omega_0 I) - A_{12}(A_{22} - j\omega_0 I)^{-1}A_{21}]\hat{u}(\mu) \| \in (0, \epsilon_{10}]$ as $\mu \to \hat{\mu}^*$.

Proof:

The proof is omitted here.

Correspondingly, (3.7.17) is bifurcation subsystem condition and (3.7.18) is geometric decoupling condition. As we will show in next chapter the bifurcation subsystem condition and geometric decoupling condition are used to identify the saddle-node or Hopf bifurcation subsystem.

It has been proven that only one of a pair eigenvectors is needed to represent the system state response. Again only one of the pair of complex conjugate eigenvectors is required to develop the bifurcation subsystem condition and geometric decoupling condition. To see this

$$\{(A - j\omega_0 I)w_i\}^H = 0$$

i.e.,

$$(A + j\omega_0 I)w_i^H = 0$$

where $-j\omega_0$ is another eigenvalue of the pair of the bifurcating eigenvalue, and w_i^H is the corresponding eigenvector.

The center manifold dynamics of the full system lies in the bifurcation subsystem since $\pm\omega_0$ are eigenvalues of A_{11}, $A_{22} - j\omega_0 I$ is nonsingular, $A_{12}[A_{22} - j\omega_0 I]^{-1}A_{21}u_i = 0$ and because the center manifold of the full system and reduced system are identical, and the center manifold periodic trajectory is sufficiently close to the equilibrium. If $A_{21}u_i = 0$ the center manifold of the full system is contained in the bifurcation subsystem. This result is extremely important because it allows the bifurcation subsystem to represent the center manifold in large systems, avoids the computation of the nonlinear transformation required to obtain the center manifold dynamics, allows one to easily find the physical variables that are bifurcation parameters, allows selecting measurements and controls for the bifurcation subsystem that stabilize the full system after bifurcation, and allows easy identification of causes and cures in terms of physically meaningful parameter changes in the bifurcation subsystem and finally allows developing robust control.

Chapter 4

Bifurcation Subsystem Identification

4.1 Objective

The objective of this chapter is to develop a bifurcation subsystem identification method which is capable of obtaining a relatively small dimensional bifurcation subsystem. The smallest bifurcation subsystems should contain the right eigenvector elements with the largest magnitudes. Thus, testing for a bifurcation subsystem using the bifurcation subsystem condition and geometric decoupling condition for increasing order bifurcation subsystem model should be performed on a system matrix reordered based on right eigenvector element magnitudes until the bifurcation subsystem condition and geometric decoupling condition are satisfied. The equivalent system produced by reordering the state matrix based on the magnitude of the right eigenvector is proven to bifurcate when the original system undergoes bifurcation. It is also proven that the geometric decoupling and bifurcation subsystem conditions must only be tested on one of the pair of complex eigenvalues/eigenvectors.

We then develop and theoretically justify a bifurcation subsystem identification algorithm. The bifurcation subsystem condition and geometric decoupling condition are extended in section 4.3, and this reveals that the existence of bifurcation subsystem requires much weaker conditions that have been required for slaving [27], model reduction [12], coherency reduction [14], and α-decomposition [22] methods.

4.2 Bifurcation Subsystem Identification Algorithm

Suppose (3.6.16) is the linearized model of system $\dot{x} = f(x)$ at an equilibrium. When the bifurcation occurs in a neighborhood of the equilibrium

$$(A - j\omega_0 I)w_i = 0 \tag{4.2.1}$$

holds strictly, where ω_0 is the imaginary part of the bifurcating eigenvalue, and $\omega_0 = 0$ for saddle node bifurcation. $w_i = \begin{bmatrix} u_i \\ y_i \end{bmatrix}$ is the corresponding eigenvector of the bifurcating eigenvalue.

Partitioning A into form of:

$$A = \begin{bmatrix} A_{11} & A_{12} \\ A_{21} & A_{22} \end{bmatrix}$$

to represent internal and external subsystems. By Schur's Theorem equation (4.2.1) can be rewritten as:

$$(A_{11} - j\omega_0 I)u_i - A_{12}(A_{22} - j\omega_0 I)^{-1}A_{21}u_i = 0 \tag{4.2.2}$$

for nonsingular $A_{22} - j\omega_0 I$, where $y_i = -A_{12}(A_{22} - j\omega_0 I)^{-1}A_{21}u_i$.

To identify the subsystem which not only experiences, produces, but also causes the

full system bifurcation to occur, (4.2.2) is broken into two separate conditions:

$$(A_{11} - j\omega_0 I)u_i = 0$$

$$A_{12}(A_{22} - j\omega_0 I)^{-1}A_{21}u_i = 0$$

which can be rewritten as:

$$\| (A_{11} - j\omega_0 I)u_i \| = 0 \tag{4.2.3}$$

$$\| A_{12}(A_{22} - j\omega_0 I)^{-1}A_{21}u_i \| = 0 \tag{4.2.4}$$

by introducing some kind of matrix norm. (4.2.3) is called bifurcation subsystem condition, and (4.2.4) is called geometric decoupling condition.

Remarks

1. When saddle-node bifurcation occurs (4.2.3) and (4.2.4) are reduced to (2.4.16) and (2.4.17).

2. When Hopf bifurcation occurs only one of the pair of the eigenvalues and the corresponding eigenvectors is required to develop the bifurcation subsystem condition and geometric decoupling condition as we have stated in Chapter 3.

We are interested in finding the relatively small-dimensional bifurcation subsystem in which very few states involves. From Proposition 3.6.1 we know that the magnitude of time response is determined by the magnitude of right eigenvector. Also, right eigenvector is an approximation of the center manifold around the equilibrium point. It is reasonable that we develop a bifurcation subsystem identification algorithm according to the magnitude of the right eigenvector. We can find a non-singular similarity transformation L, which will reorder the rows and columns of matrix $A - j\omega_0 I$ and eigenvector w_i such that bifurcation subsystem and geometric

decoupling conditions (4.2.3), (4.2.4) hold for the reordered system. The similarity transformation matrix L satisfies:

$$L^{-1} = L^T$$

The following proposition is required before giving the bifurcation subsystem identification algorithm.

Proposition 4.2.1 The full system undergoes a bifurcation, i.e., (4.2.1) is satisfied, if and only if the reordered system bifurcates.

Proof:

The reordering process is realized by pre-multiplying w_i by the unitary transformation matrix L, and pre-multiplying and post-multiplying A by L, which gives:

$$A' = L^{-1}AL$$
$$w_i' = L^{-1}w_i$$

where A' and w_i' are the reordered Jacobian and right eigenvector, respectively. Then the reordered system undergoes a bifurcation if:

$$(A' - j\omega_0 I)w_i' = 0$$

We also have:

$$\begin{aligned}(A' - j\omega_0 I)w_i' &= L^{-1}ALL^{-1}w_i - j\omega_0 L^{-1}w_i \\ &= L^{-1}Aw_i - j\omega_0 L^{-1}w_i \\ &= L^{-1}(A - j\omega_0 I)w_i \\ &= 0\end{aligned}$$

when bifurcation occurs. Since the unitary matrix L is nonsingular and the right eigenvector is nonzero, it has been shown

$$(A' - j\omega_0 I)w_i' = 0 \iff (A - j\omega_0 I)w_i = 0 \tag{4.2.5}$$

This assures that we are able to develop the bifurcation identification algorithm that searches for the bifurcation subsystem based on a reordered state matrix A' and w_i' where the elements of w_i' are ordered based on their magnitude so that the j^{th} largest element of w_i is $\{w_i'\}_j$. This process can be performed by pre-multiplying a series of similar transformation matrix L_1, L_2, $\cdots$, L_k, $0 \leq k \leq n$, and $L = L_1 L_2 \cdots L_k$, as indicated above.

Correspondingly, the reordering process for A should be performed so that all the rows and columns of A are reordered as above.

Define:

$$N_i^k = \| (A_{11}^k - j\omega_0 I)u_i^k \| \tag{4.2.6}$$

$$C_i^k = \| A_{12}^k (A_{22}^k - j\omega_0 I)^{-1} A_{21}^k u_i^k \| \tag{4.2.7}$$

$$R_i^k = \frac{N_i^k}{C_i^k} \tag{4.2.8}$$

where $k = 1, 2, \cdots, n$ which denote the k^{th} order partition of $A = \begin{bmatrix} A_{11}^k & A_{12}^k \\ A_{21}^k & A_{22}^k \end{bmatrix}$ so that A_{11}^k is k^{th}-order square matrix, and if the saddle-node bifurcation occurs, just set $\omega_0 = 0$.

N_i^k is a norm of the k-dimensional vector that measures how close the subsystem A_{11} for the i^{th} bifurcation mode is to experiencing the bifurcation. C_i^k is a norm of the k-dimensional vector and measures how small the coupling is between the k^{th}-order subsystem and the $(n-k)^{th}$-order external system for this i^{th} bifurcation mode.

Performing a series of tests on the reordered system will find a slow subsystem of the full system that has bifurcation and is decoupled from the remainder of the full system. The bifurcation subsystem identification algorithm is given here.

Algorithm 4.2.1 Bifurcation Subsystem Identification Algorithm:

1. Sort the right eigenvector based on the magnitude of each element. The element with the largest magnitude would have the smallest indices, and the element with smallest magnitude would have the largest indices in the sorted eigenvector w_i'.

2. Reorder the state matrix A by exchanging the corresponding rows and columns as performed to produce w_i' from w_i.

3. Let $k = 1$ calculate N_i^k and C_i^k using (4.2.6) and (4.2.7), respectively.

4. If both N_i^k and C_i^k are sufficiently small the bifurcation subsystem condition and geometric decoupling condition will be satisfied, thus the k^{th}-ordered system is a bifurcation subsystem. If not, set $k = k + 1$ and test the $(k+1)^{th}$-ordered subsystem using (4.2.6) and (4.2.7).

5. If $k > n$ and N_i^k and C_i^k are not sufficiently small the bifurcation subsystem identification algorithm fails.

6. End

The measure to decide what is producing the bifurcation is the ratio R_i^k. Note that $R_i^k = 0$ occurs when the real part of the eigenvalue of A_{11} is zero and bifurcation subsystem condition is satisfied. If A_{11} is singular, then the development of geometric decoupling which produces the bifurcation in the subsystem will also produce the bifurcation in the full system.

If $R_i^k \gg 1$ when the real part of the eigenvalue λ_i approaches zero, the bifurcation subsystem condition is not satisfied. Then the development of the bifurcation in the subsystem A_{11}^k produces the bifurcation subsystem and produces the bifurcation of the full system.

If $R_i^k \approx 1$ when the real part of the eigenvalue λ_i approaches zero, then both geometric decoupling condition and bifurcation subsystem condition develop together to produce the bifurcation subsystem and produce the bifurcation in the full system.

Remarks:

1. Bifurcation subsystem condition and geometric decoupling condition suggest the use of only one of the conjugate eigenvectors in the case of Hopf bifurcation. This is because we are testing the magnitude of $(A'_{11} - j\omega_0 I)u'_i$ and $A'_{12}(A'_{22} - j\omega_0 I)^{-1}A'_{21}u'_i$, and from Proposition 3.6.1 we know the magnitude of time response is determined by only the magnitude of the right eigenvector.

2. The bifurcation subsystem has been proven to experience, produce, and cause the bifurcation in the system model. The bifurcation subsystem experiences, produces, and causes the bifurcation because:

   (a) the bifurcation subsystem condition is satisfied which is a test for bifurcation in the bifurcation subsystem when the external system is assumed slow ($y = y_0$). The persistence of saddle-node and Hopf bifurcation are proven in Chapter 2, and 3 when external subsystem is slow.

   (b) the geometric decoupling condition and bifurcation subsystem condition together assure that the full system experiences bifurcation when the external subsystem is simultaneously both fast and slow. This is also proven in Chapter 2, and 3, along with the persistence of bifurcation in both the cases when the external subsystem is fast and when the external system

is slow. Thus, the bifurcation persists in the bifurcation subsystem.

The external system is considered to be simultaneously fast and slow requires the simultaneous satisfaction of bifurcation subsystem condition and geometric decoupling condition. Bifurcation is proven to occur in the bifurcation subsystem A_{11} simultaneously with that of the full system A given that the external system is slow. Given that the external system is assumed to be slow (requires testing for singularity of A_{11}) and simultaneously be fast (requires testing of singularity of $A_{11} - A_{12}A_{22}^{-1}A_{21}$), then one assures the geometric decoupling condition to be satisfied along with the bifurcation subsystem condition. This assures the external system does not respond as observed by the bifurcation subsystem when the bifurcation subsystem is experiencing bifurcation.

Thus assuming the external system is fast and slow when bifurcation occurs in the system, which is used to prove bifurcation subsystem and geometric decoupling conditions in turn justifies the assumption that the external subsystem is slow because it either does not respond, and thus is not observed by the bifurcation subsystem, or is fast to show it can respond, but is not observed by the bifurcation subsystem. The theorems in next section will clarify when external system does not respond and when it will respond and yet not be observed by the bifurcation subsystem.

(c) the change in the geometric decoupling and/or the bifurcation subsystem conditions whether it is solely the geometric decoupling condition, the bifurcation subsystem condition, or both that produces the bifurcation in the bifurcation subsystem and full system.

(d) the cause of the bifurcation in the full system is the operating change, equipment outage, or combination that results in the bifurcation subsystem condition change, the geometric decoupling condition change, or both

that produce the bifurcation in the full system.

4.3 Extension of Bifurcation Subsystem and Geometric Decoupling Conditions

Theorem 4.3.1 Assuming the system matrix is reordered based on the magnitude of the right eigenvector elements at the bifurcation point, the bifurcation subsystem identification algorithm will find the bifurcation subsystem if $A_{22} - j\omega_0 I$ is nonsingular and A_{21} is column dependent such that $A_{21}u_i = 0$.

Proof:

When the saddle bifurcation occurs to the full system the Jacobian satisfies

$$\begin{bmatrix} A_{11} & A_{12} \\ A_{21} & A_{22} \end{bmatrix} w_i = \lambda_i(\mu) w_i = 0 \tag{4.3.9}$$

where $\lambda_i(\mu)$ is the bifurcating eigenvalue, μ is the bifurcation parameter, and $w_i = \begin{bmatrix} u_i \\ y_i \end{bmatrix}$ is the corresponding eigenvector.

From equation (4.3.9) we have

$$A_{11}u_i + A_{12}y_i = 0 \tag{4.3.10}$$

$$A_{21}u_i + A_{22}y_i = 0 \tag{4.3.11}$$

It will now be proven that both the bifurcation subsystem condition and geometric decoupling condition are satisfied.

If A_{21} is column dependent such that $A_{21}u_i = 0$, equation (4.3.11) gives

$$A_{22}y_i = 0$$

which implies $y_i = 0$ since A_{22} is nonsingular. Thus, equation (4.3.10) yields

$$A_{11}u_i = 0 \tag{4.3.12}$$

The bifurcation subsystem condition is satisfied.

Also, we have

$$y_i = -A_{22}^{-1}A_{21}u_i = 0$$

Therefore,

$$A_{12}y_i = -A_{12}A_{22}^{-1}A_{21}u_i = 0 \tag{4.3.13}$$

Equation (4.3.13) shows that the geometric decoupling condition holds.

The combination of equation (4.3.12) and (4.3.13) assures the existence of the saddle bifurcation subsystem. Therefore, ranking the magnitude of right eigenvector elements will identifying the bifurcation subsystem since the ranking of w_i will often identify a bifurcation subsystem because often $y_i = 0$ outside the bifurcation subsystem and $u_i \neq 0$ inside the bifurcation subsystem.

In the case of Hopf bifurcation condition (4.3.9) is satisfied for $\lambda_i = \pm j\omega_0$ and it can be rewritten as

$$\begin{bmatrix} A_{11} - j\omega_0 I & A_{12} \\ A_{21} & A_{22} - j\omega_0 I \end{bmatrix} \begin{bmatrix} u_i \\ y_i \end{bmatrix} = 0 \tag{4.3.14}$$

which gives

$$\begin{aligned}(A_{11} - j\omega_0 I)u_i + A_{12}y_i &= 0 \\ A_{21}u_i + (A_{22} - j\omega_0 I)y_i &= 0\end{aligned}$$

If A_{21} is column dependent such that $A_{21}u_i = 0$ we have $(A_{22} - j\omega_0 I)y_i = 0$ and $y_i = 0$ if $(A_{22} - j\omega_0 I)$ is nonsingular. Therefore,

$$[A_{11} - j\omega_0 I]u_i = 0$$

which implies the bifurcation subsystem condition holds.

On the other hand $A_{21}u_i = 0$ can be rewritten as

$$-A_{12}(A_{22} - j\omega_0 I)^{-1}A_{21}u_i = 0$$

and the geometric decoupling condition is thus satisfied. Therefore, the ranking of magnitude of right eigenvector will identify the Hopf bifurcation subsystem.

The right eigenvector is the approximation of the center manifold because the right eigenvector is tangent to the center manifold at the equilibrium point. The right eigenvector indicates the direction in which the center manifold trajectories approach the equilibrium point. When $y_i = 0$, the center manifold is totally included in the bifurcation subsystem. The external subsystem thus does not include any information on center manifold, and the bifurcation subsystem contains the center manifold.

Having completed the proof of Theorem 3.1 the discussion is resumed with $\omega_0 = 0$ for saddle-node bifurcation even though the discussion can be extended to Hopf bifurcation ($\omega_0 \neq 0$). The bifurcation subsystem not only experiences bifurcation due to the bifurcation subsystem condition ($A_{11}u_i = 0$), but also produces the bifurcation

in the full system due to geometric decoupling ($A_{12}A_{22}^{-1}A_{21}u_i = 0$) between the bifurcation subsystem and the external subsystem. In the case where $y_i = 0$, the external system does not respond at all to the bifurcation because $A_{21}u_i = 0$ which results in geometric decoupling ($A_{12}A_{22}^{-1}A_{21}u_i = 0$) without allowing response ($y_i = -A_{22}^{-1}A_{21}u_i$) in the external system. This special case more clearly points out the role of the bifurcation subsystem, i.e., a subsystem that experiences, produces, and causes the bifurcation in the system and center manifold. The bifurcation parameter change that causes bifurcation to occur in the full system is either in A_{11}, or A_{21}, or both (which represents the internal bifurcation subsystem dynamics and its coupling to the external system). The above discussion can be generalized for Hopf bifurcation.

If the dimension of A_{11} is not 1, we have a bifurcation subsystem with larger dimensions than the center manifold. This suggests the center manifold is oriented within the bifurcation subsystem so that all parameters in matrices A_{11} and A_{12} in the bifurcation subsystem play a role when bifurcation develops along the center manifold and in the full system model. The advantage that $y_i = 0$ occurs is that all the parameters that may affect the bifurcation subsystem lie within the bifurcation subsystem or its boundary. Moreover, a minimum and maximum estimate for the bifurcating eigenvalue of A_{11} may be developed [22] that determines the structural parameters of A_{11} and A_{21} which play an important role of causing bifurcation in this case. All this information will generally be lost by using a nonlinear transformation to obtain center manifold dynamics as the approximation of the full system dynamics.

The maximum estimate for the bifurcating eigenvalue of A_{11} is a measure of the satisfaction of geometric decoupling condition in the loadflow model [7]. The minimum estimate of the bifurcating eigenvalue measures the satisfaction of bifurcation subsystem condition in the loadflow model [7]. Both need to approach zero to assure the existence of bifurcation subsystem. Similar results may be derived in a differential

or differential algebraic model if maximum and minimum estimate of the bifurcating eigenvalues of bifurcation subsystem are derived and the loadflow model based diagnostic methods for identifying causes and cures of bifurcation are applied to these eigenvalues estimates.

When $y_i = -A_{22}^{-1}A_{21}u_i \neq 0$ because $A_{21}u_i \neq 0$, geometric decoupling condition $A_{12}A_{22}^{-1}A_{21}\ u_i = 0$ can still hold if $A_{12}y_i = 0$, A_{22}^{-1} is very small in some direction, or a combination of column dependency of A_{21}, column dependency of A_{12}, and smallness of A_{22}^{-1} occurs in some direction associated with the right eigenvector of the bifurcating eigenvalue of the bifurcation subsystem $\Delta\dot{x}_1 = A_{11}\Delta x_1$. The bifurcation subsystem still experiences bifurcation due to the bifurcation subsystem condition, still produces the full system bifurcation because the geometric decoupling condition holds ($A_{12}A_{22^{-1}}A_{21}u_i = 0$) even though $y_i \neq 0$ but now

1. $y_i \neq 0$ implies the external system responds to the bifurcation (it may respond more than the bifurcation subsystem $\| y_i \| > \| u_i \|$ if condition in Theorem 4.3.2 holds) and thus the energy of center manifold dynamics leaks out of the bifurcation subsystem due to strong coupling to the external system dynamics

   .

2. The external system model A_{22} and the coupling matrix A_{12} can also determine when geometric decoupling is satisfied and not just A_{21}. This does not imply that the external system model dynamics described by A_{22} is always expected to play a major role in determining when the geometric decoupling condition holds. The experience is that it can but generally column dependency of A_{21} ($A_{21}u_i = 0$) or column dependence of A_{12} ($A_{12}y_i = 0$) is the cause of geometric decoupling.

3. If y_i is large as may be possible from Theorem 4.3.2, the bifurcation subsystem still provided accurate assessment of the subsystem experiencing and

For

man

$j\omega_0$.

bifur

real a

When

decou

If A_{21}

and A_{2}

producing the bifurcation even though the modal shape (magnitude of the right eigenvector) that reflects response due to the bifurcation is large outside the bifurcation subsystem. Theorem 4.3.2 and Theorem 4.3.3 explain why this is possible and why the use of modal analysis to explain why instability occurs can be misleading.

For Hopf bifurcation, it will be proven that one can describe the surface of center manifold by the real and imaginary parts of right eigenvector for eigenvalue $\lambda_i = j\omega_0$, rather than determining the eigenvectors for both $j\omega_0$ and $-j\omega_0$. When Hopf bifurcation occurs, the center manifold is the surface that can be described by the real and imaginary parts of the eigenvector, which can be determined by

$$\begin{aligned}(A_{11} - j\omega_0 I)(Re\{u_i\} + jIm\{u_i\}) + A_{12}(Re\{y_i\} + jIm\{y_i\}) &= 0 \\ A_{21}(Re\{u_i\} + jIm\{u_i\}) + (A_{22} - j\omega_0 I)(Re\{y_i\} + jIm\{y_i\}) &= 0\end{aligned}$$

When A_{21} is column dependent the bifurcation subsystem condition, and geometric decoupling condition are both satisfied.

If A_{21} is column dependent such that

$$A_{21}(Re\{u_i\} + jIm\{u_i\}) = 0$$

and $A_{22} - j\omega_0 I$ is nonsingular it is required that

$$(A_{22} - j\omega_0 I)y_i = (A_{22} - j\omega_0 I)(Re\{y_i\} + jIm\{y_i\}) = 0$$

that implies

$$\begin{aligned} Re\{y_i\} &= 0 \\ Im\{y_i\} &= 0 \end{aligned} \tag{4.3.15}$$

or just $y_i = 0$. If $y_i = 0$, then

$$(A_{11} - j\omega_0 I)u_i = (A_{11} - j\omega_0 I)(Re\{u_i\} + jIm\{u_i\}) = 0$$

which results

$$\begin{aligned} A_{11}Re(u_i) + \omega_0 Im(u_i) &= 0 \\ A_{11}Im(u_i) - \omega_0 Re(u_i) &= 0 \end{aligned} \tag{4.3.16}$$

The geometric decoupling condition simply becomes

$$A_{21}Re(u_i) = 0$$

$$A_{21}Im(u_i) = 0$$

This again requires the real and imaginary parts of u_i and y_i satisfy the specific conditions for the Hopf bifurcation in the bifurcation subsystem. These conditions are based on only one eigenvalue $\lambda_i = j\omega_0$ rather than both $\lambda_i = j\omega_0$ and $\lambda_{i+1} = -j\omega_0$. Since the above conditions (4.3.15) and (4.3.16) are satisfied for λ_{i+1} the center manifold may be determined solely based on one eigenvector w_i since $Re\{w_i\}$ and $Im\{w_i\}$ are orthogonal and describe the surface of the orbit produced at bifurcation point. The bifurcation subsystem and geometric decoupling conditions were broken into real and imaginary parts conditions. Then the bifurcation subsystem is also determined by just one eigenvector. When $y_i = 0$, the real and imaginary parts of

eigenvector tell us if the center manifold is inside the bifurcation subsystem or not. This again shows that the external subsystem does not experience, produce, or cause bifurcation, and the bifurcation subsystem contains the center manifold orbit.

Theorem 4.3.2 The ranking of the right eigenvector elements in Algorithm 4.2.1 is incorrect for identifying the bifurcation subsystem if

$$\underline{\sigma}(A_{21}) \geq m\sqrt{\min(n-m,m)}\,\bar{\sigma}(A_{22} - j\omega_0 I)$$

where $\underline{\sigma}$ and $\bar{\sigma}$ represent the minimum and maximum singular values, n is the dimension of right eigenvector w_i, and m is the dimension of y_i.

Proof:

The singular value decomposition of A_{21} is given by

$$A_{21} = U \begin{bmatrix} \Sigma & 0 \\ 0 & 0 \end{bmatrix} V^H$$

where U, V are $m \times m$, $(n-m) \times (n-m)$ unitary matrix, respectively. $\Sigma = diag(\sigma_1, \sigma_2, ...\sigma_t), t \in [1, \min(m, n-m)]$.

Define A_{21}^+ as Moore-Penrose generalized inverse of A_{21}

$$A_{21}^+ = V \begin{bmatrix} \Sigma^{-1} & 0 \\ 0 & 0 \end{bmatrix} U^H$$

Therefore, when $\omega_0 = 0$ from equation (4.3.11) we have

$$u_i = -A_{21}^+ A_{22} y_i$$

Taking 2-norm of both sides gives

$$\begin{aligned} \| u_i \|_2 &= \| -A_{21}^{+} A_{22} y_i \|_2 \\ &\leq \| A_{21}^{+} \|_F \cdot \| A_{22} \|_F \cdot \| y_i \|_2 \\ &= \| V \begin{bmatrix} \Sigma^{-1} & 0 \\ 0 & 0 \end{bmatrix} U^H \|_F \cdot \| A_{22} \|_F \cdot \| y_i \|_2 \end{aligned}$$

i.e.,

$$\| u_i \|_2 \leq \| V \begin{bmatrix} \Sigma^{-1} & 0 \\ 0 & 0 \end{bmatrix} U^H \|_F \cdot \| A_{22} \|_F \cdot \| y_i \|_2 \tag{4.3.17}$$

Since V, U are unitary matrices equation (4.3.17) can be rewritten as

$$\| u_i \|_2 \leq \| \begin{bmatrix} \Sigma^{-1} & 0 \\ 0 & 0 \end{bmatrix} \|_F \cdot \| A_{22} \|_F \cdot \| y_i \|_2 \tag{4.3.18}$$

The following vector and matrix norm inequalities, which hold strictly

$$\| a \|_{max} \leq \| a \|_2 \leq \sqrt{m} \| a \|_{max}$$

$$\bar{\sigma}(A) \leq \| A \|_F \leq \sqrt{\min(l, m)}\, \bar{\sigma}(A)$$

where a is m-dimensional vector, and A is $l \times m$ matrix, will be used to complete the proof. We thus have

$$\| \begin{bmatrix} \Sigma^{-1} & 0 \\ 0 & 0 \end{bmatrix} \|_F \leq \sqrt{\min(n-m, m)}\, \bar{\sigma}(\begin{bmatrix} \Sigma^{-1} & 0 \\ 0 & 0 \end{bmatrix}) \tag{4.3.19}$$

$$\| A_{22} \|_F \leq \sqrt{\min(m, m)}\, \bar{\sigma}(A_{22}) \tag{4.3.20}$$

$$\| y_i \|_2 \leq \sqrt{m} \| y_i \|_{max} \tag{4.3.21}$$

Subs

Noti

we h

Since

Ineq

i.e.,

If

then

Substituting equations (4.3.19), (4.3.20), and (4.3.21) into (4.3.18) yields

$$\| u_i \|_2 \leq \sqrt{\min(n-m,m)}\ \bar{\sigma}\left(\begin{bmatrix} \Sigma^{-1} & 0 \\ 0 & 0 \end{bmatrix}\right)\sqrt{m}\ \bar{\sigma}(A_{22})\sqrt{m}\ \| y_i \|_{max}$$

Noting that

$$\| a \|_{max} \leq \| a \|_2$$

we have

$$\| u_i \|_{max} \leq m\sqrt{\min(n-m,m)}\ \bar{\sigma}\left(\begin{bmatrix} \Sigma^{-1} & 0 \\ 0 & 0 \end{bmatrix}\right)\ \bar{\sigma}(A_{22})\ \| y_i \|_{max} \tag{4.3.22}$$

Since $\Sigma = diag(\sigma_1, \sigma_2, ...\sigma_t)$ it is clear that

$$\bar{\sigma}\left(\begin{bmatrix} \Sigma^{-1} & 0 \\ 0 & 0 \end{bmatrix}\right) = \frac{1}{\underline{\sigma}\left(\begin{bmatrix} \Sigma & 0 \\ 0 & 0 \end{bmatrix}\right)} = \frac{1}{\underline{\sigma}(A_{21})}$$

Inequality (4.3.22) becomes

$$\| u_i \|_{max} \leq m\sqrt{\min(n-m,m)}\frac{1}{\underline{\sigma}(A_{21})}\bar{\sigma}(A_{22})\ \| y_i \|_{max}$$

i.e.,

$$\frac{\| u_i \|_{max}}{\| y_i \|_{max}} \leq m\sqrt{\min(n-m,m)}\frac{\bar{\sigma}(A_{22})}{\underline{\sigma}(A_{21})}$$

If

$$\underline{\sigma}(A_{21}) \geq m\sqrt{\min(n-m,m)}\bar{\sigma}(A_{22}) \tag{4.3.23}$$

then

$$\| u_i \|_{max} \leq \| y_i \|_{max}$$

must hold when the bifurcation occurs.

Therefore, the algorithm based on the ranking of the right eigenvector to identify the bifurcation subsystem will not generate the bifurcation subsystem correctly if inequality (4.3.23) is satisfied.

This result suggests that even though the right eigenvector is tangent to the center manifold at the equilibrium point it may not predict the dynamics that experience, produce, and cause the bifurcation. It is expected that the center manifold expressed in the nonlinearly transformed variables has 1 nonzero state for saddle-node bifurcation and 2 nonzero states for Hopf bifurcation. The bifurcation in the physical variables is not necessarily so clear and can be totally misleading. The center manifold lies in the bifurcation subsystem since the dynamic properties and center manifold are preserved in A_{11}, but may not contain the states where their responses are most clearly observed. This is the first theory known to suggest that this is possible.

The coupling of multiple interarea modes was observed in [25] where it is shown that the dominant part of the right eigenvectors of all coupled modes indicate the subspace of the system that experiences these oscillations, and that the right eigenvector for any individual mode does not provide this information.

Nonlinear modal coupling is known to distort the behaviors that are predicted by its linear behavior [15]. The modal coupling may be explained solely by the overlapping of bifurcation subsystems (where the bifurcation subsystems for two modes may have common states). It may be possible that modal coupling could occur when bifurcation subsystems do not overlap if their responses caused resonance outside their bifurcation subsystem as indicated in Theorem 3.2.

These effects could be investigated in future research.

Theorem 4.3.3 The bifurcation subsystem condition and the geometric decoupling condition hold when full system bifurcates if $A_{22} - j\omega_0 I$ is nonsingular and A_{12} is column dependent such that

$$\| A_{12} y_i \| = 0$$

Proof:

When the full system bifurcates equation (4.3.11) gives

$$y_i = -(A_{22} - j\omega_0)^{-1} A_{21} u_i$$

if $A_{22} - j\omega_0 I$ is nonsingular. Since A_{12} is column dependent such that

$$\| A_{12} y_i \| = 0$$

when $\omega_0 = 0$. We obtain

$$A_{12} A_{22}^{-1} A_{21} u_i = 0 \tag{4.3.24}$$

which tells that geometric decoupling condition is satisfied.

According to Schur's theorem, the bifurcation of full system occurs when

$$A_{11} u_i - A_{12} A_{22}^{-1} A_{21} u_i = 0 \tag{4.3.25}$$

From equation (4.3.24) and (4.3.25)

$$A_{11} u_i = 0 \tag{4.3.26}$$

i.e., the bifurcation subsystem condition is also satisfied.

Equations (4.3.24) and (4.3.25) assure the existence of bifurcation subsystem which experience, produces, and causes the bifurcation. When A_{12} is column independent

in the direction of y_i, bifurcation subsystem and geometric decoupling conditions can still be satisfied due to matrices A_{12}, A_{22}, A_{21}, or the combination of the matrices. It is hoped that this condition is the most common manner for producing bifurcation subsystems because it will likely identify very small-dimensional subsystems since the number of rows of A_{12} is very small and the number of columns is very large. This should make it relatively easy to find bifurcation subsystem based on $A_{12}y_i = 0$.

Theorem 4.3.4 When the smallest singular value of $A_{22} - j\omega_0 I$ is much more greater than the sum of magnitude of elements in A_{21}, i.e.,

$$\underline{\sigma}(A_{22} - j\omega_0 I) \gg \sqrt{m} \parallel A_{21} \parallel_{sum} \tag{4.3.27}$$

and $\parallel A_{12} \parallel \ll 1$, then the bifurcation subsystem exists.

Proof:

When the bifurcation occurs in the full system, equation (4.3.11) gives

$$y_i = -A_{22}^{-1} A_{21} u_i$$

when $\omega_0 = 0$, Taking 2-norm of both sides gives

$$\begin{aligned} \parallel y_i \parallel_2 &= \parallel A_{22}^{-1} A_{21} u_i \parallel_2 \\ &\leq \parallel A_{22}^{-1} \parallel_F \cdot \parallel A_{21} \parallel_F \cdot \parallel u_i \parallel_2 \\ &\leq \sqrt{\min(m,m)}\, \bar{\sigma}(A_{22}^{-1}) \parallel A_{21} \parallel_F \cdot \parallel u_i \parallel_2 \\ &= \sqrt{m} \frac{1}{\underline{\sigma}(A_{22})} \parallel A_{21} \parallel_F \cdot \parallel u_i \parallel_2 \end{aligned}$$

Since

$$\max(\bar{\sigma}(A), \parallel A \parallel_F, \parallel A \parallel_{i1}, \parallel A \parallel_{sum}) \leq \parallel A \parallel_{sum} \tag{4.3.28}$$

we have

$$\| y_i \|_2 \leq \frac{\sqrt{m} \| A_{21} \|_{sum}}{\underline{\sigma}(A_{22})} \| u_i \|_2$$

If $\underline{\sigma}(A_{22}) \gg \sqrt{m} \| A_{21} \|_{sum}$, therefore, $\| y_i \|_2 \ll \| u_i \|_2$.

Because w_i is unitary column vector we have $\| y_i \| \approx 0$, which implies that u_i is almost a unitary column vector. Since $\| A_{12} \|$ is very small by using a portion of proof of Theorem 4.3.1 we can conclude that the bifurcation subsystem and geometric decoupling conditions are both satisfied. Therefore, it will produce the bifurcation subsystem and this bifurcation subsystem can be identified by ranking the magnitude of elements in w_i.

Remarks:

1. Note Theorem 4.3.1 - 4.3.4 are stated generally for ω_0, but the proofs are given for $\omega_0 = 0$. The proofs hold for both Hopf ($\omega_0 \neq 0$) and saddle node ($\omega_0 = 0$) bifurcation.

2. It has been mentioned in Chapter 2 that external system dynamics is required to be both fast and slow for the definition of the bifurcation subsystem. This brings the question about the sequence for perturbation ϵ_1 and ϵ_2 to tend to zero. It should be noted that the perturbations do not tend to zero independently. For both saddle-node and Hopf bifurcations we first set $\epsilon_1 = 0$ in (2.2.4) and obtain the reduced system dynamics with extremely fast external dynamics, and the external dynamics can be ignored and it is represented by an algebraic model that can be absorbed into the internal system which is guaranteed by assuming the hyperbolicity of the external system and Implicit Function Theorem. This produces the slaving condition [27]. Then, we set $\epsilon_2 = 0$ to obtain the reduced system with constant external state variables, which ensures that the internal system experiences the bifurcation of

the full system. The result of $\epsilon_1 = 0$ and $\epsilon_2 = 0$ implies the geometric decoupling condition holds. The above theorems explore conditions for which the geometric decoupling condition holds and extend results of slaving [27], α-decomposition [22], modal analysis [12], and coherency reduction [14].

3. The theorems and their application will be further discussed in Chapter 5.

Chapter 5

Applications of Bifurcation Subsystem Method

5.1 Objective

In this chapter the bifurcation subsystem identification method derived in Chapter 4 is successfully applied to a two-area power system model. The bifurcation subsystem identification algorithm has been implemented in a Matlab program. Taking different parameters as the bifurcation parameter, a set of numeric examples are computed and presented in this chapter. The numeric examples here will hopefully provide significant benefits for the H_∞ controller design of power system due to the ability to protect the system from the bifurcation parameter changes that produce the instability in a specific bifurcation subsystem containing the center manifold dynamics.

This chapter is organized as follows: in section 5.2, the two-area system is described briefly. The scaling technique, which plays an important part in the application of bifurcation subsystem identification algorithm, is discussed in section 5.3. In

section 5.4 more discussions of how bifurcation subsystem develops is given. It will be shown that it requires much weaker conditions than that for slaving [27], α-decomposition [22] etc. It will also be shown that bifurcation subsystem existence is highly probable. For a single machine infinite bus system the stability depends on the synchronizing torque and damping torque, and a set of parameters K_1-K_6. This is briefly presented in section 5.5 since this could be extended to analysis for multimachine system. The Hopf bifurcation and saddle-node bifurcation examples and the classification of bifurcation are presented and discussed in section 5.6.

5.2 Two-area Example System

The two-area system is shown in Figure 5.1. Two generation and load areas are interconnected by two parallel transmission lines. There are two generators in each area. The generators and their controls are identical except that generator 3 (G3) has a power system stabilizer attached. The system is heavily stressed: it has 400MW flowing on the tie lines from area 1 to area 2. In all cases, the active load are modeled as 50% constant current and 50% constant impedance. The reactive loads are constant impedance. A Matlab program was developed to perform the system modeling and bifurcation subsystem identification. First the loadflow equation was solved. Then, the dynamic model of the two-area system was obtained by singular perturbed linearization. The states for each generator in the dynamic model are represented by the number given in Table 5.1. Variables number 1 to 6 are the states of the generators, 7 to 11 denote the states of excitation system, 12 to 14 the states of power system stabilizer, and 15 to 17 the states of turbine governor. All the detailed description of the states can be found in [34].

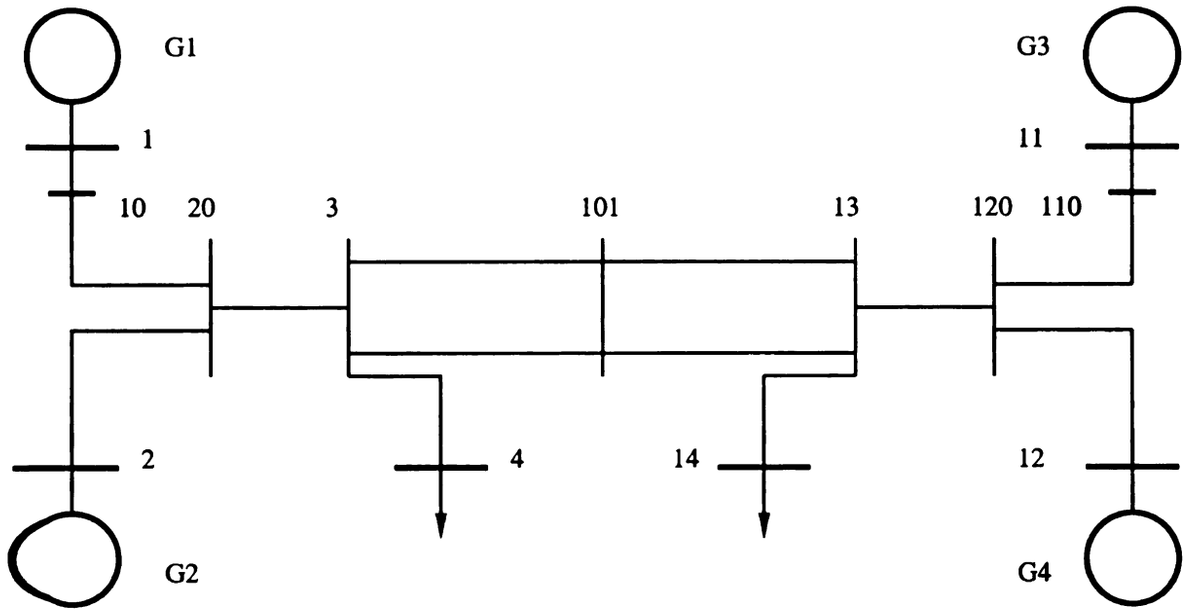

Figure 5.1: Diagram of Two-area Example System

Number	Variable	Power System State
1	δ	Machine angle
2	ω	Machine speed
3	E'_q	
4	ψ_{kd}	
5	E'_d	
6	ψ_{kq}	
7	V_{TR}	Voltage transducer output
8	V_{AS}	Regulator voltage state variable
9	V_R	Rugulator output voltage
10	E_{fd}	Exciter output voltage
11	R_f	Stabilizing transformer state
12	PSS_1	Washout state variable
13	PSS_2	First lead-lag compensator state variable
14	PSS_3	Second lead-lag compensator state variable
15	Tg_1	Governor state variable
16	Tg_2	Servo state variable
17	Tg_3	Reheater state variable

Table 5.1: States of Two-area System

5.3 Scaling

In power system analysis, it is usually convenient to use a per unit system to normalize the system variables [28]. Note that the state matrix and time must be properly scaled as indicated in [22] for the application of α-decomposition algorithm. The per unit system offers computational simplicity by eliminating units and expressing system quantities as dimensionless variables compared to the use of physical units.

$$\text{Quantity in per unit} = \frac{\text{Actual quantity}}{\text{Base value of quantity}}$$

A well-chosen per unit system not only can minimize the computational effort and simplify the evaluation, but also is necessary for the system performance analysis. For the purpose of control, the control variables should be normalized based on the expected range of their changes. Otherwise, the comparison of system performance of different control systems is obscured.

For example, the system frequencies should be maintained close to nominal. In most systems, turbine speed governors are set to have either 4% or 5% droop. This implies that the percentage change in speed for 100% (1 pu) change in system load is equal to the droop. Thus, in a 60Hz system with 4% droop , a 100% change in system load results in a steady state change in frequency of 2.4 Hz. The scaling plays a very important role in achieving success for the bifurcation identification algorithm.

5.4 More Discussions on Bifurcation Subsystem Method

In Chapter 4, the bifurcation subsystem and geometric decoupling conditions were extended. Before presenting the numerical examples we discuss the results in Chap-

ter 4 briefly since this discussion will help provide understanding of how and why bifurcation subsystems develop and that the existence of bifurcation subsystem for a full power system model is a high probability event. This discussion will help provide a foundation for understanding how and why an actual bifurcation subsystem develops in section 5.6 depends on all three causes of formation of a bifurcation subsystems developed in Chapter 4.

The results in Theorem 4.3.1 - 4.3.4 document different causes for producing a bifurcation subsystem. In Theorem 4.3.1 the column-dependency of A_{21} forces the external system eigenvector y_i to be zero. In this situation the external system does not respond to the bifurcation subsystem at all. All the information of the full system center manifold dynamics is then contained in the bifurcation subsystem. In this special case we can see all the parameters that may help cause bifurcation lie within the bifurcation subsystem.

If A_{12} is column-dependent, the geometric decoupling condition is satisfied immediately, i.e., the external system does respond and $y_i \neq 0$, but cannot be observed in the bifurcation subsystem. This can be seen in Theorem 4.3.3. The condition $y_i = 0$ is thus not necessary for the bifurcation subsystem condition and geometric decoupling condition to hold. This becomes obvious in Theorem 4.3.2. If the external subsystem is changing very slowly, the external system may not only respond to the bifurcation subsystem, but the magnitude of the external system response may be larger than the internal system response ($\| y_i \| > \| u_i \|$). The bifurcation subsystem and external system must be coupled strongly and the external system response must be slow or weak for $\| y_i \| > \| u_i \|$. As Theorem 4.3.2 indicates, the ranking of bifurcation subsystem identification algorithm fails when $\| y_i \| > \| u_i \|$. A modified bifurcation subsystem method would need to be developed to handle this case.

Theorem 4.3.4 states that if the external system is very fast and the coupling between the internal and external systems is weak, the bifurcation subsystem exists and the internal system is the bifurcation subsystem.

Theorem 4.3.4 is actually the generalization of Haken's slaving principle [27]. In [27] the slaving principle is applicable when the external system is extremely fast (A_{22} is very large); and the coupling between external and internal systems is weak (this could be shown to correspond to regular A_{22} to be large and A_{12} and A_{21} are small); and the internal system is very slow. Thus, the external system is totally slaved by the internal system. Consequently, the full system dynamics is dominated by the internal system.

From Theorem 4.3.4 it is clear that the occurrence of slaving could be the precursor of the existence of the bifurcation subsystem provided that A_{22} is invertible since in this situation the slaving system (the slow internal subsystem) must be the bifurcation subsystem. When slaving occurs, the full system dynamics is totally determined by internal system. On the other hand, the bifurcation subsystem, which can contain the center manifold of the full system, is not just trying to dominate the full system dynamics, but contains the unstable dynamics which experiences, produces, causes, and can cure the bifurcation in the full system.

In [22] the successful application of α-decomposition, which transforms a class of autonomous linear systems into a clustered semi-decoupled dynamic model that approximates a block diagonal matrix, reveals that the weak boundary can be eliminated without changing the system dynamics in the sense that the lower and upper bounds of eigenvalues the decomposed state matrix can be considered constant. The α-decomposed system includes the intercluster (usually slow) dynamics and intracluster (usually fast) dynamics which are respectively weakly decoupled. From Theorem 4.3.1 and 4.3.3, we can conclude that the bifurcation of the full system can be caused

by the weak boundary between fast external system and slow internal system. When α-decomposition is applicable, the system has weak boundaries between subsystems. This indicates the property of power systems. Therefore, the bifurcation subsystem method is a good method to study these complex system dynamics.

Theorems in Chapter 4 indicate the special cases when a bifurcation can occur. The extreme sparse nature of the power systems makes it easier to obtain column-dependent A_{12} and A_{21}. The power system may consists of 10,000 interconnected buses and 1,000 generators, where no more than five interconnections can be connected at any bus. Moreover, there are numerous weak boundaries in this sparse network. This has been verified by the successful applications of α-decomposition [22]. A typical state matrix for the two-area system is shown in Appendix B.

To make this point clear, we will show that the satisfaction of linear dependence condition of A_{12} in Theorem 4.3.1 is highly probable. Suppose the probability for each element of the state matrix A_{12} to be zero or nonzero is $\frac{1}{2}$. For a 2×2 matrix $A_{12} = \begin{bmatrix} * & * \\ * & * \end{bmatrix}$, the column dependent cases are

$$\begin{bmatrix} 0 & * \\ 0 & * \end{bmatrix}, \begin{bmatrix} * & 0 \\ * & 0 \end{bmatrix}, \begin{bmatrix} 0 & 0 \\ 1 & 1 \end{bmatrix}, \begin{bmatrix} 1 & 1 \\ 0 & 0 \end{bmatrix}$$

where $*$ represents zero or nonzero elements, 0 the zero elements, and 1 the nonzero elements only.

From left to right, the number of column dependence cases are 4, 3 (because of one repeated case), 1, and 1. Thus, it is easy to verify that the probability of column dependence of a 2×2 matrix is 9/16. If we consider a 2×3 matrix by adding one more column, the probability of getting column dependence will increase to 52/64. The sparse nature of the power system will make the column dependence a very high

probability event provided the number of columns of A_{12} is sufficiently large (this is true for A_{12}). Thus it should be relatively easy to find a bifurcation subsystem for any system where A_{12} has few rows and a sufficient number of columns and is relatively sparse.

5.5 Effects on Power System Stability for SMIB Model

It has been well known that the dynamic behavior of the machine is quite different under different operating conditions. Parameters K_1 to K_6 change with loading characteristic and operating points for different machines. The definitions of K_1 to K_6 and these can be found in [16].

A brief review of synchronous and damping torque coefficients of SMIB model is given because the coefficient matrices for multiple machine models will be utilized in the subsequent results of this chapter.

At any oscillation frequency, the machine torque can be broken into synchronizing torque K_s, which is in phase with machine rotor angle δ, and damping torque K_d, which is in phase with machine rotor speed. This is broadly applied for stability study. Positive synchronizing torques are required to restore the rotor angle following an arbitrary small displacement of this angle, and positive damping torque is necessary to damp out any oscillation due to any perturbation. Therefore, a sufficient and necessary condition for system stability is that both synchronizing and damping torques are positive. For SMIB model both synchronizing and damping torque are determined by parameters K_1 to K_6. The coefficients of synchronizing and damping torque are listed in Table 5.2. where:

Lower Frequency ($\omega < 1$)		Higher Frequency($\omega \gg 1$)	
K_s	K_d	K_s	K_d
$K_1 - \frac{K_2 K_5}{K_6}$	$M \cdot F \cdot K_5$	$K_1 - \frac{K_2 K_3 K_4 b_3}{T_A T_F T_E T^2 \omega^2}$	$\frac{K_2 K_3 K_4}{\omega^2 T}$

Table 5.2: Net Synchronizing and Damping Torque for Type-1 Excitation

$$
\begin{aligned}
T &= T'_{do} K_3 \\
F &= \frac{K_a^2 K_2 K_3 K_4}{b_0^2 + b_1^2 \omega^2} \\
M &= \frac{K_F}{K_4} - K_3 K_6 \frac{K_F}{K_5}
\end{aligned}
$$

b_0, b_1, and b_3 are functions of a synchronous machine and excitation system parameters [16]. The stability of the SMIB system model depends completely on the signs of parameters K_1 to K_6.

Note Table 5.2 is based on SMIB model with a Type-1 excitation control system but there is also a formula for K_s and K_d for a thyristor based excitation system [16]. We are going to test if these conclusions still hold when bifurcation occurs to this two-area example system. There are K_1 to K_6 matrices in this system and it is assumed they are diagonally dominant so that change in a diagonal element which occurs on the element associated with a single machine, will cause saddle-node or Hopf bifurcation when K_s or K_d becomes zero or even negative, respectively on a specific machine. All the machines in the two-area example system have Type-1 excitation systems and this is why these formulas are appropriate. Only one example that corresponds to the local oscillation will be presented in section 5.6.9.

5.6 Bifurcation Subsystem Examples of Differential Model of Power System

The bifurcation subsystem method has been applied to the loadflow equation [7] to predict the discontinuous parameter and control changes that cause the bifurcation of particular eigenvalue of the loadflow Jacobian. The prediction is based on diagnosis of the analytical expressions for the upper and lower bound estimates of the bifurcating eigenvalue. The bifurcation subsystem method has also been successfully applied to power system network model to identify two classes of algebraic bifurcation and all the agents for each class [30].

In [3] a bifurcation identification method is applied to determine saddle-node and Hopf bifurcation subsystems in a SMIB model. The saddle-node bifurcation is caused by heavy local loading system stress, i.e., increasing the shunt inductance G_{sh}. When the power transferred to the infinite bus is gradually increased a Hopf bifurcation is produced. In comparison with a participation factor for a bifurcating eigenvalue, the bifurcation subsystem often gives a completely different information about states involved in the stability problem. On the other hand, participation factors indicate the states or subsystem to better observe and control the response of the system to the bifurcating eigenvalue and not the states or subsystem experiencing or producing the bifurcation observed in the full system.

The bifurcation can develop due to a number of causes such as equipment outages, faults, parameter changes, transient to steady state load model changes, disabling of excitation control when field current limiter fails due to oscillation in the system, or improperly designed control loops etc. The most important cases of improperly designed control loops are related to excitation system, governor control loops, and power system stabilizers. This will be presented in the examples on this two-area

example system model.

We are seeking the largest order bifurcation subsystem which satisfies the bifurcation subsystem and geometric decoupling conditions in order to be assured of including all the dynamics associated with the center manifold dynamics. Based on results obtained using bifurcation subsystem identification method:

1. as the order k of the subsystem increases to some number, both the values of N_k^i and C_k^i decrease until they become very small and approximately equal, which indicates the bifurcation subsystem condition and geometric decoupling condition are satisfied;

2. the values of N_k^i and C_k^i remain small as the model order continues to increase indicates the bifurcation subsystem condition and geometric decoupling condition remain satisfied;

3. after a certain order is reached, N_k^i and C_k^i start to increase and the bifurcation subsystem and geometric decoupling conditions are no longer satisfied.

We desire to determine the largest bifurcation subsystem since it should specify the most complete description of the dynamics that experience, produce, cause, and cure the bifurcation inside these dynamics.

The bifurcation of the system could be caused by several different parameters, such as changes of active power load, reactive power load, line reactance, generator reactance, power transfer between areas etc. Consequently, different bifurcation subsystems can be produced. These examples reveal what type and class of bifurcation subsystem will occur due to different bifurcation parameters, or agents with the same parameter changing at different buses, generators, or areas. The various classes of bifurcation are identified by the variables in the bifurcation subsystem. It will be found that (a) a bifurcation class, a bifurcation subsystem with a specific set of variables can

be produced by several bifurcation parameters; (b) there are many different bifurcation classes for the same type of bifurcation, and (c) that curing a bifurcation in a particular bifurcation class does not necessarily require reducing the bifurcation parameter that caused it, but another bifurcation parameter that produced that same bifurcation type and class.

The bifurcation subsystem method can identify the different classes of bifurcation (those with different variables in the bifurcation subsystem) as well as the agents for each bifurcation class (those with the same bifurcation subsystem but involving different generator, load, and network buses but the same oscillation in these devices).

The various types and classes of bifurcation are investigated as a function of the network, load or transfer level, and the load models. Two load models, steady-state and transient models, are possible. It will be shown in the following section that the steady-state model will produce saddle-node bifurcation and the transient model will produce Hopf bifurcation for a two-area multiple machine system. This result will be used to explain the blackouts in WSSC system [20] [23] [24]. It will also be noted that the type of bifurcation changes for both steady-state and transient time frame load models if the excitation system is disabled by over excitation protection.

Interarea and local oscillations refer to Hopf bifurcation. It will be shown that a local mode can be produced in this example system when very large transformer reactances are present. Otherwise, the interarea mode will be produced with different classes of bifurcation that are due to different control parameters used as bifurcation parameters.

It will be also shown the stress test on buses which are in coherent bus group in the algebraic model will produce exactly same type and class of dynamic bifurcation.

Singularity induced bifurcation has been observed in this example system as a special type of dynamic bifurcation. Although in this case it is difficult to apply bifurcation

subsystem identification algorithm due to numerical problem, it will be shown that the bifurcation subsystem still can be obtained.

The value of determining bifurcation classes is anticipated to be the ability to quickly prescribe the cures that are possible once the bifurcation type, class, and agent are identified. This anticipates that there are several agents with the same class of bifurcation as has been found in a loadflow model. Intelligent prescriptive control would first identify the type, class, and agent experiencing instability, identify constraints on control, and then quickly prescribes cure.

The bifurcation subsystem identification method developed in Chapter 4 is applied to the two-area example system with different bifurcation parameters.

5.6.1 Interarea Hopf Bifurcation: Active Power Load

The bifurcation parameter is the active power load. We ran PV-curves on several different buses in a coherent bus group to show that the same bifurcation subsystem in the differential equation model. Bus 3 was initially heavily stressed by adding active power load. The complete test results are summarized in Table 5.3 and 5.4. From Table 5.3 and 5.4 we can see that when the order of the system increases to and reaches 8 the bifurcation subsystem and geometric decoupling conditions can be considered to be finally satisfied since N_i^k, and C_i^k have decreased to a point where they can be considered small enough and equal so that a bifurcation subsystem can be assumed to exist. Having one or the other small just assures the geometric decoupling condition $(A_{12}(A_{22}-j\omega_0 I)^{-1}A_{21})$ or the bifurcation subsystem condition $(A_{11}-j\omega_0 I)$ holds, but for a bifurcation subsystem to exist $A_{11} - j\omega_0 I - A_{12}(A_{22} - j\omega_0 I)^{-1}A_{21}$ must be singular and that requires both C_i^k and N_i^k be small and equal. When the order of subsystem reaches 16, N_i^k, and C_i^k starts increasing dramatically. Therefore, the largest bifurcation subsystem is of order 15. The involved states in the largest

k	N_i^k	C_i^k	R_i^k	States involved
1	1.9504e+00	3.0640e+00	1.5710e+00	δ_4
2	2.7388e+00	3.0629e+00	1.1183e+00	δ_3
3	2.9900e+00	3.0611e+00	1.0237e+00	δ_1
4	3.0604e+00	3.0612e+00	1.0003e+00	δ_2
5	2.3585e+00	2.3593e+00	1.0004e+00	ω_4
6	1.3658e+00	1.3680e+00	1.0017e+00	ω_3
7	6.5272e-01	6.5693e-01	1.0065e+00	ω_1
8	2.0904e-02	7.7254e-02	3.6956e+00	ω_2
9	3.0027e-02	3.0083e-02	1.0019e+00	TG_3 at G1
10	3.0378e-02	3.0415e-02	1.0012e+00	V_R at G1
11	3.3701e-02	3.3735e-02	1.0010e+00	E_{fd} at G1
12	3.3706e-02	3.3754e-02	1.0014e+00	V_{AS} at G2
13	3.8093e-02	3.8144e-02	1.0014e+00	V_R at G4
14	3.8312e-02	3.8360e-02	1.0013e+00	V_R at G2
15	3.8560e-02	3.8607e-02	1.0012e+00	R_f at G1
16	1.9470e-01	1.9472e-01	1.0001e+00	E_{fd} at G4
17	1.9372e-01	1.9375e-01	1.0001e+00	ψ_{kd} at G3
18	1.9313e-01	1.9318e-01	1.0003e+00	E'_q at G3
19	1.9247e-01	1.9252e-01	1.0003e+00	V_{TR} at G1
20	1.9211e-01	1.9216e-01	1.0002e+00	E'_q at G2
21	1.9207e-01	1.9211e-01	1.0002e+00	V_{TR} at G2
22	1.8033e-01	1.8036e-01	1.0012e+00	R_f at G4
23	1.8016e-01	1.8020e-01	1.0002e+00	ψ_{kd} at G2
24	1.8016e-02	1.8020e-02	1.0002e+00	PSS_3 at G3
25	1.8016e-02	1.8019e-02	1.0002e+00	V_{TR} at G3
26	1.8007e-02	1.8008e-02	9.9995e-01	ψ_{kq} at G4
27	1.8006e-02	1.8005e-02	9.9990e-01	ψ_{kq} at G3
28	1.8000e-02	1.8004e-02	9.9989e-01	$E_{d'}$ at G4
29	1.7996e-02	1.7998e-02	9.9988e-01	ψ_{kq} at G2
30	1.7995e-02	1.7993e-02	9.9987e-01	ψ_{kd} at G1
31	1.7994e-02	1.7992e-02	9.9985e-01	ψ_{kq} at G3
32	1.7995e-01	1.7992e-01	9.9985e-01	PSS_2 at G3
33	1.7995e-01	1.7992e-01	9.9985e-01	E'_d at G3
34	1.7995e-01	1.7993e-01	9.9985e-01	$E_{d'}$ at G2
35	1.7992e-01	1.7990e-03	9.9987e-01	ψ_{kd} at G4
36	2.9112e-03	2.0161e-03	6.9254e-01	V_{TR} at G4
37	2.9400e-03	2.0573e-01	6.9978e-01	E'_d at G1
38	2.5455e-03	1.4435e-03	5.6708e-01	E'_q at G1
39	2.1026e-03	8.8266e-05	4.1980e-01	E'_q at G4
40	2.1026e-03	8.7707e-05	4.1714e-01	TG_1 at G4

Table 5.3: Increase Active Power Load on Bus 3

k	N_i^k	C_i^k	R_i^k	States involved
41	2.1026e-03	8.7160e-05	4.1454e-01	TG_1 at G3
42	2.1026e-03	8.6946e-05	4.1353e-02	TG_1 at G1
43	2.1020e-03	6.9138e-05	3.2892e-02	TG_2 at G4
44	2.1014e-03	4.5589e-05	2.1695e-02	TG_2 at G3
45	2.1012e-03	3.2041e-05	1.5249e-02	TG_2 at G1
46	2.1012e-03	3.1869e-05	1.5167e-02	TG_1 at G2
47	2.1011e-03	2.6542e-05	1.2630e-02	TG_2 at G2
48	2.1010e-03	2.4510e-05	1.1665e-02	TG_3 at G4
49	2.1010e-03	2.2358e-05	1.0642e-02	TG_3 at G3
50	2.1009e-03	7.1325e-06	3.3950e-03	PSS_1 at G3
51	2.1008e-03	3.4079e-06	1.6221e-03	TG_3 at G3
52	2.1008e-03	0	0	

Table 5.4: Increase Active Power Load on Bus 3 (continued)

bifurcation subsystem show that the inertial dynamics of all four generators are in the bifurcation subsystem and have the largest right eigenvector magnitudes. This is an interarea mode and not a local mode of oscillation since the frequency of oscillation is small. Moreover, it is hypothesized that this bifurcation is caused by excitation system on generator 1, 2, and 4, since V_R of generator 1, 2, and 4 are in the largest bifurcation subsystem. The stabilizer is also hypothesized to cause the bifurcation since states R_f and E_{fd} on generator 1 are in the largest bifurcation subsystem. The governor on generator 1 is also involved in the bifurcation subsystem since TG_3 on generator 1 is in the bifurcation subsystem.

In section 3 we discussed three cases when bifurcation subsystem exists, the measures of $A_{12}y_i$, $A_{21}u_i$, and $(A_{22}-j\omega_0 I)^{-1}A_{21}u_i$. In this typical example of Hopf bifurcation subsystem of order 15, we found that for $8 \leq k \leq 15$ the bifurcation subsystem existence was due to the smallness of of all three measures. It should be noted that $\| A_{21}u_i \|$ and $\| A_{12}y_i \|$ are large for $k < 8$ and become much more smaller for $8 \leq k \leq 15$. $\| y_i \| = \| (A_{22} - j\omega_0 I)^{-1}A_{21}u_i \|$ is small for $k < 8$ but becomes even smaller for $k > 8$, then keeps on decreasing with increasing k. At $k \geq 16$, $C_i^k = \| A_{12}y_i \|$ increases dramatically and does not decrease until $k > 34$. Then the

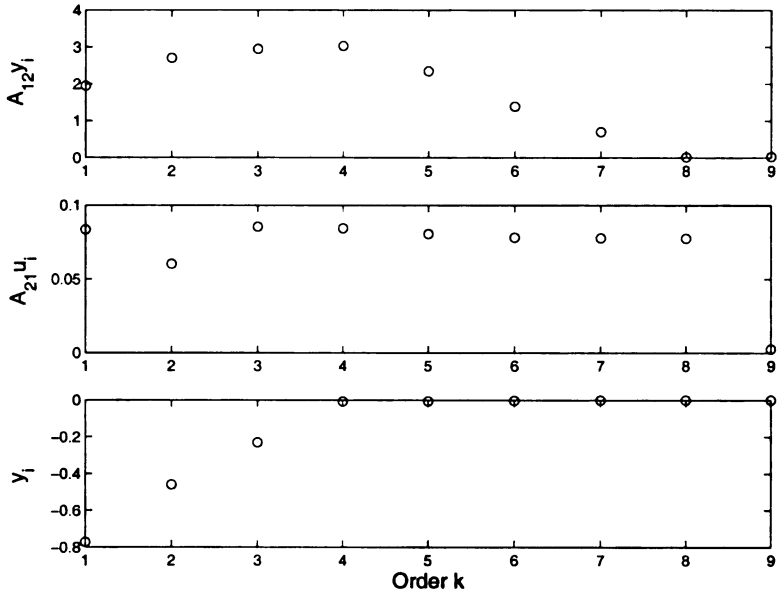

Figure 5.2: Measures: $k = 1$ to 9

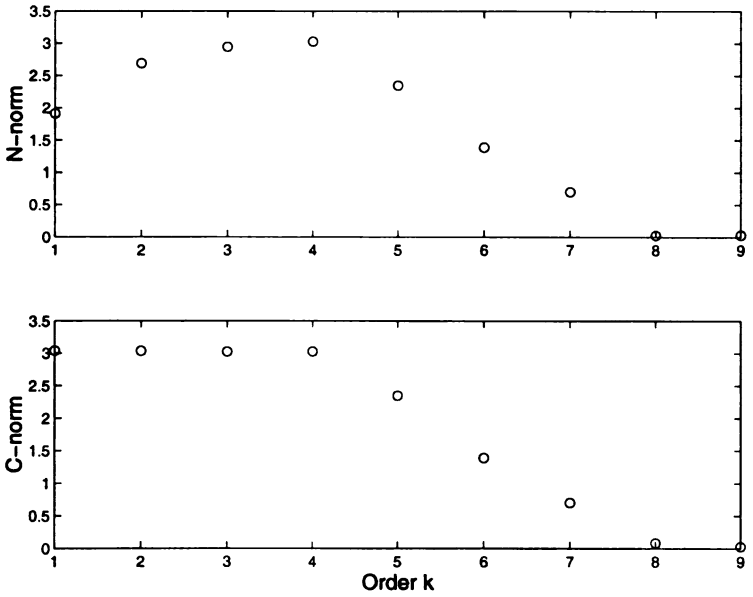

Figure 5.3: Measures: $k = 1$ to 9

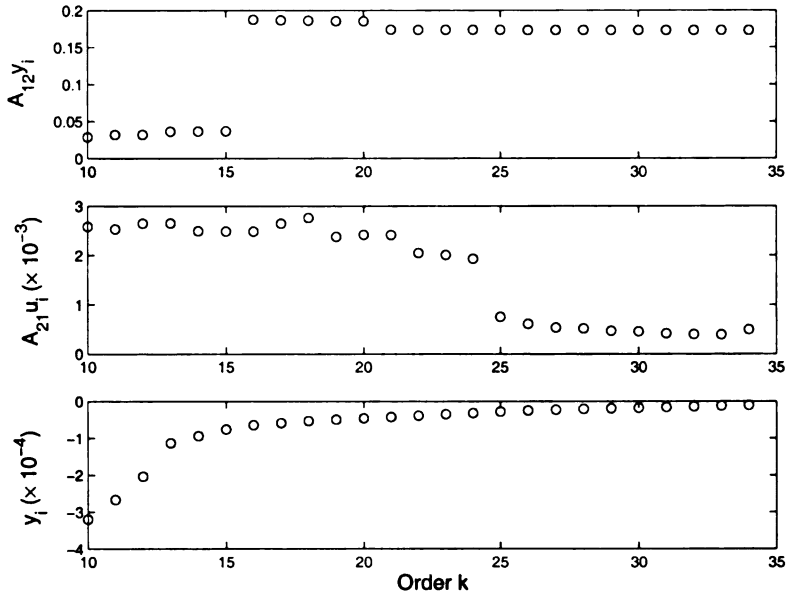

Figure 5.4: Measures: $k = 10$ to 34

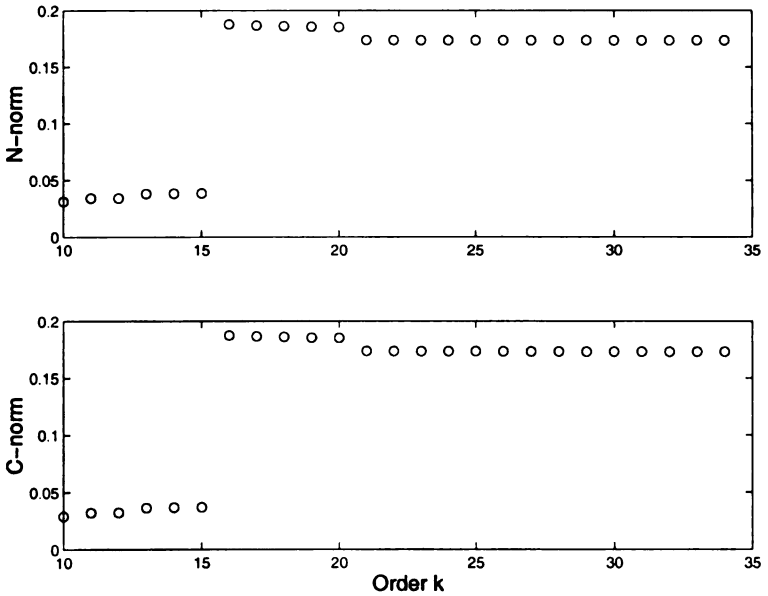

Figure 5.5: Measures: $k = 10$ to 34

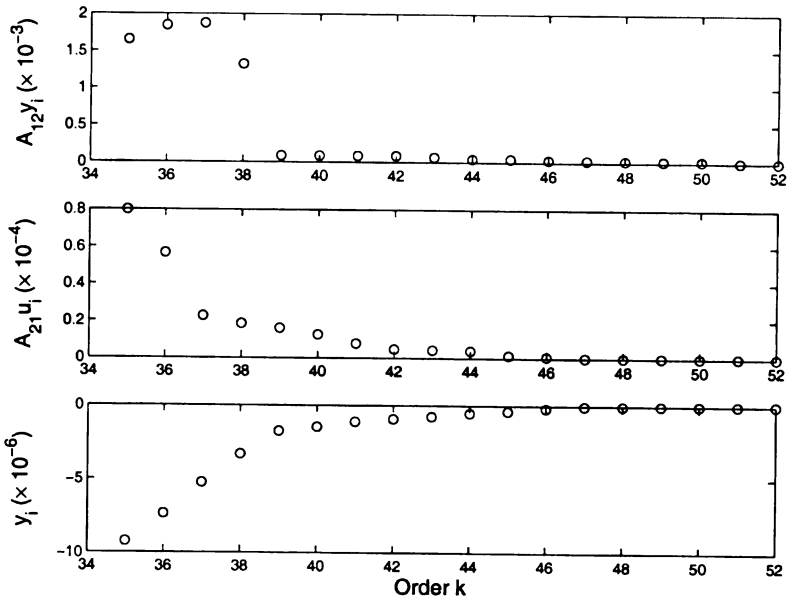

Figure 5.6: Measures: $k = 35$ to 52

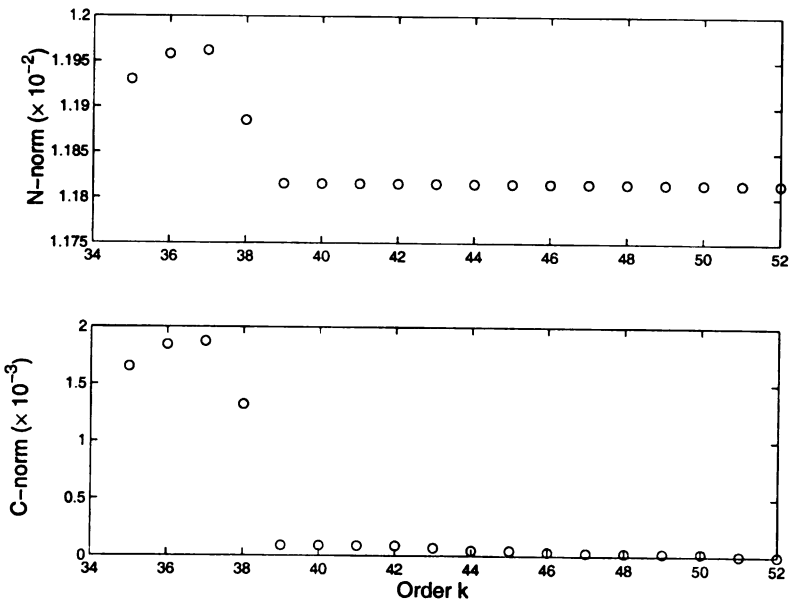

Figure 5.7: Measures: $k = 35$ to 52

decrease in $\| y_i \|$ with increasing k will override the increase in $\| A_{12}y_i \|$ causing $C_i^k = \| A_{12}y_i \|$ to again satisfy the geometric decoupling condition. Thus there are two ranges for which bifurcation subsystem exists, $8 \leq k \leq 15$ and $k \geq 34$. The bifurcation subsystem at small k is due to all three measures but principally the reduction in $\| A_{12}y_i \|$ and $\| A_{21}u_i \|$. The bifurcation subsystems for $k \geq 34$ are due to $\| (A_{22} - j\omega_0 I)^{-1} \|$ and $\| A_{21}u_i \|$ decreasing with increasing k. This shows how unpredictable the existence of bifurcation subsystems are for any specific order k because large changes can occur for integer change in order k. This suggests that the inclusion of important center manifold dynamic states may have dramatically effects on whether a bifurcation subsystem existence. The phenomena of having $\| (A_{22} - j\omega_0 I)^{-1} \|$ and $\| A_{21}u_i \|$ decrease at large k and $C_i^k = \| A_{12}u_i \|$ decrease at small k are thought to be generic phenomena. These trends can be clearly seen from Figure 5.2 - 5.7.

It is interesting to note that the active load stress on different buses generates the same bifurcation subsystem, i.e., the orders and the involved state variables of the Hopf bifurcation subsystems are the same. As an example, bus 3 and 13 were stressed by active power load simultaneously. The results are shown in Table 5.5. This suggests there are several bifurcation parameters for this bifurcation subsystem, and this interarea mode is excited by loading at all load buses in either case. From Table 5.3 and Table 5.5 we can see that the two bifurcation subsystems have the same dimensions, and the same states are involved in the bifurcation subsystem. The bifurcation subsystem involves excitation systems on generator 1, 2, and 4, and governor control loop in generator 1. The PV-curve on other buses (4, 14, and both 4 and 14) have been obtained and all the bifurcation subsystems are the same. This implies this interarea mode is excited by loading at all load buses in either case.

Actually the network containing buses 3, 4, 13, and 14 is a coherent bus group if the two lines provide a stiff connection between the two areas. This coherent bus group

k	N_i^k	C_i^k	R_i^k	States involved
1	1.8976e+00	4.9990e+00	2.6343e+00	δ_4
2	2.6705e+00	3.7947e+00	1.4210e+00	δ_3
3	2.9140e+00	3.2123e+00	1.1024e+00	δ_1
4	2.9911e+00	2.9922e+00	1.0004e+00	δ_2
5	2.3121e+00	2.3135e+00	1.0006e+00	ω_4
6	1.3473e+00	1.3498e+00	1.0018e+00	ω_3
7	6.7489e-01	6.7967e-01	1.0071e+00	ω_1
8	2.0500e-02	8.1228e-02	3.9624e+00	ω_2
9	2.8595e-02	2.8804e-02	1.0073e+00	TG_3 at G1
10	2.8905e-02	2.9059e-02	1.0053e+00	V_R at G1
11	3.2008e-02	3.2141e-02	1.0042e+00	E_{fd} at G1
12	3.2012e-02	3.2150e-02	1.0043e+00	V_{AS} at G2
13	3.6140e-02	3.6250e-02	1.0030e+00	V_R at G4
14	3.6343e-02	3.6433e-02	1.0025e+00	V_R at G2
15	3.6555e-02	3.6644e-02	1.0024e+00	R_f at G1
16	1.8754e-01	1.8756e-01	1.0001e+00	

Table 5.5: Increase Active Power Load on Bus 3 and Bus 13

would be an agent of the network model that experiences, produces, and causes instability in the network if the QV-curve computed at any bus in that coherent bus group cause the same set of generators to exhaust reactive reserves (reactive reserve basin) and the same QV-curve voltage minimum and reactive minimum as that computed at any other bus in that coherent bus group [30]. The agent composed of the coherent bus group and its reactive reserve basin, which is the subset of generators that exhaust at the QV-curve minima, will thus experience voltage instability for QV-curve computed in its test voltage control area. Several agents form a voltage collapse sequence if these reactive reserve basins are nested. A critical agent will experience voltage collapse for a PV curve computed in a voltage collapsed region composed of the coherent bus groups of several agents in a voltage collapse sequence [30].

The coherent bus group composed of 3, 4, 13, and 14 appears to be the only agent in this small system and the reactive reserve basin contains none of the generators since QV-curve run at bus 3 in Table 5.6 exhausts none of the generators reactive

k	N_i^k	C_i^k	R_i^k	States involved
1	1.9424e+00	1.9430e+00	1.0003e+00	δ_3
2	2.7363e+00	2.7388e+00	1.0009e+00	δ_4
3	3.0003e+00	3.0023e+00	1.0007e+00	δ_1
4	3.0740e+00	3.0763e+00	1.0008e+00	δ_2
5	2.3826e+00	2.3857e+00	1.0013e+00	ω_3
6	1.4009e+00	1.4058e+00	1.0035e+00	ω_4
7	6.6922e-01	6.7912e-01	1.0148e+00	ω_1
8	2.5878e-02	1.1811e-02	4.5641e+00	ω_2
9	3.2072e-02	3.2150e-02	1.0024e+00	TG_3 at G1
10	3.2443e-02	3.2525e-02	1.0025e+00	V_R at G1
11	3.2450e-02	3.2548e-02	1.0030e+00	V_{AS} at G2
12	3.5850e-02	3.5935e-02	1.0024e+00	E_{fd} at G1
13	4.0034e-02	4.0100e-02	1.0019e+00	V_R at G4
14	4.0301e-02	4.0372e-02	1.0018e+00	V_R at G2
15	4.0579e-02	4.0649e-02	1.0017e+00	R_f at G1
16	1.9501e-01	1.9501e-01	1.0000e+00	

Table 5.6: Increase Reactive Power Load on Bus 3

reserves before the system experiences bifurcation. The coherent bus group is the critical agent since it is the only agent. The increase in active load at any bus or collection of buses in this coherent bus group in Table 5.6 produces the same type of bifurcation (Hopf) and the same bifurcation subsystem in the differential model and this bifurcation occurs before the network model experiences bifurcation which occurs when one of its eigenvalues becomes negative.

It appears that the bifurcation subsystem of the network and how it is impacted by active and reactive load or contingency will determine the bifurcation subsystem of the equivalent differential system obtained by eliminating the network.

5.6.2 Interarea Hopf Bifurcation: Reactive Power Load

The bifurcation is produced by running QV-curve on bus 3. None of the generators exhausts reactive reserve before the differential model experiences Hopf bifurcation. Table 5.6 shows the results of increasing the reactive power load on bus 3. From

k	N_i^k	C_i^k	R_i^k	States involved
1	1.8167e+00	1.8201e+00	1.0018e+00	δ_4
2	2.5523e+00	2.5534e+00	1.0004e+00	δ_3
3	3.0380e+00	3.0392e+00	1.0004e+00	δ_1
4	3.0768e+00	3.0779e+00	1.0004e+00	δ_2
5	2.4832e+00	2.4844e+00	1.0005e+00	ω_4
6	1.7183e+00	1.7201e+00	1.0010e+00	ω_3
7	4.8759e-01	4.9232e-01	1.0097e+00	ω_1
8	3.3173e-02	7.3424e-02	2.2134e+00	ω_2
9	4.2051e-02	4.2185e-02	1.0032e+00	$PSS1$ at G3
10	4.2803e-02	4.2945e-02	1.0033e+00	V_R at G1
11	4.9250e-02	4.9365e-02	1.0023e+00	E_{fd} at G1
12	4.9255e-02	4.9388e-02	1.0027e+00	V_{AS} at G2
13	5.2028e-02	5.2156e-02	1.0024e+00	V_R at G2
14	5.2620e-02	5.2746e-02	1.0024e+00	ψ_{kd} at G1
15	5.2819e-02	5.2931e-02	1.0021e+00	E_{fd} at G4
16	4.5031e-01	4.5234e-01	1.0045e+00	V_{TR} at G1

Table 5.7: Increase Reactance on Generator 1

Table 5.6 we can see that another 15^{th} order bifurcation subsystem is obtained and excitation systems on generator 1, 2, and 4 cause the bifurcation since V_R of generator 1,2, and 4 are in the largest bifurcation subsystem, stabilizer on generator 1 since states R_f and E_{fd} on generator 1 are also in the largest bifurcation subsystem, and the generator state TG_3 on generator 1 is also in the bifurcation subsystem. Moreover, we can see that the bifurcation subsystem contains exactly same states as those in Table 5.3 and 5.5. Therefore, active and reactive power load appear to cause the same bifurcation and same interarea mode bifurcation subsystem. This Hopf bifurcation class appears rather generic for network based QV and PV-curve stress tests.

5.6.3 Interarea Hopf Bifurcation: Generator Reactance

A Hopf bifurcation occurs due to the increase of the reactance at generator 1. The bifurcation was caused by power system stabilizer (on generator 3) , excitation controls

k	N_i^k	C_i^k	R_i^k	States involved
1	2.1828e+00	2.1835e+00	1.0003e+00	δ_1
2	2.8493e+00	2.8501e+00	1.0003e+00	δ_2
3	2.8661e+00	2.8667e+00	1.0002e+00	δ_4
4	2.8710e+00	2.8717e+00	1.0002e+00	δ_3
5	1.8650e+00	1.8659e+00	1.0005e+00	ω_1
6	3.5203e+00	3.5828e+00	1.0178e+00	ω_2
7	1.6725e-01	1.7918e-01	1.0714e+00	ω_4
8	1.6777e-02	1.6784e-02	1.0004e+00	ω_3
9	2.0253e-02	2.0141e-02	9.9449e-01	E_{fd} at G4
10	4.8354e-02	4.8278e-02	9.9843e-01	R_f at G4
11	4.8562e-02	4.8567e-02	1.0001e+00	ψ_{kq} at G1

Table 5.8: Active Power Transfer

on generator 1, 2, and stabilizer control loops on generator 1 and 4. This interarea mode has a different bifurcation subsystem and thus produces a different class of bifurcation than that observed in Table 5.3 - 5.6. The increase in generator reactance will decrease the frequency of the interarea mode and possibly causes the only PSS on generator 3 to lose its stabilizing effect. The change of interarea mode frequency may be out of the bandwidth for where the power system stabilizer adds damping and in fact may begin to add negative damping that produces the bifurcation. This may be why the state of PSS on generator 3 joins the bifurcation subsystem.

5.6.4 Interarea Hopf Bifurcation: Active Power Transfer

The Hopf bifurcation was caused by increasing active power transfer between two areas. The active power generation on generator 2 was increased while the active power generation on generator 3 was decreased to produce the transfer between area 1 and 2. The interarea mode bifurcation is produced by the stabilizer control on generator 4, and has a bifurcation subsystem that is considerably different than those in Table 5.7 and that found in Table 5.3 - 5.6. This is the true interarea mode bifurcation subsystem or bifurcation class since it is produced by increasing active

power transfer between two areas and only contains the stabilizer on generator 4 as non-generator inertial dynamics. The increased transfer should significantly affect this generator and may explain why its stabilizer is part of the bifurcation subsystem.

This is indeed a very important result since it shows there are three different classes of bifurcation that have an interarea mode of oscillation and yet very different bifurcation subsystems. The variables and dynamics in the bifurcation subsystem cause it to occur and are the dynamics to be controlled to cure the bifurcation. This bifurcation can most easily be cured by damping the inertial dynamics via a controllable series capacitor on one of the lines connecting the two areas or FACTS devices that control the flows between two areas because only one generator's exciter system dynamics are in the bifurcation subsystem. The bifurcation subsystem for the results in Tables 5.3 - 5.7 could possibly much more easily be cured by power system stabilizers because excitation dynamics and inertial dynamics from several generators are in the bifurcation subsystems.

5.6.5 Interarea Hopf Bifurcation: K_F-gain of PSS

Table 5.9 presents the bifurcation subsystem by increasing the K_F-gain of power system stabilizer of generator 3. Increasing K_F gain would be thought to increase damping of the interarea mode, but detunes the power system stabilizer and excitation controls on generator 4 to actually cause the interarea mode to experience bifurcation. From Table 5.9 we can see that excitation system and stabilizer on generator 4 is the bifurcation subsystem of the interarea mode. Note that generator 4 and generator 3 are in the same area as shown in Figure 5.1.

This suggests that there is yet another bifurcation class for producing interarea oscillations and that the most effective control for the oscillation should be on the generators in area 2, where K_F of generator 3 was increased to produce the bifurca-

k	N_i^k	C_i^k	R_i^k	States involved
1	1.3980e+00	1.4002e+00	1.0015e+00	δ_1
2	1.8984e+00	1.8992e+00	1.0004e+00	δ_2
3	2.0196e+00	2.0201e+00	1.0003e+00	δ_4
4	2.0210e+00	2.0216e+00	1.0003e+00	δ_3
5	1.4595e+00	1.4602e+00	1.0005e+00	ω_1
6	6.9338e-01	6.9483e-01	1.0021e+00	ω_2
7	7.4492e-02	8.7883e-02	1.1489e+00	ω_4
8	8.4576e-02	9.5004e-02	1.1233e+00	V_R at G4
9	4.9155e-02	5.7711e-02	1.1741e+00	ω_3
10	5.6532e-01	5.6613e-01	1.0014e+00	E_{fd} at G4

Table 5.9: Increase K_F-gain of Power System Stabilizer

tion. It is also noted that the bifurcation subsystem does not contain the stabilizer on generator 3 but only the outer excitation control loop variable V_R, which suggests that adjusting excitation loop gain may be most effective in curing this class of interarea mode bifurcation.

5.6.6 Interarea Hopf Bifurcation: K_A-gain of Exciter

This bifurcation is caused by decreasing the K_A-gain of the excitation system on generator 3. The results are shown in Table 5.10. The power system stabilizer on generator 3, the excitation system on generator 1, 2, and the stabilizer control loop on generator 3, and 4 are in the 22 state bifurcation subsystem. The entire set of states in the generator and exciter model of generator 1 are in the bifurcation subsystem as would be expected when exciter gain on generator 3 decreases causing the exciter control on generator 3 to lose its stabilizing effect. This class of interarea mode Hopf bifurcation is far different than those previously studied because such a large number of the excitation control system variables on all four generators are in the bifurcation subsystem.

The results show that the generator and exciter voltage dynamics on all four generators join the bifurcation subsystem suggesting that the excitation controls on all

k	N_i^k	C_i^k	R_i^k	States involved
1	2.0885e+00	2.0905e+00	1.0009e+00	δ_4
2	2.9024e+00	2.9028e+00	1.0002e+00	δ_3
3	3.3753e+00	3.3760e+00	1.0002e+00	δ_1
4	3.6159e+00	3.6167e+00	1.0002e+00	δ_2
5	2.9517e+00	2.9525e+00	1.0003e+00	ω_4
6	2.1516e+00	2.1580e+00	1.0006e+00	ω_3
7	1.2971e-01	1.2992e-01	1.0016e+00	ω_1
8	1.5260e-02	7.3622e-02	4.8245e+00	ω_2
9	1.9380e-02	1.9474e-02	1.0049e+00	PSS_1 at G3
10	1.9736e-02	1.9833e-02	1.0049e+00	V_R at G1
11	2.1857e-02	2.1940e-02	1.0038e+00	E_{fd} at G1
12	2.1861e-02	2.1953e-02	1.0042e+00	V_{AS} at G2
13	2.2127e-02	2.2204e-02	1.0035e+00	V_R at G2
14	2.2746e-02	2.2830e-02	1.0037e+00	V_R at G4
15	2.3025e-02	2.3107e-02	1.0036e+00	R_f at G1
16	1.9431e-01	1.9528e-01	1.0050e+00	E'_q at G1
17	1.8487e-01	1.9519e-01	1.0045e+00	PSS_3 at G3
18	1.9137e-02	1.9184e-02	1.0024e+00	V_{TR} at G2
19	1.8562e-02	1.8599e-02	1.0020e+00	ψ_{kq} at G4
20	1.6630e-02	1.6675e-02	1.0027e+00	ψ_{kd} at G3
21	1.2727e-02	1.2737e-02	1.0008e+00	V_{TR} at G1
22	9.1727e-03	9.1862e-03	1.0015e+00	ψ_{kd} at G2
23	1.8487e-01	1.9519e-01	1.0034e+00	E'_qat G2

Table 5.10: Decrease K_A-gain of Excitation System on Generator 3

four generators are coupled when one excitation controller is misdesigned. It suggests that changes in excitation control of the other three generators should be able to compensate for the misdesign of one exciter. Obviously fixing the design of the exciter on generator 3 should be most effective.

5.6.7 Interarea Hopf Bifurcation: Generator Terminal Voltage

This bifurcation is produced by decreasing the terminal voltage set point of generator 1. There is no lower bound for the terminal voltage set point of generator 1. The terminal voltage was decreased continuously, until the generator 1 hits the generator field current limiter based reactive limit.

This bifurcation parameter produces a QV-curve on this generator bus, which is the swing bus. This generator terminal voltage, that produces the QV-curve on the swing bus, sets the voltage reference in the system and should cause excitation system states on several generators to produce the bifurcation. This is exactly happens as is shown in Table 5.11. The power system stabilizer of generator 3, excitation system states V_R on generator 1, 2, and 4, and the stabilizer on generator 1 are involved in the bifurcation subsystem. This bifurcation subsystem is similar but not identical to that for the PV-curves at bus 3, 4, 13, and 14 and the QV-curve at bus 3 shown in Table 5.3-5.6.

This is a slightly different class of Hopf bifurcation compared with Table 5.6 because the power system stabilizer on generator 3 is in the bifurcation subsystem rather than the governor on generator 3. The bifurcation subsystem describes the states which must be measured, estimated, and controlled to stabilize the instability produced by the bifurcation.

k	N_i^k	C_i^k	R_i^k	States involved
1	1.8200e+00	1.8050e+00	9.9176e-01	δ_4
2	2.5597e+00	2.5956e+00	1.0140e+00	δ_3
3	2.8705e+00	2.8587e+00	9.9586e-01	δ_1
4	3.0050e+00	3.0043e+00	9.9977e-01	δ_2
5	2.3913e+00	2.3966e+00	1.0022e+00	ω_4
6	1.5746e+00	1.5842e+00	1.0061e+00	ω_3
7	8.8897e-01	9.0175e-01	1.0132e+00	ω_1
8	4.7959e-02	7.9277e-02	1.6530e+00	ω_2
9	5.2329e-02	2.8617e-02	5.4687e-01	PSS_1 at G3
10	5.7081e-02	3.7214e-02	6.5195e-01	V_R at G1
11	5.7185e-02	3.7477e-02	6.5536e-01	E_{fd} at G1
12	5.7188e-02	3.7364e-02	6.5336e-01	V_{AS} at G2
13	5.8215e-02	3.8848e-02	6.6731e-01	V_R at G2
14	5.8378e-02	3.9483e-02	6.7633e-01	V_R at G4
15	2.5742e-01	2.5415e-01	9.8732e-01	R_f at G1

Table 5.11: Decrease Terminal Voltage of Generator 1

5.6.8 Local Hopf Bifurcation: Generator Terminal Voltage

All of the previous Hopf bifurcation classes studied have been interarea mode bifurcations because the oscillation frequencies are small and all four generators inertial dynamics lie in the bifurcation subsystems. The generator transformer reactances in this two area model are quite small making it difficult to produce a local mode that affects dynamics on a single generator and at a frequency of oscillation that exceeds 1 Hz.

This local mode of bifurcation is produced by decreasing generator terminal voltage on generator 2 with a very large reactance line connection between bus 2 and bus 20 and large transformer reactance. Again a Hopf bifurcation occurs and the oscillation frequency= 1.19 > 1. Therefore, this is a local mode. This is confirmed by plotting the magnitude and phase of the bifurcating eigenvectors for the four generator angle states. The vector diagram of the bifurcating eigenvalue is shown in Figure 5.8. We can see that generator 3 oscillates vertically against generator 1 and 2, and all three of these generators oscillate against generator 4 horizontally. This is because that

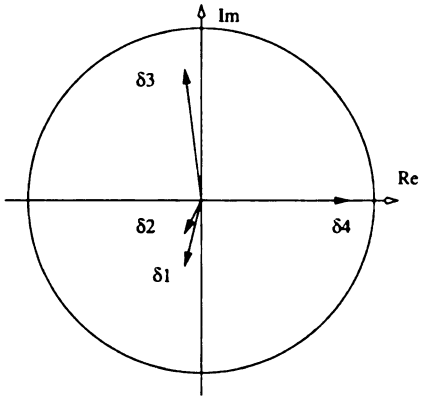

Figure 5.8: Generator Angle Vector Diagram When Bifurcating

k	N_i^k	C_i^k	R_i^k	States involved
1	5.4583e+00	7.4778e+00	1.3700e+00	δ_4
2	7.3565e+00	7.4786e+00	1.0166e+00	δ_3
3	7.4739e+00	7.4790e+00	1.0007e+00	δ_2
4	7.4827e+00	7.4790e+00	9.9951e-01	δ_1
5	5.1184e+00	5.1150e+00	9.9934e-01	ω_4
6	1.3690e+00	1.3692e+00	1.0001e+00	ω_3
7	3.6395e-01	3.6586e-01	1.0053e+00	ω_2
8	3.7678e-01	3.7852e-01	1.0046e+00	V_R at G4
9	1.0898e-01	1.1536e-01	1.0586e+00	ω_1
10	1.1020e-01	1.1010e-01	9.9910e-01	TG_3 at G3
11	1.0090e-01	1.0082e-01	9.9916e-01	E'_q at G3
12	1.0093e-01	1.0084e-01	9.9911e-01	V_R at G1
13	4.4654e-01	4.4641e-01	9.9971e-01	E_{fd} at G4

Table 5.12: Decrease Terminal Voltage of Generator 2

the transmission lines between area 1 (generator 1 and 2) and area 2 (generator 3 and 4) have large reactance and generator 2 is isolated by large reactance from the rest of the system. Generator 1 and 2 are coherent since they are in same area.

The model does not produce local mode bifurcation without increasing transformer reactances. The transformer reactances are very small in the original model and are on the order of the size of transmission line reactances. Generators must be somewhat isolated by large transformer reactances or by network reactances to have its inertial modes suffer Hopf bifurcation. Due to the large reactance between bus 2 and 20, decreasing the terminal voltage on generator 2 will decrease the voltage

at bus 20. The other three generators will attempt to compensate for the voltage drop at bus 20. This can be see from Table 5.12, where excitation system states of generator 1, 3, and 4 are involved in the bifurcation subsystem, rather than those of generator 2.

5.6.9 Local Hopf Bifurcation: K_F-gain of Internal Stabilizer

This Hopf bifurcation is produced by decreasing the K_F-gain of the internal stabilizer on generator 2 for the case where generator 2 is isolated by increasing line reactance between bus 2 and bus 20. The oscillation frequency is $1.46 > 1$. It is again a local mode due to the large generator and transformer reactance. The vector diagram of

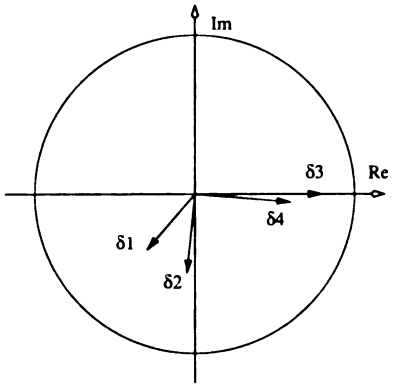

Figure 5.9: Generator Angle Vector Diagram When Bifurcating

bifurcating eigenvalue is shown in Figure 5.9, where generator 1 oscillates horizontally against generator 3 and 4, and generator 1 and 2 oscillate vertically against other generators. In Table 5.13 we can see that most of states involved in the 17 states bifurcation subsystem are those of generator 2. This electrical modes are what we expected since the bifurcation is produced by decreasing the internal stabilizer gain of the excitation system on generator 2, and the generator 2 is isolated. When this local oscillation occurs the parameter K_4 on generator 2 changes sign. It can be seen from Table 5.2 that damping torque $K_d = \frac{K_2 K_3 K_4}{\omega^2 T}$ changes sign when K_4 changes

k	N_i^k	C_i^k	R_i^k	States involved
1	5.4796e+00	3.1715e+00	5.7879e-01	δ_3
2	7.3209e+00	9.3097e+00	1.2717e+00	V_R on G2
3	8.2242e+00	9.3109e+00	1.1321e+00	δ_1
4	8.8326e+00	9.3109e+00	1.0542e+00	δ_2
5	9.2725e+00	9.3104e+00	1.0041e+00	δ_4
6	9.2831e+00	9.2959e+00	1.0014e+00	V_{AS} at G2
7	1.0240e+01	1.0272e+01	1.0032e+00	TG_3 on G2
8	9.5590e+00	9.6689e+00	1.0115e+00	E'_q at G2
9	9.2804e+00	9.5578e+00	1.0299e+00	ψ_{kd} at G2
10	7.9050e+00	7.9075e+00	1.0003e+00	V_{TR} at G2
11	7.9154e+00	7.9157e+00	1.0000e+00	V_R at G1
12	5.7122e+00	5.7136e+00	1.0003e+00	ω_3
13	4.3116e+00	4.3128e+00	1.0003e+00	ω_1
14	2.8659e+00	2.8675e+00	1.0006e+00	ω_2
15	2.9776e+00	2.9780e+00	1.0001e+00	V_R at G4
16	9.5003e-01	9.4977e-01	9.9973e-01	ω_4
17	9.5123e-01	9.5095e-01	9.9971e-01	E_{fd} at G1
18	3.0612e+00	3.0617e+00	1.0002e+00	E_{fd} at G4

Table 5.13: Decrease K_F-gain of Internal Stabilizer on Generator 2

sign, which explains why this local mode bifurcates from Table 5.2.

5.6.10 Saddle-node Bifurcation: Generator Terminal Voltage

An example of saddle-node bifurcation is presented here for the original model where reactance between bus 2 and 20 has not been increased. This original model is used in the remainder of the results in this chapter except for section 5.6.13.

The saddle-node bifurcation also occurs when decreasing the terminal voltage of generator 2. In this case the excitation system $G_e(s)$ is almost disabled by making the exciter dynamics very fast and decreasing the loop gain of $G_e(s)$ to 1. Disabling excitation system may happen due to malfunction of the exciter, inability of the field current limiter to maintain the current under the field current limit capability of the generator, and could be disastrous for power system. Results in [29] and [31] show

k	N_i^k	C_i^k	R_i^k	States involved
1	0.0000e+00	2.6837e-01	0.0000e+00	V_{AS} at G2
2	3.5803e-02	3.9211e-01	1.0952e+01	R_f at G1
3	1.3965e-01	3.1361e-01	2.2457e+00	V_{TR} at G1
4	1.6472e-01	3.2105e-01	1.9490e+00	V_{TR} at G1
5	2.3174e-01	3.0773e-01	1.3279e+00	E'_q at G4
6	2.3886e-01	3.1279e-01	1.3095e+00	ψ_{kd} at G4
7	8.3984e-01	8.5094e-01	1.0132e+00	E'_q at G3
8	3.5256e+00	3.3280e+00	1.0007e+00	ψ_{kd} at G3

Table 5.14: Decrease Terminal Voltage of Generator 2 without Exciters

that a saddle-node bifurcation should develop whenever the exciter is disabled as it does and that the bifurcation should occur in the generator flux decay dynamics. As we expect, the inertial dynamics are not involved in the bifurcation subsystem and this is clear in Table 5.14. Instead, the states of the excitation systems on all the generators appears in the bifurcation subsystem.

This is very strong indication that the bifurcation subsystem describes the dynamics causing the bifurcation.

5.6.11 Saddle-node Bifurcation: Reactive Power Load

In this case, the exciter is disabled and the time constant of the flux decay dynamics is reduced. If the flux decay dynamics as well as excitation system dynamics are eliminated as is occurring in this example, the theory in [31] suggests the bifurcation should be saddle-node and should occur in the inertial dynamics [8]. This saddle-node bifurcation occurs when the reactive power load on generator bus 2 increases after the network is made capacitive by increasing the line charging on the transmission lines. The bifurcation subsystem is shown in Table 5.15. Only the inertial dynamics is involved in the bifurcation subsystem. This confirms the theoretical results in [31] [32].

k	N_i^k	C_i^k	R_i^k	States involved
1	0.0	5.2665e-02	0.0	δ_2
2	0.0	7.3753e-02	0.0	δ_3
3	0.0	5.9953e-02	0.0	δ_4
4	0.0	1.2155e-03	0.0	δ_1
5	5.9051e-04	1.0535e-03	1.7840e+00	ω_2
6	8.3511e-04	1.0457e-03	1.2522e+00	ω_3
7	1.0228e-03	5.9940e-04	5.8604e-01	ω_4

Table 5.15: Increase Reactive Power Load on Bus 2

5.6.12 Saddle-node Bifurcation: Active Power Transfer

All of the previous results were obtained when the load model was assumed to be constant current/impedance. In reality, the load model changes over time from constant current/impedance to constant power. This phenomena has been widely studied [17] and is quite important in attempting to correctly identify why the blackout occurred. In one classic case two different power industry experts came to different conclusions on what caused a particular blackout on the WSCC system because one used a constant current model and the other used a dynamic load model that transitioned from a constant current/impedance model to a constant power load over a period of minutes. One study conducted that the cause of the blackout was due to growing interarea oscillations [20] and the other concluded that the cause was voltage collapse via saddle-node bifurcation without any evidence of oscillation and certainly no growing oscillation.

The conclusion is that the power system must remain stable for the period when the load is modeled by constant current/impedance load model and then must remain stable as the load changes to constant power to be considered stable. The WSCC system has experienced blackouts due to growing oscillations and due to saddle-node bifurcation for the three different events that produced blackout [20] [23] [24]. The result being developed will help explain why and when a system will experience

k	N_i^k	C_i^k	R_i^k	States involved
1	0.0	6.0717e-02	0.0	δ_2
2	0.0	4.9928e-02	0.0	δ_1
3	0.0	6.9224e-02	0.0	δ_3
4	0.0	4.3831e-04	0.0	δ_4
5	2.2109e-04	3.7750e-04	1.7075e+00	ω_2
6	3.1267e-04	3.0603e-04	9.7877e-01	ω_1
7	3.8294e-04	2.6117e-04	6.8202e-01	ω_3

Table 5.16: Active Power Transfer

blackout due to saddle-node bifurcation and why and when a system will experience blackout due to Hopf bifurcation. It will be shown that for the initial transient interval the system load model appears to be like a constant current/impedance load model and Hopf bifurcation is most likely to occur. If this bifurcation does not occur, the system will most likely suffer saddle-node bifurcation when the load model appears to be like constant power. These hypothesized results correlate with those observed for the three blackouts recorded on the WSCC system [20] [23] [24].

The above results and conclusions for constant current/impedance load modeling has been established in the results already presented in Table 5.8. The results to be presented will now validate the hypothesis for constant power load model.

The results in the remaining example utilized a constant power load and the type of bifurcation that develops is saddle-node bifurcation and singularity induced bifurcation rather than Hopf bifurcation for the change in same bifurcation parameter since the load model is constant power rather than constant current/impedance as long as the excitation control system is not disabled.

This saddle-node bifurcation is caused by increasing the active power transfer under constant active power load with both excitation system and flux decay dynamics present. The increasing active power on generator 2 will transfer the active power to generator bus 1, which is the swing bus of the two-area system. The bifurcation subsystem is shown in Table 5.16. From above analysis, the increase in active power

generation on generator 2 will cause the active power transfer between generator 1 and 2. It is clear that both generator angles and speeds of generator 1 and 2 are involved in the bifurcation subsystem.

It should be noted that this saddle-node bifurcation subsystem, which includes the generator inertial dynamics $\delta_1 - \delta_4$, and ω_1, and ω_2, is a subset of the Hopf bifurcation subsystem in Table 5.8. In both cases the bifurcation parameter is active power transfer between two areas. The transition from Hopf to saddle-node bifurcation is caused by the load model, i.e., constant current/impedance load and constant power load, which correspond to the transition from transient state and steady state of the power system load dynamics. This indicates that both saddle-node and Hopf bifurcation can develop at different time frames for the nearly identical bifurcation subsystem. This result shows that the bifurcation parameter stresses very similar bifurcation subsystem but the type of bifurcation depends on whether the load model is constant current/impedance or constant power. These are quite amazing results since one would have expected two very different bifurcation subsystems would produce saddle-node and Hopf bifurcation even when the same bifurcation parameter causes the bifurcation and only the load model has changed.

If we increase the active power transfer and disable the excitation systems under constant power load, then, Hopf bifurcation develops rather than saddle-node bifurcation as in section 5.6.10 when a transient load model is used for the case where the excitation system is disabled. The bifurcation subsystem produced contains only excitation variables on the generators where the excitation systems are not disabled as was the case in section 5.6.10 for saddle-node bifurcation. Excitation systems on generators were actually disabled by the malfunction of the over excitation limiter in the August, 1996 blackout studied in [20]. This appears to explain the development of Hopf bifurcation rather than saddle-node bifurcation in the steady-state time frame. It would appear that Hopf bifurcation is also possible in the transient time

frame when a constant current/impedance model is valid with results that might be similar to that shown in Table 5.8. Then as one approaches the steady-state time frame one would expect a saddle-node bifurcation to possibly occur regardless of whether Hopf bifurcation has occurred in the transient time frame where the bifurcation subsystem is possibly similar to that in Table 5.16. The disablement of excitation systems due to malfunction of the over excitation limiter appears to have produced a Hopf bifurcation in the August 10, 1996 blackout [20] in quite a different (steady-state load model) bifurcation subsystem made up of excitation system variables of all generators close to but not including those of the generator where the excitation system is disabled for the two area system.

No inertial dynamics are involved in the bifurcation subsystem suggests that the power system stabilizer might not be effective as would an excitation system control modification on the generator where the excitation control is disabled, so that stabilization controls remain active when the ac regulator excitation control is disabled. This requires excitation system stabilization functions be added to the dc regulator so that they remain active when the ac regulator is disabled.

It should be noted if the excitation system were disabled in the transient time frame that saddle-node bifurcation would occur. This result suggests that disablement of excitation system causes a change in the type of bifurcation observed in both the transient and steady-state time frames.

5.6.13 Singularity Induced Bifurcation Example

In this section a singularity induced bifurcation example is presented. This bifurcation is caused by increasing the active power generation on generator 2 and again, isolating generator 2 by increasing line reactance between bus 2 and 20.

For differential-algebraic equations the singular surface is defined as the set in which

the algebraic model becomes singular. It consists of transversal singular points, at each of them two trajectories either approach or leave the singularity transversally, and pseudoequilibrium points, which are the equilibrium points of the singularly transformed system Z^T [17]. Special singular points include transverse sources, and transverse sinks, which form the impasse surface. For the differential-algebraic equations transverse sources are called backward impasse points and transverse sinks are forward impasse points. The transformed vector field Z^T is globally smooth and leaves the constraint surface. The standard mathematical analysis can be applied to Z^T and analyze the singular dynamics of the original differential-algebraic model.

When the bifurcation parameter approaches the bifurcation point, the system equilibrium approaches singular surface in state space. This singular surface causes the dynamic structure change. The property of singularity induced bifurcation is that the eigenvalues of the differential equation model bifurcate virtually simultaneously with the bifurcation of the algebraic model, rather than prior to the algebraic model bifurcation as in all the previous cases. The eigenvalues of the equivalent linearized differential equation model, where the linearized algebraic model is reduced, cross imaginary axis and after that one eigenvalue crosses back to left hand plane, and another one possibly goes back to be stable via infinity. More details about singularity induced bifurcation can be found in [17].

The jumping behavior of the eigenvalues associated with singularity induced bifurcation is now explained. This jumping phenomena is observed on the computational results to be presented. For singularity induced bifurcation it can be shown that there exists an invariant manifold that passes through the singularity. Also, this invariant manifold is locally attracting on one side and repelling on the other side such that the trajectories cross the singularity. This will generate radically different, fast moving trajectories after approaching the singularity. The differential-algebraic equations can not provide sufficient information to predict where the continuation

of the trajectories will cause the system dynamics to leave and land on the singular surface again. The dynamics will look like random process, such as the jumping phenomenon of the eigenvalues. The lack of convergence difficulties of the Newton-Rapheson algorithm when the magnitude of eigenvalue of the loadflow Jacobian is small can also help the switching of solution from the stable to unstable path of solutions as the bifurcation develops.

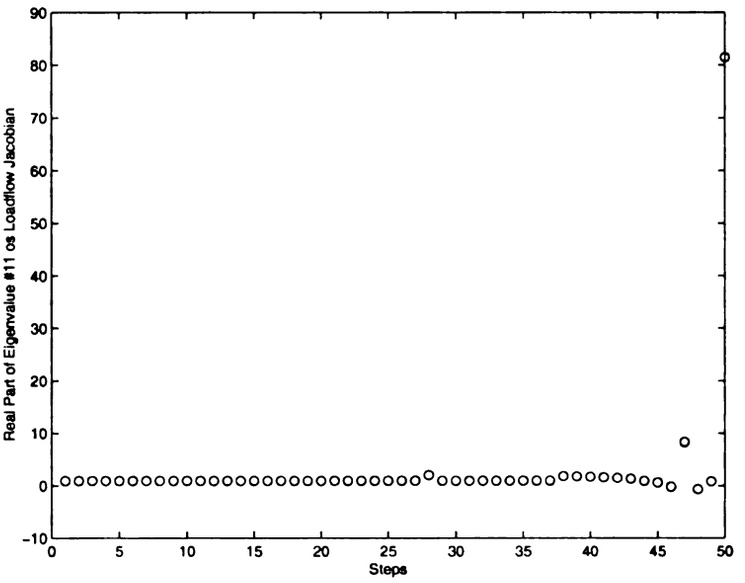

Figure 5.10: An Eigenvalue of Loadflow Jacobian

This singularity induced bifurcation is caused by the bifurcation of network equations, i.e., the loadflow Jacobian goes to unstable first, then the equivalent differential model bifurcates. This can be seen from Figure 5.10 and 5.11. As the active power of the generator is increased in the algebraic model, Figure 5.10 shows that one of the algebraic model eigenvalues becomes negative and unstable at step 48.

Figure 5.11 shows the real part of the bifurcating eigenvalue of the equivalent differential model as the loadflow bifurcation develops. The real part of this eigenvalue switches to much more negative value at step 45 and 46, to large positive values at stops 47 and 48 indicating the Hopf bifurcation occurs. The real part of the eigenvalue again switches to negative at stop 49 and 50 that reflects that the trajectories

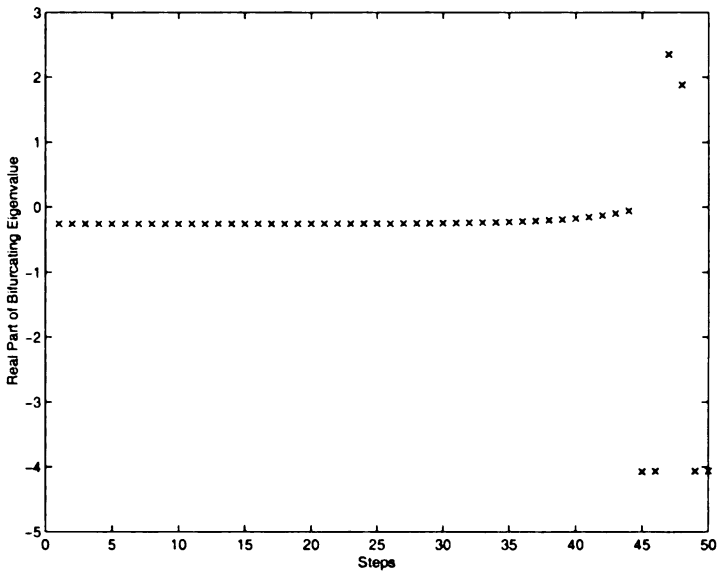

Figure 5.11: An Eigenvalue of State Matrix

pass through the pseudoequilibrium randomly. When approaching the singularity the trajectories are so fast that it is impossible to capture when and where it will cross the singularity since it won't stay at the singular surface. The numerical convergence difficulties could also contribute the switching from stable to unstable paths of solutions in the algebraic model that occurs at bifurcation in the algebraic model. This singularity induced bifurcation is produced by the network instability. Therefore, the cause and cure for this bifurcation are in the algebraic model rather than in the dynamic model. The equilibrium point and bifurcation point for dynamic model is very difficult to find because (a) the trajectories near singular surface move extremely fast due to the singularity of load flow Jacobian; (b) the points on singular surface which are not pseudoequilibrium can be sources and sinks, which makes it difficult to predict the trajectory behaviors near or on singular surface; (c) attempting to compute a pseudoequilibrium point could most possibly result in obtaining other points on singular surface rather than itself due to the numerical problems near singularity. Without the determination of equilibrium point and bifurcation point of the dynamic model it is very difficult to calculate the dynamic bifurcation

subsystem for singularity induced bifurcation. The only result for dynamic model we can obtain is the generator vector diagrams when algebraic approaches bifurcation.

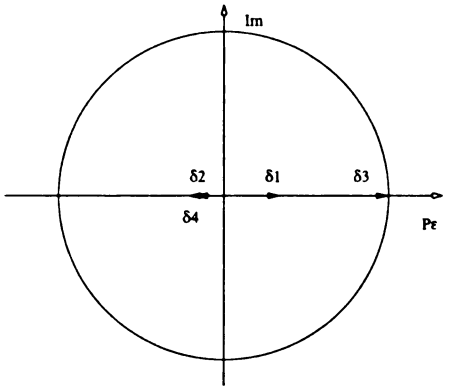

Figure 5.12: Generator Angle Vector Diagram Before Bifurcating

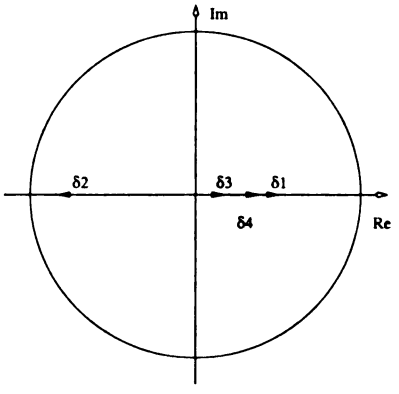

Figure 5.13: Generator Angle Vector Diagram When Bifurcating

Figure 5.12 and 5.13 give the vector diagram of the bifurcating eigenvalue. Before the singularity induced bifurcation occurs generator 1 and 3 oscillate against generator 2 and 4 horizontally, and when the bifurcation is occurring it turns that generator 2 oscillate solely against the other three generators. Generator 2 is isolated from the rest of the system by large reactance, but does not impact the vector diagram until bifurcation occurs. For the loadflow equations the large reactance reduces the lower bound on the eigenvalues associated with the voltage control area [30]. Figure 5.14 shows the PV-curve at bus 20 that occurs as generation out of generator 2 is increased. The decrease in voltage at bus 20 with increase generation is pronounced

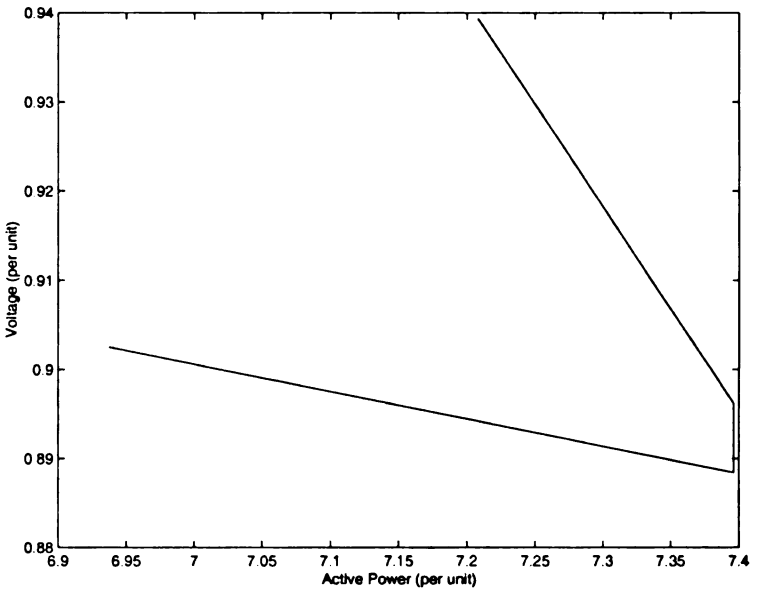

Figure 5.14: PV-curve on Bus 20

until the nose of PV-curve occurs. The voltage drops steps at the flat nose and then increases. The upper part of the nose are stable operating points. The lower part of the nose are unstable operating points. The nose corresponds to step 47 in Figure 5.11.

The bifurcation subsystem analysis which identifies causes and cures for this singularity induced bifurcation will be based on the algebraic mode and is now discussed.

The eigenvector of the eigenvalue, which is changing to negative, of the loadflow Jacobian is shown in Table 5.17. The loadflow Jacobian is defined as:

$$Jac = \begin{bmatrix} J_{n\times n} & J_{n\times m} \\ J_{m\times n} & J_{m\times m} \end{bmatrix} = \begin{bmatrix} \frac{\partial P}{\partial \delta} & \frac{\partial P}{\partial V} \\ \frac{\partial Q}{\partial \delta} & \frac{\partial Q}{\partial V} \end{bmatrix}$$

where n is the number of non-swing buses, and m is the number of buses which are neither swing nor generator buses. For this two-area example system $n = 12$, and $m = 8$, respectively.

Bus	Eigenvector of Eigenvalue 11 = $5.7709e-01$
2	-1.2803e-03
3	-3.9921e-03
4	6.2568e-03
10	-7.2387e-03
11	-7.0151e-03
12	-6.7639e-03
13	-6.7936e-03
14	1.3256e-02
20	-5.3387e-03
110	-7.1689e-03
120	5.9449e-03
3	-2.4401e-02
4	-2.4852e-02
10	-1.6768e-02
13	-5.3334e-05
14	-6.3045e-05
20	-4.2032e-02
110	1.0775e-05
120	-4.6064e-06

Table 5.17: Eigenvector of Loadflow Jacobian Near Singularity

For this singularity induced bifurcation the bifurcation subsystem method for loadflow model can be applied even though the eigenvalues are not changing continuously. The right eigenvector represents the sensitivity of active and reactive power to the angles and voltages on buses. The eigenvector has the largest elements in the voltage variables. This suggests that the algebraic bifurcation occurs in the reactive power voltage Jacobian. It can be found in Table 5.17 that the voltage eigenvector elements of bus 3, 10, and 20 have the same signs, and their magnitudes are close to each other. The eigenvector shows that the bus group 3, 10, and 20 is a coherent bus group in network voltage change and that line 2-20 is on the boundary of this coherent group [30]. The cause of the bifurcation is either internal or on the boundary of the coherent group. This suggests that the increased line reactance and the reactive loss on that element produces the algebraic bifurcation that in turn produces the singularity induced bifurcation in the differential algebraic model. The line reactance

between bus 2 and 20, bus 3 and 101 are very large. Also, the reactance between bus 3 and load bus 4 is large due to the transformer connecting the load bus 4. Thus, the geometrically neighboring bus 3, 10, and 20 form a coherent group, and it can considered as the bifurcation subsystem of the algebraic model.

It should be pointed out that singularity induced bifurcation is generic phenomena for power system. Power system dynamics always are constrained by network equations and turn to be differential-algebraic model. Then, the singularity of network equations exists. This singularity is very important since it may be stability boundaries, trajectory sources or sinks, and it can cause further bifurcations.

Remark:

Voltage instabilities are generally caused (at least partially) in the loadflow model due to losing control of voltage via generator field current limiters. Each of above bifurcation subsystems contains the generator inertial dynamics, exciters and/or stabilizer control loop. For large systems the bifurcation occurs in these dynamics first before it occurs in the algebraic model, but the stress on the algebraic model produces the bifurcations.

Chapter 6

Robust Control Design for Power System

6.1 Objective

Bifurcation phenomena for power system has been discussed in detail in the previous chapters, especially in Chapter 5. As we have mentioned, Hopf bifurcation, which refers to the interarea and local oscillations, can cause the voltage stability problem and it has been well known that interarea oscillations are difficult to control. The oscillations can be increasing if a subcritical Hopf bifurcation occurs and these can lead to action of protective relays that produces a blackout. Another class of bifurcations, saddle-node bifurcation, could also be disastrous for power systems. Saddle-node bifurcation has been observed in the blackouts that occurred in WSCC system [20] [23] [24]. Both of them can cause power system instability problems.

Many regulators are required to maintain the power supply, voltage, frequency, and damping control in a power system. Automatic voltage regulators (AVR) and governors normally meet specifications that are associated with the steady-state power

system performance and constrained by the thermal limit on elements and devices of the system. FACTS devices are used to control the voltage or power flow through transmission lines and can be used to damp oscillations. Power system stabilizers can add damping to the generator inertial oscillation by controlling its excitation system using auxiliary stabilizing signals. Although many of these regulators have been carefully designed there remain numerous stability problems without solution or with ineffective solutions.

The origins of need for control are:

1. to stabilize the unstable plant;
2. to reject disturbance and make the system robust to parametric variation and uncertainty;
3. to track the reference signals.

Our objectives in this thesis is to utilize control to stabilize an unstable plant that has experienced bifurcation of a particular type, class, and agent due to a specific disturbance or parameter variation. This objective may be extended to consider several classes of one bifurcation type due to more than one disturbance or parametric variation. These objectives will be pursued using robust control because each bifurcation produces instability for a specific bifurcation due to change in a very specific parameter. The change in parameter can be modeled either as parameter variation or as input and output uncertainty. The robust control could focus on maintaining stability for that change in bifurcation parameter. The ability to identify a bifurcation subsystem within a full system model allows one to focus on the center manifold dynamics that are experiencing, producing, and causing the instability. The use of the powerful design tools of robust control and their modification to accomplish stabilization of bifurcation subsystem dynamics and yet accomplish system based goals

is studied in this research.

The control objective of tracking the reference signals is not part of the thesis. Regulation of power generation and voltage to set point values is part of the control design in this thesis. The limitation on the proposed research is imposed because the instability caused by inability to track power or voltage set point change is assumed to be slow enough that good robust regulation should be adequate because, otherwise, it complicates this initial investigation of the application of robust control to stabilize a bifurcation.

6.2 Control Structure Design

The control structure design is closely related to the achievement of control objectives and is associated with the following steps [35]:

1. selection of controlled outputs (a set of variables which are to be controlled to achieve a set of specific objectives);

2. selection of manipulations and measurements (sets of variables which can be manipulated and measured for control purposes);

3. selection of control configurations (a structure interconnecting measurements/ commands and manipulated variables);

4. selection of a controller type (control law specification, e.g. PID controller, decoupler, LQG etc).

MIMO system may have a number of states and it should be careful to choose the controlled outputs such that the overall system goal can be achieved although they may not appear to be important variables in themselves. The outputs should be

selected such that the inputs have a large effect on outputs and the output errors are easy to control. This is related to the property of direction in MIMO system.

Selection of inputs and outputs has been known as a combinational problem and is very difficult for a large system model. This problem can be avoided by using relative gain array (RGA matrix) of the large system transfer function as a screening tool. RGA matrix was first introduced as a steady-state measure of interaction for decentralized control for MIMO system and has a number of useful control properties. In most cases, the RGA matrix at frequencies close to the crossover frequency ω_c is very important. RGA is a good indicator of sensitivity to uncertainties when an element has value much greater than 1.0. Around crossover ω_c the plant with large RGA elements is fundamentally difficult to control since it is very sensitive to the input uncertainty. This provides very important information for the choice of input and output pairs. RGA columns and rows where all elements have small magnitudes also indicate which control input does not have effect on any system output and which output can not be controlled. The RGA matrix can identify subsystem outputs that have one effective control. The decoupling of subsystems is observed by the lack of competition for control of a specific subsystem outputs by controls that are effective in other subsystems of output variables. It is noted that RGA is scaling independent and needs to be computed only once. More details about RGA can be found in [35].

Control configuration are the restrictions imposed on the overall controller by decomposing it into a set of local controllers with predetermined links and with a possibly predetermined design sequence where subcontrollers are designed locally [35]. Some elements of control configuration include cascade controllers, decentralized controllers, selectors etc and each of them has its own characteristic. For example, cascaded or decentralized control saves on modeling effort since they depend strongly on feedback rather than on the model, and partial control involves controlling only a subset of the outputs for which there is a control objective. These structures may be

needed to design controllers for bifurcation subsystems that are uncoupled or that are coupled for a particular type and class of bifurcation or different types and classes of bifurcation.

The control law specification is also important. Bifurcation is a nonlinear phenomena and normally one would expect to utilize nonlinear control for stabilization. For example, nonlinear feedback linearization can cancel the nonlinearities in the system and thus could be one of the choices. However, it is required that the decoupling matrix is nonsingular to apply this method [48] and this is difficult especially when bifurcation occurs. Also, it is very difficult to be applied to power system since the system model is generally very large. Moreover, it can not handle the uncertainty and this uncertainty is unavoidable in power system model. This suggests that good performance of nonlinear control is difficult to achieve for a power system.

For a power system the main problem related to the control design is that the system always experiences changes of power generation, transmission and load conditions, and the optimal settings depend on specific operating point. This makes it difficult to achieve the desired performance by using only the nominal model, as has been observed in power system control design. The performance of the designed controller may be unacceptable under some operating conditions. Therefore, robust control is necessary to ensure that system stability and performance is acceptable despite the parameter variation and operating condition changes, i.e., the existence of various uncertainties.

A control system is robust if it is insensitive to differences between the actual system and the model of the system which was used to design the controller. These differences refer to model uncertainty. Linear representation of the nonlinear uncertainty is difficult but very important in robust controller design.

Model uncertainties can be grouped into three classes: parametric uncertainties caused by uncertain parameters, neglected and unmodeled dynamics, and lumped uncertainties which is actually a combination of above two kinds of uncertainties. For MIMO system the uncertainties have structures, i.e., structured uncertainties in the form of diagonal complex matrix, which is mostly originated from the independent scalar uncertainty in each input or output channel and is always present, and unstructured uncertainties in the form of full complex matrix. For MIMO system the uncertainty is associated with the plant directionality. As a consequence MIMO system may experience much larger uncertainty than SISO system, especially for ill-conditioned plants. This should be carefully considered while trying to lump various uncertainties together or move uncertainty from input to output. In this situation the magnitude of RGA or the condition number of the plant is required for the decision on the uncertainty representation.

6.3 Robust Control

6.3.1 Uncertainty Modeling of General System

The system uncertainty plays a very important role in order to achieve the desired design performance despite the fact that the modeling of the system uncertainties is difficult. Model uncertainties can be grouped into three classes: (1) parametric uncertainties caused by uncertain parameters; (2) neglected and unmodeled dynamics; and (3) lumped uncertainties which is actually a combination of the other two kinds of uncertainties. For a MIMO system the uncertainties have structures, i.e., structured uncertainties in the form of a diagonal or block diagonal complex matrix. This diagonal or block diagonal complex matrix can model the independent scalar uncertainty in each input or output channel that is always present. Unstructured

uncertainties have the form of a full complex matrix. For a MIMO system the uncertainty are generally associated with the plant directionality and thus more difficult to model.

Due to the complexity of power system only simplified models can be obtained by omitting some dynamics of both generators and load devices. Unmodeled dynamics, which are often highly nonlinear, always exist in actual power systems. This poses a gap between the control performance we expect and the control performance we can achieve when applying the designed control to the actual power systems. The operating conditions for power system are always changing due to various parameter variations, such as active and reactive power load, power generation, line reactance, or even outages of generators, lines, or transformers due to electrical faults, maintenance, or scheduling. These make it more difficult to design power system control. In this thesis we are concerned about the parametric uncertainty caused by the change of operating conditions. These uncertainties contribute a large portion of the power system uncertainties in a power system model and play a significant role in causing different types and classes of bifurcation as we have shown in Chapter 5.

The design of robust control depends on the uncertainty modeling of the system over the change of operating point and parameter variation. Usually the parametric uncertainty modeling can be translated into the frequency domain [35]. The uncertainty region of the perturbed transfer function can be approximated by a "disc" or "circle". This variation can thus be approximated by the weighting matrix transfer function evaluated at some nominal operating conditions. This uncertainty modeling method has been used broadly, as we noted in [36] [37] [38] [25]. However, this method usually leads to a conservative design since the uncertainty region has to be approximated by the largest disc-shaped region.

Another approach of uncertainty modeling considers the structural information and

how the elements of the system matrix are affected by specific parameter variations. This generates the LFT representation of structured parametric uncertainties and have been used in [39][40][41]. A general LFT representation of high order matrix polynomials is presented in this section.

Considering a linearized model $(A(\delta), B(\delta), C(\delta), D(\delta))$, of a nonlinear system with a single uncertain parameter δ. We take the parameter dependent matrix $B(\delta) \in R^{n_1 \times n_2}$ as an example.

$$\eta = B(\delta)\zeta$$

where

$$B(\delta) = B_0 + \delta B_1 + \delta^2 B_{11} + \cdots$$

B_0 is the system matrix at nominal operating point.

In most cases the second order polynomial is able to provide the satisfactory approximation of the parametric uncertainty:

$$\eta = B_0\zeta + \delta B_1\zeta + \delta^2 B_{11}\zeta$$

Defining

$$\begin{aligned} y_{\Delta_1} &= B_1\zeta + u_{\Delta_2} \\ y_{\Delta_2} &= B_{11}\zeta \\ u_{\Delta_1} &= \delta y_{\Delta_1} \\ u_{\Delta_2} &= \delta y_{\Delta_2} \end{aligned}$$

gives

$$\begin{aligned}\eta &= B_0\zeta + \delta(B_1\zeta + \delta B_{11}\zeta) \\ &= B_0\zeta + u_{\Delta_1}\end{aligned}$$

Collecting the above equations we have:

$$\begin{bmatrix} y_{\Delta_1} \\ y_{\Delta_2} \\ \eta \end{bmatrix} = \begin{bmatrix} O_{n_1\times n_1} & I_{n_1\times n_1} & B_1 \\ O_{n_1\times n_1} & O_{n_1\times n_1} & B_{11} \\ I_{n_1\times n_1} & O_{n_1\times n_1} & B_0 \end{bmatrix} \begin{bmatrix} u_{\Delta_1} \\ u_{\Delta_2} \\ \zeta \end{bmatrix} \tag{6.3.1}$$

$$= B_f \begin{bmatrix} u_{\Delta_1} \\ u_{\Delta_2} \\ \zeta \end{bmatrix}$$

$$u_\Delta = \Delta(\delta) y_\Delta \tag{6.3.2}$$

where $u_\Delta = \begin{bmatrix} u_{\Delta_1} \\ u_{\Delta_2} \end{bmatrix}$, $y_\Delta = \begin{bmatrix} y_{\Delta_1} \\ y_{\Delta_2} \end{bmatrix}$, $\Delta(\delta)$ is defined as a diagonal real matrix $\Delta(\delta) = \delta I_{n_1\times n_1}$ and represents the parameteric uncertainty. Note that this uncertainty is structured and is shown in Figure 6.1.

In this example it is important to note that the general uncertainty at the component level becomes the structured uncertainty at the interconnection level. Unstructured uncertainty is represented as a full complex perturbation matrix and is compatible with the dimension of the plant, where at each frequency $\bar{\sigma}(\Delta(j\omega)) \leq 1$ is satisfied. They are usually in 3 forms: (1) additive uncertainty; (2) multiplicative input uncertainty; and (3) multiplicative output uncertainty.

Thus, the LFT form representation of $B(\delta)$ is:

$$B(\delta) = B_u(B_f, \Delta(\delta))$$

This leads to the upper LFT form of the system representation in state space, as shown in Figure 6.1. For parametric uncertainty the unknown perturbation Δ is structured since it is diagonal or block diagonal. This uncertainty represents the relationship between input and output in a LFT feedback manner. The uncertainty

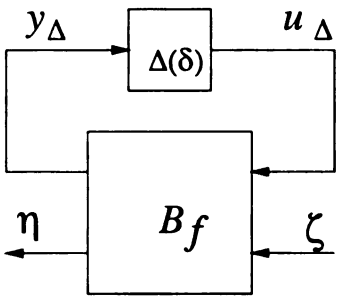

Figure 6.1: LFT Form of Uncertain System Representation

should be normalized, i.e., $\delta \in [-1, 1]$, to represent deviation of the change of parameters. $\delta = 1$ indicates the maximum parameter variation in the positive direction and $\delta = -1$ indicates the maximum parameter variation in the negative direction. The coefficient matrices B_1 and B_{11} need to be solved to obtain the uncertainty model. Here we are going to introduce a straightforward method that determines these matrices.

Each element b_{ij} of $B(\delta)$ can be represented as:

$$b_{ij} = b_{0_{ij}} + \begin{bmatrix} b_{1_{ij}} & b_{11_{ij}} \end{bmatrix} \begin{bmatrix} \delta \\ \delta^2 \end{bmatrix}$$

This represents a mapping between $\delta \in [-1, 1]$ and the element variation $b_{ij} - b_{0ij}$. Therefore, by taking different values of δ between 1 and -1 and the corresponding element variation the coefficients $b_{1_{ij}}$ and $b_{11_{ij}}$ can be solved using least-square method over the parameter change range and differences between the corresponding variation of the system matrix and the nominal system matrix.

For a single parameter perturbation the order of $B_f(\delta)$ is $3n_1 \times (2n_1 + n_2)$. It is

also applicable to multiple parameter situation and higher order representation of uncertainty. For multiple parameter variations the reduction of matrix $B_f(\delta)$ order is possible [40].

The LFT representation of a perturbed system $(A(\delta), B(\delta), C(\delta), D(\delta))$ with w as input and z as output is shown in Figure 6.2, where *int* indicates the integral block, A_f, B_f, C_f, and D_f are augmented system matrices including the uncertainty channels, and $u_{\Delta_{a,b,c,d}}$ and $y_{\Delta_{a,b,c,d}}$ are the outputs and the inputs of uncertainty block, respectively. w are the exogenous inputs such as reference signals, and z are the system outputs such as the errors to be minimized. H_∞ controller K can be designed, where v are the measurements and u are the control signals to be applied to the system. This leads to the general configuration of the H_∞ control design. The interconnection shown in Figure 6.2 is very easy to implement with Matlab. The A_f, B_f, C_f, and D_f matrices include the system matrices at nominal operating conditions. If uncertainty Δ_a, Δ_b, Δ_c, and Δ_d are incorporated into the A_f, B_f, C_f, and D_f matrices it would produce the system matrices at the bifurcation value μ^*.

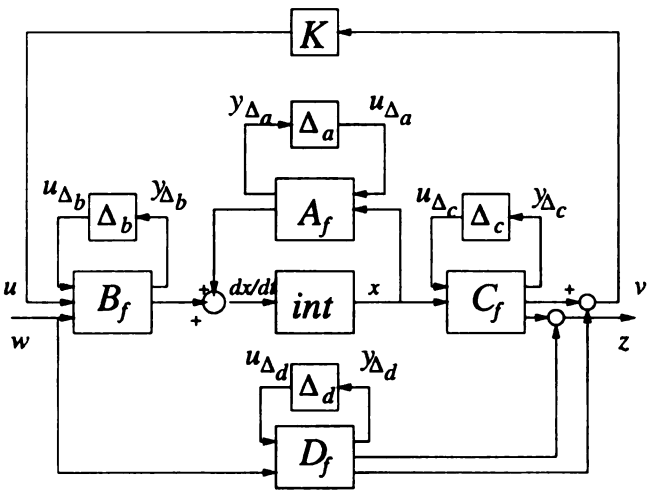

Figure 6.2: LFT Representation of System in State Space Form

6.3.2 General Robust Control Design

For the purpose of general robust controller design, the control problem is recast into LFT form as Figure 6.3 by pulling out all of the model uncertainties. Block Δ parameterizes all of the known model uncertainty in the problem. P is the open loop connection of the system containing all the nominal system elements, performance weighting functions, input and output weighting functions, and uncertainty weighting functions. There are 3 kind of inputs to P: (1) uncertainty block output u_Δ; (2) exogenous inputs w consisting of disturbances, noises, and reference signals; and (3) control output signal u. The outputs of P are (1) y_Δ, the input to the uncertainty; (2) the error signal z to be minimized; and (3) the measurements v. The controller K to be designed is also pulled out. If controller K is given the closed-loop uncertain

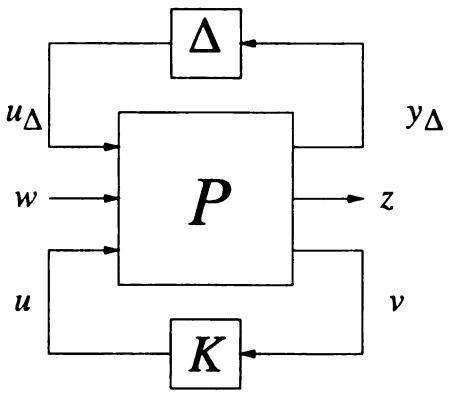

Figure 6.3: General Control Configuration

system can be analyzed with $N\Delta$-structure shown in Figure 6.4, where the given controller K is absorbed into the system by

$$\begin{aligned} N &= P_{11} + P_{12}K(I - P_{22}K)^{-1}P_{21} \\ &= \begin{bmatrix} N_{11} & N_{12} \\ N_{21} & N_{22} \end{bmatrix} \end{aligned}$$

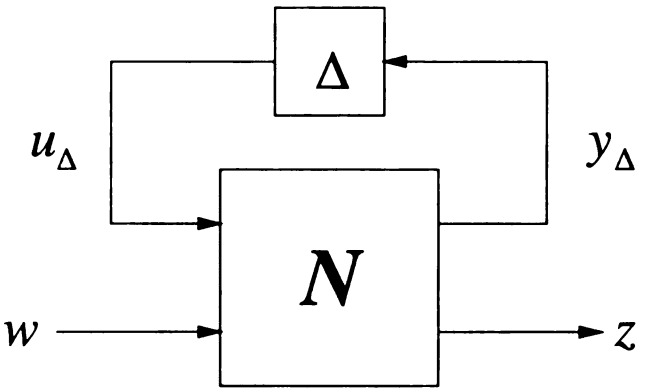

Figure 6.4: $N\Delta$-Structure for Analysis

In Figure 6.4 the uncertain closed-loop system transfer function from w to z, $z = Fw$, can be obtained with upper LFT by absorbing the uncertainty:

$$F = F_u(N, \Delta) = N_{22} + N_{21}\Delta(I - N_{11}\Delta)^{-1}N_{12}$$

In terms of the $N\Delta$ structure in Figure 6.4 the requirements for nominal stability (NS), nominal performance (NP), robust stability (RS) and robust performance (RP) are defined as [35]:

$$\begin{aligned}
\text{NS} &\iff \text{N is internally stable} \\
\text{NP} &\iff \| N_{22} \| < 1; \text{and NS} \\
\text{RS} &\iff F = F_u(N, \Delta) \text{ is stable } \forall \Delta, \| \Delta \|_\infty \leq 1, \text{and NS} \\
\text{RP} &\iff \| F \|_\infty < 1, \forall \Delta, \| \Delta \|_\infty \leq 1; \text{and NS}
\end{aligned}$$

Remark:

H_∞-norm of a linear stable system corresponds to the peak of the largest singular value at the worst direction and the worst frequency. The H_2-norm is defined as the sum of the squares of singular values over all the frequencies, i.e., at the average direction and the average frequency. The fact that H_∞-norm is applied in robust

control is because it provides natural representation of the unstructured uncertainty. H_∞ control theoretically provides optimal or suboptimal control for a system where the uncertainty is largest and at the worst frequency. The robust design methodology coordinates the uncertainty, frequency, and subsystem where the control has effect. The frequency is the bifurcation frequency ($\omega = 0$ for saddle-node bifurcation and $\omega = \omega_0$ for Hopf bifurcation) of the specific bifurcation to be controlled; the uncertainty is the nonlinear change in the linearized model that occurs due to bifurcation parameter change to the bifurcation value; and the subsystem controlled is the bifurcation subsystem which experiences, produces, and causes the bifurcation in the full system model.

The robust stability of $N\Delta$-structure in Figure 6.4 is equivalent to the stability of $M\Delta$-structure [35] shown in Figure 6.5, where $M = N_{11}$.

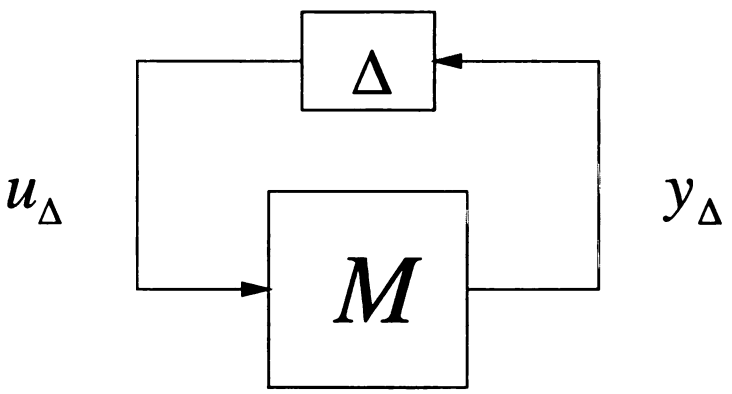

Figure 6.5: $M\Delta$-Structure for Analysis

The robust stability and performance of a system with structured perturbations can be analyzed by the structural singular value μ, which is a generalization of the maximum singular value and spectral radius. For the $M\Delta$-structure system shown in Figure 6.5 assuming that the nominal system M and Δ are stable, then the necessary and sufficient condition for $M\Delta$ system to be stable is that $\mu(M(j\omega)) < 1, \forall\omega$.

The structured singular value μ of a given complex matrix M is defined as

$$\mu(M) = \frac{1}{\min\{k_m | \det(I - k_m M\Delta) = 0 \text{ for structured } \Delta, \bar{\sigma}(\Delta) \leq 1\}}$$

If no such a structured Δ exists then $\mu(M) = 0$. By scaling the uncertainty Δ with factor k_m we look for the smallest k_m that represents the stability margin $\mu(M)$. The $\mu(M(j\omega)) < 1$ condition for stability requires the minimum k_m scaling of uncertainty value must be greater than 1.0.

From the definition of the robust performance and the equivalence of stability of $M\Delta$ in Figure 6.5 and $N\Delta$ structure in Figure 6.4, the robust performance of $N\Delta$ system is satisfied if and only if $\mu_{\tilde{\Delta}}(N(j\omega) < 1, \forall\omega$, where $\tilde{\Delta} = diag\{\Delta, \Delta_P\}$ is an augmented uncertainty structure, where Δ_P represents the uncertainty in the output error z and exogenous input dynamics. The conditions for NS, NP, RS, and RP can be redefined with μ:

$$\begin{aligned}
\text{NS} &\iff \text{N is internally stable} \\
\text{NP} &\iff \sigma(N_{22}) = \mu_{\Delta_p} < 1, \ \forall\omega, \text{ and NS} \\
\text{RS} &\iff \mu_{\Delta}(N_{11}) < 1, \forall\omega, \text{ and NS} \parallel \Delta \parallel_{\infty} \leq 1 \\
\text{RP} &\iff \mu_{\tilde{\Delta}}(N) < 1, \ \forall\omega, y < 1, \forall\Delta, \text{ and NS}
\end{aligned}$$

where $\tilde{\Delta} = \begin{bmatrix} \Delta & 0 \\ 0 & \Delta_P \end{bmatrix}$, and Δ_P is a full complex perturbation matrix that specifies the uncertainty in system dynamics between z and w, and is a fictitious uncertainty block.

Δ_P represents the uncertainty of the closed-loop system N_{22}. The performance of a given controller can be analyzed via μ-value. μ-analysis can also be used to design the controller. The goal is to find the controller that minimizes the peak μ value of

the closed-loop system, and thus achieves robust stability and robust performance of the closed-loop system for all the possible perturbations. Δ is the uncertainty used to assure the robust stability when N is stable.

DK-iteration, which combines μ analysis and H_∞ synthesis, is available to seek the optimal controller that minimizes a given μ-condition. Because the μ value is bounded by the spectral radius and the maximum singular value for the complex perturbation and the scaling does not change the μ value if the scaling matrix commutes with the uncertainty Δ, i.e., $D\Delta = \Delta D$, for the $N\Delta$ structure shown in Figure 6.4 the upper bound of μ value can be replaced by:

$$\mu(N) \leq \min_{D \in \mathcal{D}} \bar{\sigma}(DND^{-1})$$

where for every $D \in \mathcal{D}$, $D\Delta = \Delta D$ is satisfied. Therefore, the goal of the controller K design is to minimize the peak μ value of this upper bound

$$\min_{K}(\min_{D \in \mathcal{D}} \parallel DN(K)D^{-1} \parallel_\infty)$$

with respective to D and K alternatively. For each ω, the two step algorithm determines both K and D using the following three step procedures: 1) K-step, the H_∞ controller is synthesized by holding D constant, i.e., $\min_K \parallel DN(K)D^{-1} \parallel_\infty$; 2) D-step, scaling matrix $D(j\omega)$ is pursued with K obtained in K-step such that $\sigma(DND^{-1})$ is minimized; and 3) fit the magnitude of $D(j\omega)$ element to a stable and minimum phase transfer function $D(s)$. This is an iterating process and can be implemented via μ-synthesis toolbox provided in Matlab.

Remarks:

The above DK algorithm is based on the following logic:

1. μ can be seen from the definition as finding a Δ with $\bar{\sigma}(\Delta) \leq 1$ radius that has

maximum impact on M and requires a minimum value of k_m scaling such that $\det(I - k_m M\Delta) = 0$. k_m measures how close the system is to the instability with the worst uncertainty;

2. Since $\mu(M) \leq \bar{\sigma}(M)$ and $\mu(DMD^{-1}) = \mu(M)$ (Pg. 314 and 315 in [35]), the scaling matrix D with $D\Delta = \Delta D$ has no effect on μ value but can have effect on its upper bound $\bar{\sigma}(M)$;

3. We desire to find the weakest direction in which M is susceptible to the uncertainty by selecting Δ in remark 1. The μ value can not be directly computed but $\bar{\sigma}(M)$ can be computed and provides an approximation to $\mu(M)$. Therefore, using the $= mu$ value we find an improved upper bound on μ by scaling since $\mu(M) = \mu(DMD^{-1}) \leq \min \bar{\sigma}(DMD^{-1})$. We can not scale μ to find lower value since μ already does that by definition but we can scale $\bar{\sigma}(M)$ to find the lowest upper bound and the best approximation for $\mu(M)$, that measures the weakness of M to uncertainty.

6.3.3 *RGA* Matrix Analysis

The *RGA* matrix plays an important role in the system performance analysis. *RGA* matrix has been been known and yet ignored for a long time. The *RGA* matrix of a transfer function G is defined as:

$$RGA(G) = G \times (G^{-1})^T$$

where $\times$ indicates the Hadamard or Schur product.

RGA matrix is independent of input and output scaling and has a number of other control properties that can be found in [35]. It is also a good indicator of system sensitivity to uncertainty. The magnitude of a *RGA* matrix element should not be

too small. A very small magnitude of a RGA element indicates a weak direction of the corresponding control. Also the magnitude of RGA element should not be too large. A large magnitude for a element indicates that the system is very sensitive to the disturbance in this input-output direction. A system with large RGA element magnitudes around the crossover frequency implies that the plant is fundamentally difficult to control due to uncertain or unmodeled actuator dynamics. This tells us that the input i and output j which are linked by the element (i, j) of magnitude close to 1 are good pairs since this means that the gain from input i to output j is not affected by closing other loops.

The elements in RGA matrix reveal the effective control direction and disturbance rejection directions of the system. RGA matrix also reflects the control performance of the system. Therefore, the evaluation of a control design should be based on the RGA matrix structure by the robust controller. The RGA matrix should be evaluated at steady state, the crossover frequency, and the bifurcation frequency. This will tell us the steady state performance, the transient response, and the control performance when bifurcation occurs. All the controllers to be designed will be discussed in terms of RGA matrix.

The RGA matrix can capture bifurcation subsystem by producing a block diagonal matrix of the RGA matrix of the bifurcation subsystem in the upper diagonal block, RGA matrix of the external system in the lower diagonal block with zero off diagonal blocks. The diagonal effectiveness of the control in each subsystem is shown by having at least one large element in each row for each subsystem suggesting each output has one and only one effective control. If one control is used for controlling all outputs in the subsystem then one column in that subsystem will have large elements near 1.0 which is the column associated with the effective control. All the other columns will be small in that block diagonal matrix. Having more than one column large with large elements in the same rows suggests competition for control

of those outputs. Thus, the bifurcation subsystem could experience noncompetitive effective control if each output had only one large element appearing in row of the RGA matrix associated with it. The results suggest each output of the bifurcation subsystem had different effective noncompetitive controls and disturbance resistant controls (all output frequency differences were controlled by the robust control, and excitation system voltage outputs were controlled by excitation systems on those generators)

The robust control design methodology that is used in the design of the PSS and SVC controls has the following four components. The first component of this methodology is the use of the RGA analysis to show that the robustness produced by this methodology, breaks the external system into subsystems that are decoupled from one another and from the bifurcation subsystem. Each subsystem including the bifurcation subsystem is shown via RGA matrix to have one and only one effective control for each output variable so that there is no competition for control in any subsystem. The RGA matrix shows that the control in each subsystem is effective (one element near 1.0) and resistant to disturbance or noise on any subsystem (no element above 1.0). The RGA matrix can also show how the control structure change for $\omega = 0$, the Hopf bifurcation frequency, and the cutoff frequency for the control. The RGA matrix is theoretically shown to capture the bifurcation subsystem and can be used to show the bifurcation subsystem structure exists long before the bifurcation parameter reaches the bifurcation value and may imply that the external subsystem may be other bifurcation subsystems that could experience bifurcation if the correct control is used. The second component of the robust design methodology is to use a structured uncertainty that captures the nonlinear change in linear model due to the bifurcation parameter change from the nominal value to the bifurcation value. The structured uncertainty principally captures the uncertainty in the bifurcation subsystem that experiences, produces, and causes the bifurcation in

the full system model. This structured uncertainty produces a 50% increase in the feasibility region in the direction of the bifurcation parameter but does not produce the subsystem structure of the external system. A dynamic system uncertainty that in combination with the structured uncertainty is shown to produce the subsystem structure of the external system. The third component is the use of the bifurcation subsystem model for design of the controller rather than the full system. The resultant SISO controller is then the order of the bifurcation subsystem rather than the order of the full system model. The computation required to obtain the μ-synthesis controller is also reduced and makes application of μ-synthesis control to very large power system models feasible without model reduction that does not capture the small bifurcation subsystem that experiences, produces, and causes the bifurcation and retains the dynamic system properties associated with the bifurcation of the full system model. The fourth component is the selection of the performance index, weighting matrix, measurements and control that are based on the bifurcation and the bifurcation subsystem being stabilized.

H_∞ control attempts to find the control that minimize the performance index for the possible uncertainty that occurs at the frequency where the system is most vulnerable. The design methodology preselects and coordinates the frequency uncertainty and subsystem at which the robust controller should have effect. The frequency where the system is most vulnerable is the bifurcation frequency ($\omega = 0$ for saddle-node bifurcation and $\omega = \omega_0$ for Hopf bifurcation. The uncertainty is the nonlinear change in the linearized model caused by the change in the bifurcation parameter that produced the bifurcation subsystem, and the subsystem where the control has effect in increasing the feasibility region, and the nonlinear modal coupling is the bifurcation subsystem. This coordination within this design methodology enables the very significant control performance improvements obtained.

6.4 μ-synthesis Power System Stabilizer (MPSS)

6.4.1 μ-synthesis Power System Stabilizer Design

This section follows the standard μ-synthesis and analysis procedures for the power system stabilizer design.

The two-area example power system upon which a robust power system stabilizer is to be designed, consists of two generation and load areas and the network for this example system diagram is shown in Figure 5.1. The bifurcation subsystem method has been applied to this example system and various types and classes of bifurcation subsystem were obtained. It is concluded that this two-area system is vulnerable to saddle-node, Hopf and singularity induced bifurcation.

As we have shown in Chapter 5, active power load variation is an important bifurcation parameter that causes the interarea oscillation. Running active power load test on buses in the network will cause Hopf bifurcation and lead to instability of the full system. Hopf bifurcation will result in the oscillations in the power system response. They can be interarea oscillations or local oscillations. The growing oscillations can become a voltage stability problem as a transient load model (that is voltage dependent) becomes a steady state load model (constant power). This transition from interarea oscillations to voltage collapse occurs because (1) the load model transitions from a transient model to a steady state model and (2) a voltage dependent load is vulnerable to Hopf bifurcation where the same bifurcation subsystem is vulnerable to saddle-node bifurcation when the load model is constant power from results in Chapter 5. The purpose of this robust control design in the initial design is to damp the interarea oscillation (Hopf bifurcation) caused by the active power load increase as well as maintaining the voltage output by increasing the bifurcation value μ^* of the bifurcation parameter μ.

The resulting linearized full system is similar to Figure 6.2. The two-area system is stressed by increasing the active power load on bus 2 continuously. For each level of active power load, the system is linearized using the Power System Toolbox in Matlab and the system matrices (A_f, B_f, C_f, D_f) are obtained. The uncertainty coefficient matrices A_1, A_{11}, $\cdots$, D_1, D_{11} are calculated with least-square method. Using equation (6.3.1) and (6.3.2) the LFT form of system is represented along with matrix (A_f, B_f, C_f, D_f). The uncertain system can be computed for any parameter variation in the same way. It is easy to perform these steps using the μ-toolbox.

The basic function of a power system stabilizer (PSS) is to add damping to the generator rotor oscillations by controlling its excitation using an auxiliary stabilizing signal. To provide the damping the stabilizer must produce a component of electrical torque in phase with the rotor speed deviations. This is equivalent to changing the set point of the automatic voltage regulator (AVR).

The conventional PSS (CPSS) design approximates an inverse control by approximating $G^{-1}(j\omega)$, where $G(j\omega)$ is the transfer function relating generator terminal voltage and the frequency deviation of that generator. The PSS is then a damping control since the input to PSS is the rotational frequency deviation of the generator. The conventional PSS uses a fairly simple lead network compensator to adjust the input signal to give it the correct phase over the range of frequencies where the local or interarea inertial oscillation is expected to occur. The input to the stabilizer may be the generator shaft speed, electrical power or accelerating power, or terminal bus frequency, or a combination of these variables. The power signal is almost proportional to the negative of the rate of change of speed. The input is first passed through a washout to eliminate the input's steady state value.

With the development of FACTS control, where complex nonlinear, adaptive, and robust algorithms can be used to design controller, the use of such controls within a

digital AVR and PSS in order to achieve better performance [49] were investigated. However, the results initially obtained were not clearly superior to the inverse control PSS [46].

The μ-synthesis power system stabilizer is designed in this section. The purpose of MPSS design is to make the closed-loop system robust with respect to the active power load variation of bus 2 up to the bifurcation, which causes a Hopf bifurcation to occur to the open-loop system. Since the changes of some parameters do not necessarily destabilize the system, the bifurcation parameter should be selected as the source of the uncertainties because it is guaranteed to result in instability. The load at bus 2 produces the interarea oscillation mode, which has been studied on the example system. This will be used in uncertainty modeling.

The following procedures are used for the robust power system stabilizer design that will be used through this thesis. Before designing the power system stabilizer we should define the performance index to be minimized, i.e., what kind of performance we expect to achieve via this control design. When Hopf bifurcation begins to develop the angle vector diagram of the system has the form shown in Figure 6.6. We can see that generator 4 oscillates against the rest of generators of the system. This suggests that speed differences between generator 4 and rest of the generators should be controlled around the bifurcation frequency as well as the bus voltages. Therefore, a μ-synthesis based power system stabilizer (MPSS) will be designed for generator 4 in order to eliminate the Hopf bifurcation. For a power system stabilizer design the damping increase is obtained by using auxiliary input to excitation system voltage set point. That means the voltage set-point will be changed and the generator terminal voltage will be slightly different from the desired value. For conventional power system stabilizer design (CPSS) it is impossible to compensate this voltage error. For MPSS design the bus voltage difference between the actual output and desired voltage level at any of the thirteen different buses in the network can be

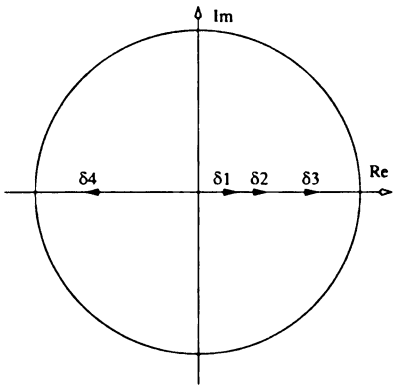

Figure 6.6: Generator Angle Vector Diagram

also included in the performance index. This will hopefully produce better voltage control. The last terms in the performance index is the error between the mechanical power set points P_{m_i} and the active power generation P_{G_i} of four generators, where $i = 1, 2, \cdots, 4$.

The following notation is introduced: $P_{REF_i} = P_{m_i}$ and $P_{OUT_i} = P_{G_i}, i = 1, 2, \cdots, 4$, indicate the input power references and active power outputs on generator bus $1, 2, 11, 12$. V_{REF_i} and V_{OUT_i}, $i = 1, 2, \cdots, 5$, indicate the voltage references and measured voltage outputs on generator terminal bus $1, 2, 11, 12$, and SVC bus 101, respectively. $V_{OUT_i}, i = 6, \cdots, 13$, represent the voltage outputs on other buses $3, 4, 10, 13, 14, 20, 110, 120$. $\omega_i, i = 1, 2, \cdots, 4$, represent the frequency on generator bus $1, 2, 11, 12$. The variables are redefined as noted above so that the errors can be easily determined for each variable and the performance index is clear.

The performance index of this μ-controller is defined as:

$$\begin{aligned} J &= \min[\Sigma_{i=1}^{4}|P_{REF_i} - P_{OUT_i}| + \Sigma_{i=1}^{5}|V_{REF_i} - V_{OUT_i}| \\ &+ \Sigma_{i=1}^{3}|\omega_i - \omega_4|] \end{aligned} \tag{6.4.3}$$

This performance index is important in the sense that it clearly suggests that this control design is to suppress the oscillations between generator 4 and rest of the

generators. It is more reasonable to minimize the frequency deviations with respect to generator 4 rather than the speed set point on each generator because damping the oscillation in ω_i would not necessarily damp the interarea mode and would certainly not effectively damp this interarea mode.

Note that the tracking performance is not required in the control design for a power system. Therefore, the integral action and large gain over the frequency range in the performance weighting function is not necessary.

The weighting function is used to shape the system error output and the desired upper bound of the subsequent errors are represented by $1/w_p(\omega)$. $w_p(s)$ is the performance weighting function:

$$w_p(s) = \frac{0.1s + 1}{0.01s + 1}$$

The weighting function here indicates that bandwidth is approximately 10 rad/s, and at low frequency the performance requirement is not stringent since at low frequency $|w_p(\omega)| \approx 1$ and only at high frequency $|w_p(\omega)| \approx 10$. The bandwidth is chosen so the response is reasonable fast and $w_p(0)$ is chosen so the low frequency gain is sufficient to make steady state errors small. The $w_p(s)$ chosen here does not specify stringent control performance requirement.

From above discussion the system is rearranged in the form shown in Figure 6.7, where Δ consists of all the uncertainties of system and is in the form of $diag\{\Delta_a, \Delta_b, \Delta_c, \Delta_d\}$. $pck(A_f, B_f, C_f, D_f)$ represents the LFT realization of the full system, which is obtained previously. K is the controller to be designed. The inputs are the references of the power system. P_{REF_i} and EP_i, $i = 1, 2, \cdots, 4$ indicate the mechanical power references and power output errors on generator i, $V_{REF_1}, \cdots, V_{REF_5}$ and $EV_1, \cdots, EV_5$ are the voltage references and voltage output errors on the four generator buses and SVC bus 101, respectively. ω_4, the speed on generator 4, is the only

measurement. $W_P = diag\{w_p, w_p, \cdots, w_p\}$ is the performance weighting matrix.

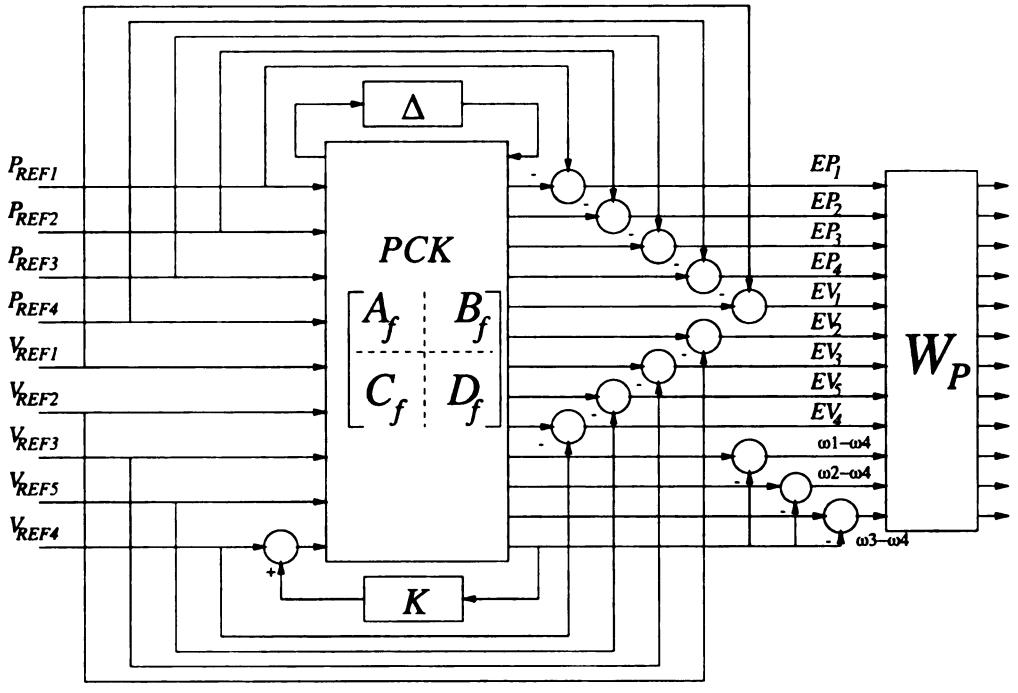

Figure 6.7: Control Configuration of Power System Stabilizer

The control configuration shown in Figure 6.7 is very flexible. Multiple controllers can be designed by pulling out the inputs and outputs and connect them to the controller. For example, if another excitation system on generator 2 needs to be designed, we need only connect the generator 2 terminal voltage output measurement to controller K and connect controller output to the summer for the generator 2 voltage set point. The performance index can be easily modified for different control purposes.

Based on system block diagram in Figure 6.2 and control configuration in Figure 6.7 DK-iteration is used to obtain a μ-controller. The μ-controller to be design has one input from the measurement of generator 4 speed, and one output to the voltage set point of excitation system voltage reference on generator 4. The μ value of the closed-loop system is shown in Figure 6.8. The μ-value is less than 1 over frequency range $\omega \in [10^{-3}, 10^{3}]$. The peak μ-value occurs between $\omega = 2$ rad/sec

and $\omega = 4$ rad/sec, which corresponds to the interarea oscillation frequency. This guarantees the robust performance of the closed-loop system over the parameter variation. Actually if the μ peak value is different than 1, then at this frequency the controller can tolerate $1/\mu$-times more uncertainty and the performance can still be satisfied with a margin of $1/\mu$. For this controller the robust performance can be assured with $1/\mu = 1.01$-times uncertainty. This makes sense because the bifurcation parameter range includes the point of bifurcation for the uncontrolled system. The μ-synthesis approach should produce a flat and small value over the control frequency range which is approximate 0.2 Hz to 60 Hz with the exception of the value at the oscillation frequency. The μ value at this frequency suggests robust stability even for a 1% increase in bifurcation parameter. This initial design is certainly not very robust.

The MPSS designed here is actually a local controller rather than a global controller since it only needs the measurement from generator 4 itself and performs control only on generator 4. It does not need the communication link to access the measurements from other generators or buses and does not need to communicate the one measurement on generator to a controller at any other generator.

The controller obtained is of high order and is difficult to implement. By using the bifurcation subsystem rather than the full system model to design the controller, the order of the controller can be reduced from the order of the full system to the order of the bifurcation subsystem, which is 15. This will be further discussed in section 6.5.2.

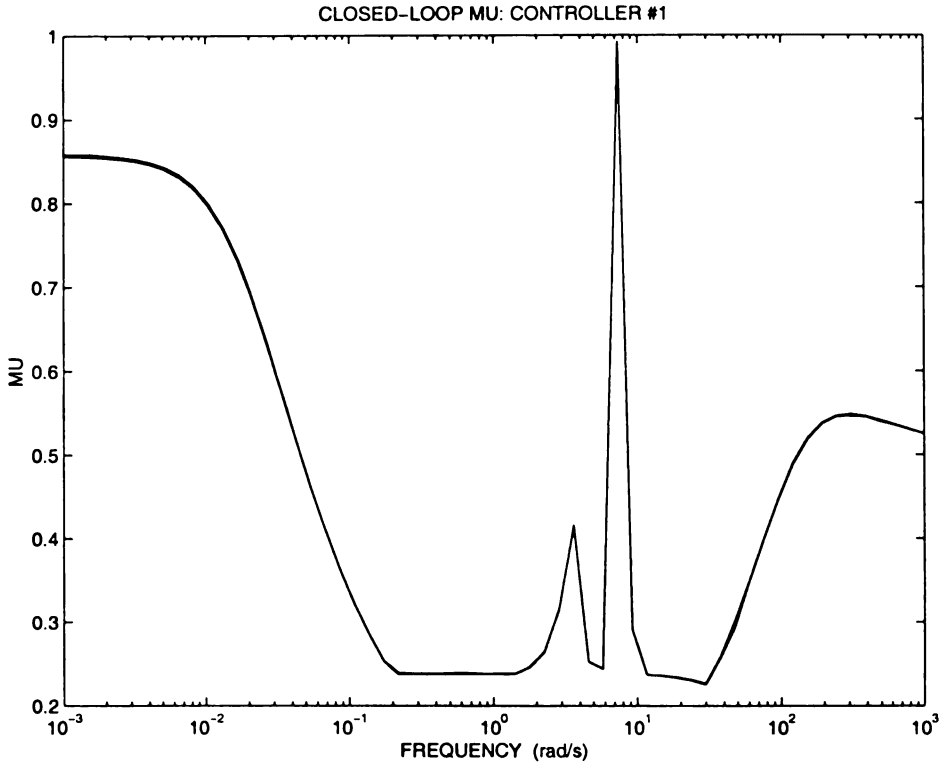

Figure 6.8: μ-value of Closed-loop System with MPSS

6.4.2 *RGA* Matrix Analysis for μ-synthesis Power System Stabilizer

The *RGA* matrix of the open loop system without MPSS at steady state ($\omega = 0$) is shown in Table 6.1. Here P_{REF_i}, V_{REF_i}, V_{OUT_i} have been defined previously. The corresponding elements indicate if the control is effective and if the system is sensitive to the input disturbance.

In Table 6.1 we can see that at steady state the elements (P_{REF_1}, P_{OUT_1}), $\cdots$, (P_{REF_4}, P_{OUT_4}) are much less than one, and (V_{REF_1}, V_{OUT_1}), $\cdots$, (V_{REF_5}, V_{OUT_5}) are much greater than one. This suggests respectively that the controls on power are not effective, and the controls on voltage are very sensitive to input uncertainty. By inspecting each column or row in Table 6.1 we find that there are a number of element magnitudes that are close to each other. This implies there are conflicts

among the controls since each control is trying to stabilize a number of outputs and each output is affected by several controls. The elements related to the generator speed have extremely small values and it reflects that the controls do not have much effect on the generator speed. This is true because generator speed is not directly controlled by power inputs and voltage inputs. This also explains why this two area example system is vulnerable to the interarea oscillations. It should be noted that the two area system is equipped with exciters, a conventional power system stabilizer on generator 3, and the SVC control at bus 101 at the midpoint of the lines that connects the two areas. Although the control devices of the open loop system are well designed and carefully tuned, the control performance is still not satisfactory for stabilizing this interarea oscillation. This also suggests that conventional control design methodology is not capable of achieving good control performance for the overall system.

Table 6.2 shows the RGA matrix of the closed-loop system with MPSS at steady state. From Table 6.2 we can see that element magnitude of the control pair $(P_{REF_1}, P_{OUT_1}), \cdots, (P_{REF_4}, P_{OUT_4})$, $(V_{REF_1}, V_{OUT_1}), \cdots, (V_{REF_5}, V_{OUT_5})$ are all close to 1. This indicates that the control input, especially power inputs, on each generator or bus is effective and is not sensitive to input uncertainties. This is in contrast to the system with only the CPSS. Inspecting the rest of the elements we find that most of them are much more smaller that 1. There are no two elements in any row with large elements but only one so that two or more controls are no longer fighting for control of an output. This is again in contrast with the system with CPSS. There is an almost decoupled control structure obtained by this robust control design because the MPSS on generator 4 has effects on the bus voltages where the extra control is needed in CPSS and because each generator and the SVC has control of the bus voltages in the vicinity of its terminal bus.

The MPSS has tremendously increased the magnitude of the elements related to the

generator speed compared to Table 6.1 from 10^{-17} to 0.005 in Table 6.2. Moreover, the frequency related elements under control of MPSS (V_{REF_4}) are the largest. This is clear by noting that the element magnitudes relating V_{REF_4} and $\omega_i, i = 1, 2, 3, 4$, and magnitudes of the rest of the elements in the ω_1, ω_2, ω_3, and ω_4 rows in Table 6.2. Therefore, the MPSS dominates the control actions of the generator speed. This is why MPSS dramatically decreases the interarea oscillations as shown in time simulations.

This MPSS not only dramatically improves the damping and control of the interarea oscillations of the dynamics contained in the bifurcation subsystem composed of δ_i, ω_i, $i = 1, 2, \cdots, 4$, but also provides a global structured control of voltage and power in the system

The global decoupled control structure of the voltages at network buses close to generator or SVC buses was not true for CPSS and logically should not be true for MPSS. The addition of the uncertainty in the system dynamics Δ_P relating z and w could explain why effective control of voltage at every bus is achieved with no fighting for control of certain bus voltages (where there are two or more large elements in a row) and very poor of control of other bus voltages with CPSS (where there are no large element in a row).

These results suggest an incredible level of control improvement via MPSS versus CPSS. This strongly contrasts with results found in [46], where it was difficult to obtain improvements using a robust control over that of a conventional power system stabilizer.

It anticipated that MPSS with inverse dynamics of the exciter system on generator 4 has better robust control performance than MPSS only. The RGA matrix of the closed-loop system with MPSS and inverse dynamics is shown in Table 6.3. From Table 6.3 it can be seen that an almost decoupled control structure is obtained

	P_{REF_1}	P_{REF_2}	P_{REF_3}	P_{REF_4}	V_{REF_1}
P_{OUT_1}	2.0122e-01	5.4940e-02	4.9468e-02	4.5633e-02	1.9901e-02
P_{OUT_2}	7.3241e-02	5.8099e-02	6.4694e-02	5.9171e-02	2.3407e-02
P_{OUT_3}	4.9381e-02	4.8561e-02	2.4306e-01	4.3897e-02	1.3832e-02
P_{OUT_4}	6.1719e-02	6.0172e-02	6.0655e-02	6.8637e-02	1.9699e-02
V_{OUT_1}	6.3270e-03	5.6395e-03	4.3453e-03	4.7831e-03	7.4752e-01
V_{OUT_2}	1.5971e-01	1.5839e-01	1.0530e-01	1.0866e-01	6.1495e-02
V_{OUT_6}	4.6791e-01	5.0714e-01	1.1412e-02	8.6905e-02	2.0189e-01
V_{OUT_7}	5.4669e-01	5.9361e-01	2.1501e-02	1.3209e-01	2.3546e-01
V_{OUT_8}	2.7831e-01	2.3012e-01	2.9681e-01	3.2250e-01	2.0031e+00
V_{OUT_3}	5.0657e-02	5.6469e-02	7.7372e-02	6.2509e-02	1.8649e-02
V_{OUT_4}	8.8706e-02	9.5712e-02	1.1995e-01	1.1043e-01	1.6749e-02
V_{OUT_9}	4.5400e-03	7.9490e-02	2.4420e-01	2.2972e-01	3.5690e-01
$V_{OUT_{10}}$	1.8105e-04	8.9868e-02	2.8902e-01	2.7113e-01	4.2977e-01
$V_{OUT_{11}}$	1.4812e-01	1.3935e-01	2.8112e-02	8.9879e-02	3.3373e-02
V_{OUT_5}	6.7254e-01	6.8109e-01	6.0622e-01	5.6385e-01	5.4493e-02
$V_{OUT_{12}}$	1.7343e-01	2.2125e-01	3.7940e-01	3.0226e-01	2.0382e-01
$V_{OUT_{13}}$	2.6434e-02	3.0909e-02	2.4767e-01	1.9841e-01	2.8566e-01
ω_1	6.6097e-14	1.2006e-18	2.3682e-18	4.3358e-18	2.7118e-19
ω_2	6.6204e-14	3.3906e-18	3.4301e-18	6.5364e-19	2.1276e-18
ω_3	6.6152e-14	5.5736e-19	1.3935e-18	9.1547e-19	3.3488e-19
ω_4	6.6163e-14	9.0147e-20	1.2116e-18	9.3615e-19	8.9884e-20
	V_{REF_2}	V_{REF_3}	V_{REF_4}	V_{REF_5}	
P_{OUT_1}	2.2113e-01	2.9037e-02	1.2899e-01	1.7218e-0	
P_{OUT_2}	3.0010e-01	4.2180e-02	1.8328e-01	2.3603e-01	
P_{OUT_3}	1.5314e-01	5.0814e-02	1.8643e-01	1.3539e-01	
P_{OUT_4}	2.0781e-01	5.3018e-02	2.2633e-01	1.7295e-01	
V_{OUT_1}	2.3218e-02	3.5323e-03	7.8761e-03	1.6712e-03	
V_{OUT_2}	1.3462e+00	2.6109e-02	1.6950e-02	3.0039e-01	
V_{OUT_6}	2.9699e+00	7.3347e-01	2.5797e+00	2.6832e-01	
V_{OUT_7}	3.2417e+00	8.2745e-01	2.8729e+00	3.3651e-01	
V_{OUT_8}	8.7573e-01	2.2550e-01	3.8370e-01	1.3186e+00	
V_{OUT_3}	6.1857e-02	1.1460e+00	2.6464e-01	2.7972e-02	
V_{OUT_4}	1.4313e-02	1.0727e-01	1.2673e+00	2.4954e-01	
V_{OUT_9}	2.5764e+00	3.1617e-01	2.5100e+00	3.8238e-01	
$V_{OUT_{10}}$	3.1117e+00	3.7947e-01	3.0432e+00	4.7068e-01	
$V_{OUT_{11}}$	4.0576e+00	4.9322e-01	1.5049e+00	2.1986e+00	
V_{OUT_5}	2.0367e+00	1.7718e-01	1.8977e+00	7.4764e+00	
$V_{OUT_{12}}$	1.0423e+00	3.0569e+00	9.1927e-01	1.6207e+00	
$V_{OUT_{13}}$	1.9078e+00	1.4786e-01	3.8524e+00	1.7270e+00	
ω_1	2.3879e-17	3.4597e-18	1.6231e-17	1.1048e-18	
ω_2	1.3125e-17	1.3600e-18	1.8060e-18	1.5227e-17	
ω_3	8.7529e-18	1.1983e-18	4.6431e-18	2.3261e-18	
ω_4	8.7227e-18	1.3183e-18	2.1026e-18	7.5682e-19	

Table 6.1: *RGA* of Open Loop System (CPSS) at Steady-state

	P_{REF_1}	P_{REF_2}	P_{REF_3}	P_{REF_4}	V_{REF_1}
P_{OUT_1}	1.0421e+00	9.8045e-03	5.7993e-03	7.9243e-03	4.4766e-03
P_{OUT_2}	8.6996e-03	1.0289e+00	5.5868e-03	3.6881e-03	2.0239e-03
P_{OUT_3}	3.3982e-03	6.1331e-03	1.0304e+00	4.4285e-03	2.0839e-03
P_{OUT_4}	7.8079e-03	3.2827e-03	4.9044e-03	1.0422e+00	2.6569e-03
V_{OUT_1}	3.1906e-04	2.7905e-04	3.3533e-04	1.3825e-04	7.1816e-01
V_{OUT_2}	6.4673e-03	5.6374e-03	5.2328e-03	5.0340e-03	6.0229e-04
V_{OUT_6}	2.3187e-02	2.5693e-02	9.4237e-03	1.2835e-02	1.4976e-03
V_{OUT_7}	2.6579e-02	2.9569e-02	1.1719e-02	1.5544e-02	1.5885e-03
V_{OUT_8}	1.8751e-02	1.9239e-02	2.2664e-02	2.3485e-02	2.0855e-01
V_{OUT_3}	2.8440e-03	2.7411e-03	2.9442e-03	3.1354e-03	9.0100e-04
V_{OUT_4}	7.2625e-02	1.0522e-01	1.1721e-01	1.0657e-01	1.7093e-02
V_{OUT_9}	1.0331e-02	1.3890e-02	2.5684e-02	2.4595e-02	2.8376e-02
$V_{OUT_{10}}$	1.2051e-02	1.6278e-02	3.0674e-02	2.9303e-02	3.4373e-02
$V_{OUT_{11}}$	1.4554e-02	1.2694e-02	1.1077e-02	1.3143e-02	1.0739e-03
V_{OUT_5}	3.0460e-02	3.0943e-02	3.1264e-02	3.1202e-02	1.8624e-03
$V_{OUT_{12}}$	1.2429e-02	2.0363e-02	2.5314e-02	2.2075e-02	1.3410e-02
$V_{OUT_{13}}$	1.1826e-02	1.0741e-02	2.9092e-02	2.5323e-02	2.6215e-02
ω_1	1.1405e-03	1.3636e-03	1.3639e-03	1.4120e-03	4.6358e-04
ω_2	1.1444e-03	1.3774e-03	1.3642e-03	1.4221e-03	4.6357e-04
ω_3	1.1434e-03	1.3718e-03	1.3650e-03	1.4183e-03	4.6390e-04
ω_4	1.1434e-03	1.3721e-03	1.3650e-03	1.4185e-03	4.6388e-04
	V_{REF_2}	V_{REF_3}	V_{REF_4}	V_{REF_5}	
P_{OUT_1}	2.8174e-02	4.2142e-03	4.3515e-02	2.6843e-02	
P_{OUT_2}	2.2932e-02	3.0933e-03	4.6339e-02	1.8858e-02	
P_{OUT_3}	1.6225e-02	5.9527e-03	5.4443e-02	1.8082e-02	
P_{OUT_4}	1.8341e-02	4.5893e-03	5.9078e-02	1.6288e-02	
V_{OUT_1}	2.5197e-04	1.0783e-05	1.5970e-03	1.2659e-05	
V_{OUT_2}	5.1800e-01	1.3314e-03	1.2626e-02	1.0867e-02	
V_{OUT_6}	1.8376e-02	2.6979e-02	2.9808e-01	5.9522e-04	
V_{OUT_7}	2.1017e-02	3.0344e-02	3.3503e-01	1.3076e-03	
V_{OUT_8}	2.7492e-02	1.1279e-02	1.2688e-01	5.7251e-02	
V_{OUT_3}	2.9045e-03	6.7092e-01	3.0183e-03	1.4842e-03	
V_{OUT_4}	2.8921e-02	1.0420e-01	2.0170e-01	2.6411e-01	
V_{OUT_9}	1.6528e-01	1.1468e-02	8.6102e-02	2.3403e-02	
$V_{OUT_{10}}$	2.0080e-01	1.3807e-02	1.0320e-01	2.8945e-02	
$V_{OUT_{11}}$	8.8708e-03	1.8709e-02	2.1507e-01	6.4250e-02	
V_{OUT_5}	5.3447e-02	7.8854e-03	6.3043e-02	5.2428e-01	
$V_{OUT_{12}}$	5.6270e-02	1.1712e-01	1.5427e-01	8.1657e-02	
$V_{OUT_{13}}$	1.3903e-01	4.4153e-03	1.2770e-02	1.2194e-01	
ω_1	1.4185e-03	5.1687e-04	5.4351e-03	1.1694e-03	
ω_2	1.4295e-03	5.1486e-04	5.4773e-03	1.1762e-03	
ω_3	1.4253e-03	5.1612e-04	5.4612e-03	1.1739e-03	
ω_4	1.4255e-03	5.1609e-04	5.4620e-03	1.1740e-03	

Table 6.2: *RGA* of System with MPSS at Steady State

between different buses by inspecting the element magnitudes of the control pair (P_{REF_1}, P_{OUT_1}), (P_{REF_2}, P_{OUT_2}), $\cdots$, (V_{REF_5}, V_{OUT_5}), i.e., the corresponding element magnitudes are also very close to 1. More important is that in Table 6.3, all the elements related to generator speed are very small except those correspond to voltage input control V_{REF_4} on generator 4. Therefore, for system with MPSS and inverse dynamics the interarea oscillations are damped mainly by generator 4 voltage input. In the same time the MPSS voltage control on generator 4 is also trying to control the voltages of the buses that are close to generator 4. This can be seen from the column under control V_{REF_4}, where element (V_{REF_4}, V_{OUT_6}), (V_{REF_4}, V_{OUT_7}), (V_{REF_4}, V_{OUT_9}), $(V_{REF_4}, V_{OUT_{10}})$, $(V_{REF_4}, V_{OUT_{11}})$, and $(V_{REF_4}, V_{OUT_{13}})$ are of large magnitude close to 1.0.

The RGA matrix of the open loop system at bifurcation frequency is also reviewed here because this indicates the control performance and the capability of disturbance rejection of the system at bifurcation frequency. It is important to know how much better the control performance can be achieved with a robust controller over different frequencies in the frequency range. The RGA matrix of the open loop system (CPSS) at bifurcation frequency is shown in Table 6.4. It can be seen from Table 6.4 that the magnitude of the control pair elements $(P_{REF_1}, P_{OUT_1}), \cdots, (V_{REF_5}, V_{OUT_5})$ are also close to 1. However, this does not mean that an almost decoupled control structure has been obtained for CPSS because in many rows of the RGA matrix we can still find more than one large element, which suggests there are conflicts among different control devices. There are some rows with no large elements, which suggests there is poor control of this variable. The open loop system has a conventional power system stabilizer on generator 3. This explains why the generator speed related element magnitudes are large under V_{REF_3}. It also suggests that the conventional power system stabilizer was well designed.

The RGA matrix of the closed-loop system with MPSS at bifurcation frequency is

	P_{REF_1}	P_{REF_2}	P_{REF_3}	P_{REF_4}	V_{REF_1}
P_{OUT_1}	9.3141e-01	6.4292e-05	7.3759e-05	6.8993e-05	1.4454e-04
P_{OUT_2}	8.6091e-05	9.4182e-01	7.3028e-05	6.7311e-05	2.2092e-04
P_{OUT_3}	2.1184e-04	1.3694e-04	9.4634e-01	1.2187e-04	6.3311e-05
P_{OUT_4}	5.6873e-05	7.8630e-06	3.2027e-05	9.5340e-01	9.2856e-06
V_{OUT_1}	4.2852e-04	2.0419e-05	2.0441e-05	2.1992e-05	7.2155e-01
V_{OUT_2}	6.4080e-04	1.4077e-03	1.0762e-04	1.1416e-04	1.8116e-03
V_{OUT_6}	5.7499e-03	4.0603e-03	3.5127e-04	5.0051e-04	1.2168e-02
V_{OUT_7}	6.5023e-03	4.6127e-03	4.3397e-04	6.0208e-04	1.3832e-02
V_{OUT_8}	3.1561e-03	7.6255e-04	4.5287e-04	4.8795e-04	2.8535e-01
V_{OUT_3}	4.4813e-04	5.0012e-04	6.7762e-05	5.2762e-04	1.6214e-04
V_{OUT_4}	6.5525e-02	7.1044e-02	8.7708e-02	7.9407e-02	1.2252e-02
V_{OUT_9}	3.0562e-03	5.5978e-03	9.2290e-03	9.1314e-03	1.0607e-02
$V_{OUT_{10}}$	3.5213e-03	6.6010e-03	1.1043e-02	1.0899e-02	1.2875e-02
$V_{OUT_{11}}$	2.9096e-03	1.4198e-03	3.0868e-04	3.8245e-04	4.9738e-03
V_{OUT_5}	1.3510e-04	3.7855e-04	5.3609e-03	5.3316e-03	8.9055e-04
$V_{OUT_{12}}$	4.2758e-03	5.1267e-03	5.8462e-03	6.0366e-03	3.7953e-03
$V_{OUT_{13}}$	3.2344e-03	5.5820e-03	1.1619e-02	1.0432e-02	1.1581e-02
ω_1	1.4771e-05	1.6421e-05	1.6816e-05	1.7468e-05	5.9286e-06
ω_2	1.4775e-05	1.6417e-05	1.6816e-05	1.7468e-05	5.9428e-06
ω_3	1.4778e-05	1.6425e-05	1.6808e-05	1.7465e-05	5.9406e-06
ω_4	1.4787e-05	1.6435e-05	1.6823e-05	1.7471e-05	5.9442e-06
	V_{REF_2}	V_{REF_3}	V_{REF_4}	V_{REF_5}	
P_{OUT_1}	2.0922e-04	4.0030e-05	2.0031e-02	1.3229e-04	
P_{OUT_2}	3.0010e-04	4.7574e-05	2.3878e-02	1.0412e-04	
P_{OUT_3}	4.4790e-04	1.1437e-04	2.5175e-02	4.0094e-04	
P_{OUT_4}	5.1926e-05	2.8558e-04	2.8778e-02	3.1345e-04	
V_{OUT_1}	7.2495e-04	8.4032e-06	4.5352e-03	1.0441e-05	
V_{OUT_2}	5.5158e-01	1.7249e-05	8.5263e-03	1.5222e-03	
V_{OUT_6}	8.0355e-02	3.3560e-04	1.5784e-01	6.8161e-04	
V_{OUT_7}	8.7001e-02	3.7743e-04	1.7822e-01	1.1791e-03	
V_{OUT_8}	2.0930e-02	1.4404e-04	8.6816e-02	7.0479e-03	
V_{OUT_3}	5.0948e-04	6.8763e-01	5.2982e-03	2.1884e-04	
V_{OUT_4}	2.0276e-02	7.6873e-02	1.6681e-02	1.9087e-01	
V_{OUT_9}	5.9684e-02	1.4133e-04	1.5456e-01	4.6626e-03	
$V_{OUT_{10}}$	7.2657e-02	1.7016e-04	1.8707e-01	5.7799e-03	
$V_{OUT_{11}}$	1.3340e-01	2.3342e-04	1.2502e-01	2.0702e-02	
V_{OUT_5}	1.5259e-02	9.3740e-05	1.1268e-02	7.9077e-01	
$V_{OUT_{12}}$	1.5310e-02	2.3387e-01	9.2654e-02	1.8203e-02	
$V_{OUT_{13}}$	5.8125e-02	5.4094e-05	1.4694e-01	4.1559e-02	
ω_1	1.7406e-05	6.3748e-06	3.7618e-03	1.4800e-05	
ω_2	1.7395e-05	6.3747e-06	3.7617e-03	1.4802e-05	
0 ω_3	1.7409e-05	6.3665e-06	3.7617e-03	1.4802e-05	
ω_4	1.7419e-05	6.3800e-06	3.7617e-03	1.4812e-05	

Table 6.3: *RGA* of System with MPSS and Inverse Dynamics at Steady State

	P_{REF_1}	P_{REF_2}	P_{REF_3}	P_{REF_4}	V_{REF_1}
P_{OUT_1}	1.0592e+00	5.5052e-02	3.3637e-02	1.3865e-02	5.5112e-02
P_{OUT_2}	9.5436e-02	9.0366e-01	2.8474e-02	8.8770e-03	3.8256e-02
P_{OUT_3}	4.6264e-02	8.4417e-03	1.1387e+00	9.7959e-02	2.3755e-01
P_{OUT_4}	5.8721e-02	1.4911e-02	1.7069e-01	1.1945e+00	2.4382e-01
V_{OUT_1}	2.4558e-01	9.9354e-02	3.1215e-02	2.2522e-02	1.5998e+00
V_{OUT_2}	5.9846e-02	1.5685e-01	1.9095e-02	1.1006e-02	6.0310e-01
V_{OUT_6}	6.9690e-02	9.1770e-02	8.2159e-03	2.0479e-02	1.4784e-01
V_{OUT_7}	7.6301e-02	1.0045e-01	9.0098e-03	2.2393e-02	1.6181e-01
V_{OUT_8}	1.9624e-01	3.9824e-02	2.6302e-02	2.3685e-02	9.1772e-01
V_{OUT_3}	3.3444e-02	1.9970e-02	1.5531e-01	6.7571e-02	1.1959e-02
V_{OUT_4}	3.9773e-03	5.9342e-04	1.5396e-02	4.6101e-02	2.7734e-02
V_{OUT_9}	1.2526e-02	9.2052e-04	1.5488e-02	2.0564e-02	1.6519e-02
$V_{OUT_{10}}$	1.5279e-02	1.1220e-03	1.8893e-02	2.5087e-02	2.0153e-02
$V_{OUT_{11}}$	5.4168e-02	9.5932e-02	1.0181e-02	1.9453e-02	1.4884e-01
V_{OUT_5}	4.9286e-02	6.3871e-03	2.4424e-02	4.6508e-03	5.8712e-03
$V_{OUT_{12}}$	1.3611e-02	1.0731e-02	9.0910e-02	1.4605e-02	2.4417e-02
$V_{OUT_{13}}$	4.7302e-03	1.2503e-03	1.8034e-02	3.2043e-02	2.6189e-02
ω_1	2.3971e-01	1.2572e-01	2.7859e-01	2.5060e-01	5.8319e-04
ω_2	1.0925e-01	1.1523e-01	2.1464e-01	1.9292e-01	2.3941e-04
ω_3	3.9120e-01	2.7356e-01	2.4953e-01	1.7340e-01	3.1521e-05
ω_4	3.9719e-01	2.7824e-01	1.9570e-01	2.1718e-01	9.4899e-05
	V_{REF_2}	V_{REF_3}	V_{REF_4}	V_{REF_5}	
P_{OUT_1}	2.7901e-01	4.9958e-02	7.8554e-02	6.9552e-02	
P_{OUT_2}	1.7235e-01	4.0388e-02	6.8929e-02	4.8178e-02	
P_{OUT_3}	8.3525e-02	1.8776e-01	1.5667e-01	8.5294e-02	
P_{OUT_4}	8.7629e-02	4.2549e-02	1.3263e-01	7.3531e-02	
V_{OUT_1}	7.2068e-01	1.2633e-02	2.2452e-02	2.2328e-02	
V_{OUT_2}	1.3580e+00	2.2311e-02	3.8624e-02	1.3585e-01	
V_{OUT_6}	3.3260e-01	2.4372e-02	9.1134e-02	4.7844e-02	
V_{OUT_7}	3.6402e-01	2.6663e-02	9.9743e-02	5.2363e-02	
V_{OUT_8}	3.8557e-01	1.8828e-02	4.9047e-03	3.3653e-02	
V_{OUT_3}	2.7155e-02	8.4068e-01	1.8799e-01	3.4056e-02	
V_{OUT_4}	3.3032e-02	1.3452e-01	7.5764e-01	6.8557e-02	
V_{OUT_9}	3.5772e-02	9.9105e-03	8.8024e-02	4.1461e-02	
$V_{OUT_{10}}$	4.3641e-02	1.2092e-02	1.0739e-01	5.0581e-02	
$V_{OUT_{11}}$	5.1103e-01	2.4511e-02	2.9226e-02	4.4068e-02	
V_{OUT_5}	1.8863e-01	1.0909e-02	7.9734e-02	9.1525e-01	
$V_{OUT_{12}}$	1.2401e-02	4.6595e-01	1.0838e-01	2.6100e-02	
$V_{OUT_{13}}$	1.1700e-02	2.2024e-02	1.9487e-01	1.5008e-02	
ω_1	4.8437e-04	1.5903e-01	1.2293e-04	4.9451e-05	
ω_2	4.8523e-04	1.2346e-01	4.7813e-05	2.7842e-05	
ω_3	1.4023e-04	1.6296e-01	3.0535e-04	6.0176e-05	
ω_4	1.0588e-04	1.0958e-01	5.6129e-04	8.1034e-05	

Table 6.4: *RGA* of Open Loop System (CPSS) at Bifurcation Frequency

	P_{REF_1}	P_{REF_2}	P_{REF_3}	P_{REF_4}	V_{REF_1}
P_{OUT_1}	1.2161e+00	6.1762e-02	4.0091e-02	1.3570e-02	1.0785e-01
P_{OUT_2}	1.0853e-01	9.4014e-01	2.7910e-02	1.1178e-02	4.9444e-02
P_{OUT_3}	5.3702e-02	1.0519e-02	1.1745e+00	1.0944e-01	2.6676e-01
P_{OUT_4}	7.0908e-02	1.9048e-02	1.9673e-01	1.2674e+00	2.8827e-01
V_{OUT_1}	3.1631e-01	1.1327e-01	3.7478e-02	2.7864e-02	1.7814e+00
V_{OUT_2}	7.2303e-02	1.6338e-01	2.0853e-02	1.1450e-02	6.9322e-01
V_{OUT_6}	8.4526e-02	9.9429e-02	9.0782e-03	2.3483e-02	1.8054e-01
V_{OUT_7}	9.2652e-02	1.0897e-01	9.9672e-03	2.5710e-02	1.9783e-01
V_{OUT_8}	2.4831e-01	4.5325e-02	3.1070e-02	2.8541e-02	1.0387e+00
V_{OUT_3}	3.6347e-02	2.0118e-02	1.6429e-01	7.5012e-02	1.3046e-02
V_{OUT_4}	4.5701e-03	6.0988e-04	1.7156e-02	6.1704e-02	3.1558e-02
V_{OUT_9}	1.3657e-02	1.3448e-03	1.6092e-02	2.2667e-02	1.7823e-02
$V_{OUT_{10}}$	1.6678e-02	1.6411e-03	1.9654e-02	2.7685e-02	2.1770e-02
$V_{OUT_{11}}$	6.5538e-02	1.0353e-01	1.1180e-02	2.2071e-02	1.8256e-01
V_{OUT_5}	5.8444e-02	8.0955e-03	2.6486e-02	5.4218e-03	5.9390e-03
$V_{OUT_{12}}$	1.4581e-02	1.0481e-02	9.5878e-02	1.6450e-02	2.6718e-02
$V_{OUT_{13}}$	5.4039e-03	9.4129e-04	1.9176e-02	3.7796e-02	2.9091e-02
ω_1	2.8635e-01	1.3461e-01	3.0465e-01	2.8088e-01	6.5648e-04
ω_2	1.2443e-01	1.2754e-01	2.2830e-01	2.1033e-01	2.9231e-04
ω_3	4.3331e-01	2.8057e-01	2.6573e-01	1.9423e-01	3.5876e-05
ω_4	4.6282e-01	3.0031e-01	2.2538e-01	2.4811e-01	1.1467e-04
	V_{REF_2}	V_{REF_3}	V_{REF_4}	V_{REF_5}	
P_{OUT_1}	3.2938e-01	5.2836e-02	7.0947e-02	6.5501e-02	
P_{OUT_2}	1.6650e-01	4.5008e-02	6.2013e-02	4.1142e-02	
P_{OUT_3}	8.4271e-02	1.9770e-01	1.7818e-01	9.2088e-02	
P_{OUT_4}	9.2616e-02	4.8654e-02	1.7133e-01	8.4354e-02	
V_{OUT_1}	8.3276e-01	1.5608e-02	2.9419e-02	2.6511e-02	
V_{OUT_2}	1.4584e+00	2.3512e-02	5.0008e-02	1.4911e-01	
V_{OUT_6}	3.7543e-01	2.7038e-02	9.7278e-02	5.3134e-02	
V_{OUT_7}	4.1138e-01	2.9615e-02	1.0659e-01	5.8221e-02	
V_{OUT_8}	4.4140e-01	2.2295e-02	1.0517e-02	3.9681e-02	
V_{OUT_3}	2.8171e-02	8.7087e-01	2.0876e-01	3.5124e-02	
V_{OUT_4}	3.5779e-02	1.5061e-01	8.0615e-01	5.3224e-02	
V_{OUT_9}	3.5220e-02	1.0814e-02	9.2877e-02	3.7256e-02	
$V_{OUT_{10}}$	4.3019e-02	1.3210e-02	1.1344e-01	4.5506e-02	
$V_{OUT_{11}}$	5.7207e-01	2.7131e-02	2.6301e-02	4.9060e-02	
V_{OUT_5}	2.0371e-01	1.2023e-02	9.1448e-02	9.2365e-01	
$V_{OUT_{12}}$	1.2957e-02	4.8690e-01	1.1774e-01	2.6249e-02	
$V_{OUT_{13}}$	1.1503e-02	2.3782e-02	2.0741e-01	1.3679e-02	
ω_1	5.6064e-04	1.7388e-01	3.0718e-02	4.5497e-05	
ω_2	5.2506e-04	1.3133e-01	2.3177e-02	2.1831e-05	
ω_3	1.3760e-04	1.7213e-01	2.0537e-02	6.0827e-05	
ω_4	1.0289e-04	1.2643e-01	2.7341e-02	9.4642e-05	

Table 6.5: *RGA* of System with MPSS at Bifurcation

shown in Table 6.5. From Table 6.5 we can see that although the magnitudes of some element that do not belong to the control pairs (P_{REF_i}, P_{OUT_i}), $i = 1, 2, \cdots, 4$, (V_{REF_i}, V_{OUT_i}), $i = 1, 2, \cdots, 5$, increase the control structure is still decoupled since the control pair elements are still dominant in each column. The RGA matrix subsystem in the network are not the same at the bifurcation frequency as for $\omega = 0$. This is expected since at $\omega = 0$ voltage control is accomplished and at the bifurcation damping of the oscillation is accomplished. It should be noted that the conventional power system stabilizer is still effective by inspecting the frequency related elements under column V_{REF_3} which occurs due to the fact that the CPSS has been assigned to be effective in damping the interarea oscillation with control V_{REF_3}. Also, MPSS is effective in controlling the frequencies since the frequency elements under control V_{REF_4} have relatively large elements but the MPSS is not as effective as the conventional power system stabilizer. Table 6.6 shows the RGA matrix of the closed-loop system with MPSS and the inverse dynamics of generator 4. It is noted that the frequency related elements under control V_{REF_4} increase in comparison with Table 6.5. Therefore, it is anticipated that better frequency control can be achieved. The rest of the RGA matrix elements are similar to those in Table 6.5.

6.4.3 Time Simulation of MPSS Design

The CPSS design uses a fairly simple lead network compensator to adjust the input signal (generator shaft speed, electrical power, or accelerating power) to give it the correct phase to effectively damp the generator rotor oscillations. The CPSS is designed by adding inverse dynamics of exciter and flux decay dynamics at the nominal operating point of the generator. Generally, a CPSS is fairly robust for small perturbations because it is designed by trial and error. Relatively large uncertainty

	P_{REF_1}	P_{REF_2}	P_{REF_3}	P_{REF_4}	V_{REF_1}
P_{OUT_1}	1.1180e+00	5.7887e-02	3.7908e-02	1.2517e-02	9.8373e-02
P_{OUT_2}	9.9824e-02	8.7851e-01	2.6374e-02	1.0300e-02	4.1621e-02
P_{OUT_3}	5.1573e-02	1.0104e-02	1.1617e+00	1.0269e-01	2.5619e-01
P_{OUT_4}	6.4711e-02	1.7374e-02	1.7948e-01	1.2189e+00	2.6301e-01
V_{OUT_1}	2.8831e-01	9.9580e-02	3.5473e-02	2.5768e-02	1.7080e+00
V_{OUT_2}	6.5828e-02	1.4410e-01	1.9745e-02	1.0595e-02	6.4862e-01
V_{OUT_6}	7.6745e-02	8.8391e-02	8.5979e-03	2.1739e-02	1.6797e-01
V_{OUT_7}	8.4122e-02	9.6869e-02	9.4398e-03	2.3800e-02	1.8405e-01
V_{OUT_8}	2.2631e-01	3.9851e-02	2.9409e-02	2.6395e-02	9.8552e-01
V_{OUT_3}	3.5457e-02	1.9625e-02	1.6241e-01	7.1665e-02	1.2731e-02
V_{OUT_4}	4.2422e-03	5.5744e-04	1.6167e-02	4.8763e-02	2.9807e-02
V_{OUT_9}	1.3611e-02	1.3251e-03	1.6008e-02	2.1811e-02	1.8038e-02
$V_{OUT_{10}}$	1.6622e-02	1.6170e-03	1.9551e-02	2.6640e-02	2.2032e-02
$V_{OUT_{11}}$	5.9592e-02	9.1616e-02	1.0585e-02	2.0421e-02	1.7065e-01
V_{OUT_5}	5.4193e-02	7.4387e-03	2.5465e-02	5.1331e-03	5.5763e-03
$V_{OUT_{12}}$	1.4300e-02	1.0269e-02	9.4714e-02	1.5610e-02	2.6248e-02
$V_{OUT_{13}}$	5.2009e-03	8.9859e-04	1.8517e-02	3.3686e-02	2.8275e-02
ω_1	2.5765e-01	1.2609e-01	2.8807e-01	2.5910e-01	5.9927e-04
ω_2	1.1480e-01	1.1559e-01	2.1574e-01	1.9382e-01	2.4575e-04
ω_3	4.1600e-01	2.6932e-01	2.5957e-01	1.8222e-01	3.4726e-05
ω_4	4.2231e-01	2.7403e-01	2.0566e-01	2.2640e-01	1.0457e-04
	V_{REF_2}	V_{REF_3}	V_{REF_4}	V_{REF_5}	
P_{OUT_1}	2.9365e-01	5.0017e-02	8.0044e-02	7.1957e-02	
P_{OUT_2}	1.4919e-01	4.2602e-02	6.9346e-02	5.0963e-02	
P_{OUT_3}	8.0929e-02	1.9408e-01	1.6433e-01	8.9003e-02	
P_{OUT_4}	8.4501e-02	4.4379e-02	1.3723e-01	7.6971e-02	
V_{OUT_1}	7.7260e-01	1.4779e-02	2.5392e-02	2.4146e-02	
V_{OUT_2}	1.3908e+00	2.2265e-02	4.2032e-02	1.3750e-01	
V_{OUT_6}	3.4907e-01	2.5605e-02	9.6575e-02	4.9335e-02	
V_{OUT_7}	3.8250e-01	2.8045e-02	1.0582e-01	5.4059e-02	
V_{OUT_8}	4.0972e-01	2.1111e-02	5.8131e-03	3.6160e-02	
V_{OUT_3}	2.7492e-02	8.4843e-01	1.9757e-01	3.4581e-02	
V_{OUT_4}	3.3799e-02	1.3630e-01	7.6082e-01	7.0389e-02	
V_{OUT_9}	3.5637e-02	1.0187e-02	8.8729e-02	4.1511e-02	
$V_{OUT_{10}}$	4.3529e-02	1.2444e-02	1.0838e-01	5.0703e-02	
$V_{OUT_{11}}$	5.3441e-01	2.5692e-02	3.0355e-02	4.5157e-02	
V_{OUT_5}	1.9120e-01	1.1423e-02	8.4989e-02	9.1569e-01	
$V_{OUT_{12}}$	1.2729e-02	4.7066e-01	1.1127e-01	2.6830e-02	
$V_{OUT_{13}}$	1.1180e-02	2.2403e-02	1.9659e-01	1.5786e-02	
ω_1	4.9970e-04	1.6460e-01	1.3026e-02	5.0073e-05	
ω_2	4.7026e-04	1.2431e-01	5.6349e-02	2.6935e-05	
ω_3	1.3233e-04	1.6897e-01	3.2133e-02	5.9110e-05	
ω_4	9.3853e-05	1.1537e-01	5.9321e-02	8.6095e-05	

Table 6.6: *RGA* of System with MPSS and Inverse Dynamics at Bifurcation

can cause the deviation of the operating point, which causes the closed-loop system with CPSS to go unstable. This will be seen in next example. The previously designed MPSS is also tested here. This MPSS is designed for generator 4 with speed on generator as input. Figure 6.9 shows the simulation result of open loop and closed-loop system with 50% increase in active power load on generator 2. In this case, the open loop system with CPSS can not maintain the system stability in terms of voltage control and frequency control. The active power load perturbation causes the interarea oscillation between generator 4 and the rest of the generators and these oscillations can not be damped by the CPSS. MPSS still achieves very good damping. The oscillations are eliminated in 20 seconds. It should be noted that the period of the waveforms shown in Figure 6.9 verifies that these oscillations are interarea oscillations ($T \approx 2.0$s).

The fact that CPSS achieves effective damping by using inverse dynamics of the excitation system and flux decay dynamics suggests the performance of MPSS could be improved by including the inverse dynamics in the design. The time simulation of closed-loop system with MPSS adding inverse dynamics is shown in Figure 6.10. The same active power load perturbation is applied to generator bus 2. The performance improvement is obvious. It can be seen that the transient time is reduced dramatically. The interarea oscillations are now damped out in 10 seconds rather than 20 seconds. Comparing Figure 6.9 and 6.10, it can be seen that the first swing in Figure 6.10 is little larger than that in Figure 6.9. This indicates that more control effort is applied by the controller. It should be pointed out that the inverse dynamics block be connected to the μ-controller output in order to achieve better performance. This result supports the conclusions reached based on the RGA matrix results.

From the above simulation results both MPSS designs achieve very robust and good control performance for this single bifurcation. However, as a local control device (local measurement and local control action) PSS has its limitation when damping

interarea oscillations because it can not always effectively control the oscillation in power between the two areas. This will be shown when multiple bifurcations develop.

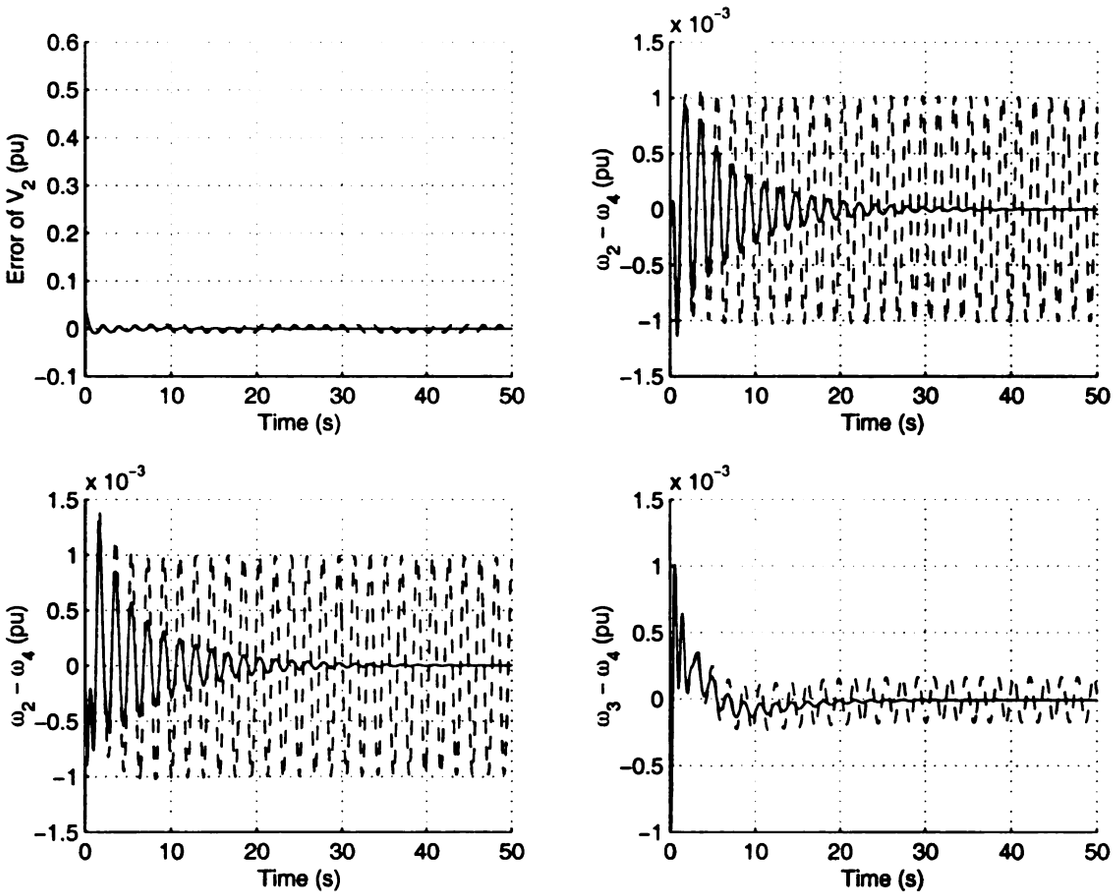

Figure 6.9: Open Loop system with CPSS (- -) and Closed-loop System with MPSS (-)

6.5 μ-synthesis SVC Control (MSVC)

6.5.1 Full System Based μ-synthesis SVC Control Design

For SVC controller, the measurement output can be

1. frequency at any bus;

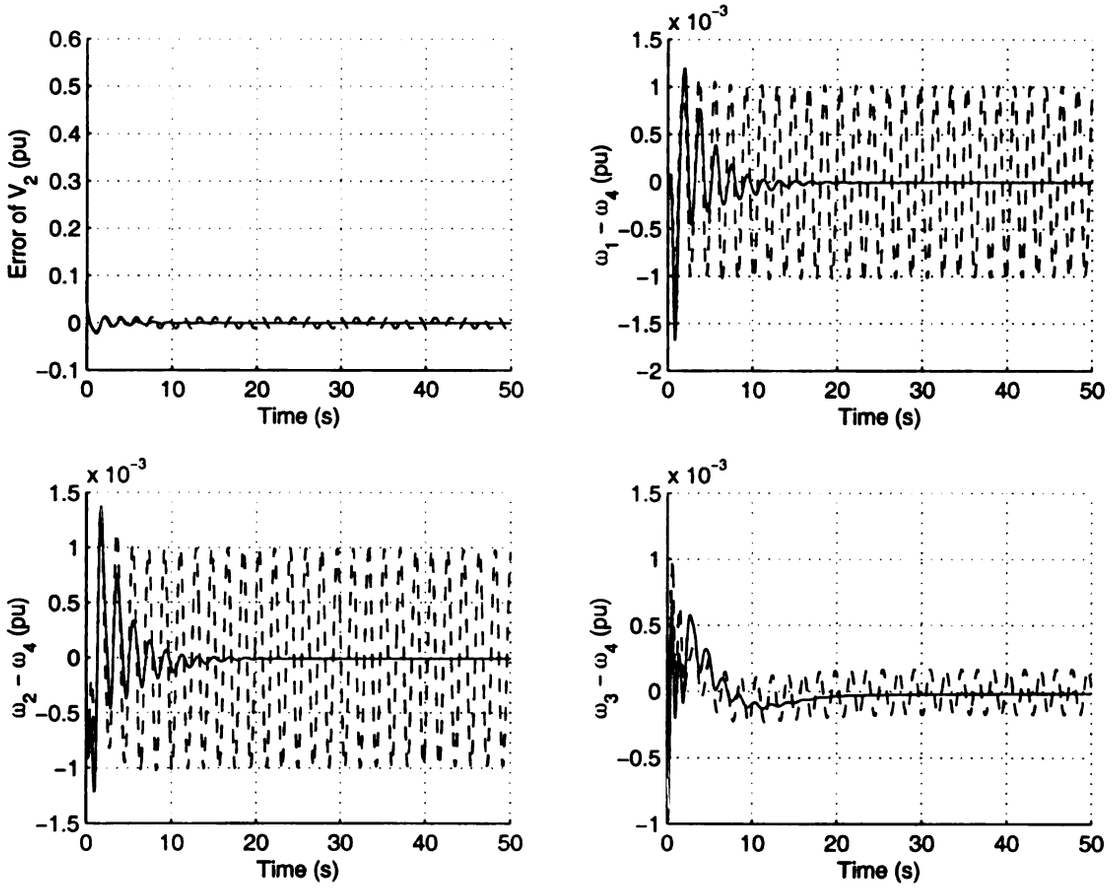

Figure 6.10: Open Loop System with CPSS (- -) and Closed-loop System with MPSS and Inverse Dynamics (-)

2. speed at any synchronous machine;

3. accelerating power of any synchronous machine;

4. power flow over any line;

5. voltage angle deviation at any bus;

The bifurcation subsystem method is again utilized to design the robust SVC controller following the same procedures used for MPSS.

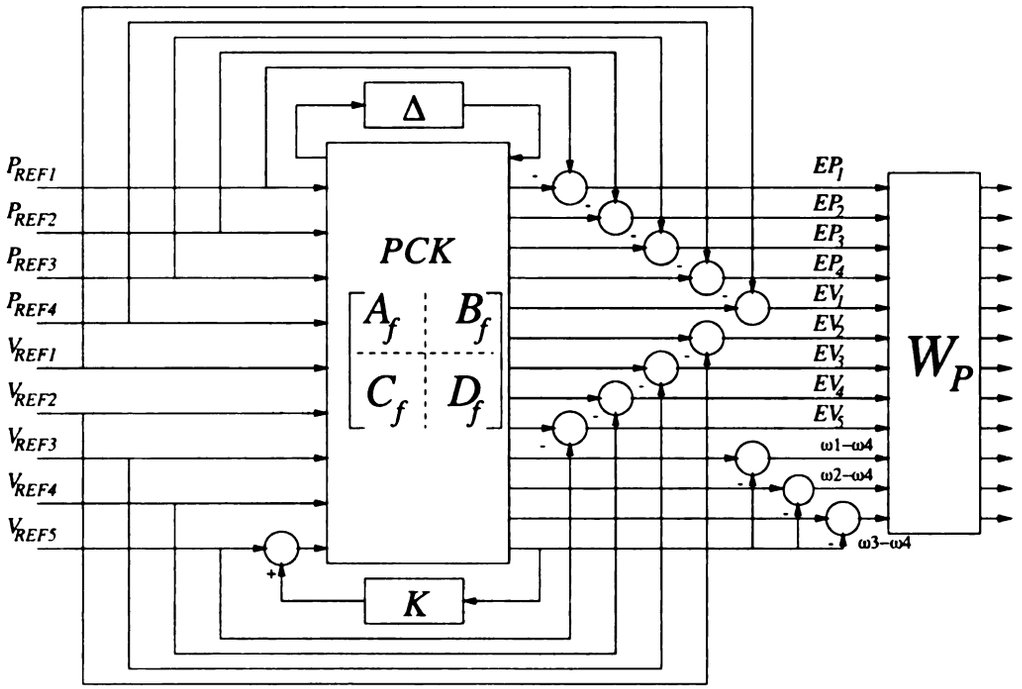

Figure 6.11: Control Configuration of MSVC

MSVC is first designed based on the full system model. The general control configuration is shown in Figure 6.11, which is very similar to Figure 6.7 for the MPSS design. To suppress the interarea oscillations caused by the active power load on bus 2, the speed of generator 4 is selected as the measured output signal and the controller output will be the voltage set point of SVC bus 101 from generator angle phase diagram in Figure 6.6. The MPSS performance index defined in equation (6.4.3) and the MPSS performance weighting function are used for the MSVC design.

The MSVC is synthesized in the same way as power system stabilizer design. The closed-loop μ-value is shown in Figure 6.12. The maximum μ value is about 0.72, which occurs around the Hopf bifurcation frequency. This maximum μ suggests a $\frac{1}{\mu_{max}}$ increase in uncertainty could be sustained to maintain the control performance requirement without experiencing instability. This uncertainty contrasts with only 1% for MPSS.

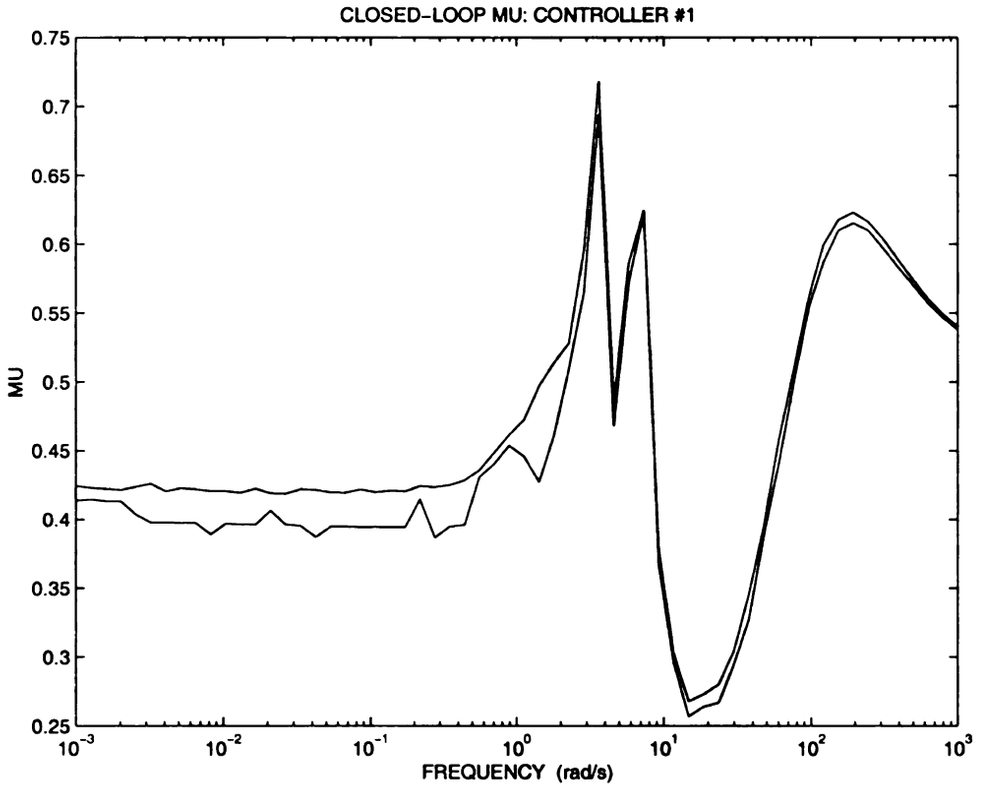

Figure 6.12: μ-value of Closed-loop System with MSVC

Robust SVC controller is anticipated to be more effective than robust power system stabilizer. Interarea oscillations can be effectively damped and voltage control performance can also be guaranteed even for very large uncertainties. Before analyzing the control performance we first show the *RGA* matrices of the system with MSVC controller at various frequencies range over the bandwidth of the controller.

The *RGA* matrices of the open loop system (CSVC) at steady state and bifurcation frequency have been shown in previous sections. Therefore, only the *RGA* matrices

of the closed-loop system with MSVC are shown here. At steady state RGA matrix of the closed-loop system with MSVC controller is shown in Table 6.7. The element magnitude of the control pair (P_{REF_1}, P_{OUT_1}), (P_{REF_2}, P_{OUT_2}), $\cdots$, (V_{REF_5}, V_{REF_5}) are very close to 1 just as with MPSS. These elements are dominant compared to the rest of them in the respective rows except for the column corresponds to SVC control input V_{REF_5}. From Table 6.7, MSVC has relatively strong voltage control at bus 3, 4, 13, 14, 20, and 120. All these buses are electrically close to SVC bus 101 as shown in Figure 5.1. Therefore, the network is controlled by MSVC centered to achieve excellent overall voltage control performance of the network of this example system. This contrasts to the decoupled structure using the MPSS where many of the network bus voltages are controlled by the MPSS on generator bus 4 rather than the MSVC at bus 5. This suggests that again an almost decoupled control structure is obtained but different than obtained with MPSS.

The power system stabilizer on generator 3 would not be expected to and did not have significant control effect on generator speeds at steady state due to the washout of the PSS at low frequencies. The RGA elements related to generator speeds in Table 6.7 show that generator 3 has very little control of frequencies. On the other hand, MSVC has tighter control on generator frequencies at steady state. This is very clear in Table 6.7 since the elements associated with speeds ω_i are only large for V_{REF_5} at bus 101, where the SVC is located. This is in contrast to the MPSS where the effective control of the CPSS on generator 3 is far more effective at $\omega = 0$ than the MPSS on generator 4. This contrast is due to the effectiveness of an SVC is controlling power flow across the interface connecting the two areas and thus the interarea frequency oscillation $\omega_i - \omega_4$, $i = 1, 2, 3$. The power system stabilizer on generator 4 just dampens ω_4 change only, which may have little effect on $\omega_i - \omega_4$, $i = 1, 2, 3$.

	P_{REF_1}	P_{REF_2}	P_{REF_3}	P_{REF_4}	V_{REF_1}
P_{OUT_1}	9.4163e-01	1.1242e-04	8.6694e-05	8.1317e-05	6.5504e-05
P_{OUT_2}	5.0174e-06	9.4508e-01	8.9223e-06	6.3128e-06	2.2200e-04
P_{OUT_3}	1.1753e-05	7.3172e-05	9.4716e-01	6.6417e-05	2.7860e-05
P_{OUT_4}	3.5712e-05	1.9010e-05	4.3746e-05	9.5895e-01	1.2103e-05
V_{OUT_1}	5.4104e-05	2.3014e-06	9.2685e-06	1.0164e-05	7.1655e-01
V_{OUT_2}	1.9586e-04	9.7300e-04	4.9833e-04	5.1415e-04	1.3144e-03
V_{OUT_6}	6.1718e-03	6.7149e-03	3.6633e-03	5.1936e-03	5.5827e-03
V_{OUT_7}	7.0207e-03	7.6633e-03	4.6575e-03	6.3548e-03	6.4313e-03
V_{OUT_8}	6.2027e-05	5.8109e-04	1.8142e-03	1.9297e-03	2.7909e-01
V_{OUT_3}	8.3432e-05	8.9916e-05	6.3927e-04	8.3704e-05	2.0862e-05
V_{OUT_4}	3.4941e-04	3.7451e-04	2.8599e-04	2.6427e-04	5.3888e-05
V_{OUT_9}	3.7749e-03	4.2708e-03	6.1360e-03	6.5769e-03	4.6204e-03
$V_{OUT_{10}}$	4.4779e-03	5.0735e-03	7.3465e-03	7.8634e-03	5.5826e-03
$V_{OUT_{11}}$	1.2103e-03	1.3966e-03	2.0741e-03	2.6595e-03	1.2387e-03
V_{OUT_5}	8.3219e-02	8.3964e-02	8.0529e-02	7.5344e-02	5.7637e-03
V_{OUT_4}	1.1779e-03	1.2560e-03	7.1775e-05	1.3570e-03	6.1211e-04
$V_{OUT_{13}}$	1.7417e-03	1.9077e-03	2.4827e-03	2.9801e-03	2.1310e-03
ω_1	2.7852e-05	2.9510e-05	3.0462e-05	3.1733e-05	8.7997e-06
ω_2	2.7848e-05	2.9515e-05	3.0464e-05	3.1734e-05	8.7885e-06
ω_3	2.7844e-05	2.9507e-05	3.0473e-05	3.1738e-05	8.7897e-06
ω_4	2.7845e-05	2.9508e-05	3.0468e-05	3.1744e-05	8.7899e-06
	V_{REF_2}	V_{REF_3}	V_{REF_4}	V_{REF_5}	
P_{OUT_1}	8.5939e-04	6.3441e-05	2.8828e-04	2.1487e-02	
P_{OUT_2}	7.5174e-04	1.0972e-05	4.8961e-05	2.3075e-02	
P_{OUT_3}	3.0935e-04	1.3723e-04	7.5344e-04	2.5291e-02	
P_{OUT_4}	1.1287e-04	3.4298e-04	2.9933e-04	2.9581e-02	
V_{OUT_1}	1.5274e-04	5.2642e-06	1.1912e-05	9.2960e-04	
V_{OUT_2}	5.0234e-01	1.0413e-04	6.7681e-05	6.1243e-03	
V_{OUT_6}	4.0652e-02	1.1253e-02	4.0210e-02	1.7081e-01	
V_{OUT_7}	4.3811e-02	1.2505e-02	4.4111e-02	1.9334e-01	
V_{OUT_8}	1.1091e-02	9.6165e-04	1.6619e-03	6.0527e-02	
V_{OUT_3}	7.5128e-05	6.9441e-01	1.6394e-03	5.8404e-03	
V_{OUT_4}	4.8091e-05	1.3202e-03	5.3044e-01	3.0835e-03	
V_{OUT_9}	3.5499e-02	3.2270e-03	2.6957e-02	1.5625e-01	
$V_{OUT_{10}}$	4.3020e-02	3.8836e-03	3.2777e-02	1.8828e-01	
$V_{OUT_{11}}$	9.9894e-02	4.6450e-03	1.4417e-02	1.2164e-01	
V_{OUT_5}	2.2570e-01	2.1394e-02	2.2754e-01	1.6850e-02	
$V_{OUT_{12}}$	3.3548e-03	2.6615e-01	1.0756e-02	9.0598e-02	
$V_{OUT_{13}}$	1.5184e-02	3.2851e-03	9.3630e-02	1.3472e-01	
ω_1	2.8289e-05	1.2255e-05	1.5993e-05	4.0257e-03	
ω_2	2.8299e-05	1.2256e-05	1.5994e-05	4.0258e-03	
ω_3	2.8288e-05	1.2264e-05	1.5995e-05	4.0257e-03	
ω_4	2.8289e-05	1.2255e-05	1.5999e-05	4.0256e-03	

Table 6.7: *RGA* of System with MSVC at Steady-state

The RGA matrix of the closed-loop system with MSVC at bifurcation frequency provides important information on the control performance when bifurcation occurs. This is shown in Table 6.8. In Table 6.8, we can see the RGA matrix indicates an almost decoupled structure. The element magnitudes of the control pairs (P_{REF_i}, P_{OUT_i}), $i = 1, \cdots, 4$, and (V_{REF_i}, V_{OUT_i}), $i = 1, \cdots, 5$ are dominant in their respective rows.

The power inputs significantly affects the generator speed at the Hopf bifurcation frequency. The conventional power system stabilizer on generator 3 again becomes more effective than the MSVC associated with V_{R_5}. Note that the difference between Table 6.4 and 6.8 is that MSVC has much more control over generator frequencies than for the open loop system equipped with CSVC. This explains why better damping can be achieved.

It is clear the at bifurcation frequency $\omega \approx 3$ rad/s the structure of RGA matrix is still reasonably decoupled but the MSVC control of network bus voltages at steady state does not exist at bifurcation. The control of bus voltage is undertaken by the generators in a manner very similar to that of the MPSS at the bifurcation frequency. This makes sense because the control of voltage at steady state focuses on the effectiveness of the MSVC ($\omega = 0$), but at bifurcation frequency the control of the inertial dynamics becomes the dominant concern of power controls P_{R_i} and the power system stabilizer on generator 3. The RGA matrix for MPSS and MSVC at bifurcation frequency have similar structure even for control of voltage at buses in the network. This excellent global decoupled control structure at bifurcation frequency explains the excellent performance when the active power stress is applied to the example system.

The RGA matrix at crossover frequency is also studied here. Since each different combination of inputs and outputs has a different crossover frequency, we just select

some combinations and provide the following results.

$(P_{REF_1}, P_{OUT_1}) = 0.7664, \omega = 0.2$ rad/sec

$(P_{REF_2}, P_{OUT_2}) = 0.7852, \omega = 0.2$ rad/sec

$(V_{REF_3}, V_{OUT_3}) = 0.4601, \omega = 0.015$ rad/sec

$(V_{REF_4}, V_{OUT_4}) = 0.5176, \omega = 1.0$ rad/sec

$(V_{REF_5}, V_{OUT_4}) = 0.0296, \omega = 2.5$ rad/sec

$(V_{REF_5}, V_{OUT_7}) = 0.0153, \omega = 0.01$ rad/sec

This again suggests that the decoupled control structure is obtained since the output is almost totally controlled by its own control input, and the control input does not have much effect on other outputs. These examples show that the decoupled control structure is preserved by the μ-controller and tight control can still be achieved at crossover frequency. This reflects the anticipated dynamic performance of the closed-loop system based on the RGA matrix results.

The simulation results will now be presented and compared to test the MSVC controller design.

The original system is equipped with various controls and is stable at the nominal operating point. In fact, for small perturbation in bifurcation parameter the open loop system still possesses the stability and satisfactory control performance due to its own control system. For a relatively large increase in bifurcation parameter perturbation, the control performance degenerates quickly and the open loop system goes unstable. Therefore, the performance of the system with and without MSVC controller is only studied for a large perturbation in the bifurcation parameter.

From the phase plane analysis given in Figure 6.6 this interarea oscillation is caused by the oscillation between generator 4 and rest of the generators. The speed of generator 4 is used as the measurement output signal. It is expected that this

	P_{REF_1}	P_{REF_2}	P_{REF_3}	P_{REF_4}	V_{REF_1}
P_{OUT_1}	9.8097e-01	5.7623e-02	3.0045e-02	1.2486e-02	7.4244e-02
P_{OUT_2}	7.6225e-02	8.3704e-01	2.3151e-02	1.0134e-02	1.8980e-02
P_{OUT_3}	3.6862e-02	2.2995e-02	1.1216e+00	8.7172e-02	1.7591e-01
P_{OUT_4}	4.9516e-02	3.0915e-02	1.5749e-01	1.1908e+00	1.8099e-01
V_{OUT_1}	2.4611e-01	9.7754e-02	2.5729e-02	1.8269e-02	1.5728e+00
V_{OUT_2}	7.9217e-02	1.5307e-01	2.6847e-02	1.4952e-02	6.0700e-01
V_{OUT_6}	6.1469e-02	9.2484e-02	6.1067e-03	2.1679e-02	1.5535e-01
V_{OUT_7}	6.7414e-02	1.0140e-01	6.7107e-03	2.3743e-02	1.7029e-01
V_{OUT_8}	1.9372e-01	3.9927e-02	2.3662e-02	2.0992e-02	8.9516e-01
V_{OUT_3}	3.2796e-02	1.8603e-02	1.5019e-01	6.1830e-02	9.6603e-03
V_{OUT_4}	3.9027e-03	1.8123e-03	1.2998e-02	3.1739e-02	1.8454e-02
V_{OUT_9}	1.0170e-02	2.4762e-03	1.2553e-02	1.3789e-02	8.9703e-03
$V_{OUT_{10}}$	1.2428e-02	3.0248e-03	1.5341e-02	1.6852e-02	1.0964e-02
$V_{OUT_{11}}$	4.2275e-02	9.5303e-02	1.3569e-02	2.1077e-02	1.5835e-01
V_{OUT_5}	6.8317e-02	1.2966e-02	2.9852e-02	4.3248e-03	1.2912e-02
$V_{OUT_{12}}$	1.2750e-02	7.5460e-03	8.3893e-02	1.2577e-02	1.7677e-02
$V_{OUT_{13}}$	4.0234e-03	1.6579e-03	1.5392e-02	2.3179e-02	1.6471e-02
ω_1	2.2730e-01	1.1827e-01	2.7039e-01	2.3967e-01	5.0473e-04
ω_2	9.1741e-02	1.1174e-01	2.0937e-01	1.8630e-01	1.6874e-04
ω_3	3.9051e-01	2.7502e-01	2.5455e-01	1.6166e-01	3.1621e-05
ω_4	3.9821e-01	2.8104e-01	1.8766e-01	2.2119e-01	8.3257e-05
	V_{REF_2}	V_{REF_3}	V_{REF_4}	V_{REF_5}	
P_{OUT_1}	2.0494e-01	5.1027e-02	7.0642e-02	8.0069e-02	
P_{OUT_2}	1.1219e-01	4.2713e-02	6.2736e-02	5.5722e-02	
P_{OUT_3}	8.9200e-02	1.7947e-01	1.2941e-01	9.2729e-02	
P_{OUT_4}	8.7027e-02	3.7657e-02	1.2559e-01	8.4172e-02	
V_{OUT_1}	6.8407e-01	1.1467e-02	1.9862e-02	2.5234e-02	
V_{OUT_2}	1.3856e+00	2.1950e-02	4.4744e-02	1.3031e-01	
V_{OUT_6}	3.4097e-01	2.3946e-02	8.6271e-02	4.9069e-02	
V_{OUT_7}	3.7378e-01	2.6238e-02	9.4571e-02	5.3791e-02	
V_{OUT_8}	3.6035e-01	1.7607e-02	5.1314e-03	3.5221e-02	
V_{OUT_3}	2.6967e-02	7.8329e-01	1.4577e-01	3.4732e-02	
V_{OUT_4}	3.1487e-02	1.2193e-01	7.1596e-01	7.3955e-02	
V_{OUT_9}	2.0358e-02	8.7393e-03	7.6798e-02	3.9940e-02	
$V_{OUT_{10}}$	2.4883e-02	1.0683e-02	9.3865e-02	4.8816e-02	
$V_{OUT_{11}}$	5.1989e-01	2.4003e-02	2.4199e-02	4.2097e-02	
V_{OUT_5}	2.0493e-01	1.2731e-02	8.9634e-02	9.1628e-01	
$V_{OUT_{12}}$	1.6273e-02	4.3176e-01	8.8967e-02	2.6628e-02	
$V_{OUT_{13}}$	6.2630e-03	2.0006e-02	1.7525e-01	1.8972e-02	
ω_1	4.0852e-04	1.5502e-01	1.1958e-04	1.6065e-02	
ω_2	4.1601e-04	1.2105e-01	3.8321e-05	1.1531e-02	
ω_3	1.1092e-04	1.6340e-01	2.5401e-04	3.2592e-02	
ω_4	7.6568e-05	1.0548e-01	5.3999e-04	3.0515e-02	

Table 6.8: *RGA* of System with MSVC at Bifurcation Frequency

MSVC should improve damping of the interarea oscillation from the performance index definition. Moreover, the voltage errors should be reduced at each of the buses because these voltage errors are also minimized during μ-synthesis controller design. This will be verified by the time simulation.

When active power load is increased by 50% above the nominal load value on bus 2, the system with CSVC goes unstable and oscillations keep growing. The Hopf bifurcation will be initiated by a slow increase in bifurcation parameter as expected. With MSVC the system remains stable and the interarea oscillations are damped effectively. This can be seen in Figure 6.13. It should be noted the bus voltages

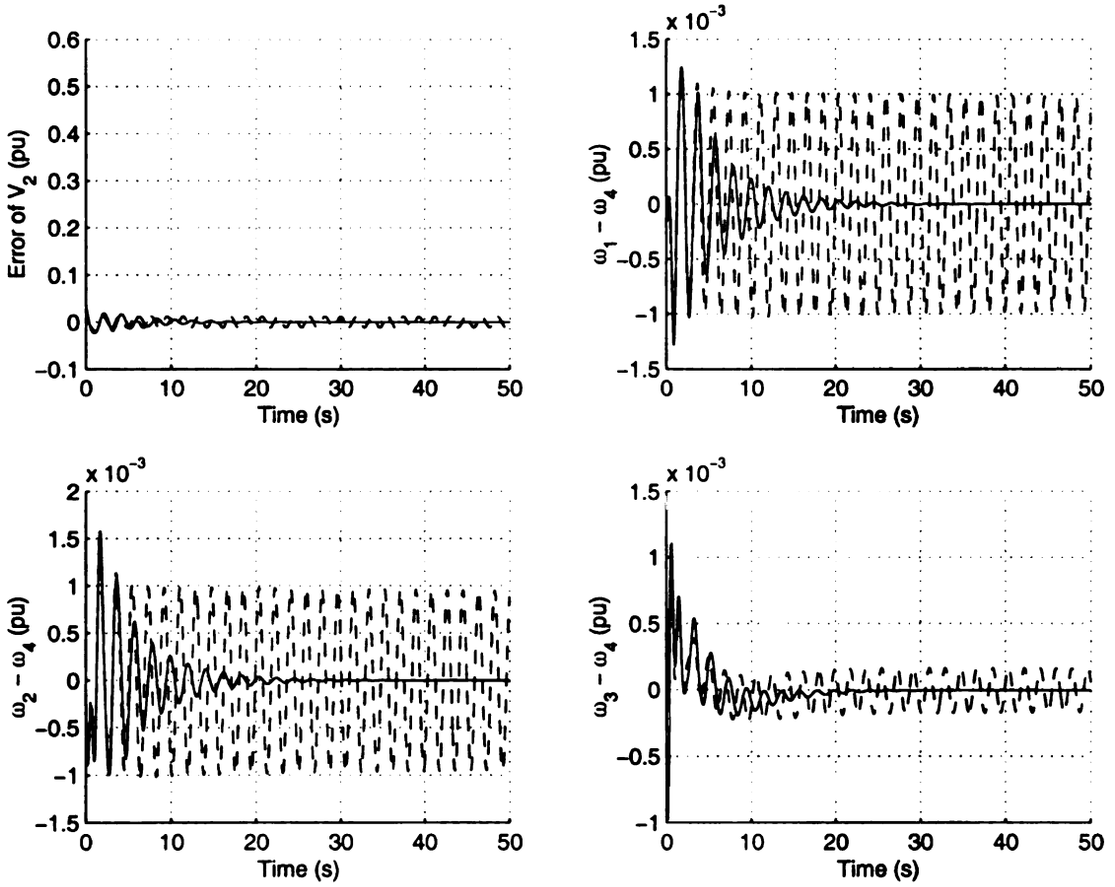

Figure 6.13: Open Loop System with CSVC (- -) and Closed-loop System with MSVC (-)

are also better controlled in addition to decreasing the speed deviations as expected. In fact, the active power load, the bifurcation parameter, can be increased by 50%

above the nominal load value for MSVC controller closed-loop system and the system still remains stable.

Both the CSVC and μ-synthesis based controller MSVC are stable and able to damp the interarea oscillation effectively for small active power increase. However, the MSVC is able to damp the frequency deviation much more quickly, which is quite obvious from Figure 6.13. The simulation results, which show that MSVC can handle even a larger than 50% increase in bifurcation parameter above the nominal load value without losing stability, are not presented here.

To further test the performance of μ-synthesis controller a fault is applied to generator 2 by placing a very small shunt reactance on generator 2. The fault is cleared after 0.05 second. The faulted time responses of the open loop system with CSVC and the closed-loop system with MSVC are shown in Figure 6.14. The oscillations observed on the terminal bus voltage on generator 2 is quickly damped for the MSVC controlled closed-loop system MSVC and is unstable for the open loop system. On the other hand, although MSVC is not designed to handle this fault uncertainty, Figure 6.14 show that the closed-loop system with MSVC is still stable and the oscillations are damped out quickly while CSVC does not have the ability to stabilize the system. This reveals that this MSVC controller is able to handle different faults and disturbances than the bifurcation parameter change that it was designed for.

The voltage and frequency control are the most important objectives in the power system controller design. However, in the performance index definition the power outputs are included as one of the objectives and the performance weighting is the same as that for outputs voltage deviations $V_{OUT_i} - V_{REF_i}$, $i = 1, 2, \cdots, 5$, and the interarea oscillations in frequency difference $\omega_i - \omega_4$, $i = 1, 2, 3$. The reason is that this performance index term $\Sigma_{i=1}^{4}(P_{OUT_i} - P_{REF_i})$ improves the control performance of voltages and frequencies. This power error control contains information on voltage

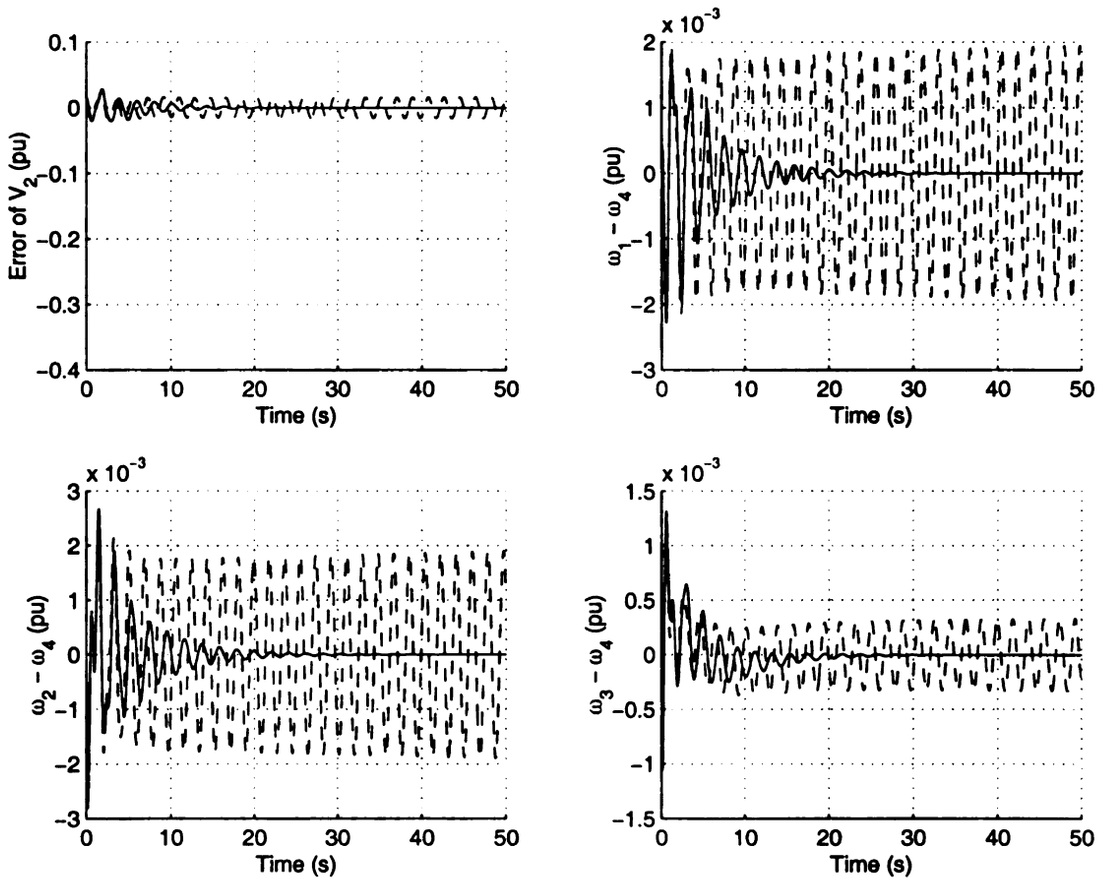

Figure 6.14: After Fault on G2: Open Loop System (- -) and Closed-loop System with MSVC (-)

which results in better control of voltage and frequency. This occurs because the deviation in generator terminal voltage is affected by the generator angle via feedback term $K_5\delta$ in Figure 6.15. Figure 6.15 shows the general block diagram of exciter and generator, where $G_e(s)$ represents the dynamics of excitation system, T'_{do} is the d-axis open-circuit time constant, M is the inertia of the generator, T_R is the time constant of transducer, D is the local damping of the generator, E'_a is the generator internal voltage, and E_{fd} is the field voltage output of the excitation system. The magnitude of the generator angle is directly related to the magnitude of the electric power generation. Thus including the power output error in the performance index should improve control of voltages, angles, and frequencies in the network. This is verified via simulation and comparing the peak response in Figure 6.16 and Figure 6.13 since we can see that both the voltage and frequency peak deviation increase without including the power output in the performance index. The damping of the oscillation are more rapid when the power output is not included in the performance index. If rapid damping of the oscillation was more important than reducing the peak deviation then the performance index without including power output can be used.

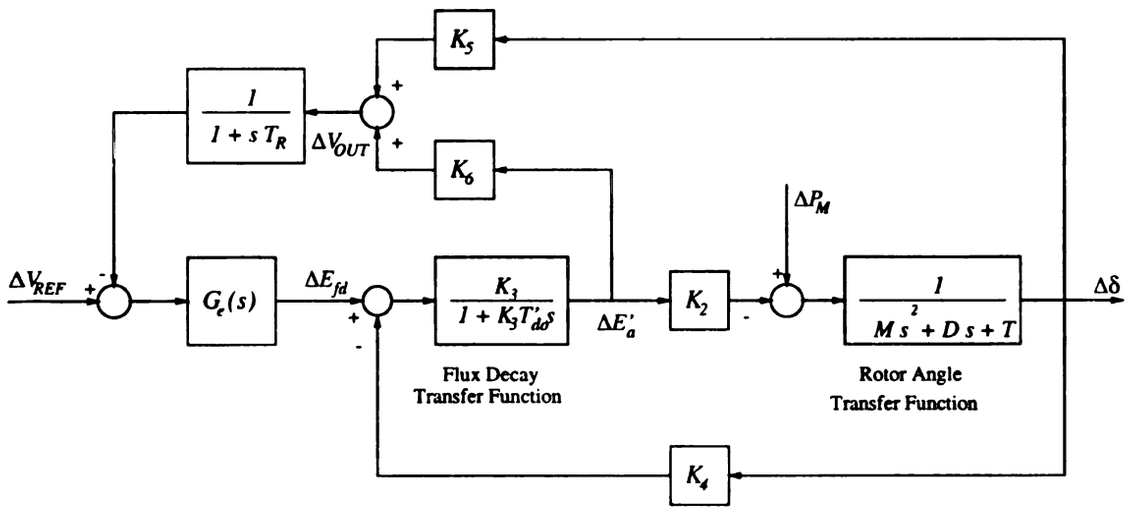

Figure 6.15: Diagram of Excitation System and Generator

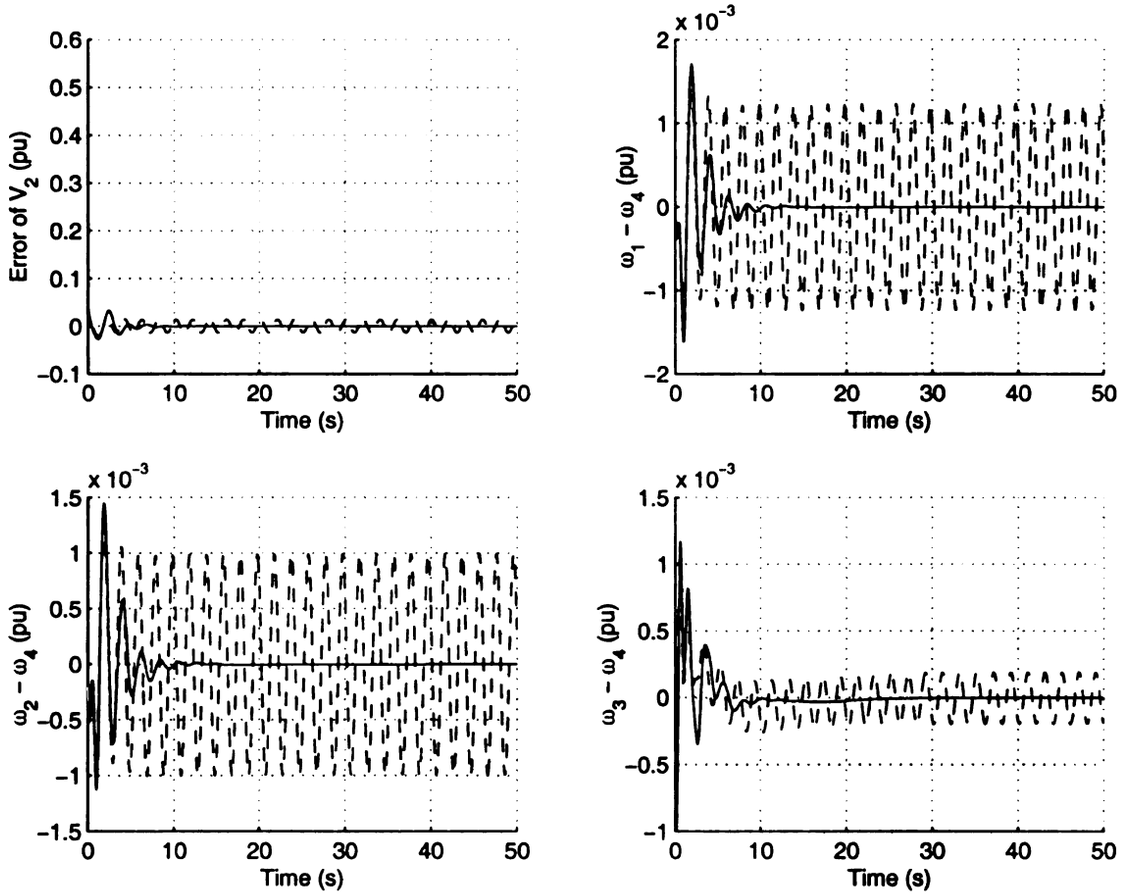

Figure 6.16: Open Loop System with CSVC (- -) and Closed-loop System with MSVC (No Power Output Performance Requirement)

The main objective of this robust SVC controller is to damp the interarea oscillations when Hopf bifurcation occurs in the example system. In Chapter 5 it has been shown that the power system can develop a different type of bifurcations in different time frame because the load model changes from a constant current in the transient time frame to a constant power model in the steady state time frames. The system with a constant current load model is vulnerable to Hopf bifurcation but the system with a constant power load model is vulnerable to saddle-node bifurcation. When active power transfer between two areas increases, a saddle-node bifurcation occurs when the load model changes from a constant current model to a constant power model. This implies that if the system is equipped with the robust controller, it is important that this controller should also be able to provide control in both the transient and steady-state time frame as is shown via the RGA matrix and time simulation results.

It has been verified in the MPSS design that including the inverse dynamics of generator enhances the control performance. A MSVC is designed by utilizing the inverse dynamics of generator 4. Figure 6.17 shows the improvement of the control performance of the closed-loop system with this MSVC and inverse dynamics. The overall performance is improved in terms of both maximum swings of the frequency deviation and transient period. Comparing the results of Figure 6.17 with Figure 6.13, it can be seen that the frequency deviation is smaller and the transient time is obviously shorter.

6.5.2 Reduced Order MSVC

The MSVC obtained here has 64 states, which is the same as the state number as the open loop system. It is difficult to implement such a high order controller.

A Hankel norm can be used for model reduction [46]. The reduced order model can be found by minimizing the optimal Hankel norm error between the original model

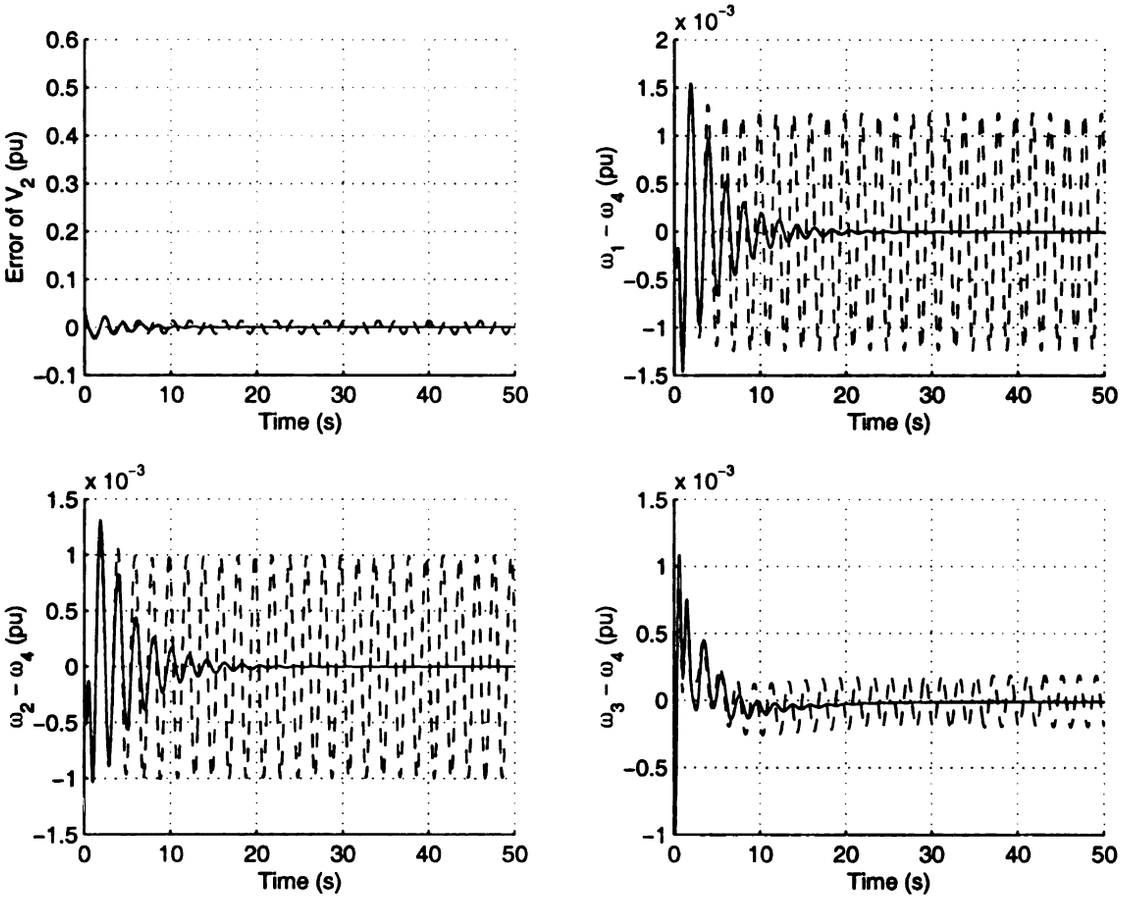

Figure 6.17: Open Loop System with CSVC (- -) and Closed-loop System with MSVC and Inverse Dynamics (-)

and the reduced order model. Hankel norm method has not been used to reduce the controller order in any previous work [36] [37] [38] [41] [46] [25] except in [42]. There is no method to determine the order of the reduced model should be or the dynamics that should be retained in the reduced model except for trial-and-error. In this section we will use a Hankel norm to obtain a reduced order μ-controller with the help of bifurcation subsystem method.

Bifurcation subsystem method claims that although a large number of states may be involved in the instability, only a subset of them, which constitutes the bifurcation subsystem, experiences, produces, and causes the full system bifurcation. The bifurcation subsystem information will be used to simplify the controller. The bifurcation subsystem for the Hopf bifurcation associated with the interarea oscillation produced by increasing active power load as bifurcation parameter is of 15^{th} order. This suggests the order of the μ-synthesis controller could be 15^{th} order to achieve the control objective of damping the interarea oscillation since the rest of the system can be truncated in terms of studying what produces or causes the full system model bifurcation, and thus need not be controlled. Actually, the order of MSVC can be further reduced. It is pointed out that the largest subsystem that satisfies both bifurcation subsystem condition and geometric decoupling condition is considered as the bifurcation subsystem in order to provide the greatest control design flexibility for the bifurcation that is experienced, produced, and caused within it. This implies the redundancy of bifurcation subsystem and the controller order can be decreased further. The smallest order bifurcation subsystem for this bifurcation is 8^{th} order. A Hankel norm reduction of the controller is used to produce an 8^{th} order controller. The result, is that an 8^{th} order MSVC preserves the control performance and the system stability in the presence of the uncertainty in a manner similar to that of the full system based MSVC controller. The *RGA* matrices of the closed-loop system with reduced order MSVC at steady state and at bifurcation frequency are shown

in Table 6.9 and 6.10, respectively. From Table 6.9 and 6.10 we can see that the *RGA* matrix determined decoupled control structure of the closed-loop system are still comparable the *RGA* matrix of the system with full order MSVC controller. Thus, it is expected that same control performance should be achieved for reduced order MSVC. The details of this *RGA* matrix is not further discussed here.

Figure 6.18 shows the response of the closed-loop system with this reduced order MSVC for the same perturbation shown in Figure 6.17 and we can see the control performance is almost the same as that for the full order MSVC.

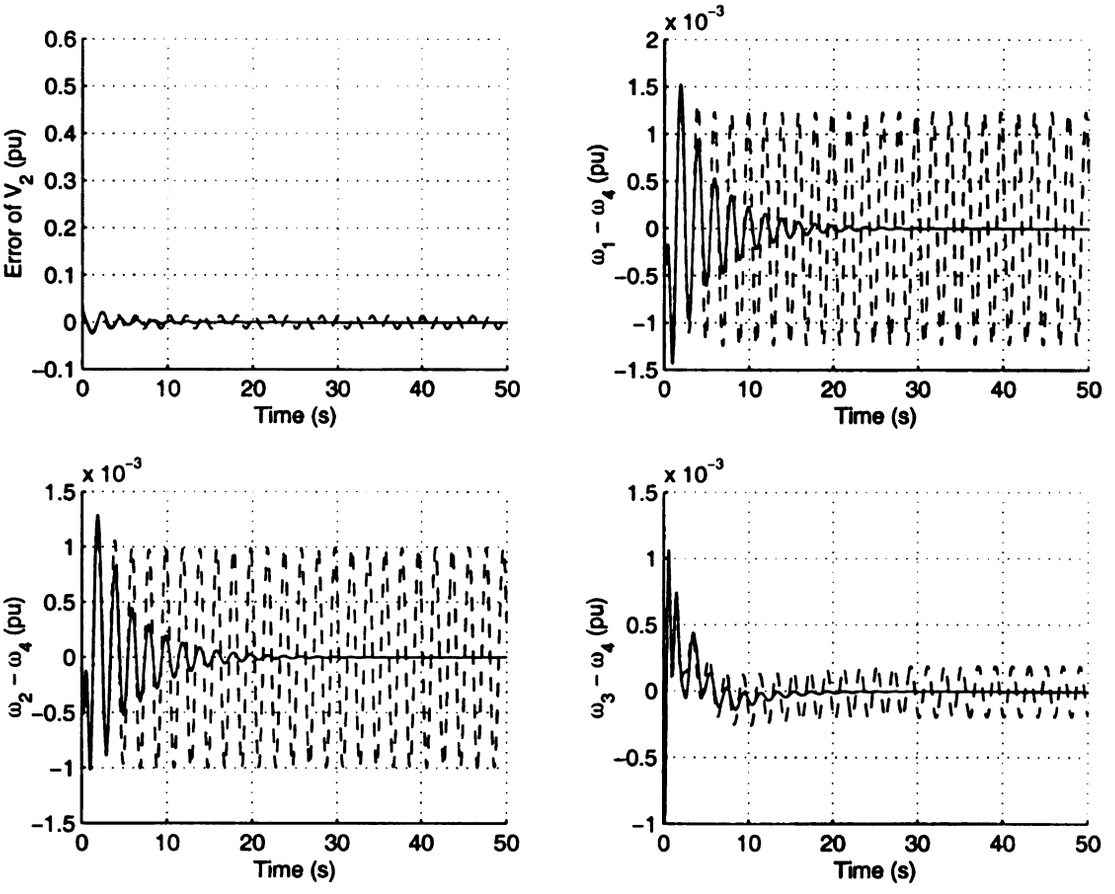

Figure 6.18: Open Loop System (- -) and Closed-loop System with Reduced Order MSVC (-)

	P_{REF_1}	P_{REF_2}	P_{REF_3}	P_{REF_4}	V_{REF_1}
P_{OUT_1}	9.3050e-01	1.5716e-04	1.1515e-04	1.0874e-04	2.7684e-04
P_{OUT_2}	1.2029e-05	9.3559e-01	1.0396e-05	8.3552e-06	2.6922e-04
P_{OUT_3}	2.0382e-05	9.5933e-05	9.4156e-01	8.2128e-05	4.3011e-05
P_{OUT_4}	2.7762e-05	3.7073e-05	5.8498e-05	9.5158e-01	2.3704e-05
V_{OUT_1}	4.4751e-04	2.6570e-05	6.5681e-05	6.9857e-05	7.2147e-01
V_{OUT_2}	1.3432e-04	6.3173e-04	6.2739e-04	6.4993e-04	1.5860e-03
V_{OUT_6}	5.9116e-03	6.1260e-03	3.6318e-03	4.9300e-03	8.3926e-03
V_{OUT_7}	6.6716e-03	6.9691e-03	4.4715e-03	5.9136e-03	9.5381e-03
V_{OUT_8}	1.3570e-03	7.4514e-04	2.3220e-03	2.4423e-03	2.7911e-01
V_{OUT_3}	7.4756e-05	7.8053e-05	6.0857e-04	7.5093e-05	2.2282e-05
V_{OUT_4}	3.2369e-04	3.4677e-04	2.6885e-04	2.6995e-04	5.1620e-05
V_{OUT_9}	2.3563e-03	2.0476e-03	4.7407e-03	4.8633e-03	5.6303e-03
$V_{OUT_{10}}$	2.7553e-03	2.3765e-03	5.6712e-03	5.8007e-03	6.8393e-03
$V_{OUT_{11}}$	1.0095e-03	1.3999e-03	2.6464e-03	3.1355e-03	4.3765e-03
V_{OUT_5}	8.8840e-02	8.5641e-02	8.3239e-02	7.8111e-02	6.9720e-03
$V_{OUT_{12}}$	1.0318e-03	9.5950e-04	5.7215e-05	1.1667e-03	7.3532e-04
$V_{OUT_{13}}$	1.1674e-03	8.3773e-04	2.0351e-03	2.2968e-03	2.6384e-03
ω_1	3.0837e-05	2.8863e-05	3.1007e-05	3.2104e-05	1.1159e-05
ω_2	2.8743e-05	3.0981e-05	3.1007e-05	3.2104e-05	1.1144e-05
ω_3	2.8743e-05	2.8862e-05	3.3387e-05	3.2110e-05	1.1146e-05
ω_4	2.8744e-05	2.8863e-05	3.1013e-05	3.4625e-05	1.1147e-05
	V_{REF_2}	V_{REF_3}	V_{REF_4}	V_{REF_5}	
P_{OUT_1}	1.0341e-03	6.5517e-05	2.9814e-04	2.2143e-02	
P_{OUT_2}	2.5569e-05	8.5892e-06	6.1856e-05	1.8739e-02	
P_{OUT_3}	2.8957e-04	1.5453e-04	7.4161e-04	2.3546e-02	
P_{OUT_4}	1.4384e-04	3.0619e-04	1.4861e-04	2.7018e-02	
V_{OUT_1}	6.8115e-04	3.2416e-05	6.4861e-05	4.2892e-03	
V_{OUT_2}	5.5181e-01	1.6048e-04	1.9053e-04	9.1092e-03	
V_{OUT_6}	4.3657e-02	1.0231e-02	3.6771e-02	1.7306e-01	
V_{OUT_7}	4.7323e-02	1.1383e-02	4.0489e-02	1.9515e-01	
V_{OUT_8}	1.7540e-02	1.0860e-03	1.6636e-03	8.9201e-02	
V_{OUT_3}	7.4386e-05	6.9005e-01	1.6818e-03	5.0732e-03	
V_{OUT_4}	9.2853e-05	1.3221e-03	5.2490e-01	2.3365e-03	
V_{OUT_9}	3.1805e-02	2.7285e-03	2.8810e-02	1.4306e-01	
$V_{OUT_{10}}$	3.8744e-02	3.2949e-03	3.5240e-02	1.7319e-01	
$V_{OUT_{11}}$	1.0261e-01	4.2398e-03	1.2524e-02	1.3042e-01	
V_{OUT_5}	1.8453e-01	2.2688e-02	2.3416e-01	1.0793e-02	
$V_{OUT_{12}}$	3.0552e-03	2.6954e-01	9.9389e-03	8.1761e-02	
$V_{OUT_{13}}$	1.3491e-02	2.1629e-03	9.6416e-02	1.2265e-01	
ω_1	3.2505e-05	1.1725e-05	1.3793e-05	3.6351e-03	
ω_2	3.2513e-05	1.1726e-05	1.3795e-05	3.6351e-03	
ω_3	3.2491e-05	1.1737e-05	1.3804e-05	3.6354e-03	
ω_4	3.2494e-05	1.1727e-05	1.3807e-05	3.6355e-03	

Table 6.9: *RGA* of Closed-loop System with Reduced Order MSVC at Steady State

	P_{REF_1}	P_{REF_2}	P_{REF_3}	P_{REF_4}	V_{REF_1}
P_{OUT_1}	1.0856e+00	5.4835e-02	3.4428e-02	1.1685e-02	1.0919e-01
P_{OUT_2}	8.6946e-02	8.3883e-01	2.1900e-02	1.1447e-02	3.5391e-02
P_{OUT_3}	5.0394e-02	1.0044e-02	1.2004e+00	1.0377e-01	2.7209e-01
P_{OUT_4}	6.4662e-02	1.7287e-02	1.8767e-01	1.2679e+00	2.8055e-01
V_{OUT_1}	3.1366e-01	1.0643e-01	3.8506e-02	2.7754e-02	1.7893e+00
V_{OUT_2}	6.8800e-02	1.4953e-01	1.9323e-02	9.4495e-03	6.8600e-01
V_{OUT_6}	8.4603e-02	9.4375e-02	1.0378e-02	2.1410e-02	1.8197e-01
V_{OUT_7}	9.2777e-02	1.0347e-01	1.1398e-02	2.3448e-02	1.9948e-01
V_{OUT_8}	2.4578e-01	4.2308e-02	3.1247e-02	2.7671e-02	1.0369e+00
V_{OUT_3}	3.7062e-02	1.9923e-02	1.7218e-01	7.3762e-02	1.3445e-02
V_{OUT_4}	3.1175e-03	4.4102e-04	1.4325e-02	3.9141e-02	2.6737e-02
V_{OUT_9}	1.1691e-02	1.4206e-03	1.3888e-02	1.6404e-02	1.5116e-02
$V_{OUT_{10}}$	1.4283e-02	1.7345e-03	1.6969e-02	2.0044e-02	1.8472e-02
$V_{OUT_{11}}$	6.5577e-02	9.6979e-02	9.8768e-03	2.0024e-02	1.8493e-01
V_{OUT_5}	7.6537e-02	1.2126e-02	3.2038e-02	5.9559e-03	6.9418e-03
$V_{OUT_{12}}$	1.3745e-02	9.5586e-03	9.5894e-02	1.5017e-02	2.6726e-02
$V_{OUT_{13}}$	5.3849e-03	3.8832e-04	1.7236e-02	2.7859e-02	2.5522e-02
ω_1	2.5828e-01	1.2377e-01	2.8917e-01	2.5629e-01	5.4536e-04
ω_2	1.0510e-01	1.1088e-01	2.1210e-01	1.8836e-01	1.9890e-04
ω_3	4.5194e-01	2.8412e-01	2.8937e-01	1.9329e-01	3.7330e-05
ω_4	4.6079e-01	2.9039e-01	2.2396e-01	2.5230e-01	1.1022e-04
	V_{REF_2}	V_{REF_3}	V_{REF_4}	V_{REF_5}	
P_{OUT_1}	2.7563e-01	5.0388e-02	7.6052e-02	7.6918e-02	
P_{OUT_2}	1.2592e-01	4.2909e-02	6.5416e-02	5.4705e-02	
P_{OUT_3}	8.2804e-02	2.0195e-01	1.5931e-01	9.0510e-02	
P_{OUT_4}	8.6624e-02	4.5700e-02	1.4413e-01	8.2573e-02	
V_{OUT_1}	8.1205e-01	1.6265e-02	2.6700e-02	2.6566e-02	
V_{OUT_2}	1.4471e+00	2.2306e-02	4.3618e-02	1.4372e-01	
V_{OUT_6}	3.6637e-01	2.6318e-02	9.9464e-02	5.1211e-02	
V_{OUT_7}	4.0163e-01	2.8838e-02	1.0904e-01	5.6139e-02	
V_{OUT_8}	4.2956e-01	2.2539e-02	6.2521e-03	3.9606e-02	
V_{OUT_3}	2.8470e-02	8.1889e-01	1.8072e-01	3.8102e-02	
V_{OUT_4}	2.9766e-02	1.2639e-01	7.2532e-01	7.4724e-02	
V_{OUT_9}	2.8830e-02	8.8894e-03	7.8099e-02	4.3529e-02	
$V_{OUT_{10}}$	3.5229e-02	1.0864e-02	9.5434e-02	5.3191e-02	
$V_{OUT_{11}}$	5.5840e-01	2.6327e-02	3.0992e-02	4.8448e-02	
V_{OUT_5}	2.4356e-01	1.4908e-02	1.0488e-01	9.4740e-01	
$V_{OUT_{12}}$	1.2762e-02	4.5126e-01	9.8712e-02	2.7639e-02	
$V_{OUT_{13}}$	9.6382e-03	2.0661e-02	1.8031e-01	1.7661e-02	
ω_1	4.5562e-04	1.6542e-01	1.1802e-04	1.7301e-02	
ω_2	4.0150e-04	1.2245e-01	4.6397e-05	1.2790e-02	
ω_3	1.2609e-04	1.8281e-01	3.0707e-04	3.7041e-02	
ω_4	9.0633e-05	1.2573e-01	6.0688e-04	3.4992e-02	

Table 6.10: *RGA* of Closed-loop System with Reduced Order MSVC at Bifurcation

6.5.3 MSVC for Uncertainty on Coherent Group Buses

In Chapter 5, it has been concluded that both active and reactive power load stress tests on buses of a coherent group produce exactly same bifurcation subsystem. This implies that the μ-synthesis controller designed to reject active power variation could also be effective in rejecting reactive power load variation if the reactive power load increase occurs at the buses in the coherent group with generator bus 2. In this example system, the bus 3, 4, 13, and 14 is a coherent bus group. In this section, a MSVC is designed with the active power load variation at bus 3 as uncertainty parameter. The details of MSVC design is similar to that in the previous section.

Figure 6.19 shows the simulation results of the closed-loop system with this MSVC control design for active power stress on bus 3. Again, 50% active power load above the nominal value can be applied to bus 3 without losing stability.

The reactive power stress test is run on bus 3 and the time simulation result is shown in Figure 6.20. Bus 3 and 4 are in a coherent bus group. Figure 6.21 shows the time simulation for reactive power uncertainty at bus 4. It can be seen that this MSVC design is fully able to reject reactive power uncertainty at bus 3. Satisfactory control performance can still be achieved despite the fact that reactive power load variation at bus 3 or bus 4 is not the bifurcation parameter that was used to design the MSVC control.

In fact, this simulation provides a verification of bifurcation subsystem method, i.e., the bifurcation subsystem itself provides the cures for the full system bifurcation. The conclusions reached in this section include:

1. although MSVC can achieve good control performance for the system with large uncertainties caused by active and reactive power load increase over the frequency range as well as for the fault on generator, it can not be guaranteed that MSVC is able to deal with all kinds of operating condition change induced

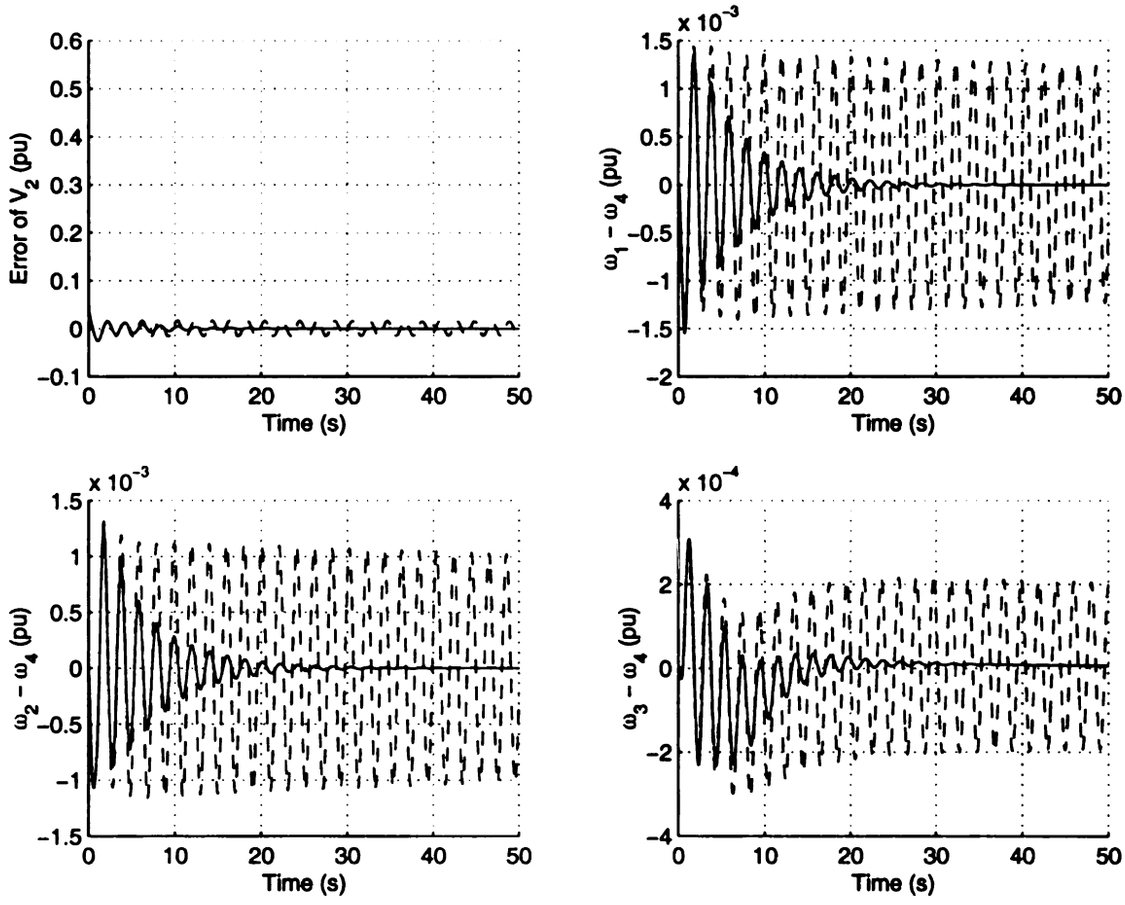

Figure 6.19: CSVC (- -) and MSVC (-) for Active Power Uncertainty at Bus 3

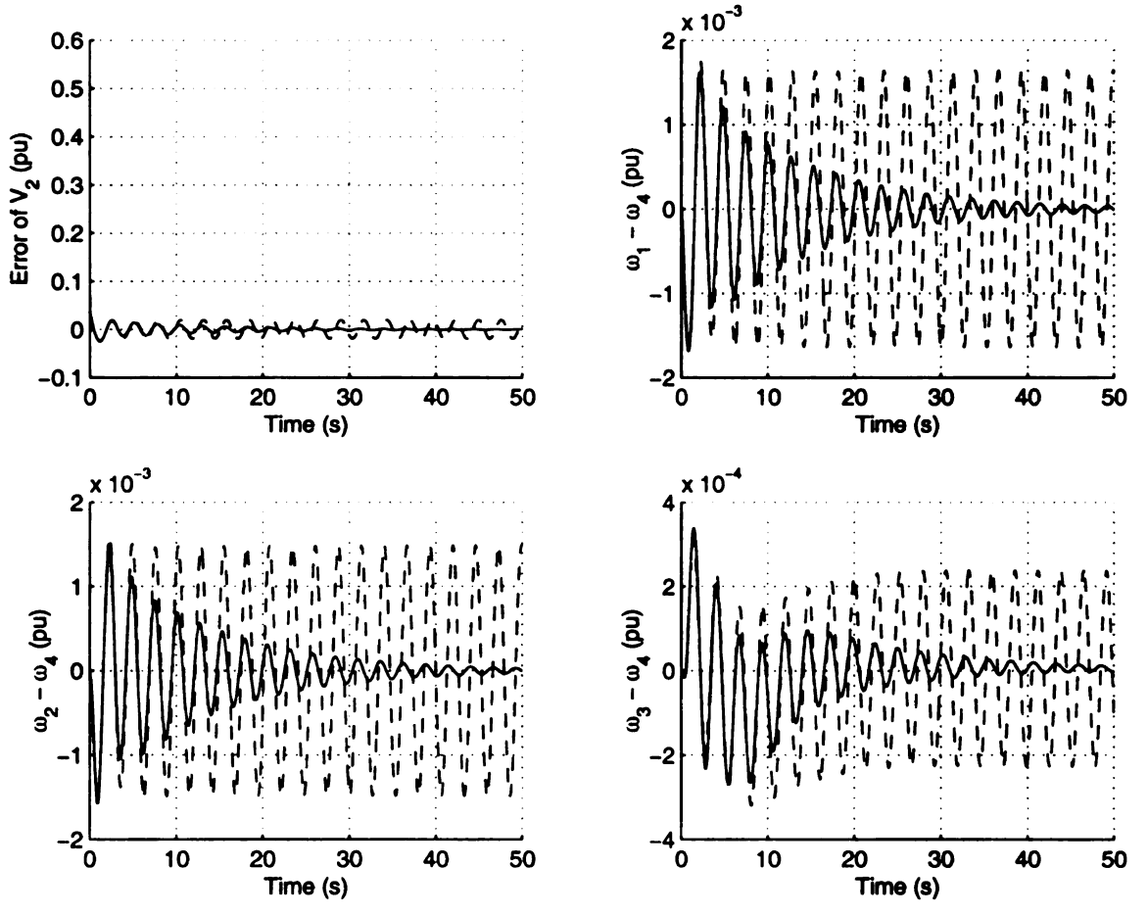

Figure 6.20: CSVC (- -) and MSVC (-) for Reactive Power Uncertainty at Bus 3

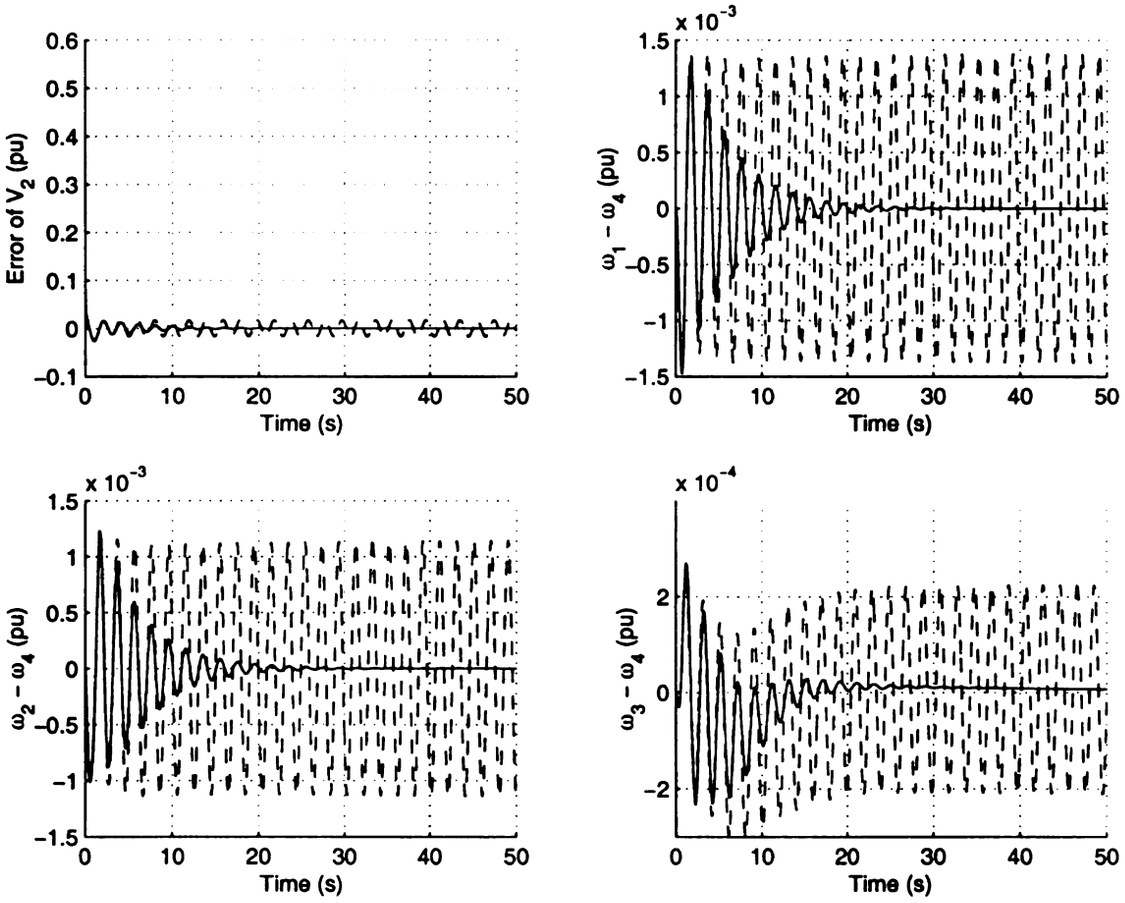

Figure 6.21: CSVC (- -) and MSVC (-) for Reactive Power Uncertainty at Bus 4

uncertainties that are not considered in the design. The study shows that MSVC designed for an active power bifurcation parameter can not achieve good performance for the uncertainty caused by generator reactance variation because the bifurcation subsystem is different than the bifurcation subsystem produced by active or reactive power load at bus 2, 3, and 4. These reqults also confirm that the same robust control design can stabilize different types of bifurcation as long as they are associated with the same bifurcation subsystem. This verifies that the bifurcation subsystem preserves the dynamics of the full system;

2. if all kinds of uncertainties are simultaneously modeled to design μ-synthesis based controller, the resulting system may be quite complicated. It is not guaranteed that μ-synthesis algorithm can converge and generate the desired control design;

3. MSVC is designed based on the fact that the parametric uncertainty is structured, i.e., the uncertainty matrix Δ is diagonal. If very large unstructured perturbation is applied to the system the control performance can become unacceptable or even result in the closed-loop system becoming unstable. This has been verified by simulation but the simulation results are not shown here. It should be noted that it is highly improbable that the unstructured parameter variation will ever be close to those values.

6.5.4 Bifurcation Subsystem Based SVC (BMSVC) Design

Bifurcation subsystem method has been used to guide the controller design and the order reduction of controller that was introduced in previous section. As we have mentioned that bifurcation subsystem method proves that the bifurcation subsystem not only experiences, produces, and causes the full system bifurcation, but also

provides the cures for the bifurcation. By inspecting the involved states it provide the lower order model that includes these states. Based on this reduced order model the controller designed is expected to stabilize the full system.

After applying the bifurcation identification, the linearization of the full system is represented as:

$$\begin{aligned} \dot{x}_1 &= A_{11}x_1 + A_{12}x_2 + B_1u \\ \dot{x}_2 &= A_{21}x_2 + A_{22}x_2 + B_2u \\ y &= C_1x_1 + C_2x_2 + Du \end{aligned}$$

where x_1 is the state variables associated with the bifurcation subsystem, and x_2 represents the external system states. For a specific bifurcation parameter the bifurcation subsystem method is applied and the truncated bifurcation subsystem model is:

$$\begin{aligned} \dot{x}_1 &= A_{11}x_1 + B_1u \\ y &= C_1x_1 + Du \end{aligned} \tag{6.5.4}$$

Parameter change in A_{11} will cause the Hopf bifurcation. It has been proven that the center manifold dynamics of the full system lie in or are totally contained in the nonlinear model associated with the bifurcation subsystem. Therefore, the controller can be designed based on the bifurcation subsystem, and thus applied to the full nonlinear system to cure the bifurcation.

Bifurcation subsystem is claimed to be able to provide a lower order model for control system design. In this section, μ-synthesis SVC controller based on the truncated bifurcation subsystem model is designed and tested using the same design procedures as in the previous section. The bifurcation subsystem is also produced by increasing

the active power load on generator bus 2. By using the bifurcation identification algorithm, a 15^{th} order bifurcation subsystem is obtained. As we mentioned in Chapter 5, the maximum ordered bifurcation subsystem is selected in order to provide the greatest control design flexibility. Therefore, a μ-synthesis robust SVC control is designed based on the bifurcation subsystem in the form of (6.5.4). Note the control configuration is similar to that shown in Figure 6.11. The same inputs and outputs are involved in the design, and only the states involved in the bifurcation subsystem are used. Clearly, this will reduce the dimension of the controller designed and require much less computational effort.

In this BMSVC design the uncertainty modeling and the performance index definition in the previous section are used. The system matrix, input and output matrix are reorganized to match the bifurcation subsystem states involved in the reduced order dynamics. The information associated with the external dynamics is lost since the bifurcation subsystem is obtained by eliminating the states outside of bifurcation subsystem. Once the bifurcation subsystem based MSVC (BMSVC) is obtained, the order of the controller is further reduced to 8 according to the order of the minimum bifurcation subsystem using the Hankel norm method. The resulting BMSVC is applied to the full system in order to stabilize the full system when the uncertainty caused by active power load on bus 2 is added to the system. The closed-loop μ-value is obtained and is shown in Figure 6.20. The peak μ value is around 0.9 around bifurcation frequency. This result implies that the bifurcation parameter can increase by $1/0.9 = 1.11$ and remain robustly stable. This compares with $1/0.72$ for the full model MSVC and $1/0,99$ for the full model MPSS.

It has been shown that a decoupled control structure is obtained for system with MSVC or MPSS and the control performance achieved by either of these controllers is greatly improved compared to the at both steady state and bifurcation frequency. The performance of the BMSVC is expected to be excellent but not as good as

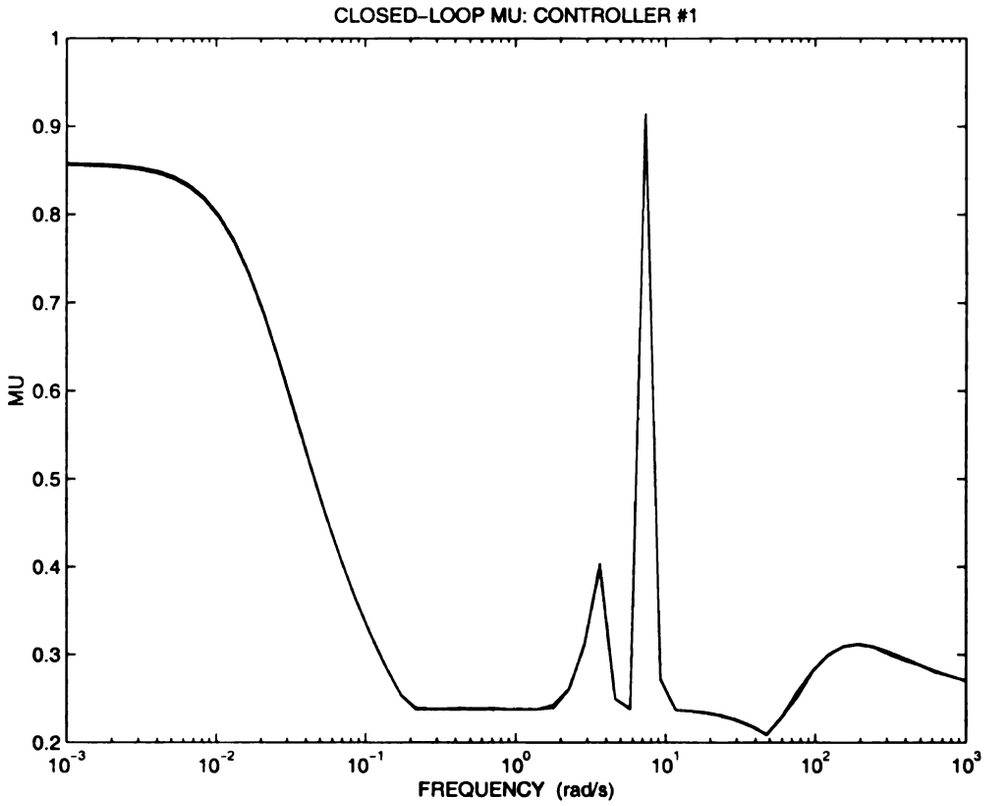

Figure 6.22: Closed-loop μ-value of Closed-loop System with BMSVC

the MPSS and MSVC, which were designed based on the full system model. As an example, the RGA matrices of the system with BMSVC at steady state and bifurcation frequency are shown in Table 6.11 and 6.12. Table 6.11 shows that at steady state the effectiveness of control degenerates (by comparing Table 6.11 and 6.7) in the sense that the closed-loop system is only weakly decoupled because the control pair elements, (P_{REF_i}, P_{OUT_i}), $i = 1, 2, 3, 4$, (V_{REF_i}, V_{OUT_i}), $i = 1, 2, \cdots, 5$, are no longer dominant. The excellent control structure of the MSVC where network voltage control is dominant by the MSVC at bus 5 is not true for BMSVC and now more than one element in each row is large. This can be seen from the RGA structure where there is only one dominant element in each row for V_{OUT_5}, V_{OUT_6}, V_{OUT_9}, $V_{OUT_{10}}$, $V_{OUT_{11}}$, $V_{OUT_{12}}$, and $V_{OUT_{13}}$ for the MSVC at bus 5. Therefore, there is fighting for control of these buses using BMSVC that does not occur for the MSVC. However, no output is subject to disturbance or noise is still preserved. This is true

since almost none of the RGA matrix element magnitudes are greater than one at steady state.

This structural robustness occurs because Δ_P, the uncertainty in the dynamics relating error z and output w, represents the uncertainty only in the bifurcation subsystem for the BMSVC but represents the uncertainty in both the bifurcation subsystem and the external system dynamics for the MSVC when the full system model is used to design the control. The uncertainty components of Δ_P associated with the external system produced the excellent control structure for the external system in the MSVC.

The same degradation of the control structure is not observed in Table 6.12 at the bifurcation frequency but the control structure of BMSVC has changed so network voltage control of the BMSVC is now assumed in part by the generators as it is for the MSVC. The omission of the dynamics external to the bifurcation subsystem thus has very little effect on control structure at bifurcation frequency (comparing Table 6.12 and 6.8). The control of power, P_{OUT_i}, $i = 1, 2, \cdots, 4$, and V_{OUT_i}, $i = 1, 2, \cdots, 5$, for the BMSVC, are not susceptible to disturbance because their magnitudes are very close to one as for the MSVC. Moreover, there should be no fighting for control of output variables because there is only one dominant element in each row. Thus, the control structure at bifurcation for BMSVC is still fine although it is expected that the control performance will degrade comparing with MSVC, especially for the control of voltage at steady state. From Table 6.11 and 6.12 it is still anticipated that the BMSVC significantly enhances the control performance of the system at both steady state and bifurcation frequency comparing with CSVC. This will be verified by time simulation.

The time response of the closed-loop system with BMSVC is shown in Figure 6.21 when the active power load is increased by 50% above the nominal load value for the

	P_{REF_1}	P_{REF_2}	P_{REF_3}	P_{REF_4}	V_{REF_1}
P_{OUT_1}	6.4091e-01	3.9668e-02	1.3932e-02	8.8237e-03	3.6621e-02
P_{OUT_2}	1.2735e-01	8.6022e-01	1.4029e-02	1.4352e-02	7.1711e-02
P_{OUT_3}	5.3061e-02	1.2611e-02	9.3716e-01	1.3679e-01	3.1913e-01
P_{OUT_4}	7.1160e-02	2.0194e-02	2.0891e-01	1.0760e+00	3.1652e-01
V_{OUT_1}	3.1699e-01	1.7973e-01	3.1095e-02	2.0154e-02	1.3916e+00
V_{OUT_2}	8.0288e-02	2.7279e-01	1.6656e-02	7.7844e-03	6.3204e-01
V_{OUT_6}	1.3078e-01	1.8876e-01	1.7657e-02	1.3381e-02	1.9435e-01
V_{OUT_7}	1.4369e-01	2.0719e-01	1.9494e-02	1.4549e-02	2.1314e-01
V_{OUT_8}	2.6521e-01	6.4335e-02	1.8798e-02	1.5251e-02	8.2340e-01
V_{OUT_3}	5.8376e-02	3.1802e-02	1.8374e-01	1.1652e-01	1.6959e-02
V_{OUT_4}	6.6569e-03	7.5180e-03	1.3056e-02	1.3693e-01	4.9918e-02
V_{OUT_9}	5.5046e-02	1.4674e-02	3.6398e-02	9.3113e-02	4.9657e-02
$V_{OUT_{10}}$	6.7233e-02	1.7904e-02	4.4470e-02	1.1380e-01	6.0704e-02
$V_{OUT_{11}}$	9.0984e-02	1.8090e-01	3.6868e-03	1.0693e-02	1.7344e-01
V_{OUT_5}	5.6230e-01	8.9808e-02	1.5467e-01	3.5070e-02	4.2881e-02
$V_{OUT_{12}}$	1.1871e-02	8.2272e-03	7.4478e-02	2.0194e-02	3.0436e-02
$V_{OUT_{13}}$	2.1605e-02	7.6903e-03	2.0984e-02	8.3378e-02	4.4718e-02
ω_1	1.0066e-01	9.5292e-02	1.6399e-01	1.5633e-01	1.4032e-04
ω_2	1.6080e-01	1.0151e-01	1.7784e-01	1.8647e-01	4.2163e-04
ω_3	5.7697e-01	3.5511e-01	3.1751e-01	2.8375e-01	6.5393e-05
ω_4	5.6084e-01	3.4430e-01	2.7687e-01	3.0097e-01	4.4116e-05
	V_{REF_2}	V_{REF_3}	V_{REF_4}	V_{REF_5}	
P_{OUT_1}	1.6422e-01	3.0217e-02	5.0548e-02	1.7970e-01	
P_{OUT_2}	1.0900e-01	3.6543e-02	6.7768e-02	1.3808e-01	
P_{OUT_3}	9.3678e-02	1.8820e-01	2.3303e-01	1.2288e-01	
P_{OUT_4}	9.4102e-02	5.0771e-02	1.5986e-01	2.4439e-01	
V_{OUT_1}	6.7661e-01	1.3149e-02	1.9086e-02	4.5985e-02	
V_{OUT_2}	1.2518e+00	1.9943e-02	3.7485e-02	1.9347e-01	
V_{OUT_6}	3.7441e-01	2.1189e-02	9.7519e-02	8.5607e-02	
V_{OUT_7}	4.1061e-01	2.3166e-02	1.0694e-01	9.3702e-02	
V_{OUT_8}	3.6111e-01	1.5146e-02	4.6555e-03	7.6777e-02	
V_{OUT_3}	3.5134e-02	2.5297e-01	3.4653e-01	2.1982e-01	
V_{OUT_4}	5.4168e-02	1.0670e-01	7.4895e-01	1.2988e-01	
V_{OUT_9}	9.0809e-02	1.0542e-02	1.5294e-01	1.0864e-01	
$V_{OUT_{10}}$	1.1100e-01	1.2892e-02	1.8697e-01	1.3277e-01	
$V_{OUT_{11}}$	4.9699e-01	1.9550e-02	2.5965e-02	1.1975e-01	
V_{OUT_5}	1.5838e+00	8.2471e-02	8.9176e-01	9.3881e-01	
$V_{OUT_{12}}$	1.4231e-02	1.8346e-01	1.0532e-01	7.8432e-02	
$V_{OUT_{13}}$	1.6113e-02	1.4884e-02	2.1783e-01	7.6250e-02	
ω_1	2.8419e-04	9.9537e-02	1.0570e-04	2.1795e-01	
ω_2	3.3995e-04	1.0684e-01	7.7375e-05	1.6206e-01	
ω_3	2.2398e-04	1.8786e-01	4.9536e-04	4.7175e-01	
ω_4	1.2286e-04	1.5328e-01	6.5759e-04	4.4503e-01	

Table 6.11: *RGA* of Closed-loop System with BMSVC at Steady State

	P_{REF_1}	P_{REF_2}	P_{REF_3}	P_{REF_4}	V_{REF_1}
P_{OUT_1}	1.1019e+00	5.7585e-02	3.7552e-02	1.2345e-02	9.6924e-02
P_{OUT_2}	9.6914e-02	8.6738e-01	2.6025e-02	1.0120e-02	3.9752e-02
P_{OUT_3}	5.2543e-02	1.0297e-02	1.1733e+00	1.0417e-01	2.6107e-01
P_{OUT_4}	6.5975e-02	1.7717e-02	1.8301e-01	1.2342e+00	2.6818e-01
V_{OUT_1}	2.9315e-01	1.0266e-01	3.5948e-02	2.6058e-02	1.7265e+00
V_{OUT_2}	6.7153e-02	1.4869e-01	2.0044e-02	1.0724e-02	6.5889e-01
V_{OUT_6}	7.8473e-02	9.1388e-02	8.7418e-03	2.2059e-02	1.7098e-01
V_{OUT_7}	8.6017e-02	1.0015e-01	9.5977e-03	2.4151e-02	1.8735e-01
V_{OUT_8}	2.3022e-01	4.1092e-02	2.9811e-02	2.6700e-02	9.9785e-01
V_{OUT_3}	3.6153e-02	2.0008e-02	1.6570e-01	7.2677e-02	1.2978e-02
V_{OUT_4}	4.1250e-03	5.3864e-04	1.5774e-02	4.6136e-02	2.9026e-02
V_{OUT_9}	1.2963e-02	1.2550e-03	1.5388e-02	2.0337e-02	1.7278e-02
$V_{OUT_{10}}$	1.5831e-02	1.5316e-03	1.8794e-02	2.4840e-02	2.1104e-02
$V_{OUT_{11}}$	6.0779e-02	9.4553e-02	1.0749e-02	2.0686e-02	1.7335e-01
V_{OUT_5}	6.0191e-02	8.4784e-03	2.7554e-02	5.5248e-03	6.0878e-03
$V_{OUT_{12}}$	1.4409e-02	1.0340e-02	9.5294e-02	1.5578e-02	2.6456e-02
$V_{OUT_{13}}$	5.0555e-03	8.7158e-04	1.8088e-02	3.2069e-02	2.7563e-02
ω_1	2.5350e-01	1.2544e-01	2.8540e-01	2.5556e-01	5.9047e-04
ω_2	1.1161e-01	1.1250e-01	2.1293e-01	1.9053e-01	2.3490e-04
ω_3	4.2392e-01	2.7446e-01	2.6454e-01	1.8483e-01	3.5395e-05
ω_4	4.3062e-01	2.7942e-01	2.0970e-01	2.3085e-01	1.0662e-04
	V_{REF_2}	V_{REF_3}	V_{REF_4}	V_{REF_5}	
P_{OUT_1}	2.8878e-01	4.9564e-02	7.8733e-02	7.4295e-02	
P_{OUT_2}	1.4499e-01	4.2059e-02	6.8054e-02	5.2614e-02	
P_{OUT_3}	8.2458e-02	1.9743e-01	1.6379e-01	9.0109e-02	
P_{OUT_4}	8.6142e-02	4.5248e-02	1.3989e-01	7.6613e-02	
V_{OUT_1}	7.8338e-01	1.4986e-02	2.5611e-02	2.4912e-02	
V_{OUT_2}	1.4119e+00	2.2625e-02	4.2463e-02	1.4069e-01	
V_{OUT_6}	3.5523e-01	2.6064e-02	9.7670e-02	4.9249e-02	
V_{OUT_7}	3.8925e-01	2.8548e-02	1.0702e-01	5.3965e-02	
V_{OUT_8}	4.1550e-01	2.1413e-02	5.8698e-03	3.7373e-02	
V_{OUT_3}	2.8034e-02	8.4185e-01	1.9377e-01	3.6141e-02	
V_{OUT_4}	3.2926e-02	1.3343e-01	7.4927e-01	7.1179e-02	
V_{OUT_9}	3.4130e-02	9.8380e-03	8.5133e-02	4.2751e-02	
$V_{OUT_{10}}$	4.1688e-02	1.2018e-02	1.0398e-01	5.2217e-02	
$V_{OUT_{11}}$	5.4268e-01	2.6106e-02	3.0654e-02	4.6779e-02	
V_{OUT_5}	2.0887e-01	1.2551e-02	8.9660e-02	9.3302e-01	
$V_{OUT_{12}}$	1.2835e-02	4.6577e-01	1.0787e-01	2.7473e-02	
$V_{OUT_{13}}$	1.0894e-02	2.1947e-02	1.9140e-01	1.5782e-02	
ω_1	4.9151e-04	1.6311e-01	1.2567e-04	5.1015e-03	
ω_2	4.5730e-04	1.2273e-01	4.9085e-05	3.7291e-03	
ω_3	1.3487e-04	1.7188e-01	3.2225e-04	1.0889e-02	
ω_4	9.5707e-05	1.1763e-01	6.0289e-04	1.0272e-02	

Table 6.12: *RGA* of System with BMSVC at Bifurcation Frequency

open loop system.

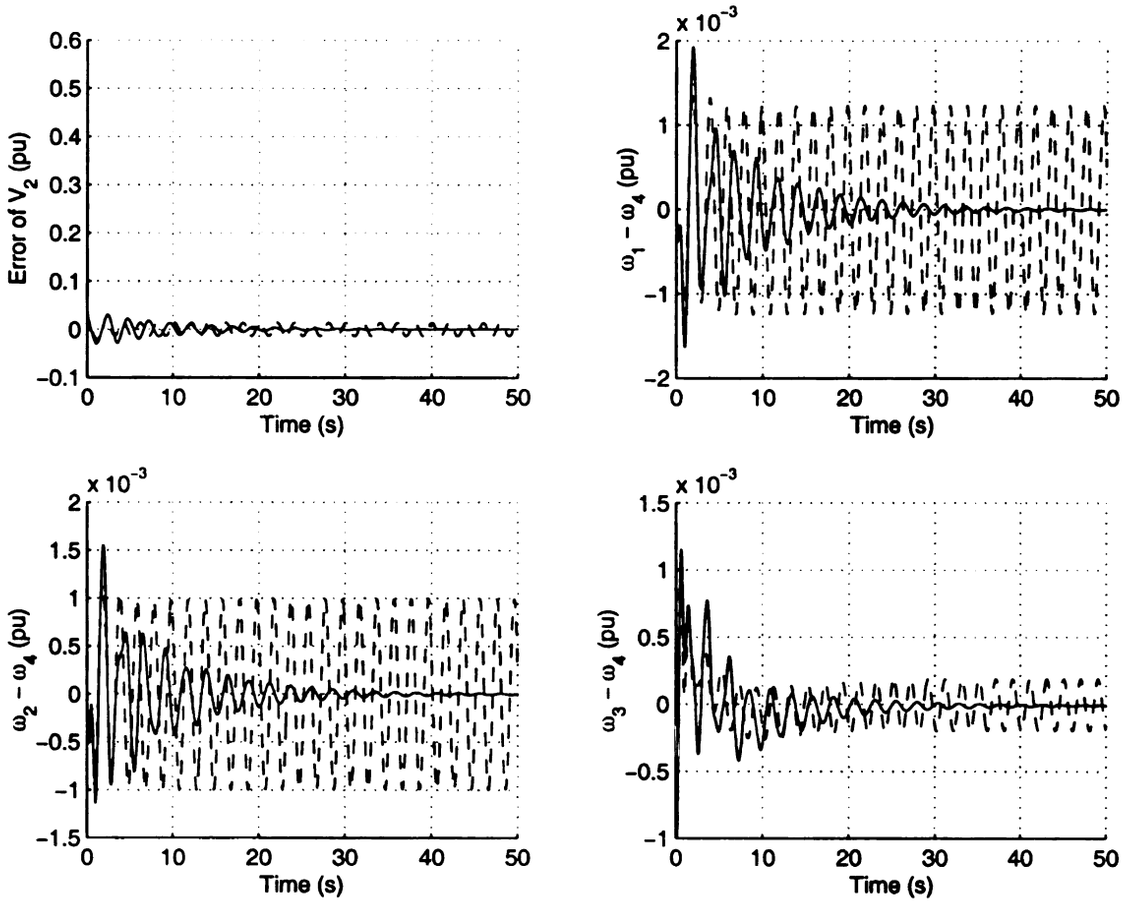

Figure 6.23: Open Loop System (- -) and Closed-loop System with BMSVC (-)

From Figure 6.21 the control performance of BMSVC is still very satisfactory although the control performance somewhat slightly degrades compared to MSVC design based on the full system model. This is expected because (a) the states of the external system that are computationally considered irrelevant are discarded as well as (b) the dynamic uncertainty associated with these discarded states omitted on the BMSVC control design shown in Figure 6.21 but is not discarded in the MSVC full system design. The uncertainty components of Δ_P associated with the subsystem external to the bifurcation subsystem assures (a) better control of steady state voltage; (b) improved decoupling between subsystems in the external system, and between those subsystems and the bifurcation subsystem; and (c) assignment of only one control for each subsystem and for the external system.

The most important conclusion shown by this simulation result is that it again computationally justifies the bifurcation subsystem method since the BMSVC designed based on the bifurcation subsystem robustly stabilizes the full system. It implies that the center manifold of the full system lies in or is contained in the bifurcation subsystem. It should be noted that the order of this BMSVC can be further decreased via Hankel norm reduction to order 8 without the loss of control performance. This occurs because the order of the minimum bifurcation subsystem is 8.

6.5.5 μ-synthesis SVC Controller for Input Uncertainty

In control system design the input uncertainty, which stems from the inability to know the exact value of the manipulated inputs, is always present. In this case the input becomes:

$$u' = (1 + \epsilon)u$$

where u is the desired control input computed by the controller, and u' is the actual control applied to the plant. In this section, both input uncertainty and parameteric uncertainty are included in the system model.

The plant with input uncertainty and parameteric uncertainty is shown in Figure 6.24 and we have

$$G' = G(I + E_I)$$

where G is the "nominal plant" that contains the parameteric uncertainty and G' is the plant perturbed by input uncertainty. Here the parameteric uncertainty is caused by the active power load variation on generator bus 2 as we have used in previous sections. Usually the input uncertainty is associated with the individual input channel. Thus, E_I also represents the diagonal structure uncertainty. Here we are going to design μ-controller to overcome the input uncertainty and interarea

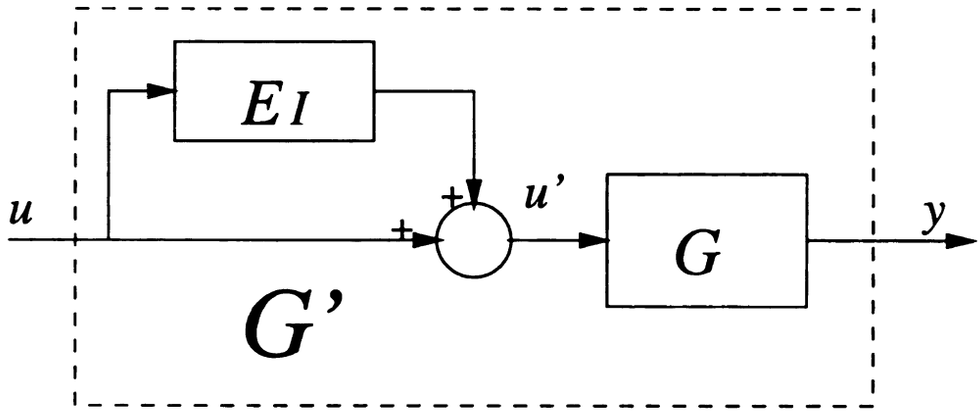

Figure 6.24: Plant with Input Uncertainty

oscillations as well as the voltage deviation from the desired values. The uncertainty weighting we are using here is represented by

$$E_I = \frac{s + 0.2}{0.5s + 1}$$

This input weighting function represents the 20% input uncertainty at low frequency since $lim_{s\to 0} E_I(s) = 0.2$. At high frequency $E_I(s)$ represents about 200% gain error since $lim_{s\to\infty} E_I(s) = 2$. The design procedures and performance index are defined as before. Obviously, more control effort is needed to achieve the robust stability and robust performance. The μ-controller is designed based on the full system for active power load variation. The closed-loop μ-value is shown in Figure 6.25. The peak μ-value is around 0.991 and it shows the robust stability and performance can be maintained for up to 20% input uncertainty. Note that the input uncertainty drastically decreased the possible increase in bifurcation parameter uncertainty from 1/0.72 to 1/0.991 by comparing the peak value in Figure 6.12 with that in Figure 6.25.

The *RGA* matrices of the closed-loop system with this controller at steady state and bifurcation frequency are shown in Table 6.13 and 6.14, respectively. The excellent control structure for network voltage for the MSVC in Table 6.7 is somewhat

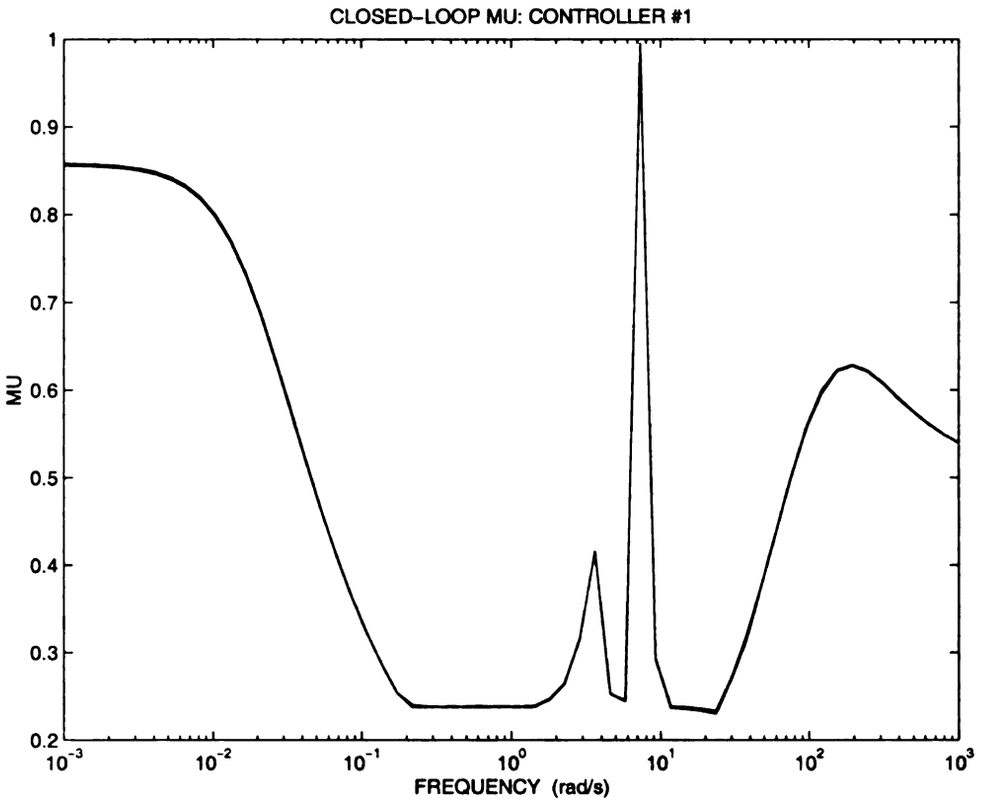

Figure 6.25: Closed-loop μ-value with Input Uncertainty

destroyed by the large input uncertainty level in Table 6.13 because the elements (P_{REF_i}, P_{OUT_i}), $i = 1, 2, \cdots, 4$, and (V_{REF_i}, V_{OUT_i}), $i = 1, 2, \cdots, 5$, are above one. The MSVC no longer controls the network bus voltage V_{OUT_6}, V_{OUT_7}, V_{OUT_9}, $V_{OUT_{10}}$, $V_{OUT_{11}}$, and $V_{OUT_{13}}$ but now are effective for only V_{OUT_2} and V_{OUT_5}. There is not much fighting at steady state for control of network voltage in this RGA matrix since there is one and only one dominant row element in Table 6.13. However, some control loops may be subject to disturbance because we note that magnitude of element (P_{REF_1}, P_{OUT_1}), (P_{REF_3}, P_{OUT_3}), (P_{REF_4}, P_{OUT_4}), (V_{REF_1}, V_{OUT_1}), and (V_{REF_2}, V_{OUT_2}) are above one. On the other hand, MSVC gives good control to SVC bus and generator bus 2, where the active power load stress test is run. This is indicated by the magnitude of (V_{REF_5}, V_{OUT_2}) and (V_{REF_5}, V_{OUT_5}) since they are the largest elements in the column under V_{REF_5}.

The RGA matrix of the closed-loop system with the MSVC at bifurcation frequency

is shown in Table 6.14. The RGA matrix structure in Table 6.14 degrades compared to Table 6.8 and 6.12. The magnitude of element (P_{REF_i}, P_{OUT_i}), $i = 1, 2, \cdots, 5$, and (V_{REF_i}, V_{OUT_i}), $i = 1, 2, 3, 4$ are less than 1, and (V_{REF_5}, V_{OUT_5}) is much greater than 1. However, these elements are still dominant in each row. This suggests decent if not good voltage control can still be achieved. There is no single dominant element at several buses in the network and thus there is some fighting between controls. The generator speeds are under control of this MSVC at bifurcation frequency as would be expected. This can be seen from the large magnitude of elements of (V_{REF_5}, ω_i), $i = 1, 2, 3, 4$. The MSVC has even more control than the PSS on generator 3 over generator speed at the bifurcation frequency.

The performance of the control design with input uncertainty is simulated. The time responses are shown in Figure 6.26 and 6.27. It should be noted that the bifurcation parameter uncertainty is stressed with a 50% active power increase above the nominal load value applied to bus 2 for the open loop CSVC system. From Figure 6.26 it can be seen that the transient responses of the power and voltage outputs is worse than the previous cases. The errors decay quickly to steady state values. However, the steady state error values do not converge to zero even though the steady state errors are very small. This is because the input uncertainty weighting function is not zero at steady state but has a 20% input bias. There is no approximate integral effect in the closed-loop system. Since the power system stabilizer achieves tight control over the frequency the small steady state error of power output is not surprising. The frequency deviations are shown in Figure 6.27. The interarea oscillations are eliminated quickly. The input uncertainty has slight effects on control of the frequency ω_i, $i = 1, 2, \cdots, 4$ as shown by comparing Figure 6.13 and 6.27. The damping of transient response of frequency deviation is almost same and the steady state error of frequency is zero. However, the peak of the transients $\omega_i - \omega_4$, $i = 1, 2, 3$, has doubled comparing to those shown in Figure 6.13.

	P_{REF_1}	P_{REF_2}	P_{REF_3}	P_{REF_4}	V_{REF_1}
P_{OUT_1}	1.1321e+00	5.7304e-02	3.5488e-02	1.2167e-02	1.1497e-01
P_{OUT_2}	9.6979e-02	8.6197e-01	2.2679e-02	1.1942e-02	4.0993e-02
P_{OUT_3}	4.9811e-02	9.9342e-03	1.1899e+00	1.0433e-01	2.6906e-01
P_{OUT_4}	6.3693e-02	1.7037e-02	1.8495e-01	1.2506e+00	2.7648e-01
V_{OUT_1}	3.1089e-01	1.0308e-01	3.8101e-02	2.7717e-02	1.7735e+00
V_{OUT_2}	6.7967e-02	1.4490e-01	1.9084e-02	9.4294e-03	6.7880e-01
V_{OUT_6}	8.3358e-02	9.1148e-02	1.0226e-02	2.1325e-02	1.7985e-01
V_{OUT_7}	9.1411e-02	9.9935e-02	1.1232e-02	2.3355e-02	1.9715e-01
V_{OUT_8}	2.4341e-01	4.0960e-02	3.0903e-02	2.7620e-02	1.0272e+00
V_{OUT_3}	3.6698e-02	1.9727e-02	1.6919e-01	7.4366e-02	1.3311e-02
V_{OUT_4}	3.4925e-03	4.9727e-04	1.5674e-02	4.7385e-02	2.9773e-02
V_{OUT_9}	1.3962e-02	1.7218e-03	1.5981e-02	2.0986e-02	1.7786e-02
$V_{OUT_{10}}$	1.7058e-02	2.1022e-03	1.9527e-02	2.5643e-02	2.1734e-02
$V_{OUT_{11}}$	6.4768e-02	9.3856e-02	9.7497e-03	1.9966e-02	1.8298e-01
V_{OUT_5}	6.2698e-02	9.3324e-03	2.8524e-02	5.3122e-03	5.9375e-03
$V_{OUT_{12}}$	1.4011e-02	9.7538e-03	9.7416e-02	1.5732e-02	2.7206e-02
$V_{OUT_{13}}$	6.0084e-03	4.3579e-04	1.8792e-02	3.3005e-02	2.8323e-02
ω_1	2.7419e-01	1.2930e-01	2.9801e-01	2.6680e-01	5.7428e-04
ω_2	1.1676e-01	1.2018e-01	2.1958e-01	1.9643e-01	2.2970e-04
ω_3	4.4697e-01	2.8100e-01	2.8433e-01	1.9432e-01	3.7204e-05
ω_4	4.5413e-01	2.8619e-01	2.2072e-01	2.4851e-01	1.0880e-04
	V_{REF_2}	V_{REF_3}	V_{REF_4}	V_{REF_5}	
P_{OUT_1}	2.9470e-01	5.1910e-02	7.9466e-02	7.5029e-02	
P_{OUT_2}	1.3673e-01	4.4394e-02	6.8247e-02	5.3497e-02	
P_{OUT_3}	8.1885e-02	1.9857e-01	1.6721e-01	9.1418e-02	
P_{OUT_4}	8.5368e-02	4.5041e-02	1.4203e-01	7.8352e-02	
V_{OUT_1}	8.0642e-01	1.6076e-02	2.6882e-02	2.5711e-02	
V_{OUT_2}	1.4269e+00	2.2002e-02	4.3938e-02	1.4138e-01	
V_{OUT_6}	3.6246e-01	2.5894e-02	1.0007e-01	5.0048e-02	
V_{OUT_7}	3.9734e-01	2.8373e-02	1.0970e-01	5.4865e-02	
V_{OUT_8}	4.2641e-01	2.2266e-02	6.2919e-03	3.8471e-02	
V_{OUT_3}	2.8188e-02	8.4540e-01	1.9795e-01	3.6098e-02	
V_{OUT_4}	3.3140e-02	1.3378e-01	7.5038e-01	7.1981e-02	
V_{OUT_9}	3.3912e-02	9.7054e-03	8.5341e-02	4.2650e-02	
$V_{OUT_{10}}$	4.1440e-02	1.1861e-02	1.0428e-01	5.2117e-02	
$V_{OUT_{11}}$	5.5306e-01	2.5954e-02	3.1184e-02	4.7148e-02	
V_{OUT_5}	2.0880e-01	1.2808e-02	9.1134e-02	9.3246e-01	
$V_{OUT_{12}}$	1.2991e-02	4.6796e-01	1.0903e-01	2.7635e-02	
$V_{OUT_{13}}$	1.0694e-02	2.1842e-02	1.9202e-01	1.6158e-02	
ω_1	4.8689e-04	1.7038e-01	1.2328e-04	5.5186e-03	
ω_2	4.3562e-04	1.2665e-01	4.8384e-05	4.0768e-03	
ω_3	1.2462e-04	1.7975e-01	3.2224e-04	1.1804e-02	
ω_4	8.9396e-05	1.2391e-01	5.9811e-04	1.1144e-02	

Table 6.13: *RGA* of System with MSVC and Input Uncertainty at Steady State

	P_{REF_1}	P_{REF_2}	P_{REF_3}	P_{REF_4}	V_{REF_1}
P_{OUT_1}	3.4548e-01	4.4217e-02	3.8143e-02	3.5449e-02	2.1733e-02
P_{OUT_2}	2.8238e-02	4.7207e-01	2.6074e-02	2.4482e-02	1.3652e-02
P_{OUT_3}	1.7246e-02	3.7587e-02	4.8674e-01	2.5339e-02	1.1203e-02
P_{OUT_4}	2.0940e-02	3.5382e-02	2.7811e-02	4.6893e-01	1.3470e-02
V_{OUT_1}	3.1122e-03	1.9040e-03	1.5411e-03	1.7014e-03	7.2625e-01
V_{OUT_2}	4.8918e-02	3.8818e-02	2.8429e-02	2.9201e-02	1.6754e-02
V_{OUT_6}	1.9891e-01	1.6154e-01	5.2213e-02	7.0543e-02	6.9884e-02
V_{OUT_7}	2.2716e-01	1.8534e-01	6.4876e-02	8.5404e-02	8.0133e-02
V_{OUT_8}	1.5690e-01	1.0160e-01	1.2978e-01	1.3575e-01	7.4729e-01
V_{OUT_3}	1.1898e-02	1.0918e-02	1.6425e-02	1.2881e-02	3.8767e-03
V_{OUT_4}	2.0416e-02	1.7479e-02	2.4483e-02	2.2647e-02	3.2270e-03
V_{OUT_9}	3.4963e-02	3.0862e-02	7.6847e-02	6.9681e-02	9.0483e-02
$V_{OUT_{10}}$	4.0677e-02	3.5798e-02	9.1582e-02	8.2804e-02	1.0949e-01
$V_{OUT_{11}}$	1.1266e-01	8.0105e-02	6.3289e-02	7.4901e-02	2.3085e-02
V_{OUT_5}	2.1200e-01	2.2841e-01	1.9206e-01	1.7983e-01	2.0470e-02
$V_{OUT_{12}}$	6.0671e-02	5.9025e-02	9.8336e-02	7.8404e-02	4.8850e-02
$V_{OUT_{13}}$	2.3958e-02	2.7159e-02	7.7503e-02	6.3817e-02	7.1398e-02
ω_1	7.1656e-03	6.7033e-03	7.4277e-03	7.6809e-03	2.5390e-03
ω_2	7.1277e-03	6.7408e-03	7.4265e-03	7.6795e-03	2.5385e-03
ω_3	7.1285e-03	6.7030e-03	7.4635e-03	7.6804e-03	2.5385e-03
ω_4	7.1284e-03	6.7033e-03	7.4274e-03	7.7159e-03	2.5386e-03
	V_{REF_2}	V_{REF_3}	V_{REF_4}	V_{REF_5}	
P_{OUT_1}	1.5344e-01	1.9868e-02	9.5740e-02	1.5635e-01	
P_{OUT_2}	1.2036e-01	1.8878e-02	8.6581e-02	1.2692e-01	
P_{OUT_3}	8.5145e-02	3.1426e-02	1.1877e-01	1.0598e-01	
P_{OUT_4}	9.7485e-02	2.6963e-02	1.1998e-01	1.1399e-01	
V_{OUT_1}	5.8353e-03	9.5998e-04	1.9820e-03	1.0196e-03	
V_{OUT_2}	7.5222e-01	7.9565e-03	9.4267e-03	6.5933e-02	
V_{OUT_6}	6.5868e-01	1.5680e-01	5.6368e-01	1.1679e-01	
V_{OUT_7}	7.1966e-01	1.7624e-01	6.2704e-01	1.3823e-01	
V_{OUT_8}	3.0736e-01	6.5800e-02	1.0081e-01	4.4798e-01	
V_{OUT_3}	1.2592e-02	7.7753e-01	5.4668e-02	4.3937e-03	
V_{OUT_4}	5.6374e-03	2.3858e-02	6.7624e-01	5.4449e-02	
V_{OUT_9}	5.1099e-01	5.9686e-02	6.2967e-01	1.1716e-02	
$V_{OUT_{10}}$	6.2006e-01	7.1861e-02	7.6788e-01	1.6776e-02	
$V_{OUT_{11}}$	9.5668e-01	1.0744e-01	3.1754e-01	6.0235e-01	
V_{OUT_5}	5.1849e-01	5.6926e-02	5.8778e-01	2.7694e+00	
$V_{OUT_{12}}$	2.0240e-01	8.6752e-01	1.8552e-01	3.8513e-01	
$V_{OUT_{13}}$	3.6562e-01	2.1225e-02	9.4401e-01	4.5151e-01	
ω_1	7.7847e-03	2.8147e-03	3.3101e-03	8.8402e-03	
ω_2	7.7834e-03	2.8145e-03	3.3108e-03	8.8389e-03	
ω_3	7.7814e-03	2.8154e-03	3.3129e-03	8.8379e-03	
ω_4	7.7818e-03	2.8151e-03	3.3123e-03	8.8379e-03	

Table 6.14: *RGA* of System with MSVC and Input Uncertainty at Bifurcation Frequency

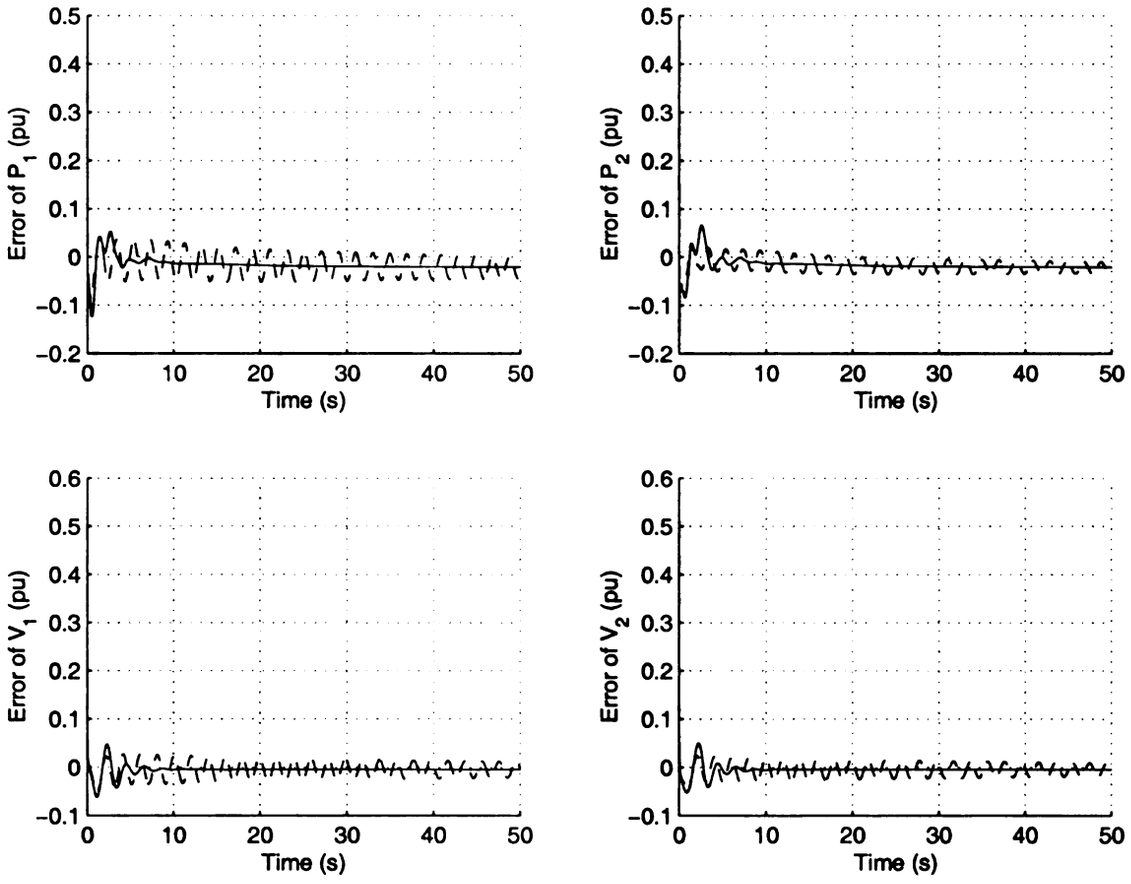

Figure 6.26: Power and Voltage Output Errors for Input Uncertainty

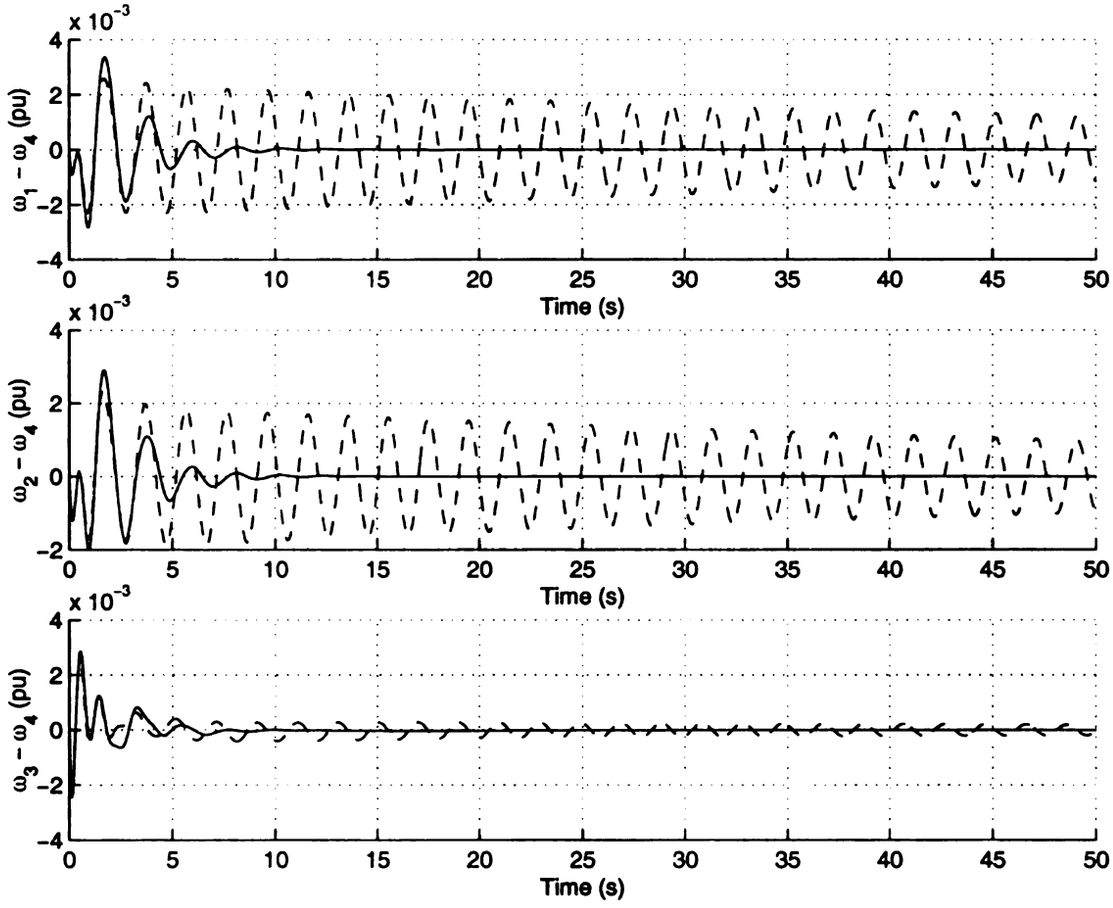

Figure 6.27: Frequency Deviation for Input Uncertainty

The 10% measurement noise is now added to the output channel to μ-controller in addition to the presence of input uncertainty. This is reflected in the power outputs shown in Figure 6.28. The system is still robustly stable but the magnitude of performance of power and voltage set points degrade. However, the frequency deviation is suppressed quickly. This can be seen in Figure 6.29. The simulation

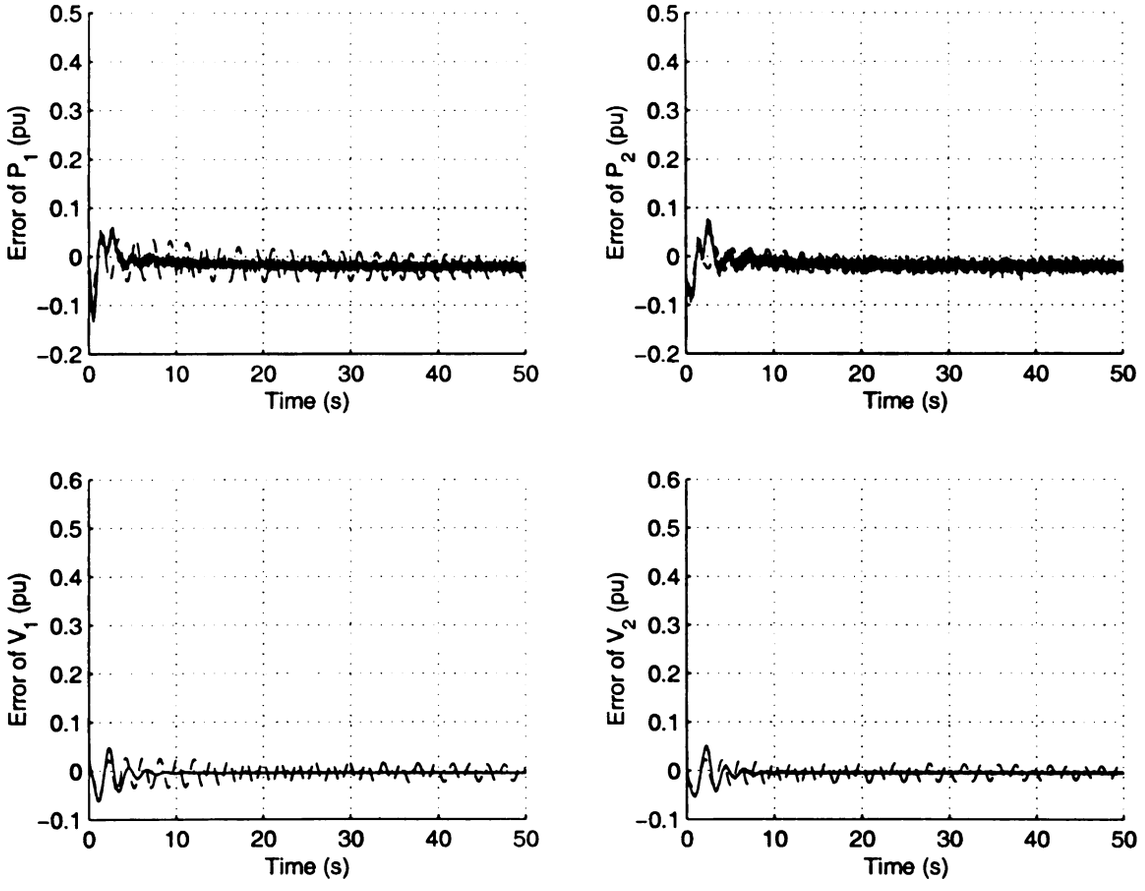

Figure 6.28: Power and Voltage Output Errors for Measurement Noise

results show that the input uncertainty and measurement noise do not affect the oscillations between generators.

6.5.6 Redesigned BMSVC for Saddle-node Bifurcation

In this section, BMSVC is designed in order to stabilize the saddle-node bifurcation, which is caused by active power transfer between two areas for constant power load

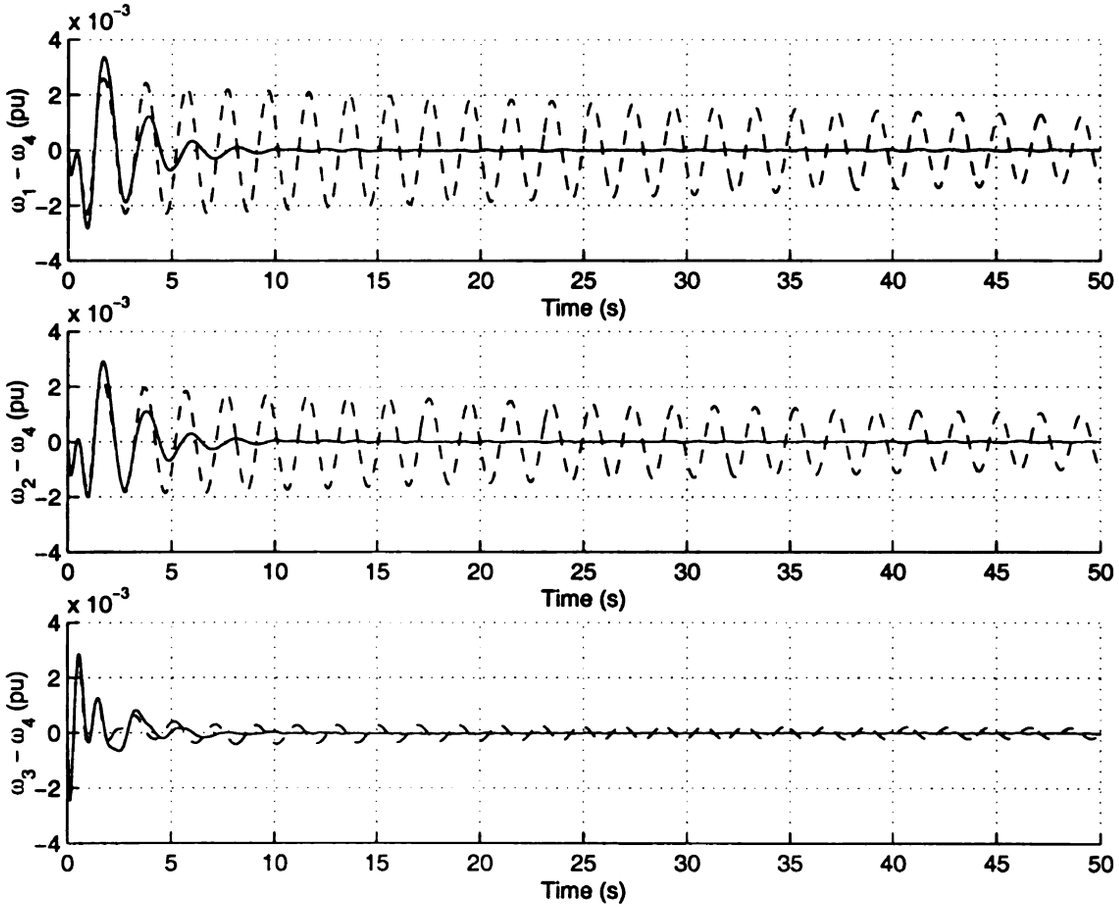

Figure 6.29: Frequency Deviation for Measurement Noise

model. From Table 5.16 the saddle-node bifurcation is of order 7. Following the control design procedures a 8^{th}-order BMSVC is designed. This saddle-node bifurcation is expected to be easy to stabilize since very few states and only inertial dynamics are involved.

The *RGA* matrix of the system with MPSS redesigned for saddle-node bifurcation is shown in Table 6.15. It has a very robust control structure that has very excellent decoupled control of P_{OUT_i}, $i = 1, 2, \cdots, 4$ and V_{OUT_i}, $i = 1, 2, \cdots, 5$, where there is no fighting for control and no susceptibility to disturbance. The control of ω_i, $i = 1, 2, \cdots, 4$, is likely to be poor because there is no large element in the *RGA* row for ω_i, $i = 1, 2, \cdots, 4$. However, this is of little concern for saddle-node bifurcation.

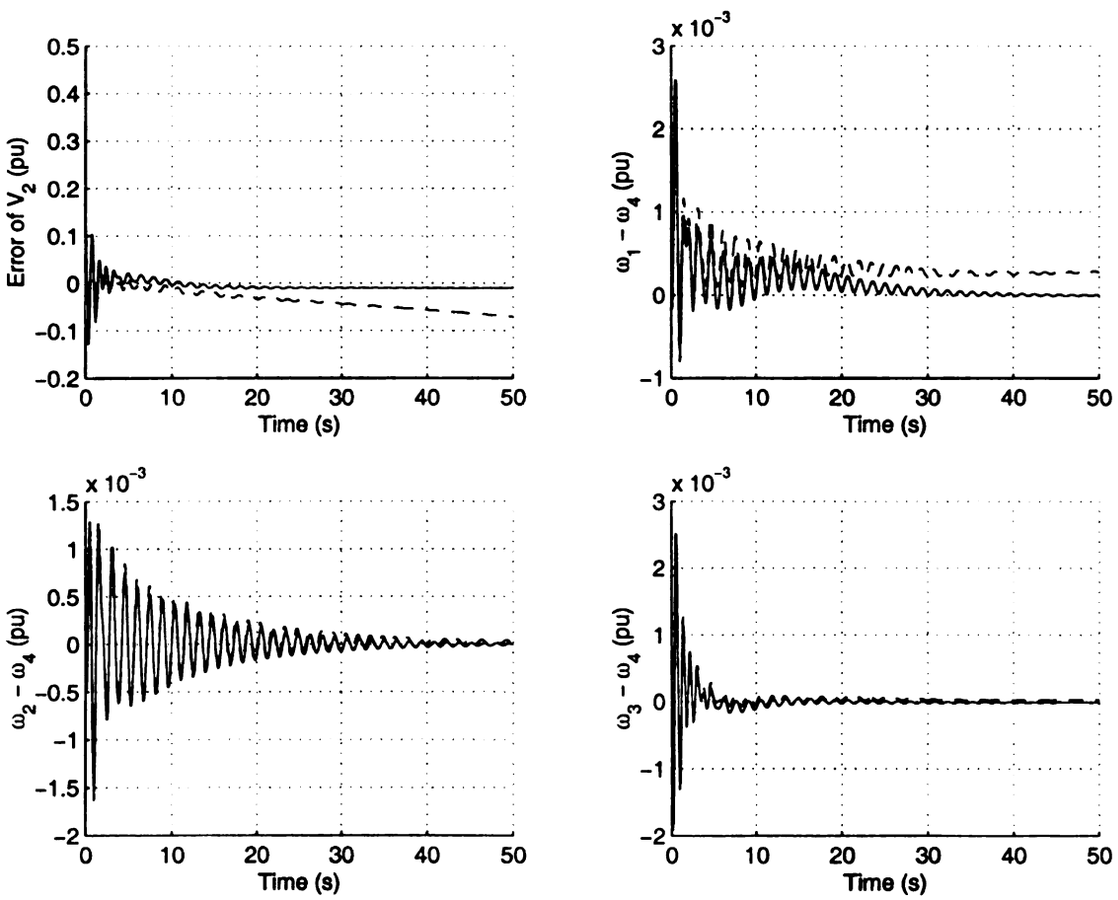

Figure 6.30: Open Loop System (- -) and Closed-loop System with Redesigned BMSVC (-) for Saddle-node Bifurcation

This saddle-node bifurcation is produced by increasing the active power transfer

	P_{REF_1}	P_{REF_2}	P_{REF_3}	P_{REF_4}	V_{REF_1}
P_{OUT_1}	9.4951e-01	5.5594e-04	5.5234e-04	5.2442e-04	4.0195e-04
P_{OUT_2}	4.9961e-04	9.5521e-01	4.8134e-04	4.4679e-04	2.3172e-04
P_{OUT_3}	2.6927e-04	2.7525e-04	9.6134e-01	2.9825e-04	3.0907e-04
P_{OUT_4}	2.6038e-04	2.5753e-04	3.2747e-04	9.6674e-01	3.3395e-04
V_{OUT_1}	2.9792e-04	1.3422e-04	1.2715e-04	1.3258e-04	6.8266e-01
V_{OUT_2}	1.9200e-03	2.0901e-03	1.0867e-03	1.1551e-03	1.7515e-03
V_{OUT_6}	1.8162e-02	1.6597e-02	6.8724e-03	7.1911e-03	4.8030e-03
V_{OUT_7}	2.0942e-02	1.9216e-02	8.2444e-03	8.6162e-03	5.1037e-03
V_{OUT_8}	4.3860e-03	2.4517e-03	3.5135e-03	3.5265e-03	2.9697e-01
V_{OUT_3}	1.7261e-04	2.0005e-04	9.2275e-04	3.2240e-04	3.2170e-05
V_{OUT_4}	7.8284e-05	9.1786e-05	1.0532e-04	1.6159e-04	7.7342e-06
V_{OUT_9}	7.7864e-04	1.1338e-03	3.7264e-03	2.4883e-03	7.2772e-04
$V_{OUT_{10}}$	6.7993e-04	1.0698e-03	3.9857e-03	2.5589e-03	8.2353e-04
$V_{OUT_{11}}$	8.9534e-03	6.9736e-03	4.8578e-03	4.9072e-03	1.1648e-02
V_{OUT_5}	4.8069e-03	4.6369e-03	2.3490e-03	1.9250e-03	8.7304e-04
$V_{OUT_{12}}$	1.3755e-03	1.6167e-03	5.1444e-03	2.7893e-03	4.7510e-04
$V_{OUT_{13}}$	8.6980e-04	1.1202e-03	4.6153e-03	2.8768e-03	6.3662e-04
ω_1	1.0848e-04	1.2260e-04	1.7871e-04	1.8365e-04	1.9851e-05
ω_2	1.0640e-04	1.2484e-04	1.7872e-04	1.8366e-04	1.9850e-05
ω_3	1.0640e-04	1.2261e-04	1.8142e-04	1.8366e-04	1.9846e-05
ω_4	1.0641e-04	1.2261e-04	1.7872e-04	1.8641e-04	1.9847e-05
	V_{REF_2}	V_{REF_3}	V_{REF_4}	V_{REF_5}	
P_{OUT_1}	1.6294e-03	3.5051e-04	1.1002e-03	8.5900e-04	
P_{OUT_2}	1.8606e-03	3.9824e-04	1.2264e-03	1.0184e-03	
P_{OUT_3}	1.0701e-03	7.6746e-04	2.1850e-03	5.5203e-04	
P_{OUT_4}	1.1796e-03	7.1422e-04	1.6296e-03	6.6689e-04	
V_{OUT_1}	1.9663e-04	2.1035e-05	2.0091e-05	6.3761e-05	
V_{OUT_2}	6.5066e-01	3.2534e-04	7.6201e-04	2.1938e-03	
V_{OUT_6}	9.5668e-02	1.0198e-03	3.0545e-03	4.3870e-02	
V_{OUT_7}	1.0493e-01	1.1941e-03	3.3355e-03	4.8702e-02	
V_{OUT_8}	5.7772e-03	2.0360e-04	2.7468e-03	4.6484e-03	
V_{OUT_3}	2.0582e-04	6.6569e-01	4.1963e-03	3.0678e-04	
V_{OUT_4}	1.1279e-04	1.7739e-03	5.2112e-01	1.2025e-03	
V_{OUT_9}	3.6600e-03	3.5884e-03	1.3636e-01	3.0985e-02	
$V_{OUT_{10}}$	4.1288e-03	4.5760e-03	1.6647e-01	3.8392e-02	
$V_{OUT_{11}}$	1.5461e-01	2.5591e-04	2.8482e-03	1.5521e-03	
V_{OUT_5}	6.9510e-03	2.5819e-03	2.2545e-02	8.6107e-01	
$V_{OUT_{12}}$	1.9868e-03	3.2124e-01	4.8511e-03	6.7457e-03	
$V_{OUT_{13}}$	2.6822e-03	8.4970e-03	2.0136e-01	9.3452e-03	
ω_1	1.0911e-04	1.4055e-05	4.1211e-05	1.4782e-05	
ω_2	1.0910e-04	1.4058e-05	4.1207e-05	1.4782e-05	
ω_3	1.0905e-04	1.4080e-05	4.1146e-05	1.4767e-05	
ω_4	1.0906e-04	1.4066e-05	4.1171e-05	1.4764e-05	

Table 6.15: *RGA* of System with Redesigned BMSVC for Saddle-node Bifurcation

between two areas. The load is modeled as constant power model. The saddle-node bifurcation subsystem can be found in Table 5.16. By increasing the active power transfer the saddle-node bifurcation develops. This corresponds to the voltage stability problem of the two area system. The time simulation result is shown in Figure 6.30. The closed-loop system with this redesigned controller is extremely robust. Increasing the structural parameter uncertainty by 50% does not cause voltage instability because the closed-loop system is still stable and effective voltage control can still be achieved. For the open loop system, the voltage stability problem starts developing even for very small increase in structural parameter. The voltage on generator bus 2 is unstable as shown in Figure 6.30. Furthermore, the frequency error no longer approaches zero. Figure 6.30 shows the robust control of voltage, frequency and power for this saddle-node BMSVC predicted by the *RGA* matrix. The excellent control of voltage by this saddle-node BMSVC is absolutely necessary to prevent voltage collapse and saddle-node bifurcation.

6.6 μ-synthesis Control Design for Multiple Bifurcations

6.6.1 Multiple Bifurcations

In this section a multiple bifurcation phenomena is studied. Usually multiple bifurcations are produced by more than one bifurcation parameter variation. More complex system behaviors are expected if more than one bifurcation develop simultaneously and the corresponding bifurcation subsystems overlap. It is much more difficult to stabilize the system under this situation.

A double-bifurcation is produced by increasing the active power load on generator

bus 2 and the susceptance at generator bus 2, respectively. It should be noted that a constant power load model is used here. It has been pointed out that a saddle-node bifurcation generally develops when a constant power load model is used. However, in this case the Hopf bifurcation develops first instead of saddle-node due to the interaction of the two bifurcation parameters. Two kinds of Hopf bifurcations, a local Hopf bifurcation (frequency of oscillation around 1 Hz) and an interarea Hopf bifurcation (frequency of oscillation less than 0.5 Hz) are observed in this study. The generator angle vector diagrams of the interarea and the local Hopf bifurcation are shown in Figure 6.31 and 6.32, respectively. It is expected that the dynamic behaviors of the system with multiple bifurcations are more complicated because of the interaction between the interarea and local oscillations.

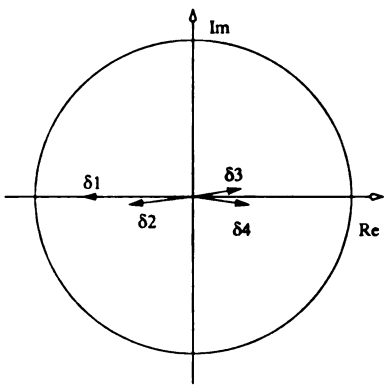

Figure 6.31: Generator Angle Vector Diagram of Interarea Hopf Bifurcation

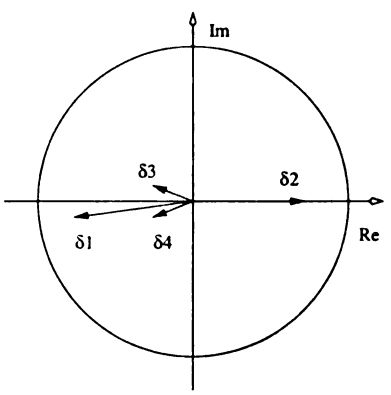

Figure 6.32: Generator Angle Vector Diagram of Local Hopf Bifurcation

Figure 6.31 verifies that an interarea Hopf bifurcation develops since the two generation areas (δ_1, δ_2) and (δ_3, δ_4) oscillate against each other. Figure 6.32 shows that the Hopf bifurcation is a local oscillation between generator 2 and the other generators in the system. It is also noted that the two bifurcation subsystems of the bifurcations overlap each other because the inertial dynamics of all four generator belong to the bifurcation subsystems for both bifurcations.

With the complexity and stress increased on current power systems, multiple bifurcations are more likely to develop. In WSCC system it has been verified that there could exist up to 6 interarea oscillations in the same time and these interarea oscillations turn out to be very difficult to control since they appear to be strongly coupled to each other. Typically a control that stabilizes one interarea oscillation destabilizes others [25]. It should be noted that it is not as easy to produce multiple bifurcation for this small two area system as in large power system.

As a very first but important step, a single robust controller is developed in this section in order to stabilize multiple bifurcations. In section 6.4 it has been shown that μ-synthesis based robust power system stabilizer (MPSS) is very effective to stabilize the system with a single bifurcation. In section 6.5 μ-synthesis based robust SVC (MSVC) was shown to be even more effective than MPSS for system with a single bifurcation in terms of the overall control performance. Now we are going to design MPSS and MSVC when multiple bifurcations develop.

6.6.2 μ-synthesis Power System Stabilizer for Multiple Bifurcations

As shown in section 6.6.1 multiple bifurcations develop in the different locations (generators) of the two area system. It is thus anticipated that more measurements or controls are either required or are able to improve the control of the system

experiencing multiple bifurcations. Therefore, three increasing more complex μ-synthesis robust power system stabilizer designs are considered in this section that have.

1. a single measurement and a single control on generator 2. Considering that the interarea oscillations are more difficult to control, generator 4 speed is taken as the measurement. The voltage excitation control set point on generator 2 is the single control. This is a typical local controller but is sited to affect the interarea oscillation between generator 1 and 2 and generator 3 and 4 and for the local oscillation between generator 2 and generators 1, 3, and 4.;

2. two measurements and a single control on generator 2. From the generator vector diagram a local oscillation develops for generator 2 in addition to the interarea oscillations. Thus, the measurements used by the controller should contain both generator 2 and generator 4 speed information. This controller is not local any more since a communication link will be needed for the measurement on generator 4 to wherever the controller is located on generator 2. The control is chosen to be on the excitation voltage set point on generator 2 since it should provide control over the interarea and local oscillation. The measurement on generator 2 and 4 should provide information on both areas containing generators 1 and 2 and the other area containing generators 3 and 4 as well as the local oscillation of generator 2 against generators 1, 3, and 4. This controller should perform better than the local controller since it has measurements that should capture both oscillations;

3. two measurements and two controls on generator 2 and 4. The measurements of the speed on generator 2 and 4 are used as in the case above. The control actions should be taken on the excitation system voltage set point on generator 2 as well as generator 4 due to the nature of the multiple bifurcations. This

is expected to achieve better control performance than either of the above two designs since one has both sufficient information to detect and estimate the states associated with both oscillations and since there is also sufficient control to independently control both oscillations.

The above three types of MPSS can be designed by slightly modifying the control configuration of MPSS shown in Figure 6.7. Note in the control configuration the only difference from Figure 6.7 is the number of inputs and/or outputs of MPSS (labeled as K in Figure 6.7) to be designed. The previously used performance index in equation (6.4.3) and the performance weighting matrix are still adopted here. Note here minimizing the frequency deviations between ω_4 and the rest of generator frequencies is still one of the control objectives for multiple bifurcations. The reason is that control objective is to keep the generators to be synchronized with one specific generator (generator 4 in this case) despite the fact there exists a Hopf bifurcation between two areas or the fact that there exists a local bifurcation between generator 2 and the rest of the system.

In order to improve the control performance the inverse of the electrical dynamics of the corresponding generators are included in the control design. Using the same procedures of μ-synthesis control design, the MPSS is obtained and the closed-loop system μ value with a single measurement and a single control MPSS (case 1) is shown in Figure 6.33. The order of the controller is again reduced using Hankel norm and the bifurcation subsystem information. In Figure 6.33, two local maximum points appear around 3 and 8 rad/sec that correspond to the frequencies of the interarea and the local oscillation. This suggests that it is difficult to control the oscillations at both of these frequencies. Another fact is that the peak μ value of the closed-loop system occurs at low frequencies and is great than one. This suggests the voltage control performance is very poor. However, we are not concerned because it occurs

at very low frequency and because the frequency range is below that of the local and interarea modes for which the control is being designed. This control would not provide effective voltage control where values of μ at low frequencies should be much smaller than 1.0 if effective steady state voltage regulation is to be achieved. The μ values of the closed-loop system with two measurements and a single control MPSS (case 2) and two measurements and two controls MPSS (case 3) are not shown here since they are similar to Figure 6.32.

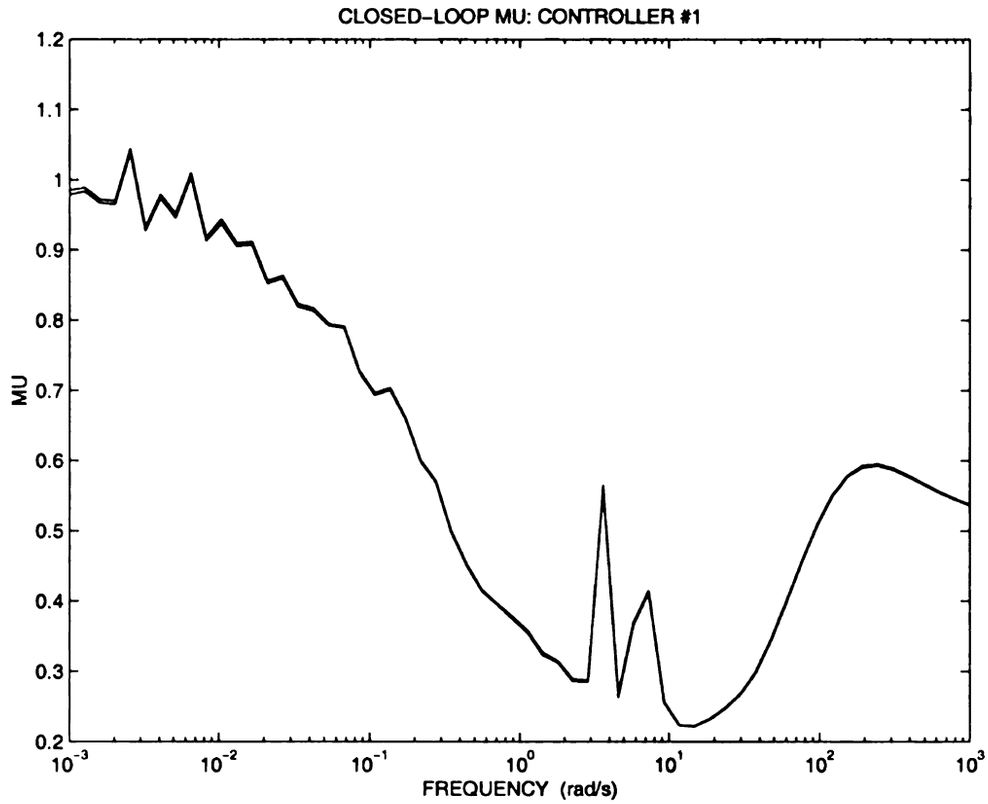

Figure 6.33: Closed-loop μ Value with MPSS of Measurement ω_4

The *RGA* matrix of the closed-loop system with a single measurement (ω_4) and a single MPSS control (on generator 2) at interarea bifurcation frequency is shown in Table 6.16. It can be seen that the decoupled control structure is lost since the *RGA* elements of the control pairs are no longer dominant in each column. There also exist the fighting of the controls since there are several large elements in each row. Some *RGA* element magnitudes are very large and this indicates that the system is

susceptible to disturbances.

40% increase in active power load at generator 2 and 40% increase in susceptance on the line connected to generator 2 were applied. The time response of the closed-loop system with one measurement ω_4 and one MPSS control on generator 2 is given in Figure 6.34. The results show that the control it is not able to achieve good control performance for multiple bifurcations as predicted by the *RGA* matrix results. It is able to stabilize the perturbed system because the oscillations decay with time. However, the transition time is too long. The oscillations are not completely damped out even after 100 seconds. Therefore, the single measurement and single control MPSS is not a good choice when multiple bifurcations develop.

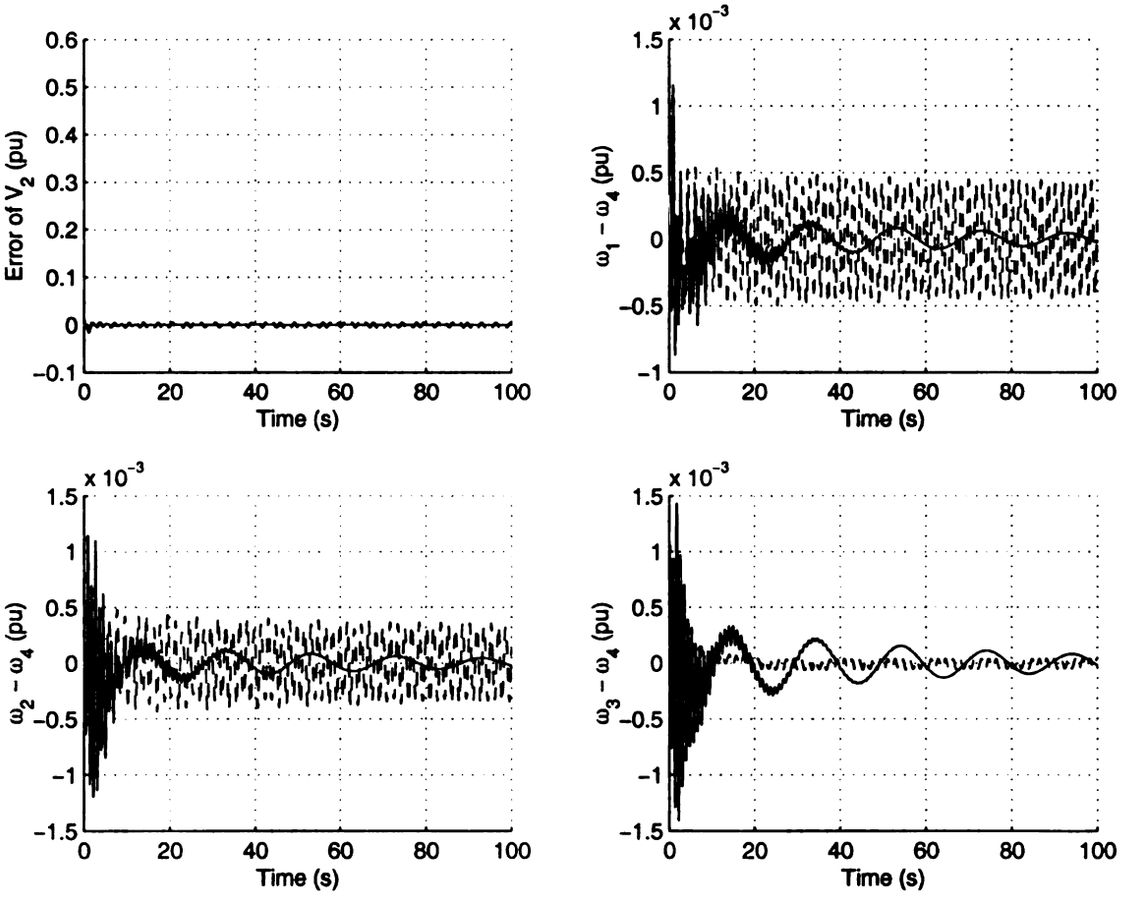

Figure 6.34: 1-input 1-output MPSS (-) and Open Loop System (- -) for Multiple **Bifur**cations

	P_{REF_1}	P_{REF_2}	P_{REF_3}	P_{REF_4}	V_{REF_1}
P_{OUT_1}	1.0122e+02	7.7417e+01	1.4069e+00	4.0385e+00	1.1382e+00
P_{OUT_2}	6.8894e+01	4.9237e+01	9.7148e-01	3.1248e+00	1.0421e+00
P_{OUT_3}	1.5951e-01	2.3214e-01	8.8184e-01	7.8843e-03	5.2292e-03
P_{OUT_4}	1.9023e+00	1.7131e+00	2.7918e-02	4.8244e-01	9.5431e-03
V_{OUT_1}	2.0157e+01	1.6243e+01	2.8022e-02	5.3375e-01	5.8769e-01
V_{OUT_2}	6.1827e+00	5.2396e+00	6.8879e-03	1.6577e-01	3.6293e-02
V_{OUT_6}	2.5761e+00	1.8632e+00	4.9640e-02	8.3955e-03	1.9753e-03
V_{OUT_7}	2.4247e+00	1.7240e+00	4.9847e-02	3.5348e-03	3.9117e-03
V_{OUT_8}	7.9380e-01	4.0372e-01	1.8069e-01	1.7356e-01	4.0504e-01
V_{OUT_3}	1.9219e-01	1.7425e-01	1.1171e-02	2.2591e-03	4.7358e-03
V_{OUT_4}	1.0245e+00	1.0220e+00	4.1898e-02	7.0703e-02	1.4374e-02
V_{OUT_9}	3.1391e+00	3.0838e+00	2.0065e-02	1.2363e-01	1.8189e-02
$V_{OUT_{10}}$	3.7294e+00	3.6685e+00	2.6478e-02	1.5029e-01	2.1395e-02
$V_{OUT_{11}}$	1.1459e+00	7.7086e-01	8.7235e-02	6.6317e-02	2.9367e-02
V_{OUT_5}	3.0486e+00	2.7741e+00	9.2961e-02	3.3908e-03	1.3800e-01
$V_{OUT_{12}}$	1.1779e+00	1.1412e+00	9.7038e-04	4.1072e-02	2.0435e-03
$V_{OUT_{13}}$	2.7102e+00	2.6491e+00	1.3803e-02	1.0261e-01	5.6723e-03
ω_1	8.4392e-02	7.8883e-01	8.2831e-03	2.7585e-04	6.4022e-03
ω_2	1.7039e+00	1.5550e+00	2.2214e-02	2.4419e-02	1.1580e-02
ω_3	9.5025e-03	8.6637e-03	1.2569e-04	1.3619e-04	6.4587e-05
ω_4	1.0443e-02	9.5145e-03	1.3619e-04	1.5152e-04	7.0922e-05
	V_{REF_2}	V_{REF_3}	V_{REF_4}	V_{REF_5}	
P_{OUT_1}	1.7724e+00	1.7033e+00	7.6152e+00	7.5556e+00	
P_{OUT_2}	1.7754e+00	1.3770e+00	6.0762e+00	6.1116e+00	
P_{OUT_3}	5.9911e-03	5.0456e-03	1.8626e-02	1.8311e-02	
P_{OUT_4}	5.0148e-02	4.0125e-02	1.7490e-01	1.7171e-01	
V_{OUT_1}	9.2104e-01	3.8115e-01	1.5771e+00	1.7565e+00	
V_{OUT_2}	1.0888e-01	1.2494e-01	5.3500e-01	4.7977e-01	
V_{OUT_6}	6.4485e-02	5.3806e-02	2.3378e-01	2.0168e-01	
V_{OUT_7}	6.9351e-02	5.2254e-02	2.3139e-01	1.6894e-01	
V_{OUT_8}	4.5625e-02	5.7518e-03	7.6582e-02	1.4394e-01	
V_{OUT_3}	2.5246e-03	5.8293e-01	5.2265e-02	1.2374e-02	
V_{OUT_4}	3.8744e-02	6.7523e-02	1.6034e-01	1.1333e-01	
V_{OUT_9}	8.1986e-02	2.6596e-02	1.5728e-02	5.2795e-02	
$V_{OUT_{10}}$	9.7288e-02	3.1289e-02	1.3964e-02	6.2457e-02	
$V_{OUT_{11}}$	1.0597e-01	1.7946e-02	3.4854e-02	1.3729e-01	
V_{OUT_5}	2.5432e-01	3.0112e-03	2.5218e-01	5.8909e-01	
$V_{OUT_{12}}$	3.5052e-02	1.5801e-01	5.5674e-02	4.5538e-02	
$V_{OUT_{13}}$	7.9505e-02	1.1093e-02	2.9465e-03	2.5219e-02	
ω_1	4.6667e-04	6.3671e-04	2.0155e-02	9.0420e-02	
ω_2	4.1323e-02	3.3449e-02	1.2524e-01	1.4934e-01	
ω_3	2.3049e-04	1.8659e-04	6.9849e-04	8.3293e-04	
ω_4	2.5327e-04	2.0494e-04	7.6743e-04	9.1565e-04	

Table 6.16: *RGA* of System with 1-input 1-output MPSS for Multiple Bifurcations

The *RGA* matrices of the closed-loop system with two measurements (ω_2 and ω_4) and a single MPSS control (on generator 2) and two measurements (ω_2 and ω_4) and two MPSS controls (on generator 2 and 4) are shown in Table 6.17 and 6.18, respectively. In Table 6.17 it is clear that adding one more measurement has significantly improved the *RGA* structure of the closed-loop system. The decoupled control structure of different loops is again obtained. There is almost no fighting of controls for output variables and the rejection of disturbance is greatly improved since only one *RGA* element is above 1. The *RGA* matrix of the closed-loop system with two measurements and two controls MPSS shown in Table 6.18 is somewhat better than that in Table 6.17 due to the fact that there is better control of power P_{OUT_i} by P_{REF_i}, $i = 1, \cdots, 4$; there is proper control of V_{OUT_i} by V_{REF_i}, $i = 1, \cdots, 5$; there is proper control of ω_i, $i = 1, \cdots, 4$, for two measurements and two controls compared to two measurements and one control. The input P_{REF_2} provides some control of ω_i, $i = 1, \cdots, 4$. There is no effective control of ω_i, $i = 1, \cdots, 4$, from the MPSS control devices except for the PSS on generator 3 for two measurements and one control case as well as the two measurements and two controls case based on the *RGA* matrix. This implies that there is not much difference between the control performances of the two controllers.

The time response of MPSS on generator 2 with two measurements ω_4 and ω_2 and single control is shown in Figure 6.35. It can be seen that the damping of the oscillations has been increased dramatically comparing with Figure 6.34 for the single measurement and single control MPSS. Both interarea and local oscillations can be damped out in 30 seconds.

MPSS with two control outputs and two measurements is also tested in this section and time simulation is shown in Figure 6.36. Better control performance has been achieved since the oscillations are damped more quickly and transient responses are more smooth compared with the time response shown in Figure 6.35.

	P_{REF_1}	P_{REF_2}	P_{REF_3}	P_{REF_4}	V_{REF_1}
P_{OUT_1}	9.7359e-01	5.6199e-02	4.8026e-02	2.3176e-02	1.5123e-01
P_{OUT_2}	5.2552e-02	7.7273e-01	5.1863e-02	2.2550e-02	1.1314e-02
P_{OUT_3}	5.8479e-02	6.2181e-02	5.9997e-01	2.6148e-02	1.2901e-02
P_{OUT_4}	6.3786e-02	6.8081e-02	3.0774e-02	6.6666e-01	1.2948e-02
V_{OUT_1}	1.6528e-01	5.8330e-02	5.4112e-02	4.2715e-02	1.2623e+00
V_{OUT_2}	7.4029e-02	2.9804e-02	1.2136e-02	7.9867e-03	3.9317e-01
V_{OUT_6}	3.0725e-02	1.0678e-02	1.5778e-02	2.3914e-02	1.6916e-01
V_{OUT_7}	3.4339e-02	1.1840e-02	1.7664e-02	2.6727e-02	1.8855e-01
V_{OUT_8}	9.6555e-02	3.7006e-02	4.6858e-02	3.7690e-02	6.5576e-01
V_{OUT_3}	9.2942e-03	8.5937e-03	2.0884e-02	1.5008e-02	1.0225e-03
V_{OUT_4}	3.2726e-03	4.2068e-03	1.0405e-02	1.8747e-02	2.9679e-03
V_{OUT_9}	5.1857e-03	5.0271e-03	4.7541e-03	2.8087e-03	4.2483e-04
$V_{OUT_{10}}$	6.3712e-03	6.1773e-03	5.8458e-03	3.4573e-03	5.2349e-04
$V_{OUT_{11}}$	3.5536e-02	9.4537e-03	2.1783e-02	1.8516e-02	1.6491e-01
V_{OUT_5}	1.0378e-02	6.3105e-03	3.1266e-03	8.1442e-03	1.1399e-02
$V_{OUT_{12}}$	2.4092e-03	1.7897e-03	2.3374e-02	3.7219e-03	1.4052e-03
$V_{OUT_{13}}$	4.2671e-03	4.6847e-03	6.3032e-03	7.9346e-03	1.6731e-03
ω_1	1.6625e-01	6.1531e-02	2.4667e-01	2.2844e-01	3.8735e-02
ω_2	5.1857e-02	8.6118e-02	2.0285e-01	1.8777e-01	1.1531e-02
ω_3	1.3360e-01	1.2928e-01	4.0654e-02	3.4599e-02	7.3105e-03
ω_4	1.3486e-01	1.3195e-01	2.8171e-02	2.9382e-02	7.2209e-03
	V_{REF_2}	V_{REF_3}	V_{REF_4}	V_{REF_5}	
P_{OUT_1}	8.1092e-02	5.4046e-02	6.1733e-02	1.4780e-03	
P_{OUT_2}	5.5731e-02	4.4569e-02	5.5353e-02	5.8270e-03	
P_{OUT_3}	1.9536e-02	5.2098e-02	7.1227e-02	2.1267e-03	
P_{OUT_4}	1.7288e-02	3.8769e-03	5.3451e-02	5.1631e-04	
V_{OUT_1}	4.8221e-01	1.7332e-02	1.9236e-02	2.0770e-02	
V_{OUT_2}	8.4407e-01	8.2994e-03	3.9945e-02	6.9531e-02	
V_{OUT_6}	2.6768e-01	6.9396e-03	3.1810e-02	6.7212e-02	
V_{OUT_7}	2.9837e-01	7.7670e-03	3.5457e-02	7.4914e-02	
V_{OUT_8}	2.4238e-01	1.5114e-02	1.5519e-02	2.0095e-02	
V_{OUT_3}	2.6116e-03	7.3176e-01	1.2776e-01	9.4361e-03	
V_{OUT_4}	7.7886e-03	1.3663e-01	7.1959e-01	6.4475e-02	
V_{OUT_9}	2.1818e-03	1.4632e-02	8.6831e-02	6.0052e-02	
$V_{OUT_{10}}$	2.6874e-03	1.8044e-02	1.0695e-01	7.3963e-02	
$V_{OUT_{11}}$	3.7426e-01	5.5512e-03	5.8901e-03	9.9738e-03	
V_{OUT_5}	6.4098e-02	2.4726e-03	1.2090e-02	8.9392e-01	
$V_{OUT_{12}}$	2.6276e-03	4.0298e-01	8.9607e-02	9.5917e-03	
$V_{OUT_{13}}$	2.2299e-03	2.3897e-02	1.7101e-01	5.6606e-03	
ω_1	1.7072e-02	1.2289e-01	8.0895e-03	7.7285e-05	
ω_2	1.2905e-02	1.0154e-01	6.7169e-03	3.8988e-04	
ω_3	3.5996e-03	5.0497e-02	2.6858e-03	8.6312e-04	
ω_4	3.2790e-03	1.2787e-02	3.0351e-03	4.4005e-04	

Table 6.17: *RGA* of System with 2-measurement and 1-control MPSS

	P_{REF_1}	P_{REF_2}	P_{REF_3}	P_{REF_4}	V_{REF_1}
P_{OUT_1}	9.5536e-01	2.9580e-04	3.0523e-04	2.9376e-04	8.8295e-05
P_{OUT_2}	1.6290e-04	9.6809e-01	1.6595e-04	1.5487e-04	9.4875e-05
P_{OUT_3}	6.4821e-05	8.8978e-05	9.7399e-01	1.0516e-04	1.3019e-04
P_{OUT_4}	8.2294e-05	1.0170e-04	1.4361e-04	9.7805e-01	1.6755e-04
V_{OUT_1}	9.5291e-04	4.3841e-04	4.6919e-04	4.8871e-04	6.9116e-01
V_{OUT_2}	7.3437e-02	7.3649e-02	6.2020e-02	6.5399e-02	3.3696e-02
V_{OUT_6}	3.8644e-02	3.6811e-02	2.1297e-02	2.2486e-02	8.2800e-04
V_{OUT_7}	4.0595e-02	3.8214e-02	2.0356e-02	2.1598e-02	1.2176e-03
V_{OUT_8}	1.3106e-02	8.1961e-03	1.2877e-02	1.3000e-02	2.7673e-01
V_{OUT_3}	1.1007e-05	1.4871e-05	4.1640e-04	1.7544e-05	6.8237e-06
V_{OUT_4}	7.9529e-03	1.0135e-02	2.2832e-02	1.8622e-02	6.1897e-04
V_{OUT_9}	5.0112e-04	9.4897e-04	2.3307e-03	2.2959e-03	2.0920e-03
$V_{OUT_{10}}$	3.7727e-04	8.6689e-04	2.5201e-03	2.3551e-03	2.4885e-03
$V_{OUT_{11}}$	2.6403e-02	2.1397e-02	2.3081e-02	2.3513e-02	3.5907e-03
V_{OUT_5}	5.6705e-03	5.3798e-03	3.5219e-03	2.9723e-03	4.4876e-04
$V_{OUT_{12}}$	5.4122e-04	7.0075e-04	2.3863e-04	1.0930e-03	4.6530e-04
$V_{OUT_{13}}$	1.0360e-03	1.5174e-03	3.7717e-03	3.4849e-03	2.0963e-03
ω_1	3.9820e-01	3.2348e-03	2.8446e-01	2.8745e-01	1.0150e-05
ω_2	7.3483e-02	3.4844e-02	3.3870e-01	9.4847e-02	1.1504e-05
ω_3	8.8324e-02	5.3229e-02	2.3234e-02	2.8047e-03	2.0354e-05
ω_4	1.9832e-01	4.0527e-02	6.8732e-03	6.8478e-02	1.1589e-05
	V_{REF_2}	V_{REF_3}	V_{REF_4}	V_{REF_5}	
P_{OUT_1}	1.1415e-03	1.6101e-04	5.8080e-03	4.6329e-04	
P_{OUT_2}	4.9660e-03	1.3374e-04	4.7089e-03	5.2067e-04	
P_{OUT_3}	4.0495e-03	2.7775e-04	6.0978e-03	1.9703e-04	
P_{OUT_4}	5.0191e-03	3.8185e-04	5.0700e-03	3.2917e-04	
V_{OUT_1}	2.8532e-03	7.6326e-05	2.8842e-03	1.0377e-04	
V_{OUT_2}	1.2005e+00	1.2142e-02	3.4278e-01	3.8861e-02	
V_{OUT_6}	1.3124e-02	3.4818e-03	4.7807e-02	5.0922e-02	
V_{OUT_7}	7.7458e-03	3.6515e-03	4.0431e-02	5.7500e-02	
V_{OUT_8}	2.2295e-02	3.8753e-04	1.8181e-02	7.9259e-03	
V_{OUT_3}	1.1822e-04	6.6185e-01	3.0956e-03	1.7826e-04	
V_{OUT_4}	4.4418e-02	2.7885e-02	4.5593e-01	1.8441e-02	
V_{OUT_9}	5.7970e-02	2.7675e-03	2.1831e-01	2.6592e-02	
$V_{OUT_{10}}$	6.9264e-02	3.5065e-03	2.6131e-01	3.3036e-02	
$V_{OUT_{11}}$	7.9719e-02	1.5329e-04	3.5339e-02	9.0486e-03	
V_{OUT_5}	9.5038e-03	3.1061e-03	4.3771e-02	8.7766e-01	
$V_{OUT_{12}}$	1.4649e-02	2.9498e-01	4.8235e-02	3.9680e-03	
$V_{OUT_{13}}$	6.4249e-02	5.8576e-03	2.8779e-01	5.5567e-03	
ω_1	9.2386e-04	5.8476e-01	2.8435e-03	4.0021e-06	
ω_2	1.8334e-03	8.8432e-03	1.9823e-03	5.0026e-06	
ω_3	7.3545e-04	2.3954e-01	5.3845e-03	7.2432e-06	
ω_4	8.8327e-04	1.9984e-02	8.4842e-03	5.3019e-06	

Table 6.18: *RGA* of System with 2-measurement 2-control MPSS

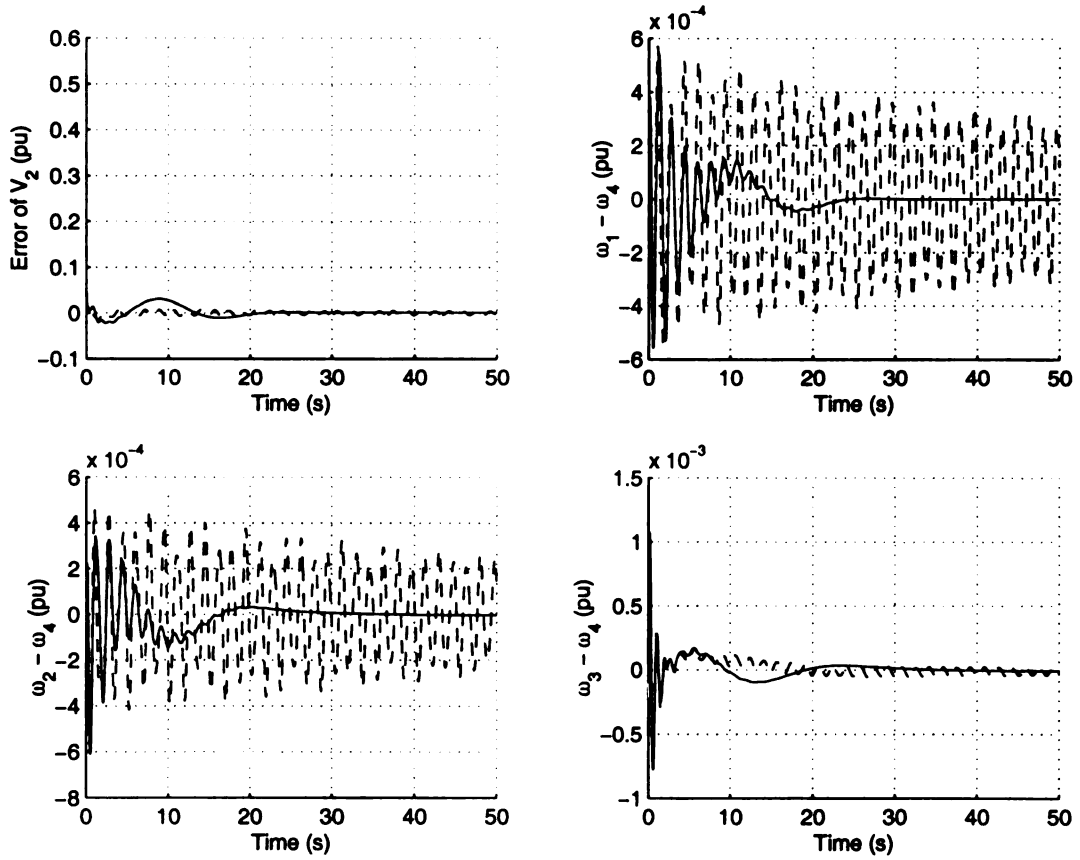

Figure 6.35: 2-measurement 1-control MPSS (-) and Open Loop System (- -) for Multiple Bifurcations

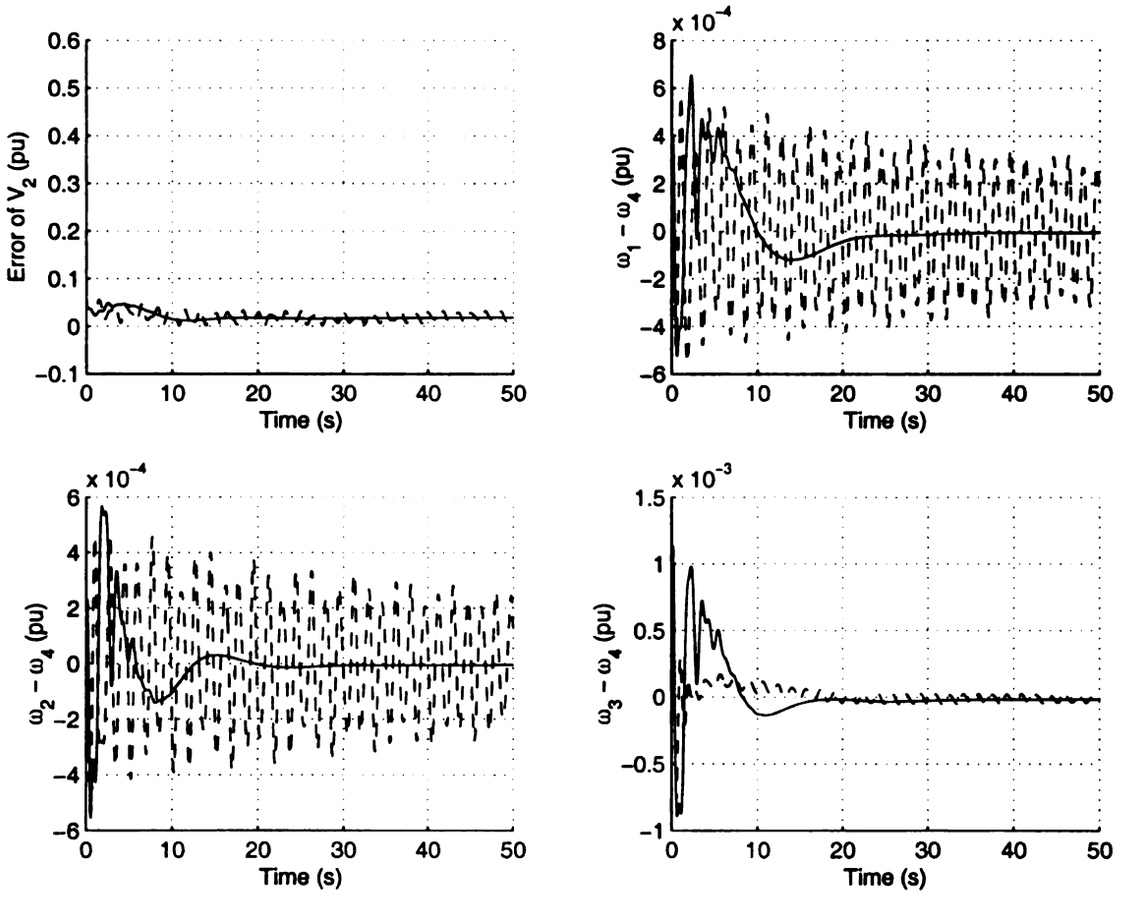

Figure 6.36: Reduced Order 2-input 2-output MPSS (-) and Open Loop System (- -) for Multiple Bifurcations

However, the voltage control of the system with two measurements and a single control MPSS and two measurements and two controls MPSS has degraded and this can be seen in Figure 6.35 and 6.36. This is predicted by *RGA* matrix analysis because the power system stabilizer increases the damping effect by directly changing the generator terminal voltage set point. Thus, the conflicted objectives of good voltage and damping control can not be obtained simultaneously by MPSS designs.

It should be noted that the system behavior is very different from that of the system with a single bifurcation. The swings of large magnitude and small magnitude appear alternatively. This is obviously the combination of interarea and local oscillations and verifies that multiple bifurcations occur due to two different bifurcation parameters, but are both nicely damped by multiple measurements and/or multiple controls MPSS. The MPSS designs are able to damp out the interarea oscillations but the voltage can not be controlled very well.

6.6.3 μ-synthesis SVC for Multiple Bifurcations

For multiple bifurcations the control performance of MPSS was shown to be less than perfect since the voltage control of network buses degraded. In section 6.5 it has been concluded that MSVC is more effective than MPSS for a single bifurcation due to the local property of power system stabilizer. In this section μ-synthesis based robust SVC controller will be developed for the purpose of improving the control of a system experiencing multiple bifurcations. Similar to MPSS designs considered in the previous section, the MSVC will be designed

1. with a single measurement (ω_4) and a single control (on generator 2);

2. with two measurements (ω_4 and ω_2) and a single control (on generator 2);

3. a mixed PSS/SVC design with two measurements (ω_4 and ω_2). The MPSS

is located on generator 2 where the local oscillation occurs, or is located on generator 4 where the interarea oscillation develops. This mixed MPSS/MSVC design will take the advantage of capability of voltage support of SVC and the damping of power system stabilizer.

Here the mixed MPSS/MSVC is designed instead of two measurements and two MSVC controls because (1) in previous section the two measurements and two controls MPSS did not have as large an improvement in control performance compared with two measurements and a single control MPSS as we expected; and (2) power system stabilizer is better in terms of damping increase and SVC is better in terms of voltage control of network buses.

The inverse dynamics are again included in the MSVC design and the same performance index and performance weighting matrix are again used. Only the closed-loop μ value with two measurements and a single control MSVC is shown here in Figure 6.37. The multiple bifurcations phenomena can be seen by inspecting the peak μ value around frequency 3 and 8 rad/sec in Figure 6.37. In order to obtain better damping of the local oscillation on generator 2, it is more reasonable to introduce another signal ω_2 as the measurement. The improved control at steady state using MSVC control is observed by the small value of μ at $\omega = 0$ compared to the MPSS design.

The *RGA* matrices of the closed-loop system with a single measurement (ω_4) and a single control MSVC, two measurements (ω_4 and ω_2) and a single control MSVC, and a mixed MPSS/MSVC design with MPSS on generator 4 and MPSS on generator 2 are shown in Table 6.19, 6.20, 6.21, and 6.22, respectively.

The *RGA* matrix of the MSVC with a single measurement (ω_4) and a single control at interarea oscillation frequency is shown in Table 6.19. The control pairs (P_{REF_i}, P_{OUT_i}), $i = 1, \cdots, 4$, and (V_{REF_i}, V_{OUT_i}), $i = 1, \cdots, 5$ are now dominant in

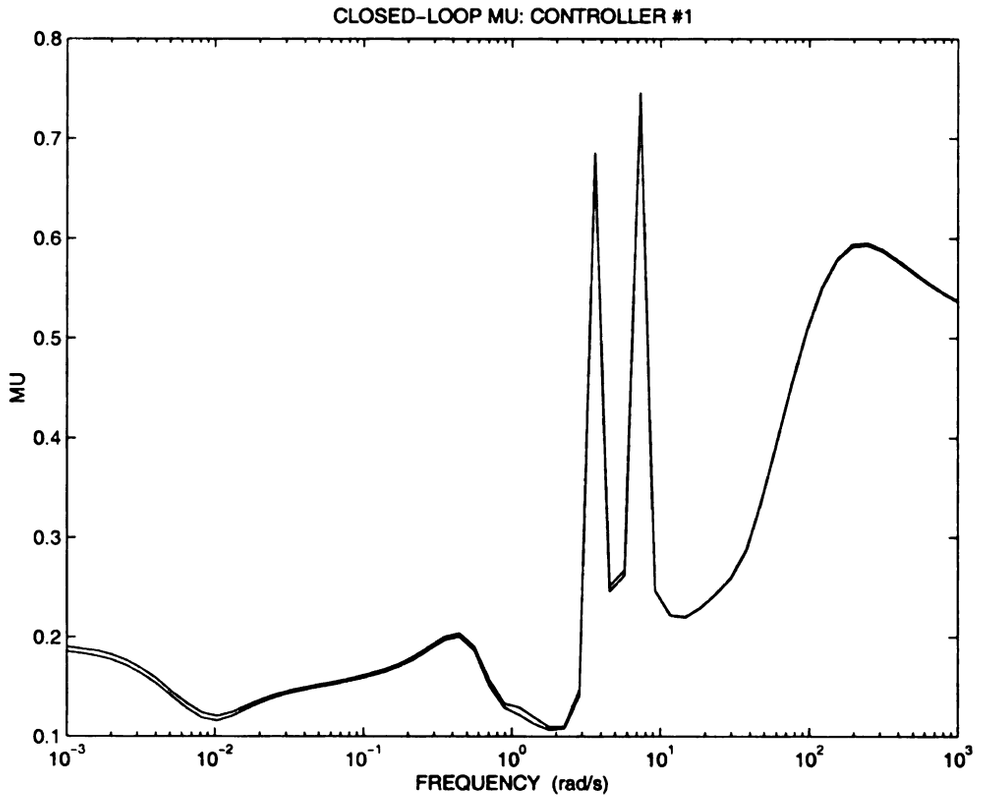

Figure 6.37: Closed-loop μ with MSVC of Measurement ω_4 and ω_2

each column and row of the RGA matrix and all of them are of magnitude close to one. This implies an almost decoupled control structure and that a better disturbance rejection capability is obtained with the MSVC than MPSS. Both the MSVC and the CPSS on generator 3 have significant control effects on the generator speeds ω_i, $i = 1, \cdots, 4$. This can be seen from the magnitudes of the element (V_{REF_3}, ω_i) and (V_{REF_5}, ω_i), $i = 1, \cdots, 4$ in Table 6.19. The control is not perfect since (a) there is one direction (V_{REF_i}, V_{OUT_1}) that is greater than 1.0; (b) there is one bus voltage with no effective control because all row elements are below 0.1; and (c) some fighting for voltage control at buses 6, 7, and 8 between generator 1 and 2 because V_{REF_1} and V_{REF_2} both have dominant similar sized elements in these rows.

The RGA matrix of the MSVC with ω_2 and ω_4 as measurements is shown in Table 6.20. The RGA matrix structure here is very similar to Table 6.19. Both of them have a good decoupled control structure and it is difficult to tell the improvement of the

control structure compared to Table 6.19 although there is very slight improvement in virtually every measure.

The *RGA* matrix of the closed-loop system of mixed MPSS/MSVC design with MPSS on generator 4 is shown in Table 6.21. In Table 6.21 we find that the control structure with this mixed design is not very well decoupled because there are output variables that are not controlled effectively by any control input. The elements of the control pairs (P_{REF_i}, P_{OUT_i}), $i = 1, \cdots, 4$, and (V_{REF_i}, V_{OUT_i}), $i = 1, \cdots, 5$, have very large values (above 1.0) and are dominant. This implies the power and voltage would be susceptible to the input disturbance. The network voltage control would not be perfect since there is a row associated with $V_{OUT_{10}}$ without perfect control. Moreover, the elements (V_{REF_4}, ω_i), $i = 1, \cdots, 4$, are not very large, which means the MPSS on generator 4 is not very effective in terms of frequency control but the existing PSS on generator 3 is made much more effective. The addition of MPSS control on generator 4 appears to have improved control of frequency and voltage at the control devices but the control of voltages in the network is not good.

Table 6.22 shows the *RGA* matrix of the closed-loop system of a mixed MPSS/MSVC design with MPSS on generator 2. By inspecting the *RGA* elements we found that the *RGA* matrix structure in Table 6.22 is similar to Table 6.19 and 6.20, but (1) the magnitudes of element (V_{REF_2}, ω_i), $i = 1, \cdots, 4$, is much larger than (V_{REF_4}, ω_i) was in Table 6.21, which means that the MPSS on generator 2 is more effective in frequency control than generator 4 was; (2) in each column the magnitudes of the elements are pretty small except the control pairs (P_{REF_i}, P_{OUT_i}), $i = 1, \cdots, 4$, and (V_{REF_i}, V_{OUT_i}), $i = 1, \cdots, 5$. These elements are much closer to 1.0 compared to the *RGA* matrix in Table 6.19 and 6.20 suggests these controls are quite effective and yet the decoupling is achieved. None of the elements is above 1.0 and susceptible to disturbance as they are when the MPSS is on generator 4. The control of network bus voltage on buses 6, 7, and 8 is now by either generator 1 or 2. This was a

problem in Table 6.19 - 6.21. The effectiveness of the control of network bus voltages by using MPSS on generator 2 rather than on generator 4 is reduced since the RGA matrix elements of (V_{REF_i}, V_{OUT_i}), $i = 1, \cdots, 5$, are reduced. This is the only advantage observed in placing the MPSS on generator 2 rather than generator 4. The siting of MPSS control where the the local oscillation occurs is thus very important to achieve excellent control of local Hopf bifurcation when control is required for multiple bifurcations. The siting of the SVC at midpoint of the line connecting the two areas is seen as important in control of the interarea oscillation. Tables 6.19, 6.20, 6.21, and 6.22 all suggest a mixed MPSS/MSVC combination provides better decoupled control structure than that of solely MPSS designs in the previous section.

The time simulation of the open loop system and closed-loop system with MSVC with one measurement ω_4 and one control is shown in Figure 6.38. By applying 50% more active power load on generator 2 and increasing susceptance by 50% on generator 2 than the bifurcation value on generator bus 2 the open loop system with conventional controls is almost unstable and neither voltage or interarea or local oscillation is controlled effectively. On the other hand, both interarea and local oscillations can be eliminated effectively by this MSVC and the voltage is maintained.

It is expected that MSVC with more measurements should improve the control performance as predicted by the RGA. This is verified in Figure 6.39, where the MSVC with two measurements ω_4 and ω_2 is applied to the system. The control performance improvement can be seen in terms of a smaller oscillation magnitude and shorter transition period compared to Figure 6.38.

Figure 6.40 shows the time response of the closed-loop system with mixed MSVC/MPSS control with the MPSS located on generator 2. It can be seen that this design gives the best overall performance. The control performance of another mixed

	P_{REF_1}	P_{REF_2}	P_{REF_3}	P_{REF_4}	V_{REF_1}
P_{OUT_1}	9.7321e-01	4.3081e-02	3.6349e-02	2.0119e-02	1.4837e-01
P_{OUT_2}	4.3626e-02	7.6444e-01	4.3106e-02	1.5164e-02	6.1116e-03
P_{OUT_3}	5.6094e-02	5.9843e-02	6.0745e-01	2.1863e-02	1.3492e-02
P_{OUT_4}	6.1510e-02	6.5741e-02	3.4017e-02	6.6398e-01	1.2741e-02
V_{OUT_1}	1.6531e-01	5.4431e-02	4.9823e-02	3.9221e-02	1.2697e+00
V_{OUT_2}	7.8401e-02	2.9688e-02	1.5457e-02	8.9529e-03	3.9830e-01
V_{OUT_6}	3.4212e-02	8.3143e-03	1.9397e-02	2.7538e-02	1.6960e-01
V_{OUT_7}	3.8252e-02	9.1905e-03	2.1720e-02	3.0789e-02	1.8904e-01
V_{OUT_8}	9.6585e-02	3.5447e-02	4.5342e-02	3.6525e-02	6.5657e-01
V_{OUT_3}	1.1268e-02	1.0483e-02	2.1424e-02	1.2157e-02	8.7448e-04
V_{OUT_4}	6.0191e-03	6.2529e-03	4.9937e-03	8.0837e-03	2.8738e-03
V_{OUT_9}	6.6646e-03	6.1867e-03	4.3495e-03	2.0145e-03	5.4024e-04
$V_{OUT_{10}}$	8.1889e-03	7.6025e-03	5.3478e-03	2.4795e-03	6.6546e-04
$V_{OUT_{11}}$	3.8059e-02	7.8111e-03	2.4525e-02	2.1121e-02	1.6539e-01
V_{OUT_5}	1.0721e-02	7.2567e-03	3.2615e-03	1.1360e-02	1.2041e-02
$V_{OUT_{12}}$	2.1302e-03	1.6215e-03	1.9578e-02	2.4978e-03	1.4312e-03
$V_{OUT_{13}}$	6.2599e-03	6.2825e-03	5.8627e-03	3.3010e-03	1.8159e-03
ω_1	1.8451e-01	6.3619e-02	2.5942e-01	2.3893e-01	3.3804e-04
ω_2	5.8547e-02	9.3595e-02	2.0958e-01	1.9275e-01	7.3582e-05
ω_3	1.4273e-01	1.3770e-01	5.3946e-02	2.7289e-02	1.6133e-05
ω_4	1.4260e-01	1.3874e-01	2.8589e-02	3.7016e-02	1.1134e-05
	V_{REF_2}	V_{REF_3}	V_{REF_4}	V_{REF_5}	
P_{OUT_1}	8.0794e-02	5.7576e-02	6.5609e-02	1.2400e-03	
P_{OUT_2}	5.8703e-02	4.5615e-02	6.3953e-02	6.3581e-03	
P_{OUT_3}	1.9200e-02	5.1659e-02	6.5038e-02	2.0293e-03	
P_{OUT_4}	1.7435e-02	4.2903e-03	4.8544e-02	3.4982e-04	
V_{OUT_1}	4.7743e-01	1.5415e-02	2.0968e-02	1.9523e-02	
V_{OUT_2}	8.4100e-01	9.3294e-03	4.4336e-02	6.9356e-02	
V_{OUT_6}	2.6757e-01	8.2231e-03	3.5138e-02	6.6012e-02	
V_{OUT_7}	2.9824e-01	9.2101e-03	3.9163e-02	7.3574e-02	
V_{OUT_8}	2.3739e-01	1.4335e-02	1.6543e-02	1.9400e-02	
V_{OUT_3}	2.4266e-03	7.2286e-01	1.1960e-01	9.7292e-03	
V_{OUT_4}	6.7612e-03	1.2083e-01	6.8357e-01	6.2390e-02	
V_{OUT_9}	2.4687e-03	1.1579e-02	8.2443e-02	6.0432e-02	
$V_{OUT_{10}}$	3.0401e-03	1.4286e-02	1.0155e-01	7.4423e-02	
$V_{OUT_{11}}$	3.7316e-01	6.7750e-03	4.3877e-03	1.0546e-02	
V_{OUT_5}	7.0528e-02	4.0776e-03	2.8210e-02	8.9013e-01	
$V_{OUT_{12}}$	2.4622e-03	3.9312e-01	8.3566e-02	9.6500e-03	
$V_{OUT_{13}}$	2.4100e-03	1.9596e-02	1.6254e-01	4.5783e-03	
ω_1	2.4429e-04	1.3288e-01	3.9669e-05	5.9672e-03	
ω_2	5.8607e-05	1.0867e-01	3.3588e-05	3.5857e-02	
ω_3	1.1324e-05	5.7243e-02	1.1863e-04	4.9248e-02	
ω_4	1.9590e-05	1.6927e-02	1.4820e-04	1.2694e-01	

Table 6.19: *RGA* of System with 1-measurement 1-control MSVC

	P_{REF_1}	P_{REF_2}	P_{REF_3}	P_{REF_4}	V_{REF_1}
P_{OUT_1}	9.6467e-01	4.0929e-02	3.6307e-02	2.0102e-02	1.4751e-01
P_{OUT_2}	3.0060e-02	7.1718e-01	4.2709e-02	1.5009e-02	5.3030e-03
P_{OUT_3}	7.6624e-02	8.1734e-02	6.1804e-01	1.9505e-02	1.8807e-02
P_{OUT_4}	7.4194e-02	7.9194e-02	3.2949e-02	6.6921e-01	1.5769e-02
V_{OUT_1}	2.5540e-01	1.0944e-01	5.3194e-02	4.2356e-02	1.3834e+00
V_{OUT_2}	1.3006e-01	5.6160e-02	1.6586e-02	9.7291e-03	4.6647e-01
V_{OUT_6}	6.1360e-02	1.8231e-02	2.1209e-02	3.0610e-02	2.0631e-01
V_{OUT_7}	6.8606e-02	2.0152e-02	2.3748e-02	3.4223e-02	2.2996e-01
V_{OUT_8}	1.5073e-01	7.1464e-02	4.8476e-02	3.9510e-02	7.3308e-01
V_{OUT_3}	1.7581e-02	1.6424e-02	2.6442e-02	1.0251e-02	1.3687e-03
V_{OUT_4}	1.5481e-02	1.6444e-02	4.7963e-03	9.1936e-03	6.5398e-03
V_{OUT_9}	2.2588e-02	2.1999e-02	4.9504e-03	8.9026e-03	1.3818e-03
$V_{OUT_{10}}$	2.7754e-02	2.7033e-02	6.0866e-03	1.0957e-02	1.7021e-03
$V_{OUT_{11}}$	6.3709e-02	1.5977e-02	2.6475e-02	2.3118e-02	1.9453e-01
V_{OUT_5}	8.4330e-02	7.3518e-02	5.9026e-03	2.2434e-02	3.9102e-02
$V_{OUT_{12}}$	3.5412e-03	2.7139e-03	2.1111e-02	1.1272e-03	2.3797e-03
$V_{OUT_{13}}$	1.5582e-02	1.5933e-02	5.6149e-03	4.4524e-03	4.0781e-03
ω_1	1.8120e-01	6.0813e-02	2.5912e-01	2.3861e-01	3.3639e-04
ω_2	4.2444e-02	7.3426e-02	2.0764e-01	1.9074e-01	6.4162e-05
ω_3	1.9758e-01	1.9087e-01	5.9665e-02	2.4663e-02	2.2103e-05
ω_4	1.7284e-01	1.6805e-01	2.7808e-02	3.9374e-02	1.3570e-05
	V_{REF_2}	V_{REF_3}	V_{REF_4}	V_{REF_5}	
P_{OUT_1}	8.0363e-02	5.7326e-02	6.5442e-02	6.4786e-03	
P_{OUT_2}	5.6285e-02	4.4166e-02	6.2738e-02	3.7847e-02	
P_{OUT_3}	2.6250e-02	5.9130e-02	6.1417e-02	2.9645e-02	
P_{OUT_4}	2.1377e-02	4.0154e-03	5.0164e-02	2.0592e-02	
V_{OUT_1}	5.1687e-01	1.8677e-02	2.4217e-02	6.4425e-02	
V_{OUT_2}	8.7987e-01	1.1449e-02	5.1791e-02	6.6137e-02	
V_{OUT_6}	2.9867e-01	1.0590e-02	4.2825e-02	5.2358e-02	
V_{OUT_7}	3.3291e-01	1.1861e-02	4.7731e-02	5.8183e-02	
V_{OUT_8}	2.5713e-01	1.7433e-02	1.9165e-02	6.0762e-02	
V_{OUT_3}	3.6686e-03	7.1692e-01	1.1078e-01	7.2748e-03	
V_{OUT_4}	1.6050e-02	1.0007e-01	6.5359e-01	4.1655e-02	
V_{OUT_9}	6.0199e-03	8.4967e-03	7.1423e-02	1.0662e-01	
$V_{OUT_{10}}$	7.4131e-03	1.0483e-02	8.7973e-02	1.3120e-01	
$V_{OUT_{11}}$	4.0584e-01	8.4428e-03	5.1954e-03	2.7552e-02	
V_{OUT_5}	1.6986e-01	1.9355e-02	1.1174e-01	1.0373e+00	
$V_{OUT_{12}}$	4.2849e-03	3.7269e-01	7.7256e-02	4.1209e-03	
$V_{OUT_{13}}$	5.7226e-03	1.6237e-02	1.4870e-01	2.7910e-02	
ω_1	2.4315e-04	1.3239e-01	3.9572e-05	6.1627e-03	
ω_2	5.6259e-05	1.0536e-01	3.2980e-05	4.4210e-02	
ω_3	1.5449e-05	6.5488e-02	1.1109e-04	1.0218e-01	
ω_4	2.3906e-05	1.5824e-02	1.5336e-04	5.3677e-02	

Table 6.20: *RGA* of System with 2-measurement 1-control MSVC

	P_{REF_1}	P_{REF_2}	P_{REF_3}	P_{REF_4}	V_{REF_1}
P_{OUT_1}	1.0856e+00	5.4835e-02	3.4428e-02	1.1685e-02	1.0919e-01
P_{OUT_2}	8.6946e-02	8.3883e-01	2.1900e-02	1.1447e-02	3.5391e-02
P_{OUT_3}	5.0394e-02	1.0044e-02	1.2004e+00	1.0377e-01	2.7209e-01
P_{OUT_4}	6.4662e-02	1.7287e-02	1.8767e-01	1.2679e+00	2.8055e-01
V_{OUT_1}	3.1366e-01	1.0643e-01	3.8506e-02	2.7754e-02	1.7893e+00
V_{OUT_2}	6.8800e-02	1.4953e-01	1.9323e-02	9.4495e-03	6.8600e-01
V_{OUT_6}	8.4603e-02	9.4375e-02	1.0378e-02	2.1410e-02	1.8197e-01
V_{OUT_7}	9.2777e-02	1.0347e-01	1.1398e-02	2.3448e-02	1.9948e-01
V_{OUT_8}	2.4578e-01	4.2308e-02	3.1247e-02	2.7671e-02	1.0369e+00
V_{OUT_3}	3.7062e-02	1.9923e-02	1.7218e-01	7.3762e-02	1.3445e-02
V_{OUT_4}	3.1175e-03	4.4102e-04	1.4325e-02	3.9141e-02	2.6737e-02
V_{OUT_9}	1.1691e-02	1.4206e-03	1.3888e-02	1.6404e-02	1.5116e-02
$V_{OUT_{10}}$	1.4283e-02	1.7345e-03	1.6969e-02	2.0044e-02	1.8472e-02
$V_{OUT_{11}}$	6.5577e-02	9.6979e-02	9.8768e-03	2.0024e-02	1.8493e-01
V_{OUT_5}	7.6537e-02	1.2126e-02	3.2038e-02	5.9559e-03	6.9418e-03
$V_{OUT_{12}}$	1.3745e-02	9.5586e-03	9.5894e-02	1.5017e-02	2.6726e-02
$V_{OUT_{13}}$	5.3849e-03	3.8832e-04	1.7236e-02	2.7859e-02	2.5522e-02
ω_1	2.5828e-01	1.2377e-01	2.8917e-01	2.5629e-01	5.4536e-04
ω_2	1.0510e-01	1.1088e-01	2.1210e-01	1.8836e-01	1.9890e-04
ω_3	4.5194e-01	2.8412e-01	2.8937e-01	1.9329e-01	3.7330e-05
ω_4	4.6079e-01	2.9039e-01	2.2396e-01	2.5230e-01	1.1022e-04
	V_{REF_2}	V_{REF_3}	V_{REF_4}	V_{REF_5}	
P_{OUT_1}	2.7563e-01	5.0388e-02	7.6052e-02	7.6918e-02	
P_{OUT_2}	1.2592e-01	4.2909e-02	6.5416e-02	5.4705e-02	
P_{OUT_3}	8.2804e-02	2.0195e-01	1.5931e-01	9.0510e-02	
P_{OUT_4}	8.6624e-02	4.5700e-02	1.4413e-01	8.2573e-02	
V_{OUT_1}	8.1205e-01	1.6265e-02	2.6700e-02	2.6566e-02	
V_{OUT_2}	1.4471e+00	2.2306e-02	4.3618e-02	1.4372e-01	
V_{OUT_6}	3.6637e-01	2.6318e-02	9.9464e-02	5.1211e-02	
V_{OUT_7}	4.0163e-01	2.8838e-02	1.0904e-01	5.6139e-02	
V_{OUT_8}	4.2956e-01	2.2539e-02	6.2521e-03	3.9606e-02	
V_{OUT_3}	2.8470e-02	8.1889e-01	1.8072e-01	3.8102e-02	
V_{OUT_4}	2.9766e-02	1.2639e-01	7.2532e-01	7.4724e-02	
V_{OUT_9}	2.8830e-02	8.8894e-03	7.8099e-02	4.3529e-02	
$V_{OUT_{10}}$	3.5229e-02	1.0864e-02	9.5434e-02	5.3191e-02	
$V_{OUT_{11}}$	5.5840e-01	2.6327e-02	3.0992e-02	4.8448e-02	
V_{OUT_5}	2.4356e-01	1.4908e-02	1.0488e-01	9.4740e-01	
$V_{OUT_{12}}$	1.2762e-02	4.5126e-01	9.8712e-02	2.7639e-02	
$V_{OUT_{13}}$	9.6382e-03	2.0661e-02	1.8031e-01	1.7661e-02	
ω_1	4.5562e-04	1.6542e-01	1.1802e-03	1.7301e-02	
ω_2	4.0150e-04	1.2245e-01	4.6397e-04	1.2790e-02	
ω_3	1.2609e-04	1.8281e-01	3.0707e-03	3.7041e-02	
ω_4	9.0633e-05	1.2573e-01	6.0688e-03	3.4992e-02	

Table 6.21: *RGA* of System with Mixed MPSS/MSVC (MPSS on Generator 4)

	P_{REF_1}	P_{REF_2}	P_{REF_3}	P_{REF_4}	V_{REF_1}
P_{OUT_1}	9.5320e-01	2.7916e-04	2.8469e-04	2.7419e-04	6.4741e-03
P_{OUT_2}	2.7358e-04	9.6436e-01	2.5233e-03	2.3564e-03	1.6662e-02
P_{OUT_3}	1.2672e-03	1.3496e-03	9.7100e-01	1.5278e-03	1.9178e-04
P_{OUT_4}	1.6025e-03	1.5616e-03	2.0673e-04	9.7422e-01	2.5043e-04
V_{OUT_1}	6.9468e-03	2.2593e-03	2.1938e-04	2.2824e-04	6.9204e-01
V_{OUT_2}	1.6028e-03	1.5935e-03	7.1980e-04	7.5601e-04	2.0985e-03
V_{OUT_6}	1.6421e-02	1.3790e-02	5.1296e-03	5.3841e-03	2.0549e-03
V_{OUT_7}	1.7142e-02	1.4183e-02	4.8043e-03	5.0664e-03	3.0094e-03
V_{OUT_8}	6.6457e-03	3.2586e-03	4.1968e-03	4.2287e-03	3.0424e-01
V_{OUT_3}	1.2754e-05	1.7284e-05	4.1071e-04	2.1472e-05	7.4215e-06
V_{OUT_4}	1.1892e-02	1.4846e-02	3.3341e-02	2.7305e-02	9.0987e-04
V_{OUT_9}	5.0936e-04	1.2250e-03	3.2339e-03	3.0061e-03	2.5646e-03
$V_{OUT_{10}}$	3.1219e-04	1.1111e-03	3.4999e-03	3.0884e-03	3.0569e-03
$V_{OUT_{11}}$	9.2133e-03	6.1403e-03	4.4197e-03	4.4829e-03	8.7760e-03
V_{OUT_5}	1.0275e-02	1.0214e-02	9.3012e-03	8.1377e-03	5.4143e-04
$V_{OUT_{12}}$	6.9473e-04	9.5533e-04	8.6250e-04	1.5442e-03	6.0379e-04
$V_{OUT_{13}}$	1.1914e-03	2.0758e-03	5.7457e-03	4.9790e-03	2.8108e-03
ω_1	4.6923e-02	3.3523e-01	8.7878e-01	6.1273e-01	1.3696e-05
ω_2	4.3417e-01	1.9562e-01	2.0083e-01	1.5415e-02	6.4009e-05
ω_3	4.1803e-02	5.2420e-01	9.3404e-02	5.0013e-02	1.4940e-05
ω_4	4.6915e-01	2.9107e-02	4.8750e-01	9.1182e-01	3.5038e-05
	V_{REF_2}	V_{REF_3}	V_{REF_4}	V_{REF_5}	
P_{OUT_1}	7.3777e-05	1.4996e-04	5.3672e-03	1.1587e-03	
P_{OUT_2}	6.1158e-04	1.9824e-04	6.9388e-03	1.8725e-03	
P_{OUT_3}	2.9210e-03	3.7753e-02	8.0245e-03	1.1603e-03	
P_{OUT_4}	3.7926e-04	4.6887e-03	7.7222e-03	1.9690e-03	
V_{OUT_1}	8.6049e-03	3.7200e-05	1.3938e-03	2.9569e-04	
V_{OUT_2}	6.0130e-01	1.5779e-04	4.3867e-03	1.6252e-04	
V_{OUT_6}	1.2132e-01	9.5874e-03	1.2903e-02	2.6145e-02	
V_{OUT_7}	1.3797e-01	9.8842e-03	1.0717e-02	3.2098e-02	
V_{OUT_8}	1.0193e-02	1.3441e-03	6.2177e-03	6.4745e-03	
V_{OUT_3}	1.9669e-05	6.6182e-01	3.0563e-03	1.0067e-04	
V_{OUT_4}	5.0625e-03	4.1611e-02	3.4816e-01	3.4871e-02	
V_{OUT_9}	6.5370e-03	2.5325e-03	1.9832e-01	2.2382e-03	
$V_{OUT_{10}}$	7.8686e-03	3.2014e-03	2.3684e-01	1.1219e-03	
$V_{OUT_{11}}$	1.7208e-01	3.2772e-05	7.4329e-03	8.6743e-03	
V_{OUT_5}	5.0683e-03	5.3734e-03	7.5605e-02	9.4573e-01	
$V_{OUT_{12}}$	9.4678e-04	2.9162e-01	4.3752e-02	8.2094e-03	
$V_{OUT_{13}}$	5.0172e-03	5.0638e-03	2.4687e-01	1.8175e-02	
ω_1	2.2783e-03	6.0366e-02	6.3071e-05	3.2206e-02	
ω_2	4.0278e-02	1.6963e-01	8.2609e-04	4.3102e-02	
ω_3	2.3281e-02	5.3841e-03	3.7002e-04	3.8801e-03	
ω_4	6.8920e-02	7.4054e-03	9.2572e-05	3.5598e-02	

Table 6.22: *RGA* of System with Mixed MPSS/MSVC (MPSS on Generator 2)

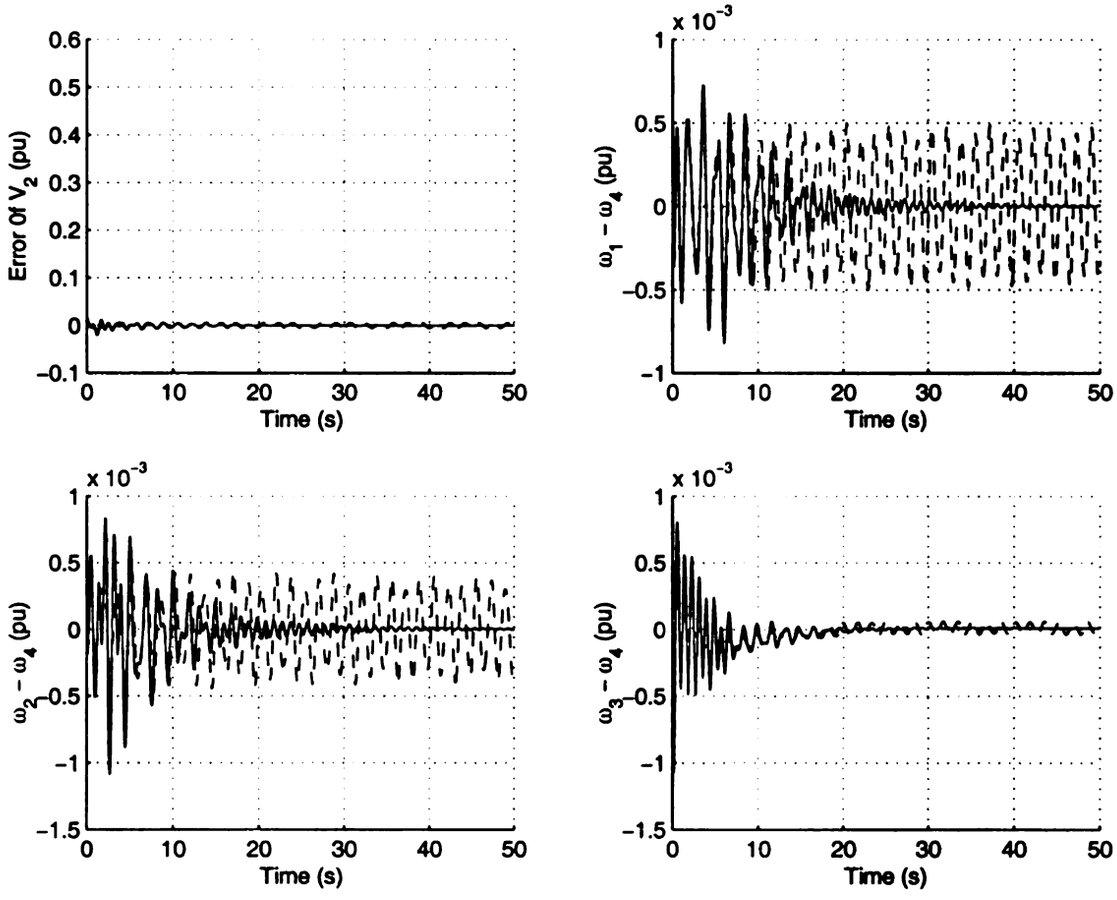

Figure 6.38: MSVC with Measurement ω_4 (-) and Open Loop System (- -)

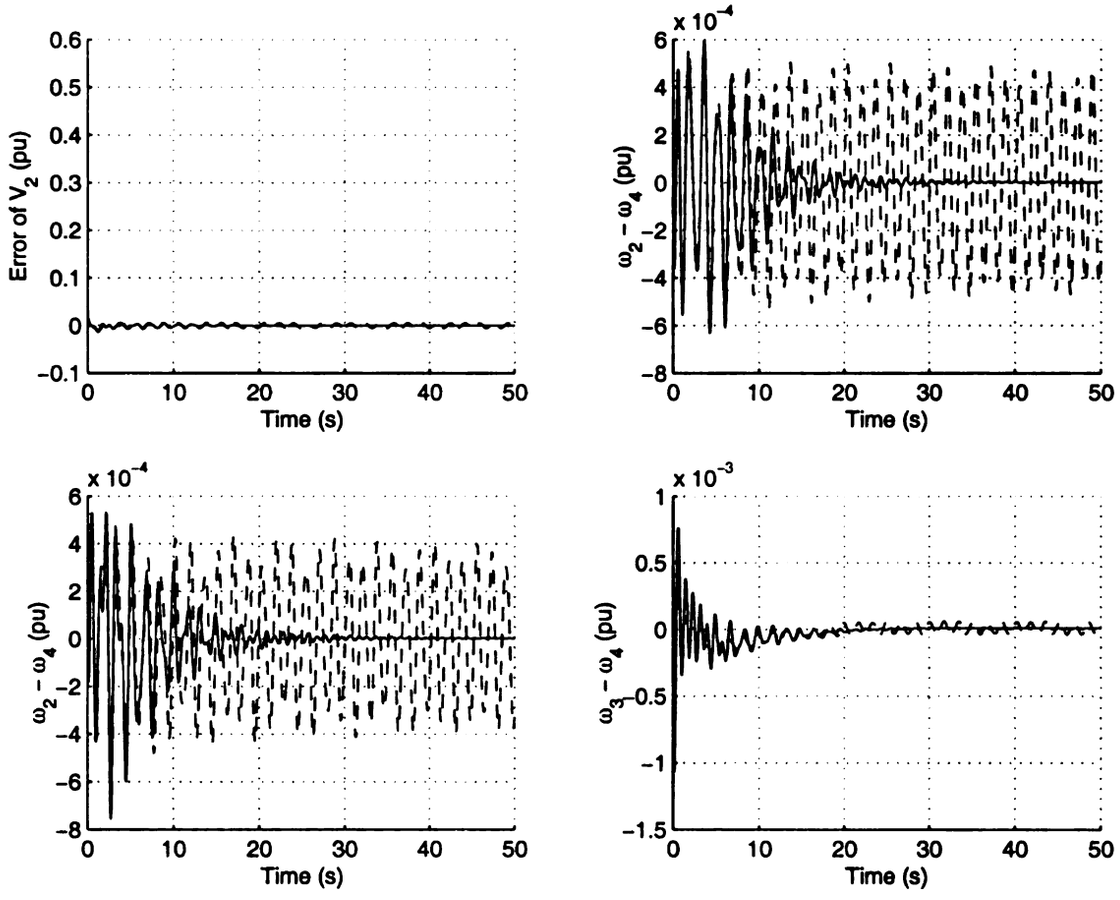

Figure 6.39: MSVC of Measurement ω_4 and ω_2 (-) and Open Loop System (- -)

MSVC/MPSS, where the MPSS is located on generator 4, is not given here since it is not as good as this design. In this design, both voltage and oscillations are very well damped with a transition period of 5 seconds rather than 10 seconds and much smaller magnitude of oscillation. The oscillations between generator 2 and the rest of the system and between generator 4 and the rest of the system are also shown in Figure 6.40. Both of the variables are well controlled. The results demonstrate the advantages of using both SVC control and a power system stabilizer that is properly sited over using only MSVC control. The addition of the MPSS on generator 2 shows a significant improvement in the damping of the oscillations produced by the double bifurcations as predicted based on the RGA matrix. The control of voltage V_{OUT_2} is shown to be degraded due to the MPSS as predicted by the RGA matrix but not seriously.

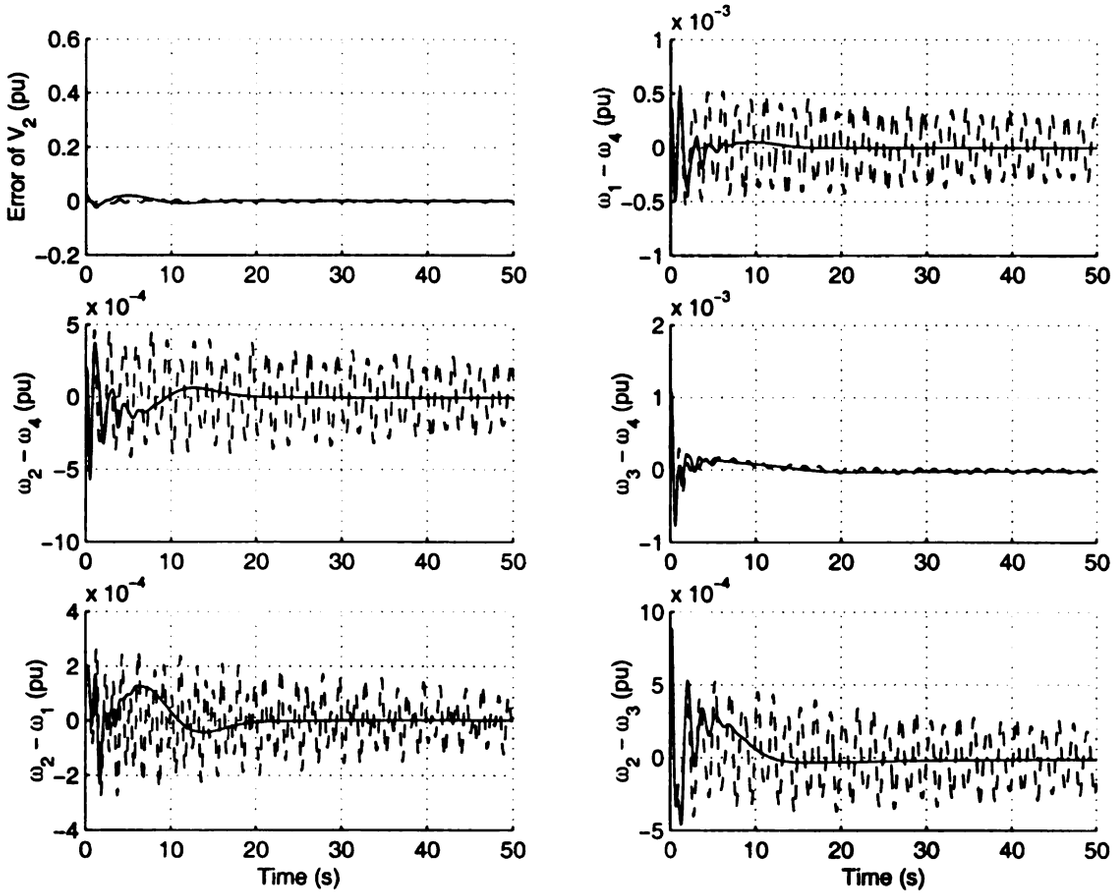

Figure 6.40: Mixed MPSS/MSVC Design(-) and Open Loop System (- -)

6.7 Nonlinear Effects of Robust Control

All the controllers designed in the previous sections are linear based on the linearized model of the system. The nonlinear structural uncertainty represents the nonlinear change in this linearized model as the bifurcation is approached. It has been shown that significant improvement in terms of control performance and robustness has been achieved with respect to bifurcation parameter variations. The control is designed for the linearized power system model, which is obtained by omitting the nonlinearity, i.e., only the first order approximation along the system trajectory is retained. According to Hartman-Grobman Theorem [21], if the equilibrium of the linearization of a general vector field $\dot{x} = f(x)$ is hyperbolic, there exists a homeomorphism defined in the neighborhood of the equilibrium taking orbits of the nonlinear flow to those of a linear flow. This homeomorphism preserves the sense of orbits. This theory along with the assumption that the control is to stabilize small variations around the equilibrium is used to justify the use of a linearized model for control system design. The designs of the CSVC and CPSS prove that there are severe limitations in designing control systems based on a linearized model without benefit of the knowledge of the bifurcation subsystem for the particular bifurcation that the controller is to stabilize and the structured uncertainty that represents the nonlinear change in the linearized model that produced the bifurcation. It should be noted that although the bifurcation subsystem is defined based on the linear model that is used for the robust control design, the bifurcation subsystem is shown to capture the nonlinear properties such as:

1. the bifurcation point for the bifurcation subsystem is close to that for the full system;

2. the bifurcating eigenvalue at the point of bifurcation is arbitrarily close to that bifurcating eigenvalue at the bifurcation point for the full system;

3. the nonlinear center manifold dynamics lie in or are contained in the bifurcation subsystem dynamics;

4. the trajectories near the center manifold in the bifurcation subsystem are arbitrarily close to those of the full system;

5. the orbits and their frequencies predicted by the bifurcation subsystem are close to those in the full system.

The robust control designed based on the linearized bifurcation subsystem (or full linearized model) and the structured uncertainty model that represents the nonlinear change in the state model as it experiences bifurcation could be expected to achieve nonlinear control performance.

Although this Hartman-Grobman Theorem suggests that the control design based the linearized model is highly applicable to the actual nonlinear system as long as the perturbations along the trajectory are sufficiently small and not close to bifurcation, this Hartman-Grobman Theorem does not imply that the bifurcation point is changed by controller to increase the feasibility region nor does it imply that the second order structure of the controlled closed-loop system is changed. It has already been shown that the bifurcation value is increased by as much as 50% by the robust control based on a bifurcation subsystem and the structural uncertainty that captures the nonlinear change in the linearized model of this bifurcation subsystem. It will now be shown that a non robust controller (the conventional excitation control) has no effect on the modal coupling of the closed-loop system that are dominated by modes associated with the inertial dynamics. The robust controller, on the other hand, will now be shown to suppress the nonlinear coupling of the modes associated with the inertial dynamics and replace it completely with a coupling to the control system dynamics. This is highly desirable change since the modal coupling is shown to make design of power system stabilizing controls very difficult due to the fact

that the stabilization of one inertial mode often causes instability of other inertial modes [25].

The closed-loop system eigenvalues and eigenvectors are usually changed by almost any controller. For the stable linearized system the right eigenvectors approximate the stable manifolds. Thus, virtually any control design will change the stable manifold of the nonlinear system. However, most linear system based control would not necessarily significantly change the bifurcation point. The robust controllers based on the bifurcation subsystem and the structured uncertainty representing the nonlinear change increased the bifurcation value by 50%, i.e., significantly changed the bifurcation point. The center manifold dynamics are related to the bifurcating eigenvalues and change with bifurcation point. Therefore, it is most possibly that the center manifold of the actual nonlinear system is significantly changed by the robust control designed based on the methodology. The dependence of all modal coupling on control dynamics would suggest that once the control is designed, the destabilizing affects of nonlinear modal coupling are at least suppressed if not eliminated. Thus, the robust controller would appear not only change the bifurcation value, the center manifold, but also the nonlinear coupling that produces additional bifurcations, all of which are nonlinear changes in the structure of the system being controlled.

6.7.1 Normal Form Representation of Nonlinear System

Normal form theory provides systematic procedure to find a sequence of nonlinear coordinate transformations to remove the inessential terms of increasing degree up to certain order from Taylor expansion of a vector field. Note equilibrium point can be nonhyperbolic. If an equilibrium point is hyperbolic, the application of normal form theory produces the formal part of Hartman's linearization. Normal form procedures

are summarized as follows.

A Taylor's series of a general vector field

$$\dot{x} = f(x)$$

where $x = [x_1, x_2, \cdots, x_n]^T$ and $f(x) = [f_1(x_1, \cdots, x_n), \cdots, f_n(x_1, \cdots, x_n)]^T$, around equilibrium is:

$$\dot{x}_i = A_i x + \frac{1}{2} x^T H_i x + H.O.T$$

where A_i is the i^{th} row of the Jacobian matrix and H_i is the Hessian matrix given by $\frac{\partial^2 f_i}{\partial x_j \partial x_k}$, i, j, and $k = 1, 2, \cdots, n$.

Letting U be the transformation matrix consisting of right eigenvectors of the Jacobian matrix A and defining:

$$x = Uy$$

give

$$\dot{y}_j = \lambda_j y_j + \Sigma_{k=1}^n \Sigma_{l=1}^n C_{kl}^j y_k y_l$$

where $C^j = [C_{kl}^j] = \frac{1}{2} \Sigma_{p=1}^n V_{jp}^T [U^T H_p U]$, and V is the matrix of the left eigenvectors of the Jacobian, and V_{jp} is the (j, p) element of V.

The nonlinear transformation that leads to the normal form is given by:

$$y_j = z_j + \Sigma_{k=1}^n \Sigma_{l=1}^n h2_{kl}^j z_k z_l$$

where $z_j = z_{j0} e^{\lambda_j t}$, and $h2_{kl}^j = \frac{C_{kl}^j}{\lambda_k + \lambda_l - \lambda_j}$.

With the normal form a closed-loop solution of the states x can be obtained as:

$$x_i(t) = \Sigma_{j=1}^n U_{ij} z_{j0} e^{\lambda_j t} + \Sigma_{j=1}^n U_{ij} [\Sigma_{k=1}^n \Sigma_{l=1}^n h2_{kl}^j z_{k0} z_{j0} e^{(\lambda_k + \lambda_l) t}]$$

where z_{j0}, z_{k0}, and z_{l0} are the initial conditions that can be calculated from the known initial conditions of x and U_{ij} is the (i,j) element of U. It can be seen that the time evolution of the system is determined by two parts: the corresponding mode i in the linear sense, and the combination of mode k and l in the second order sense. The magnitude of the time response of the second order is decided by the size of $h2^j_{kl}$, z_{k0}, and z_{l0}. The term $h2^j_{kl} z_{k0} z_{l0}$ indicates the nonlinear interaction of the second order [43] [44].

6.7.2 Nonlinear Effects of Robust Control on Transient Response of Power Systems

The two area example system in Figure 5.1 is again studied here with slight modification in order to simplify the calculation of normal form representation and show a clear picture of the effects of the robust control. The SVC control on bus 101, the power system stabilizer on generator 3, the turbine controls on all generators, and the transformers are removed from the system. Simplified excitation systems are used on all four generators. The diagram of a simple exciter is shown in Figure 6.41, where $V_{R_{max}}$ and $V_{R_{min}}$ indicate the maximum and minimum voltage regulator output, respectively. In order to obtain a nominal stable system the exciter parameters and the transmission line resistance and reactance are carefully tuned. These changes are required to assure that both the second order coupling and the μ-synthesis control can be calculated.

The active power load on generator 2 is again taken as the bifurcation parameter. A Hopf bifurcation develops with the increase of the active power load on bus 2. The generator angle vector diagram, which is not presented here, shows that this is a interarea Hopf bifurcation between the two areas and the oscillation is again between generator 4 and the rest of the system. Following the same design procedures

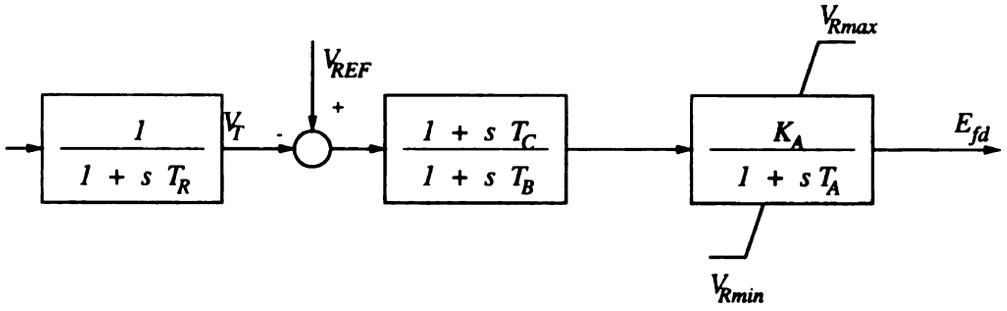

Figure 6.41: Simplified Excitation System

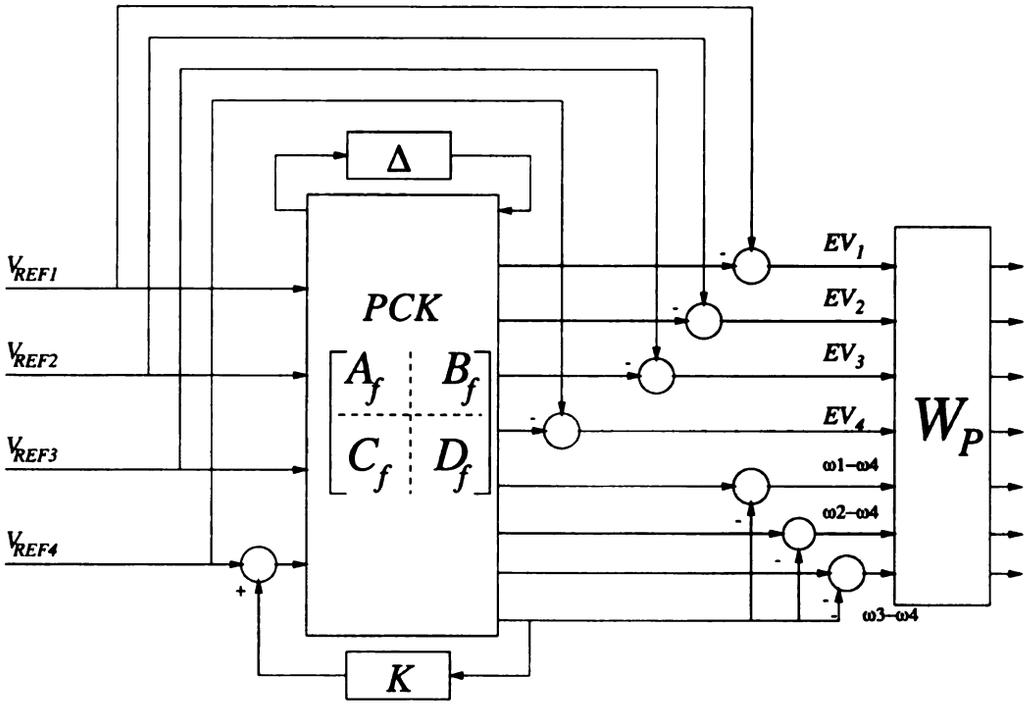

Figure 6.42: Control Configuration of MPSS

shown in the previous sections a μ-synthesis power system stabilizer on generator 4 is obtained (the control configuration is shown in Figure 6.42). When a fault occurs on generator 2 the frequency time response of the closed-loop system with MPSS is shown in Figure 6.43. Note that the open loop system time response is not shown here because it is unstable. It can be seen that the transition time period is obviously longer compared to the time response shown in the previous sections. This is due to that fact that control devices for this two area system are only simplified excitation systems. However, the overall control performance is still satisfactory.

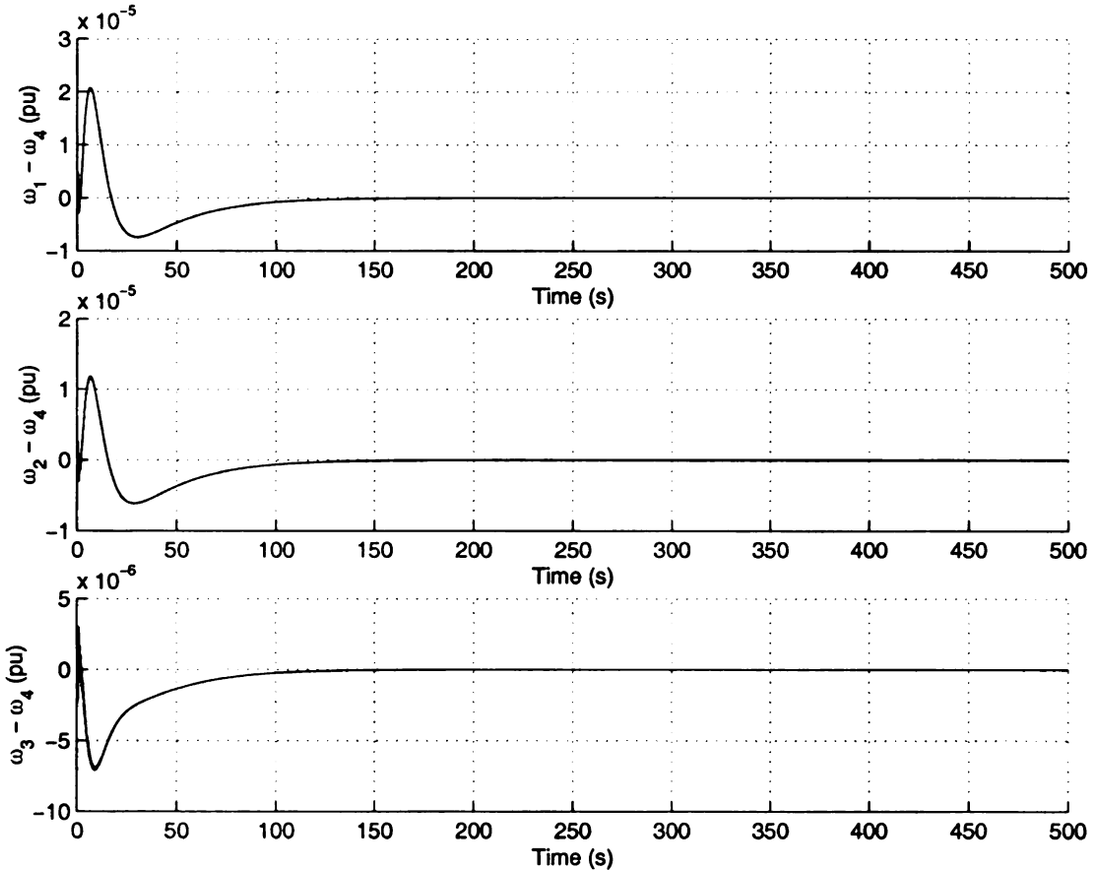

Figure 6.43: Closed-loop System with MPSS After a Fault

The second order interaction $h2^j_{kl}z_{k0}z_{l0}$ of the faulted system is calculated with a Fortran program. Table 6.23 and 6.24 show the second order interaction of the open loop system and the closed-loop system with MPSS, respectively, where mode 1, $\cdots$, 4 represent E'_{q_1}, $\cdots$, E'_{q_4}, 5, $\cdots$, 8 represent E'_{d_1}, $\cdots$, E'_{d_4}, 9, $\cdots$, 12 represent ω_1,

Mode j	$\max_{k,l}\{h2^j_{kl} z_{k0} z_{l0}\}$	Mode k	Mode l
1	0.09785	1	14
2	0.09785	2	14
3	0.46590	3	17
4	0.46590	4	17
5	0.53522	3	10
6	0.53522	4	9
7	2.76160	9	10
8	2.76160	9	10
9	3.69249	9	10
10	3.69249	9	10
11	0.00000	9	10
12	0.01318	3	4
13	0.09021	3	4
14	1.36082	9	10
15	11.19070	9	10
16	0.26531	10	13
17	1.24454	9	10
18	1.82886	14	16
19	0.13837	9	10
20	0.15227	2	17
21	0.67276	2	10
22	0.06897	16	24
23	0.13363	9	27
24	0.78005	14	25
25	1.23878	9	10
26	0.97817	9	27
27	4.00940	14	26

Table 6.23: Modal Interaction of Original System

$\cdots$, ω_4, 13, $\cdots$, 15 represent δ_{21}, $\cdots$, δ_{41} with $\delta_{i1} = \delta_i - \delta_1$, $i = 2, 3, 4$, 16, $\cdots$, 19 represent E_{fd_1}, $\cdots$, E_{fd_4}, 20, $\cdots$, 27 represent excitation control states, and 28, $\cdots$, 35 represent states of the MPSS. Thus, mode 9 to 15 are all inertial modes that are related to inertial dynamics, mode 16 to 35 are control modes including both excitation control and MPSS control. Note that MPSS takes effect through the excitation system.

Table 6.23 shows the maximum modal coupling of modes k and l for each mode j. In Table 6.23 for mode $j = 1, 2, \cdots, 8$ the interactions are primarily related to

Mode j	$\max_{k,l}\{h2^j_{kl} z_{k0} z_{l0}\}$	Mode k	Mode l
1	67.51087	1	34
2	67.51087	2	34
3	2.80985	23	34
4	2.80985	23	34
5	10.10032	23	34
6	10.10032	23	34
7	0.00041	7	26
8	0.00041	8	26
9	0.20141	11	34
10	0.20141	12	34
11	0.75560	11	26
12	0.75560	12	26
13	43.45400	23	34
14	43.45400	23	34
15	1.32449	32	34
16	1.32449	32	34
17	3.86180	23	34
18	3.86180	23	34
19	7.40299	26	34
20	7.40299	26	34
21	10.78313	26	34
22	10.78313	26	34
23	0.00000	32	34
24	0.00003	30	35
25	0.01329	11	12
26	0.03922	11	12
27	0.00619	11	12
28	0.03413	11	12
29	0.03301	11	12
30	0.08095	11	12
31	0.65977	26	34
32	2.13788	26	34
33	0.05035	26	34
34	0.11682	28	34
35	2.18197	34	34

Table 6.24: Modal Interaction of System with MPSS

inertial modes 9, 10, 11, 12, 13, 14, and 15, only mode 3 and 4 are slightly affected by excitation field mode 17, and modes 22, $\cdots$, 24, 26, 27 are slightly affected by a coupling in control modes. The largest second order interactions of noncontrol mode $j = 7, 8, 9, 10, 11, 14$, and 15 are all related to inertial dynamics 9 (ω_1) and 10 (ω_2), and none of inertial dynamics are affected by the excitation control mode. Moreover, the maximum value of the second order interaction is 11.1907. This occurs to mode $(15, 9, 10)$ and these three modes all belong to the inertial dynamics. For the excitation control modes 16, 17, $\cdots$, 27, almost all of them have coupling to at least one inertial mode except for mode 20 and 22. This indicates that (1) the inertial dynamics dominate the nonlinear response of the open loop system; (2) the excitation control is not effective and does not have much control on the inertial dynamics or on the rest of the system; and (3) the excitation system response is seriously affected by inertial dynamics. These results explain why the system is susceptible instability for parameter variation or faults. It would also explain why design of multiple PSS to improve damping on different modes would likely require iterative design because stabilizing one inertial model could destabilize others due to the dominance of inertial dynamics and the modal coupling in these inertial modes to virtually every other mode .

The modal interaction of the closed-loop system with MPSS is shown in Table 6.24. Mode $j = 1, 2, \cdots, 8$ are all related to control mode 23, 26, and 34. For inertial mode $j = 9, 10, 11, 12, 13, 14$, and 15, the maximum interaction are all now related to control mode 34, 26, 23, and 32. The control modes $j = 16, 17, \cdots, 35$ are now coupled to themselves except for mode $25, 26, \cdots, 30$. However, the value of the maximum interaction shows that all of them are pretty small and can be neglected. This shows that (1) MPSS rather than inertial modes dominates the second order part of the time response and has tremendous control effect over the system on the high order terms as well as the first (this can be seen from the time response shown in

Figure 6.43) and second order approximation of the system ; (2) the inertial dynamics are now under control of exciters and MPSS; and (3) the inertial dynamics have only slight effects over the control modes. This is exactly the purpose of this robust PSS design.

6.8 Analyses of Robust Control Design for Power Systems

As noticed in [25], the most frequently encountered problem in power system control design is that a control that stabilizes one mode destabilizes another. The local stability or control performance achieved does not guarantee the interconnected system stability or performance. For the current power systems that are very complicated and highly coupled a coordinated control could achieve a significant improvement in control performance of a power system since local PSS achieves local performance and stability for a particular mode of instability does not necessarily improve the performance or even guarantee the stability of the full system when all of these local controllers are implemented simultaneously. From results in [25], there is a need to iteratively design each local control to stabilize the modes destabilized by the last iteration. If the operating conditions change significantly the interarea modes would reappear and again require iterative control redesign for potentially all of the local controllers.

A power system stabilizer is a local controller that is located on the specific generator. The location of the power system stabilizer makes it difficult to have strong influence on controlling the interarea oscillations and the rest of the system. As a local control device, a power system stabilizer has been proved in [46] and in previous sections of this chapter to be less effective than it was claimed to be for achieving both the

interarea oscillation control and the voltage control on buses. This was confirmed by showing that a robust controller SVC is far more effective than a robust control PSS. FACTS devices have been widely used and are very promising in stabilizing power systems due to its rapid response and the ability to provide or absorb the reactive power and therefore to provide the voltage support.

The success of robust control design methodology occurs because:

1. robust control is extremely suitable for power system as we have mentioned that the operating point of the power system is changing continuously and perturbation caused by various bifurcation parameters always exists. These situations are difficult to handle by a manually-tuned conventional control (CPSS or CSVC) and most often destroy the power system steady state stability. For robust controller all of the bifurcations can be corrected as long as these perturbations are properly considered in the design process;

2. μ-synthesis is looking for the worst direction and the worst frequency of the system by using H_∞ norm and minimizing the peak μ value for the all allowable uncertainty perturbations. Thus, the nonlinear uncertainty expressed in the form of structured perturbations of the linear system for each bifurcation, can be taken care of during the control design. The robust control produced can increase the feasibility region for the directions in parametric space associated with each bifurcation included in the structured uncertainty model used to design the control. The use of the uncertainty in Δ_P, which is an uncertainty in the dynamic model, can produce a coordination of the control of the bifurcation subsystem and the subsystems within the external system. This coordination reduces or eliminates the coupling between the bifurcation subsystem and the subsystems in the external system. The coordination of control appears to remain up to the point of bifurcation. However, if the robust control

design is restricted to the bifurcation subsystem, the coordination between the bifurcation subsystem and the external system does not occur but the increase in the feasibility region direction associated with the bifurcation subsystem is almost the same as that obtained if the full system model is used in the robust control design.

The coordination using the full system model may make it difficult to use two controls effectively when controlling two bifurcation subsystems, especially when they overlap. Designing two controls separately based on their own bifurcation subsystem or together based on the their combined bifurcation subsystem may improve control performance for both bifurcations compared to designing both controls separaterly on a full system model. This hypothesis is based on the fact that the robust control designed for the full system model and one bifurcation coordinate control of all subsystems in the full system model when the full system model is used in the design. This could lead to a fighting for control of subsystems not in either bifurcation subsystem when two or more controls are designed separately based on the full system model;

3. for the two-area example system the μ-synthesis control design generates an almost decoupled closed-loop system for every subsystem in the full system model. The RGA matrix structure of the closed-loop system is very impressive in the sense that it shows that the individual local non robust control is responsible only for the output it is supposed to control while the robust controller provides excellent robust control of the bifurcation subsystem and coordinated control of the subsystems that lie in system external to the bifurcation subsystem. Also, RGA matrix structure of the closed-loop system with robust controller is preserved over wide frequency band including steady state, crossover frequency, and up to the bifurcation frequency. This clearly explains why the coordinate robust control designed based on the full system model

can achieve better control performance for a single bifurcation than could be achieved by a non coordinated robust control designed for a model of just the bifurcation subsystem;

4. the bifurcation subsystem provides very important information on control signal selection, performance index definition, location of controls, and control design simplification for control design. The bifurcation subsystem information shows this interarea oscillation occurs between generator 4 and the rest of the system. Thus, the speed frequency of generator 4 is selected as the measured output signal, and the frequency deviations of generator 1, 2, and 3 with respect to the angular speed of generator are included in the performance index definition. The robust controller and the original excitation systems, power system stabilizer, turbine governor controls are coordinated in the sense that the voltage control errors, the power control errors are also to be minimized by the robust control design;

5. for a large power system the computation and impelementation of the robust control design is almost impossible without finding a lower order model. The bifurcation subsystem for any specific bifurcation provides a much lower order model that can be used to compute and design the control that can be applied to stabilize the full system. Bifurcation subsystem based robust controller is of lower order and the control performance is still very competitive. The use of the bifurcation subsystem definitely facilitates and helps the control design but loses the ability to coordinate the control of the bifurcation subsystem and the subsystems within the external system model;

6. the uncertainty caused by the specific bifurcation parameter is properly modeled. The uncertainty modeling in the frequency domain is often conservative since the uncertainty region has to be approximated by the largest "circle"

region. The uncertainty is caused by a specific bifurcation parameter change that causes the full system bifurcation. The uncertainty captures the nonlinear change in the linearized model of the bifurcation subsystem. The relationship between the system matrix change and the parameter is approximated by least-square method. The uncertainty captures the worst uncertainty at the worst frequency ($\omega = 0$ for saddle-node bifurcation and $\omega = \omega_0$ for Hopf bifurcation) that is required to compute the H_∞ control for a specific bifurcation that is to be stabilized. Robust control did not attempt stabilization of a specific bifurcation and did not then select the worst uncertainty and the worst frequency and the subsystem to be controlled by selecting the uncertainty to produce the bifurcation in the bifurcation subsystem which in turn implies the worst frequency, the bifurcation frequency of that bifurcation;

7. the two area example system is treated as entity in the control design. In the design, all the control inputs and the outputs of the power system are included. The goal of the control design is to stabilize the interarea oscillations as well as maintaining the voltage output at all the buses and the power outputs on generator buses. This guarantees the overall system performance at the cost of more control efforts by the robust controller. Thus, we are looking for the balance between the controller complexity and all of the desired performance requirements rather than just one goal, for instance, damping of an interarea oscillation. Focus on solely on interarea oscillation damping could possibly cause a voltage control problem in the whole system. It should also be noted that in order to reduce the computation load and the controller complexity the desired control performance requirements of the weighting matrices are not very stringent;

8. we are trying to design a controller that is robust to one specific bifurcation

parameter variation rather than to all kinds of parameter changes and disturbances. However, the resulting controller shows effective control for different bifurcation parameters (active and reactive power load variation), different bifurcations (saddle-node and Hopf bifurcation), and different disturbances (faults). This is not surprising since bifurcation subsystem analysis shows that the corresponding bifurcations are caused by either the same bifurcation subsystem or a subset of the bifurcation subsystem for reactive power load change as for active power load changes;

9. SVC, one of the FACTS control devices, is usually located on one of the the long transmission lines in a large power system. It has been shown that SVC is most effective for damping when it is located at the midpoint of the transmission lines in two-area power system, as it is in this two-area example system. This is also one of the important factors to achieve good control performance. Despite that fact that a global stabilizing controller for a very large power system is impossible, a SVC does have the ability to control a relatively large area. Moreover, this ability has been drastically extended using the bifurcation subsystem method.

Chapter 7

Conclusions and Future Work

A bifurcation subsystem method is developed and justified theoretically and computationally. It is proven that the bifurcation subsystem experiences, produces, and causes the full system bifurcation. This is guaranteed by showing that the full system dynamics are preserved in the slow/fast reduced system when a saddle-node or a Hopf bifurcation develops. Bifurcation subsystem method is more than a model reduction method like coherent reduction [14], Kalman minimal realization method [13], decomposition methods [22], and quasi-steady-state approximation [9], since the center manifold dynamics of the full system are shown to lie in or be totally contained in the bifurcation subsystem. Thus, operating changes or control of the bifurcation subsystem is able to provide cures of the full system bifurcation.

The bifurcation subsystem condition and the geometrical decoupling condition assure the existence of the bifurcation subsystem for both saddle-node and Hopf bifurcation. It is shown that the conditions for the existence of the bifurcation subsystem that preserves the dynamic behaviors and the center manifold of the full system are much less stringent than slaving, modal reduction, coherent reduction, or decomposition methods because the bifurcation subsystem requires that the coupling of the bifurcation and external system be small and the response of the external system be

fast in the direction of the right eigenvector direction of the bifurcating eigenvalues rather than in all directions. A bifurcation subsystem identification algorithm provides a systematic and computationally efficient method to obtain the bifurcation subsystem. The bifurcation subsystem can be computed for any large systems without intensive computation that is required to compute a nonlinear transformation by center manifold dynamics determination. Moreover, the bifurcation subsystem is in the physical variables and contains the structural information of the full system model.

The power system bifurcations are classified using the bifurcation subsystem method and the bifurcation subsystem identification. The types (saddle-node, Hopf, or Singularity induced bifurcation), the classes of each bifurcation (a subset of the variables of generator and load dynamics, controls, and network model etc in the bifurcation subsystem), and the agents (which is associated with states of specific generators and load devices for a particular type and class of bifurcation) can be identified and thus the classification could eventually provide the causes and cures of a specific power system stability problem by the type and the class of a bifurcation.

The bifurcation subsystem method, the classification of the power system bifurcations, and the bifurcation parameter identification directly lead to the robust stabilizing control design for a specific bifurcation parameter (a single bifurcation) or multiple bifurcation parameter (multiple bifurcations) variations that always exist in any power system model.

The goal of robust power system stabilizing control design is defined to increase the damping of the interarea oscillation as well as to control the individual bus voltage in the systems. Since the major control devices are excitation control/power system stabilizer and FACTS devices, the robust power system stabilizer and robust SVC control are designed and implemented in this thesis using a μ-synthesis

H_∞ method. The success of the robust controls designed compared to those developed previously [36] [37] [38] [41] [46] [25] is that the uncertainty model represents the nonlinear change in the model caused by the bifurcation parameter change that produces bifurcation in some bifurcation subsystem. The robust controls are configured and synthesized based either on the bifurcation subsystem information on the full system model and/or based on the lower order bifurcation subsystem model. The implementation of the robust control not only shows the drastically improved closed-loop system controllability structure, the control performance, and robustness improvement, but also reveals that the robust control design based on the bifurcation subsystem information dominates the nonlinear modal coupling effects up to the second order.

The RGA matrix is proven to capture the bifurcation subsystem structure and its vulnerability to bifurcation. The RGA matrix shows that using MPSS or MSVC the external system is broken into decoupled subsystems where each subsystem has one and only one effective control, where without the RGA matrix one could not observe this structural change that occurs to MPSS or MSVC. The RGA matrix also captures the fact that the bifurcation subsystem structure exists and is preserved at bifurcation parameter value far below the bifurcation value and that the bifurcation subsystem remains decoupled from the robustly controlled external subsystems.

The uncertainty modeled by Δ and Δ_P produces the robust control discussed. The structured uncertainty captures the nonlinear change in principally the bifurcation subsystem dynamics associated with change in the bifurcation parameter that produces the bifurcation in the bifurcation subsystem that also occurs in the full system due to geometric decoupling. This uncertainty allows up to a 50% increase in the bifurcation parameter and thus in the feasibility region in the bifurcation parameter direction. The uncertainty of the dynamics in the internal and external systems, produced the global decoupled control subsystem structure that not only breaks the

external system into decoupled subsystems but also provides a single effective control that is not vulnerable to disturbances or competition from other controls.

The μ-synthesis control is looking to maximize control performance in the worst direction and worst frequency by using a H_∞ norm and minimizing the peak μ value for all allowable perturbations modeled by Δ and Δ_P. The μ-synthesis control would attempt to minimize the effects of the structured uncertainty that produces bifurcation in a specific bifurcation subsystem at the bifurcation frequency ($\omega_i > 0$ for Hopf bifurcation and $\omega_i = 0$ for saddle-node bifurcation) where it occurs. The μ-synthesis control must then cope with the nonlinear modal coupling within the power system model that allows control of one mode to produce instability in other modes. This μ-synthesis control also produces the global decoupled control structure in the process of coping with dynamic uncertainty Δ_P. The global decoupled control structure due to robustness to Δ_P and the robustness to the structured uncertainty Δ that produces bifurcation may together produce the robustness against control or operation change that affects one mode producing instability in other modes.

The knowledge of bifurcation subsystem, the structured uncertainty that occurs within the bifurcation subsystem, and the RGA matrix that captures the structure and vulnerability of bifurcation subsystem all combine to produce the control design methodology given in this thesis. The fact that the controller can be destabilized based solely on the bifurcation subsystem model and still achieve the control performance makes the control practical because (a) it can be computed for very large power system models, where normally μ-synthesis control must be restricted to small models; (b) the control does not depend on changes in the external system; and (c) it can be coordinated with controls developed for each bifurcation that effects different bifurcation subsystems even if the bifurcation subsystems overlap. The bifurcation subsystem also provides selection, reduction, and siting of controls, selection of measurements and control performance index;

7.1 Saddle-node Bifurcation Subsystem

The concept of a bifurcation subsystem [3] that experiences, produces, and causes the bifurcation in the full system model is extended. The motivation for finding a bifurcation subsystem and its advantages over model reduction [12], slaving [27], and finding the center manifold dynamics [18] are discussed. A more precise definition of what constitutes a bifurcation subsystem for saddle-node bifurcation is given than that provided in [3]. Persistence of the center manifold for the reduced models of singularly perturbed fast and slow external dynamics is shown [19]. These results are then used to show that the center manifold of the saddle-node bifurcation is in the bifurcation subsystem and is contained within the bifurcation subsystem if additional conditions are satisfied. This result is needed to justify the bifurcation subsystem advantages over the model reduction, slaving, and center manifold dynamics identification methods.

7.2 Hopf Bifurcation Subsystem

The concept of a bifurcation subsystem that experiences, produces, and causes Hopf bifurcation is introduced in [3] as only an extension of the saddle-node bifurcation subsystem. The theoretical results required in [3] for Hopf bifurcation subsystem method are incomplete. In this thesis the persistence of Hopf bifurcation as well as the preservation of equilibrium point, the bifurcation point, the bifurcating eigenvalue, the nature and size of the periodic orbits in the reduced system for the full system with slow singularly perturbed external dynamics are proven [5]. This and the theoretical results in [4] for fast external dynamics complete the requirements for proper definition of Hopf bifurcation subsystem. These results also establish that the center manifold dynamics lie in the bifurcation subsystem [4] [5]. The advantages of

bifurcation subsystem as a representation of the center manifold include being able to capture orbits, trajectories, frequency, and center manifold dynamics in a small bifurcation system in the physically meaningful variables and parameters. Computation of center manifold is currently impossible for large system because it requires computation of a nonlinear transformation which is only possible for small system. It is also shown this bifurcation subsystem can contain the center manifold dynamics of the full system and, therefore, can provide all the necessary information for the analysis and control design when Hopf bifurcation occurs. It is also justified that only one of a pair of complex conjugate eigenvectors is required to represent the system response. The test conditions for the existence of the Hopf bifurcation subsystem are developed based on use of only one of the complex bifurcating eigenvalues and its conjugate right eigenvectors.

7.3 Bifurcation Subsystem Identification

A systematic algorithm is given for identification of a bifurcation subsystem. The algorithm applies the bifurcation subsystem and the geometric decoupling condition tests to a sequence of partitioned models where the internal systems are of increasing order and are each associated with the largest right eigenvector elements. The simplicity of this algorithm makes its application to large systems possible. The bifurcation subsystem condition and geometric decoupling condition that are a sufficient condition for existence of a bifurcation subsystem are theoretically extended and given in Theorem 4.3.1 - 4.3.4 in Chapter 4. It is shown that bifurcation subsystem method is more rigorously established since specific norms are introduced to represent the different system properties that allow a bifurcation subsystem to exist. The theoretical results in Chapter 4 provide more insight into the bifurcation subsystem method and why and when a bifurcation subsystem exists. This analysis reveals

that the existence of a bifurcation subsystem requires much weaker conditions than that required for slaving [27], model reduction [12], coherency reduction [14], and α-decomposition [22] methods.

7.4 Classification of Types, Classes, and Agents of Power System Bifurcations

The bifurcation subsystem method provides a procedure for determining the classes and the agents for each bifurcation based on its type (saddle-node, Hopf, singularity induced, and algebraic). The study of the types of stability problems in power system and the identification of different classes of each type of bifurcation are required in order to prescribe cures for stabilizing a specific bifurcation. The following questions which have been raised are addressed in this thesis: (a) what is the relation between network (algebraic) and dynamic bifurcation? (b) how and why interarea and local modes are produced? (c) what are the classes and types of bifurcation for different load models? and (d) how to find the bifurcation subsystem and the behaviors when singularity induced bifurcation occurs? Bifurcation subsystem method is applied to a two-area example power system and the classification of bifurcations that can occur in this example system is studied thoroughly. The classes of saddle-node and Hopf bifurcation hypothesized in [26] are verified via numerical examples and analysis. This classification of bifurcation may permit prescriptive control of systems because knowing the bifurcation type and class and any control constraints in the specific agent, one can quickly design a control once that bifurcation appears possible.

7.5 Robust Control Design Methodology

The bifurcation subsystem based robust control design methodology has four components: The first component of this methodology is the use of the *RGA* analysis to show that the robustness produced by this methodology, breaks the external system into subsystems that are decoupled from one another and from the bifurcation subsystem. Each subsystem including the bifurcation subsystem is shown via *RGA* matrix to have one and only one effective control for each output variable so that there is no competition for control in any subsystem. The *RGA* matrix shows that the control in each subsystem is effective (one element near 1.0) and resistant to disturbance or noise on any subsystem (no element above 1.0). The *RGA* matrix can also show how the control structure change for $\omega = 0$, the Hopf bifurcation frequency, and the cutoff frequency for the control. The *RGA* matrix is theoretically shown to capture the bifurcation subsystem and can be used to show the bifurcation subsystem structure exists long before the bifurcation parameter reaches the bifurcation value. The second component of the robust design methodology is to use a structured uncertainty that captures the nonlinear change in linear model due to the bifurcation parameter change from the nominal value to the bifurcation value. The structured uncertainty principally captures the uncertainty in the bifurcation subsystem that experiences, produces, and causes the bifurcation in the full system model. This structured uncertainty produces a 50% increase in the feasibility region in the direction of the bifurcation parameter but does not produce the subsystem structure of the external system. A dynamic system uncertainty that in combination with the structured uncertainty is shown to produce the subsystem structure of the external system. The third component is the use of the bifurcation subsystem model for design of the controller rather than the full system. The resultant SISO controller is then the order of the bifurcation subsystem rather than the or-

der of the full system model. The computation required to obtain the μ-synthesis controller is also reduced and makes application of μ-synthesis control to very large power system models feasible without model reduction that does not capture the small bifurcation subsystem that experiences, produces, and causes the bifurcation and retains the dynamic system properties associated with the bifurcation of the full system model. The fourth component is the selection of the performance index, weighting matrix, measurements and control that are based on the bifurcation and the bifurcation subsystem being stabilized. The robust control completely eliminates the strong nonlinear modal coupling that makes design of PSS dampen one mode produce instability of another inertial model.

H_∞ control attempts to find the control that minimize the performance index for the possible uncertainty that occurs at the frequency where the system is most vulnerable. The design methodology preselects and coordinates the frequency uncertainty and subsystem at which the robust controller should have effect. The frequency where the system is most vulnerable is the bifurcation frequency ($\omega = 0$ for saddle-node bifurcation and $\omega = \omega_0$ for Hopf bifurcation. The uncertainty is the nonlinear change in the linearized model caused by the change in the bifurcation parameter that produced the bifurcation subsystem, and the subsystem where the control has effect in increasing the feasibility region, and the nonlinear modal coupling is the bifurcation subsystem. This coordination within this design methodology enables the very significant control performance improvements obtained.

7.6 μ-synthesis Power System Stabilizer Control

The resulting control achieves significant structural improvements that would not be thought possible by a linear control: increasing the feasibility region by 50% in the direction of the bifurcation parameter and uncertainty, elimination of the nonlinear

modal coupling producing decoupled subsystem control of the inertial mode in the external system. This is all accomplished by a SISO controller.

A μ-synthesis power system stabilizer (MPSS) design is presented for a two-area power system. The uncertainty is modeled based on the nonlinear change in the linearized model and the structural information of the system for the bifurcation parameter change that produces bifurcation. The use of this uncertainty model and knowledge of the bifurcation subsystem that experiences, produces, and causes the full system bifurcation is used to design the control. The control objective is to damp out the interarea oscillation as well as regulate the bus voltages for the variation of the uncertainty parameter. The determination of the robust control device location that is expected to give better control performance is discussed and selected according to the nature of the bifurcation. The performance index definition reflects the desired control purpose. A very flexible robust control configuration, that can be easily applied for different control designs, is shown.

The *RGA* matrix is studied to evaluate the robust power system stabilizer design. The *RGA* matrix information suggests that the control structure and capability of disturbance rejection has been drastically improved by MPSS design. Moreover, the use of the dynamic uncertainty of the full system Δ_P in addition to the bifurcation parameter directional uncertainty that affects the bifurcation subsystem breaks the external system into uncoupled subsystems and decouples these subsystems from the bifurcation subsystem. The *RGA* matrix provides a view of these structural properties that would otherwise be unobserved except for the exceptional control performance achieved. This thesis is the first use of the *RGA* matrices applied to power systems. The *RGA* matrix is proven to capture bifurcation subsystem structure. The *RGA* matrix, bifurcation subsystem, and the uncertainty that is the nonlinear change within the bifurcation subsystem together produce a new very powerful control design methodology, where the *RGA* matrix can capture the incredible

controllability improvements that are achieved via the bifurcation subsystem model and uncertainty based on μ-synthesis design. The time simulation verifies the improvement of control performance and robustness.

7.7 μ-synthesis SVC Control

Several kinds of robust SVC controls are designed to increase the damping of interarea oscillation and maintain the bus voltages. The structured uncertainty modeling, the MSVC control configuration, the performance index, and the weighting transfer function are formulated according the nature of the interarea oscillation caused by active power load change. The MSVC and the MPSS are compared and discussed. The SVC provides better damping control of the interarea oscillation and better regulation of voltage in the network. The full system and the bifurcation subsystem based robust SVC controls are designed for Hopf and saddle-node bifurcation with and without input uncertainty and measurement noise. The input and measurement uncertainty compromise the effectiveness of the control designed based on structured uncertainty for bifurcation parameter change Δ and the dynamic uncertainty Δ_P, that produced effective control in subsystems in external system, and lack of coupling between external subsystems and between the external system and the bifurcation subsystem. The measurement and control uncertainty also compromised the increase of 50% in the feasibility region in the change of the bifurcation parameter direction. It was also shown that the design of a robust control for a bifurcation produced by adding load at one bus in a coherent group was effective for adding load at any bus in that coherent group.

7.8 Multiple Bifurcations

A multiple bifurcation phenomena is observed in a two area example power system. A local bifurcation and an interarea bifurcation develop because of the multiple bifurcation parameter changes. The dynamic behaviors of the bifurcating system are complex due to the overlapping of the two different bifurcation subsystems and are shown to be difficult to control. In order to stabilize the double bifurcations produced by two bifurcation parameters, three kind of μ-synthesis robust controls are designed, (a) μ-synthesis power system stabilizer (MPSS); (b) μ-synthesis SVC control (MSVC); and (c) a mixed MPSS/MSVC control. Based on the bifurcation subsystem analysis, the measurement signals and locations of the controls are selected. The control performances and the *RGA* matrix information of three kind of controls are compared. It is shown that (a) the multiple bifurcations can not be stabilized well by a single measurement and a single control MPSS but can be stabilized by a single measurement and a single control MSVC; (b) additional appropriate measurements and/or controls improves the control performance for multiple bifurcations; and (c) the mixed MSVC/MPSS design gives the best performance. The SVC provides effective control of the interarea oscillation and the MPSS placed on the generator experiencing the local oscillation is effective. If the MPSS is placed on another generator, the effectiveness of the MPSS is very limited and the performance of the control is only slightly better than using the SVC control. This study provides the guidance of robust control design for large power systems.

7.9 Nonlinear Effects of Robust Control

The nonlinear effects of a robust power system stabilizer for a two area power system is studied. To highlight the nonlinear effects of a μ-synthesis power system stabi-

lizer (MPSS) the two area system [25] is modified and equipped with conventional simplified excitation systems only. A normal form representation of the nonlinear power system model [43] is introduced such that the nonlinear model can be approximated up to the second order. A MPSS is designed based on the bifurcation subsystem information and the second order interaction indices of the system with MPSS and conventional excitation control are calculated and compared. The analysis of the nonlinear effects shows that the nonlinear coupling now depends solely on MPSS dynamics rather than the nonlinear coupling between inertial modes and between inertial modes and electrical modes in the original system. The nonlinear coupling of inertial modes makes stabilizing multiple interarea modes very difficult since the stabilization of one inertial mode can make one or more of other inertial modes unstable. Designing PSS for systems with multiple coupled interarea modes is an iterative process and one that is very susceptible to be destabilized by changes in operating conditions. The MPSS removes this modal coupling and replaces it by a modal coupling to the controller dynamics that will not change with approaching bifurcation.

7.10 Future Work

This thesis may provide the following future research topics:

- extend the bifurcation subsystem method including the bifurcation subsystem identification and the power system classification to the very large power system;
- extend the bifurcation subsystem method based robust power system stabilizer and SVC control designs to the very large power system;
- establish the theoretical, the computational framework, and the stabilizing

control methodology for multiple bifurcation study in the large power system;

- build the intelligent control structure consisting of the learning mechanism, the knowledge representation, and the intelligence acquisition based on the bifurcation subsystem method, the classification of the bifurcations, the robust control design methodology, and the wide area sensing system.

Bibliography

[1] D. V. Anosov, "On Limit Cycles in Systems of Differential Equations with a Small Parameter in the Highest Derivatives", AMS Translations, Ser. 2 33, 1963

[2] H. D. Chiang, L. Fekih-Ahmed, "Persistence of Saddle-node Bifurcations for General Nonlinear Systems Under Unmodeled Dynamics and Applications", IEEE Proceedings of International Symposium on Circuits and Systems, June, 1993

[3] K. Ben-Kilani, R. Schlueter, "An Approach for Determining the Subsystem Experiencing and Producing a Bifurcation in a Power System Dynamics Model", IEEE Transactions on Power Systems, Vol. 15, No. 3, August, 2000

[4] E. H. Abed, "Singularly Perturbed Hopf Bifurcation", IEEE Transactions on Circuits and Systems, Vol. 32, No. 12, Dec. 1985

[5] N. Fenichel, "Geometric Singular Perturbation Method for Ordinary Differential Equations", SIAM Journal of Applied Mathematics, Vol. 31, 1979

[6] R. Schlueter, K. B. Kilani, and U. Ahn, "Impact of Modeling Accuracy on Type, Kind, and Class of Stability Problems in a Power System Model", Proc. of the ECC and NSF International Workshop on Bulk Power System Voltage Stability, Security and Control, Phenomena-III, Aug., 1994

[7] R. Schlueter, S. Liu, and N. Alemadi, "Intelligent Voltage Stability Assessment Diagnosis, and Control of Power Systems Using a Modal Structure", Division of Engineering Research Technical Report, Dec., 1998 and distributed to attendees of Bulk Power System Dynamics and Control IV Restructuring, Aug. 24-28, Santorini, Greece

[8] K. Ben-Kilani, "Bifurcation Subsystem Method and Its Application to Diagnosis of Power System Bifurcations Produced by Discontinuities", Ph.D dissertation, Michigan State University, 1997

[9] T. V. Cutsem, C. Vournas, "Voltage Stability of Electric Power Systems", Kluwer Academic Publisher

[10] P. Kokotovic, J. Allemong, J. Winkelman, and J. Chow, Singular Perturbation and Iterative Separation of Time Scales, Automatica, Jan. 1980

[11] P. Kokotovic, H. K. Khalil, J. O'Reilly, "Singular Perturbation Methods in Control: Analysis and Design", Academic Press, 1986.

[12] J. M. Undrill, J. A. Casazza, E. M. Gulachenski, and L. K. Kirchmayer, "Electromechanical Equivalents for User in Power System Stability Studies", IEEE Transactions on Power Apparatus and Systems, Vol. PAS-90, Sep./Oct., 1971

[13] B. Moore, "Principle Component Analysis in Linear Systems : Controllability, Observability, and Model Reduction", IEEE Transactions on Automatic Control, Feb. 1981

[14] A. Shayanfar, and R. A. Schlueter, "Optimal Modal Coherent Aggregation of Dynamic Equivalents for Transient Stability Studies", IEEE Transactions on Power Apparatus and Systems, Vol. PAS-103, No. 7, Jul., 1984

[15] Y. X. Ni, V. Vittal, W. Kliemann, A. A. Fouad, "Nonlinear Modal Interaction in HVDC/AC Power Systems with DC Power Modulation", IEEE Transactions on Power Systems,

[16] M. K. El-Sherbiny, D. M. Mehta, "Dynamic System Stability Part I: Investigation of the Effect of Different Loading and Excitation Systems",

[17] M. Ilic, J. Zaborszky, "Dynamics and Control of Large Electric Power Systems", John Wiley & Sons, Inc., 2000

[18] S. Wiggins, "Introduction to Applied Nonlinear Dynamic Systems and Chaos", Springer-Verlag, 1990

[19] S. Wiggins, "Normally Hyperbolic Invariant Manifolds in Dynamical Systems", Springer-Verlag, 1991

[20] D. Kosterev, C. Taylor, W. Mittelstadt, "Model Validation for the August 10, 1996 WSCC System Outage", IEEE Transactions on Power Systems, Dec., 1997

[21] J. Guckenheimer, P. Holmes, "Nonlinear Oscillations Dynamic Systems, and Bifurcations of Vector Fields", Springer-Verlag, 1983

[22] J. Zaborszky, K. W. Whang, G. M. Huang, L. J. Chiang, S. Y. Lin, "A Clustered Dynamic Model for a Class of Linear Autonomous Systems Using Simple Enumerative Sorting", IEEE Transactions on Circuits and Systems, Nov. 1982

[23] C. Taylor, J. Mechenbier, and J. Burns, "The December 14, 1994 Breakup of the Western North American Power System: Failures, Successes, and Lessons", Invited paper for V Symposium of Specialist in Electric Operational and Expansion Planning, Recile, Brazil, May 19-24, 1996

[24] C. Taylor, D. Erickson, "Recording and Analyzing the July 2 Cascading Outage", IEEE Computer Applications in Power, Jan., 1997

[25] G. Rogers, "Power System Oscillations", Kluwer's Power Electronics and Power System Series, 2000

[26] K. Ben-Kilani, and R. Schlueter, "Trends in Model Development for Stability Studies of Power Systems", Electric Power System Research, Vol. 53, No. 3, Mar., 2000

[27] H. Haken, "Advanced Synergetics: Instability Hierarchies of Self-Organizing Systems and Devices", Springer-Verlag, 1983

[28] P. Kundar, "Power System Stability and Control", Mc-Graw-Hill, 1994

[29] S. Liu, R. A. Schlueter, Intelligent Control for a Power System in a Deregulated Environment, North American Power Symposium, M. I. T., Nov, 1996

[30] R. Schlueter, S. Liu, and K. Kilani, "Justification of the Voltage Stability Security Assessment and Diagnostic Procedure Using a Bifurcation Subsystem Method", Vol. 15, No. 3, IEEE Transactions on Power Systems, Aug., 2000

[31] C. A. Canizares, Conditions for Saddle-node Bifurcations in AC/DC Power Systems, Electrical Power & Energy Systems, Vol. 17, No. 1, 1995

[32] C. A. Canizares, F. L. Alvarado, "Point of Collapse Methods Applied to AC/DC Power Systems", IEEE/PES 1991 Summer Meeting, San Diego, 1991

[33] G.H. Golub, C. E. Van Loan, "Matrix Computation", The John Hopkins University Press

[34] "Power System Toolbox Version 2.0, Loadflow Tutorial and Functions", Cherry Tree Scientific Software

[35] S. Skogestad, I. Postlethwaite, "Multivariable Feedback Control, Analysis and Design", John Wiley & Sons, 1997

[36] S. Chen, O. P. Malik, "H_∞ Optimization-based Power System Stabilizer Design", IEE Proc. Gener., Transmi. Distrib., Vol. 142, No. 2, March, 1995

[37] Q. Zhao, J. Jiang, "Robust SVC Controller Design for Improving Power System Damping", IEEE Transactions on Power System, Vol. 10, No. 4, Nov., 1995

[38] M. Klein, L. X. Le, G. J. Rogers, S. Farrokhpay, N. J. Balu, "H_∞ Damping Controller Design in Large Power Systems", IEEE Transactions on Power Systems, Vol. 10, No. 1, Feb., 1995

[39] "Mu Analysis and Synthesis Toolbox User's Guide", The Mathworks Inc.

[40] G. E. Boukarim and J. Chow, "Modeling of Nonlinear System Uncertainties using a Linear Fractional Transformation Approach", Proceedings of the American Control Conference, June, 1998

[41] M. Djukanovic, M. Khammash, V. Vittal, "Application of the Structured Singular Value Theory for Robust Stability and Control Analysis in Multimachine Power System", IEEE Transactions on Power System, Dec., 1997

[42] X. Yu, M. Khammash, and V. Vittal, "Robust Design of a Damping Controller for Static Var Compensators in Power Systems", IEEE Transactions on Power Systems, Aug., 2001

[43] J. Thapar, V. Vittal, W. Kliemann, A. Fouad, "Application of the Normal Form of Vector Fields to Predict Interarea Separation in Power Systems", IEEE Transactions on Power Systems, Vol. 12, No. 2, May, 1996

[44] S. Zhu, V. Vittal, and W. Kliemann, "Analyzing Dynamics Performance of Power Systems over Parameter Space Using Normal Forms of Vector Fields - Part I: Identification of Vulnerable Regions", IEEE Transactions on Power Systems, Vol. 16, No. 3, August, 2001

[45] N. Martins, and L. Lima, "Determination of Suitable Locations for Power System Stabilizers and Static VAR Compensators for Damping Electromechanical Oscillations in Large Scale Power Systems", IEEE Transactions on Power Systems, Vol. 5, No. 4, Nov., 1990

[46] G. E. Boukarim, S. Wang, J. H. Chow, G. N. Taranto, N. Martins, "A Comparison of Classical, Robust, and Decentralized Control Design for Multiple Power System Stabilizers", IEEE Transactions on Power Systems, Jan., 2000

[47] R. A. Horn, C. R. Johnson, "Topics in Matrix Analysis", Cambridge University Press, 1991

[48] H. Khalil, "Nonlinear Feedback Control", Class Notes of ECE 960B, Department of Electrical and Computer Engineering, Michigan State University, Fall, 2000

[49] Y. Takagi and T. Shigemasa, "An Application of State-Space Linearization to a Power System Stabilizer", Proceedings of the 29th Conference on Decision and Control, Honolulu, Hawaii, Dec., 1990

Appendix A

Singular Perturbation for Ordinary Differential Equations [5]

The singular perturbation problems are characterized by two time scales , slow time t and fast time τ. They are related by $\tau = t/\epsilon$, where ϵ is a small positive number.

Let M be an open subset of $R^n \times R^m$, and let $\mathcal{E} = M \in (R^n \times \{0\})$ be nonempty. The ordinary equation with small positive perturbation ϵ of the form:

$$\begin{aligned} \dot{x} &= f(x, y, \epsilon) \\ \epsilon\dot{y} &= g(x, y, \epsilon) \end{aligned} \tag{A.0.1}$$

defined for $(x, y) \in M$. The degenerated system is:

$$\begin{aligned} \dot{x} &= f(x, y, 0) \\ 0 &= g(x, y, 0) \end{aligned} \tag{A.0.2}$$

with assumption that $g(x, 0, 0) = 0 \quad \forall (x, 0) \in \mathcal{E}$. Suppose that the flow defined by (A.0.2) has periodic orbit $\gamma_0 : x = p(t), y = 0$.

Rescaling the (A.0.1) with $\tau = t/\epsilon$ gives:

$$\begin{aligned} x' &= \epsilon f(x, y, \epsilon) \\ y' &= g(x, y, \epsilon) \end{aligned} \tag{A.0.3}$$

where $'$ denotes the derivative with respect to fast time τ.

To study the periodic orbit structure of (A.0.1) define the suspended system:

$$\begin{aligned} x' &= \epsilon f(x, y, \epsilon) \\ y' &= g(x, y, \epsilon) \\ \epsilon' &= 0 \end{aligned} \tag{A.0.4}$$

The linearization of system (A.0.4) is given by:

$$\begin{bmatrix} \delta x' \\ \delta y' \\ \delta \epsilon' \end{bmatrix} = \begin{bmatrix} 0 & 0 & f(x,0,0) \\ 0 & D_y f(x,0,0) & D_\epsilon f(x,0,0) \\ 0 & 0 & 0 \end{bmatrix} \begin{bmatrix} \delta x \\ \delta y \\ \delta \epsilon \end{bmatrix} \tag{A.0.5}$$

The initial layer problem is obtained by setting $\epsilon = 0$:

$$\delta y' = D_y g(x, 0, 0) \delta y \tag{A.0.6}$$

It has been proved that γ_0 can be continued to a family of the periodic orbits γ_ϵ [1] if:

1. The periodic orbit of the reduced system γ_0 has 1 as a Floquet multiplier of multiplicity precisely one.

2. For each $(x, 0) \in \gamma_0$, the initial layer problem (A.0.6) has a hyperbolic equilibrium point at $\delta y = 0$.

The geometric proof can be given following that γ_ϵ and the period of γ_ϵ depend smoothly on ϵ. For simplification, assume all the eigenvalues of $D_2 g(x,0,0)$ lie in the left half plane, for all $(x,0) \in \gamma_0$, then the coefficient matrix in equation (A.0.5) has m eigenvalues in the left half plane and has zero as an eigenvalue of multiplicity $m+1$.

Denote the invariant subspace associated with the eigenvalue zero by $E^c_{(x,0)}$, which is invariant and asymptotically stable under the flow of (A.0.5), depends continuously on $(x,0)$, and is transversal to the plane through $(x,0)$ parallel to the y-axis. The global manifold theorem assures the existence of a smooth $(n+1)$-dimensional manifold χ containing γ_0, invariant and asymptotically stable under the suspended system (A.0.4), and tangent to $E^c_{(x,0)}$ at $(x,0)$, for each $(x,0) \in \chi$.

Theorem A.1: For the suspended system (A.0.4) there is a neighborhood U of $\gamma_0 \times \{0\}$, and a smooth family of m-dimensional manifolds $\mathcal{F}^s(x,y,\epsilon), (x,y,\epsilon) \in U$, such that:

1. $\mathcal{F}^s(x,0,0)$ is tangent to $E^s_{(x,0)}$, for all $(x,0,0) \in U \cap (\mathcal{E} \times \{0\})$

2. The family $\{\mathcal{F}^s(x,y,\epsilon) : (x,y,\epsilon) \in U\}$ is invariant in the sense that

$$(\mathcal{F}^s(x,y,\epsilon)) \cdot \tau \subset F^s((x,y,\epsilon) \cdot \tau)$$

   for all $(x,y,\epsilon) \in U$, for all $\epsilon \geq 0$, $\tau \geq 0$

3. For $\epsilon \geq 0$, $\mathcal{F}^s(x,y,\epsilon)$ is uniquely characterized by: $\mathcal{F}^s(x,y,\epsilon) = \{(\bar{x},\bar{y},\epsilon) \in U : |(\bar{x},\bar{y},\epsilon) \cdot \tau - (x,y,\epsilon) \cdot \tau| / e^{K\tau} \to 0 \text{ as } \tau \to \infty\}$

where $\cdot\tau$ denotes the solution operator of any system of differential equations with independent variable of fast time τ. $K < 0$ is any number greater than the real parts of all the eigenvalues of $D_g(x,0,0)$, for all $(x,0) \in \gamma_0$.

Above statements implies that for the singularly perturbed ordinary equations, the periodic orbits and the period of the periodic solutions change smoothly with the perturbation ϵ under the assumption of the hyperbolicity. The third conclusion in above theorem suggests that the trajectories through points in $\mathcal{F}^s(x, y, \epsilon)$ are asymptotically approaching the trajectories up to an error of order $e^{K,\tau}$ through (x, y, ϵ) as $\tau \to \infty$.

More general system in a form which is independent of the choice of coordinates is studied.

Let M be an open subset of $R^n \times R^m$, let $\mathcal{E}$ be a m-dimensional submanifold of M., let ϵ_0 be small positive number. The general C^r system is given by:

$$z' = h(z, \epsilon) \tag{A.0.7}$$

for $z \in M$, $\epsilon \in (-\epsilon_0, \epsilon_0)$, with $h(z, 0) = 0$. System (A.0.3) is thus only a special case of (A.0.7) with coordinates selected as fast time, i.e., $z = (x, y)$ and $h = (\epsilon f_0, g)$. The slow time system is:

$$\epsilon \dot{z} = h(z, \epsilon)$$

and the suspended systems for both slow and fast time systems are:

$$\begin{aligned} z' &= h(z, \epsilon) \\ \epsilon' &= 0 \end{aligned}$$

and

$$\begin{aligned} \epsilon \dot{z} &= h(z, \epsilon) \\ \dot{\epsilon} &= 0 \end{aligned}$$

For the coordinate-free system (A.0.7), let M be a C^{r+1} n-dimensional manifold, $1 \geq r < \infty$. Let $X : M \to TM$ be a C^r vector field on M. X maps each $m \in M$ to a tangent vector $X(m) \in T_mM$. Denote a family of vector fields on M, which is parameterized by $\epsilon \in (-\epsilon, \epsilon_0)$, by X^ϵ. Let $\mathcal{E} \in R_n$ be a C^r submanifold of M consisting entirely of equilibria of X^0. Denote the codimension of $\mathcal{E}$ in M by m. We have a linear map:

$$TX^0(m) : T_mM \to T_mM$$

and

$$T(X^0\times)(m,0) : T_{(m,0)}\{M \times (-\epsilon_0, \epsilon)\} \to T_{(m,0)}\{M \times (-\epsilon_0, \epsilon_0)\}$$

where $TX^0(m) \in R^{n+m}$, and $T(X^0 \times 0) \in R^{n+m+1}$. $TX^0(m)$ induces another linear map:

$$QX^0(m) : T_mM|T_m\mathcal{E} \to T_mM|T_m\mathcal{E}$$

on the quotient space. Actually $QX^0(m)$ is nothing but the linearization of

$$z' = X^\epsilon\phi(\phi^{-1}(z))$$

where $\phi(m)$ is a flow of the full system X^ϵ.

Theorem A.2: Let M be a C^{r+1} manifold, $2 \leq r < \infty$. Let $X^\epsilon, \epsilon \in (-\epsilon_0, \epsilon_0)$, be a C^r family of vector fields, and let $\mathcal{E}$ be a C^r submanifold of M consisting entirely of equilibrium points of X^0. Let $\gamma \in \mathcal{E}_H$ be a periodic orbit of the reduced system X_R, and suppose that γ_0, a periodic orbit of X_R, has 1 as a Floquet multiplier of multiplicity precisely one. Then, there exists $\epsilon_1 > 0$ and there exists a C^{r-1} family of closed curves $\gamma_\epsilon, \epsilon \in (-\epsilon_1, \epsilon_1)$, such that $\gamma_0 = \gamma$ and ϵ is a periodic orbits of $\epsilon^{-1}X^\epsilon$. The period of γ_ϵ is a C^{r-1} function of ϵ.

Suppose the periodic orbit γ_R of the reduced system X_R has j_+, j_-, and 0 Floquent multipliers inside, outside, and on the unit circle, and for each $m \in \gamma_R$, the lineariza-

tion $QX^0(m)$ of the reduced system has k_+, k_-, and 0 eigenvalues in the left, right half plane, and on the imaginary axis, therefore, under assumptions of Theorem, there exists $\epsilon_1 > 0$ such that:

1. There exists a C^{r-1} family of closed solution $\{\gamma_\epsilon, \epsilon \in (-\epsilon_1, \epsilon)\}$ in M such that $\gamma_0 = \gamma_R$ and for $\epsilon \neq 0$, γ_ϵ is a periodic orbit of $\epsilon^{-1}X^\epsilon$. The period of γ_ϵ is a C^{r-1} function of ϵ.

2. γ_ϵ has $j_+ + k_+$, $j_- + k_-$ Floquent multiplier inside and outside the unit circle, respectively.

3. There are C^{r-1} families of local stable and unstable manifolds $W^s_\epsilon \in R^{j_+ + k_+ + 1}$, $W^u_\epsilon \in R^{j_- + k_- + 1}$ in M, such that $W^s_\epsilon \cap W^u_\epsilon = \gamma_\epsilon$.

4. Let $A^+(U_\epsilon) = W^s_\epsilon$ and $A^-(U_\epsilon) = W^u_\epsilon$. There are C^{r-1} families of manifolds $\{\mathcal{F}^s_\epsilon(m), m \in W^s_\epsilon\}$ and $\{\mathcal{F}^u_\epsilon(m), m \in W^-\epsilon\}$ characterized by:

$$\begin{aligned} \mathcal{F}^s_\epsilon(m) &= \{\hat{m} \in A^+(U_\epsilon) : e^{-K_s t/\epsilon} d(m \cdot t, \hat{m}\cdot) \to 0 \\ \mathcal{F}^u_\epsilon(m) &= \{\hat{m} \in A^-(U_\epsilon) : e^{-K_u t/\epsilon} d(m \cdot t, \hat{m}\cdot) \to 0 \end{aligned}$$

as $t \to \infty$

Appendix B

RGA-Matrix Property of Bifurcation Subsystem

RGA is defined as:

$$\Lambda(A) = A \times (A^{-1})^T$$

where $\times$ means Hadamard product or Schur product. The system transfer function of the state space representation is given by:

$$G(s) = C(sI - A)^{-1}B$$

When B, and C are identity and at steady-state:

$$G(s) = -A^{-1}$$

Since $\Lambda(A^{-1}) = \Lambda(A^T)$ we here consider $\Lambda(A)$ only and A is partitioned as

$$A = \begin{bmatrix} A_{11_{(l\times l)}} & A_{12_{(l\times m)}} \\ A_{21_{(m\times l)}} & A_{22_{(m\times m)}} \end{bmatrix}$$

If A_{11} and A_{22} are nonsingular the RGA matrix is given by:

$$\begin{aligned}\Lambda(A) &= \begin{bmatrix} A_{11} & A_{12} \\ A_{21} & A_{22} \end{bmatrix} \times \begin{bmatrix} X_{11} & X_{12} \\ X_{21} & X_{22} \end{bmatrix}^T \\ &= \begin{bmatrix} A_{11} \times X_{11}^T & A_{12} \times X_{21}^T \\ A_{21} \times X_{12}^T & A_{22} \times X_{22}^T \end{bmatrix}\end{aligned}$$

where:

$$\begin{aligned}X_{11} &= (A_{11} - A_{12}A_{22}^{-1}A_{21})^{-1} \\ &= A_{11}^{-1} + A_{11}^{-1}A_{12}(A_{22} - A_{21}A_{11}^{-1}A_{12})^{-1}A_{21}A_{11}^{-1} \\ X_{12} &= -(A_{11} - A_{12}A_{22}^{-1}A_{21})^{-1}A_{12}A_{22}^{-1} \\ X_{21} &= -A_{22}^{-1}A_{21}(A_{11} - A_{12}A_{22}^{-1}A_{21})^{-1} \\ X_{22} &= A_{22}^{-1} + A_{22}^{-1}A_{21}(A_{11} - A_{12}A_{22}^{-1}A_{21})^{-1}A_{12}A_{22}^{-1}\end{aligned}$$

It has been discussed that the magnitude of RGA element represents specific properties of the system. The following inequality [47] holds strictly:

$$\| A \times B \|_F \leq \| A \|_F \| B \|_F$$

and will be used to estimate the upper bound of each block in $\Lambda(A)$. If A_{11} is nonsingular we have:

$$\begin{aligned}
\| \Lambda(A)(1,1) \|_F &= \| A_{11} \times (A_{11}^{-1})^T \\
&+ A_{11} \times [A_{11}^{-1} A_{12}(A_{22} - A_{21}A_{11}^{-1}A_{12})^{-1} A_{21} A_{11}^{-1}]^T \|_F \\
&\leq \| A_{11} \times (A_{11}^{-1})^T \|_F \\
&+ \| A_{11} \times [A_{11}^{-1} A_{12}(A_{22} - A_{21}A_{11}^{-1}A_{12})^{-1} A_{21} A_{11}^{-1}]^T \|_F \\
&\leq \| \Lambda(A_{11}) \|_F \\
&+ \| A_{11} \|_F \| A_{11}^{-1} A_{12}(A_{22} - A_{21}A_{11}^{-1}A_{12})^{-1} A_{21} A_{11}^{-1} \|_F \\
&\leq \| \Lambda(A_{11}) \|_F \\
&+ l\bar{\sigma}(A_{11})\bar{\sigma}(A_{11}^{-1} A_{12}(A_{22} - A_{21}A_{11}^{-1}A_{12})^{-1} A_{21} A_{11}^{-1}) \\
&\leq \| \Lambda(A_{11}) \|_F \\
&+ l\bar{\sigma}(A_{11})\underline{\sigma}^2(A_{11})\bar{\sigma}(A_{12}) \\
&\cdot \underline{\sigma}(A_{22} - A_{21}A_{11}^{-1}A_{12})\bar{\sigma}(A_{21}) \qquad \text{(B.0.1)}
\end{aligned}$$

where the second inequality follows from:

$$\begin{aligned}
\| A_{(l \times m)} \|_F &\leq \sqrt{\min(l,m)}\ \bar{\sigma}(A) \\
\bar{\sigma}(AB) &\leq \bar{\sigma}(A)\bar{\sigma}(B) \\
\bar{\sigma}(A) &= \underline{\sigma}(A^{-1})
\end{aligned}$$

$$
\begin{aligned}
\| \Lambda(A)(1,2) \|_F &\leq \| A_{12} \|_F \| [(A_{22}^{-1} A_{21}(A_{11} - A_{12}A_{22}^{-1}A_{21})^{-1}]^T \|_F \\
&\leq \sqrt{\min(l,m)}\bar{\sigma}(A_{12}) \\
&\cdot \sqrt{\min(l,m)}\bar{\sigma}(A_{22}^{-1}A_{21}(A_{11} - A_{12}A_{22}^{-1}A_{21})^{-1}) \\
&\leq \min(l,m)\bar{\sigma}(A_{12})\underline{\sigma}(A_{22}) \\
&\cdot \bar{\sigma}(A_{21})\underline{\sigma}(A_{11} - A_{12}A_{22}^{-1}A_{21}) \qquad \text{(B.0.2)}
\end{aligned}
$$

$$
\begin{aligned}
\| \Lambda(A)(2,1) \|_F &\leq \| A_{21} \|_F \| [(A_{11} - A_{12}A_{22}^{-1}A_{21})^{-1}A_{12})A_{22}^{-1}]^T \|_F \\
&\leq \min(l,m)\bar{\sigma}(A_{21})\underline{\sigma}(A_{11} - A_{12}A_{22}^{-1}A_{21}) \\
&\cdot \bar{\sigma}(A_{12})\underline{\sigma}(A_{22}) \qquad \text{(B.0.3)}
\end{aligned}
$$

$$
\begin{aligned}
\| \Lambda(A)(2,2) \|_F &= \| A_{22} \times (A_{22}^{-1})^T \\
&+ A_{22} \times [A_{22}^{-1}A_{21}(A_{11} - A_{12}A_{22}^{-1}A_{21})^{-1}A_{12}A_{22}^{-1}]^T \|_F \\
&\leq \| A_{22} \times (A_{22}^{-1})^T \|_F \\
&+ \| A_{22} \times [A_{22}^{-1}A_{21}(A_{11} - A_{12}A_{22}^{-1}A_{21})^{-1}A_{12}A_{22}^{-1}]^T \|_F \\
&\leq \| \Lambda(A_{22}) \|_F \\
&+ \| A_{22} \|_F \| A_{22}^{-1}A_{21}(A_{11} - A_{12}A_{22}^{-1}A_{21})^{-1}A_{12}A_{22}^{-1} \|_F \\
&\leq \| \Lambda(A_{22}) \|_F \\
&+ m\bar{\sigma}(A_{22})\bar{\sigma}(A_{22}^{-1}A_{21}(A_{11} - A_{12}A_{22}^{-1}A_{21})^{-1}A_{12}A_{22}^{-1}) \\
&\leq \| \Lambda(A_{22}) \|_F \\
&+ m\bar{\sigma}(A_{22})\underline{\sigma}^2(A_{22})\bar{\sigma}(A_{21})\underline{\sigma}(A_{11} - A_{12}A_{22}^{-1}A_{21})\bar{\sigma}(A_{12}) \qquad \text{(B.0.4)}
\end{aligned}
$$

Inequalities (B.0.1) - (B.0.2) show that the *RGA* matrix of the system becomes block diagonal (with off-diagonal blocks approaching zero) as $\underline{\sigma}(A_{11} - A_{12}A_{22}^{-1}A_{21}) \rightarrow 0$. The upper diagonal block approaches the *RGA* matrix of the internal system

with the external system truncated. The lower diagonal block approaches the *RGA* matrix of the external system with the internal system truncated. The control of the bifurcation subsystem is completely independent of the external system based on this *RGA* structure.

It should be noted that when bifurcation occurs A_{11} is singular, and $\| \Lambda(A)(1,1) \|_F$ is small instead of being large since A_{11} is singular and (B.0.1) does not hold any more. Instead the upper bound of $\Lambda(A)(1,1)$ is given in the following inequality:

$$\begin{aligned} \Lambda(A)(1,1) &\leq \| A_{11} \|_F \| [(A_{11} - A_{12}A_{22}^{-1}A_{21})^{-1}]^T \|_F \\ &\leq \sqrt{l}\bar{\sigma}(A_{11})\sqrt{l}\, \underline{\sigma}(A_{11} - A_{12}A_{22}^{-1}A_{21}) \\ &= l\, \bar{\sigma}(A_{11})\underline{\sigma}(A_{11} - A_{12}A_{22}^{-1}A_{21}) \end{aligned} \tag{B.0.5}$$

Since A_{11} and $A_{11} - A_{12}A_{22}^{-1}A_{21}$ both become singular as the bifurcation occurs, then $\underline{\sigma}(A_{11} - A_{12}A_{22}^{-1}A_{21})$ approaches zero as the bifurcation occurs.

Large *RGA* element magnitudes of the system indicate that the system is fundamentally difficult to control since the system is very sensitive to uncertainty. A specific small element in *RGA* matrix means that the corresponding input and output are not a good pair in the sense that closing other loops has large effects on this input/output loop gain. Therefore, it is difficult to choose control inputs and outputs for internal system when bifurcation occurs as noted in (B.0.5). Moreover, in this situation it is difficult to control internal system via external system since they are almost totally decoupled. This puts extra difficulty for stabilization. Thus, it is important to carefully consider the directionality of the bifurcation and the parameter variation in the MIMO system that translates into the input and output uncertainties in order to design the robust controller that would stabilize the system and cure the bifurcation.